Interplay Between Long-Range And Short-Range Interactions In Polymer Self-Assembly And Cell Adhesion

Thesis by

Cheng-Zhong Zhang

In Partial Fulfillment of the Requirements

for the Degree of

Doctor of Philosophy

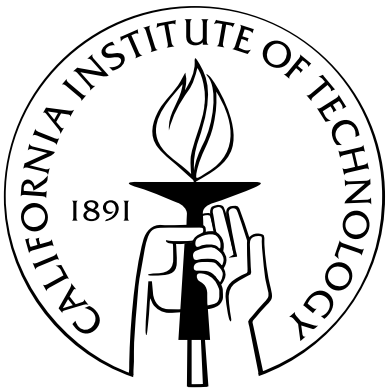

California Institute of Technology

Pasadena, California

2008

(Defended September 13, 2007)

To my parents and all friends

who have witnessed my intellectual growth,

To the great Mozart

Bach, Beethoven, Brahms, Wagner, Strauss ...

Acknowledgements

Six years has passed since I came to Caltech, which has become the longest period I ever spent at one school. Yet this past six years at Caltech has transformed me from an "A" student, to a keen problem-solver, and finally, a critical thinker. For my intellectual growth, first I need to thank my advisor, Professor Zhen-Gang Wang. In addition to his impressive depth of knowledge and insights, as an advisor, he can always gauge the right amount of help and advice, and leave the rest to myself. It could be a little stressful sometimes: whenever I made some progress and felt that I can tackle one class of problems, the next task turned out to be even more challenging. Nonetheless, it is only through this process of excellence that I learn to enjoy doing research.

Professor John Brady gave me the first lecture at Caltech. I still remember our discussions of the topics for the class project, which gave my first exposure to independent research. I am impressed by his broad interests, which are reflected in his research as well as the problems he designed for the qualifying exams: from coffee stirring to the Lost Ark. I thank him for many discussions on various subjects, in particular, for his meticulous and critical reading of my candidacy report and final thesis.

Professor Rob Phillips introduced me to the area of biophysics, or physical problems in biology. I am deeply impressed by his infinite passion in exploring all kinds of topics, but what is truly remarkable is his determination and courage in moving from mechanics into experimental biology. We have had several discussions, but attending Rob's talks or lectures, and listening to his questions or comments, impact me the most.

Theorists "are a special group of people who live upon our colleagues." As a theorist, I have had the fortune of working in collaboration with Professor David Tirrell's group. Dave, and students in his group, Kechun, and Wei, are the main resources of new ideas and new problems for us to work on. They have also been the best audience and collaborators when we want to discuss and test our results. In particular, I want to thank Dave for his encouragement when I meet difficulties.

I must say, though a cliché, that our department has the best staff members. Both as graduate student assistant and as secretary to Zhen-Gang, Kathy has been offering the most and best help that I can ever expect. Anne also did a great job in organizing the CSEM annual meetings and it has been pleasant to work with her. I need to thank Suresh—as the only computer assistant in the

department, he offers timely help and deals with all sorts of computer issues. I also want to thank Martha, Laura, Yvette, and Marcy (who has left Caltech), for receiving all my packages.

During my stay at Caltech, I have met many good friends. Justin Bois, who became "Dr. Bois" several months ago, and Jennifer Witman, are the first friends I met in the chemical engineering department, and incidentally we all joined the "Wang group", and quadrupled the size of the group then with only Andrew Spakowitz. All my group members, including the later joined Shelby Hutchens, have offered me a lot of suggestions and encouragements. I need to thank Yizhen Zhang, Xinwei Yu, and many other house mates at Braun house, for offering me a lot of help during my first year at Caltech. Zhipu Jin is the first Chinese student I met at Caltech: we shared many fun stories and experiences; Zhaoyan Zhu and I shared some of the best memories and sweetest moments, which colored my monochromatic life; Kai Shen and I have been cheering up each other in the past two years: without his help I would not have gone through the difficult moments in writing up the thesis. In addition, I want to thank Ying Huang, Rongjing Zhang and Junhua Yuan, Hua Long, George X. Ouyang, Xin Guo, Yu Liu, Changlin Pang, Jian Wu, and many others whom I have talked to and benefited from.

In the past six years I have undergone not only intellectual, but also mental growth. My parents witnessed this whole process, I am indebted to their comforts and encouragements, even though we are at two ends of the globe. Without their support I could never come to this point. I also treasure the friendship of Liang Qiao and Hongzhou Jiang: we have been arguing with each other since college, and continue to share our individual opinions on all sorts of issues.

Abstract

Interplay between long-range and short-range interactions is a common theme in soft and biological matter, which results in complicated self-assembly behaviors. We study two examples of this interplay: reversible gelation of associating polymers and ligand-receptor interactions in membrane adhesion. In associating polymer solutions, the competition between the conformation flexibility of polymer chains and the enthalpic monomer interactions results in phase-separated micro-structures at the mesoscopic scale; both gelation and the microphase order-disorder transition are manifestations of this self-assembly. We further establish that reversible gelation is similar to the glass transition: both are characterized by ergodicity breaking, aperiodic micro-structures, and non-equilibrium relaxations over a finite temperature range. In the study of ligand-receptor interactions between surfaces, we emphasize the interplay between *specific* ligand-receptor binding, and *generic* physical interactions. We find that both the finite spatial extension of receptors and their mobilities affect their binding affinity. As a special case of the interplay between receptor binding and generic interactions, we study the dynamics of membrane adhesion that is mediated by receptor binding but fulfilled through membrane deformations. We calculate the energy barrier of the adhesion as a result of membrane bending deformations and the double-well adhesion potential, and analyze the different scenarios according to the shape of the adhesion potential by scaling arguments.

Contents

List of Figures

List of Tables

Overview

In a famous paper, "*More is different*," P. W. Anderson (1972) highlighted the "hierarchical structure of science." Even though we understand the fundamental laws of basic particles or objects, the physical behavior of aggregates of these entities, usually associated with strong interactions and correlations, cannot be "understood from simple extrapolations from the properties of a few of these particles." More is different, and more leads to emergent phenomena as a result of increasing complexities as length and time scales increase. For this very reason, chemical and biological sciences, which study essentially physical phenomena from the nanometer scale up to the macroscopic scale of our living world, call upon their own principles, rather than the microscopic quantum mechanic theory.

This viewpoint is further supported by the multitude of complex behaviors of soft and biological matter, which typically involve objects of large spatial extensions, such as long polymers or membranes, and a confluent of energy and time scales of different interactions (Phillips and Quake, 2006). A key feature of mesoscopic organization in soft and biological matter is that competing interactions at different length scales can interplay with each other and result in sophisticated self-assembly. This new paradigm, which extends the classical "symmetry breaking" picture of Landau, is referred to as the "Middle Way" (Laughlin et al., 2000).

In this thesis I study two problems related to the self-assembly of soft matter as a result of competing interactions at different length scales.

In Part I, we study the physics of reversible gelation. Reversible gel is a class of materials which are macroscopic networks formed by reversible associations. Compared to irreversible gel with permanent connections, such as rubber, reversible gel is characterized by both solid-like elasticity and liquid-like relaxations. These features are characteristic of structural glasses. We choose the model of associating polymer solutions, which is a prototype for reversible gelation, and analyze the thermodynamics and phase transitions in the system. We find that gelation is intimately related to the micro-structural order-disorder transition in this system and gelation to order-disorder transition is an analog of glass transition to crystallization.

To further corroborate our conjecture regarding the nature of gelation, in particular, its relation to the microphase transition, we study the phase transitions in diblock copolymer melts, which are

characterized by the microphase spinodal as in associating polymer solutions. Using a thermodynamic replica approach, we find a micro-structural glass transition in the system which results from self-assembly due to competitions between monomer interactions and polymer chain flexibility. In particular, we find that in the mean field limit (infinitely long chains), this glass transition becomes identical to the microphase spinodal, suggesting that the microphase spinodal can be regarded as the signature for glass transitions in this class of systems. In this calculation we also propose a systematic treatment of fluctuations due to the cubic coupling term that appears in asymmetric copolymers, which is missing in the Brazovskii-Leibler-Fredrickson-Helfand theory (Brazovskii, 1975; Leibler, 1980; Fredrickson and Helfand, 1987). Chapter 3 is adapted from our paper, C.-Z. Zhang and Z.-G. Wang, *Phys. Rev. E***73**, 031804 (2006). Copyright (2006) by the American Physical Society.

In Part II we study two problems related to ligand-receptor interactions between surfaces, which is a central motif in cell adhesion and signaling. In Chapter 4[1] we analyze the thermodynamics of interactions between flat surfaces mediated by receptors that are tethered by polymer chains. This model is widely used in bioengineering applications (Garcia, 2006) and biophysical measurements (Wong et al., 1997; Jeppesen et al., 2001). From statistical thermodynamics calculations we obtain an effective two-dimensional binding constant reflecting contributions from the microscopic binding affinity as well as from stretching of the polymer tether. In addition, we distinguish between different scenarios as a result of different receptor mobilities relative to the biological process or experimental measurements. These results clarify the persistent confusion about the interpretation of experimental measurements of binding affinity (Dustin et al., 1996; Orsello et al., 2001). We also demonstrate the versatile control over surface interactions by several examples that combine different types of ligand-receptor interactions, which have both biological and bioengineering relevance.

In Chapter 5[2] we study the interplay between specific ligand-receptor binding and membrane deformations. We offer a systematic analysis of the dynamics of the first-order adhesion typical for cell and membrane adhesion mediated by specific receptors (Bruinsma et al., 2000; Bruinsma and Sackmann, 2002; Sackmann and Goennenwein, 2006). We find that the evolution of membrane deformations along the adhesion pathway is governed by the characteristic length associated with the adhesion potential, while the energetics is governed by the potential depths of the adhesion potential. The dependence of the critical radius and the energy barrier on relevant parameters, including the bending rigidity, the barrier height of the potential, and the separation of the potential minima, are obtained by scaling arguments, and verified by numerical calculations. For completeness we also give a scaling analysis of the scenario when adhesion is a weak first-order transition; this is done by a Peierls argument which accounts for the entropic corrections of irregular boundary shapes.

[1] Reproduced in part with permission from *Langmuir*, in press. Unpublished work copyright (2007) American Chemical Society.

[2] Adapted version of the manuscript submitted to *Phys. Rev. E*. Copyright (2007) by the American Physical Society

Part I

Reversible Gelation and Glass Transition: Towards a microscopic model of reversible polymer gel

Chapter 1

Introduction: Gel and gelation

A (polymer) gel is a macroscopic network of polymer chains joined at a number of connection sites. These joints can be either irreversible chemical bonds or reversible physical associations, which are called chemical (irreversible) or physical (reversible) gels. Chemical associations are usually introduced by crosslinking (e.g., vulcanization), while physical gels can involve many different types of interactions, such as hydrophobic interactions, hydrogen bonds, and electrostatic interactions between certain segments of the polymer chains.

In most cases the joints in a gel network are localized[1] and result from short-range interactions. But short-range connections have to be linked by long chains to form a macroscopic network. The assembly of long polymers by short-range connections result in a spatially extended network which is non-uniform. These two features, i.e., **local joints** connected by arms with **finite spatial extensions**, characterize most gel-forming systems.

Comparing to an ordered crystal, we find that microscopic structures in a gel network are highly random with no long-range order. The non-uniform yet aperiodic structures make a polymer gel share both liquid and solid properties. Within short time scales, the non-uniform micro-structures should have solid-like elasticity and exhibit fixed mechanical shapes. But over a long time span, the aperiodic structures in a gel are not thermally stable compared to periodic crystals; these structures should evolve slowly and exhibit liquid-like responses, such as finite shear viscosities. These features are reminiscent of another class of disordered materials—glasses.

1.1 Preparation of gels

We first briefly review the conventional ways to prepare chemical and physical polymer gels. A straightforward way to introduce chemical links is to add polyfunctional units (with 3 or more functional groups) that serve as branches in a network. Such polyfunctional units are interconnected

[1] An exception is the network generated by topological entanglements, such as in melts of very long polymer chains, or a series of interconnected rings (de Gennes, 1979).

with polymer chains generated by di-functional monomers. Alternatively one can add crosslinking agents to the system which will form inter- and intra-chain connections. A typical example is vulcanized rubber, where sulphur molecules act as the crosslinking agents (Doi, 1996).

For polymer gels prepared via crosslinking, the connections are permanent and the gelation process is irreversible. It was Flory (1953) who first calculated the amount of crosslinkers that are necessary to generate a macroscopic network (Flory-Stockmayer model) and studied the elasticity of this network ("rubber elasticity" theory). The basic model for this crosslinked network is percolation, and it is known that Flory's mean-field theory is accurate.

Reversible physical interactions that can induce gelation include hydrophobic interactions, electrostatic interactions, and hydrogen bonds. A typical example is a solution of associating A-B-A triblock copolymers where A segments associate with each other. At low concentrations, these triblock copolymers form micelles with A segments aggregating in the core and B segments in the corona. As the concentration of polymers increases, more micelles are formed with bigger sizes and finally these micelles overlap and interconnect with each other, some A-B-A chains serving as linkers among the micelles. In this case the connections are not permanent and the gelation process is reversible, i.e, the gel can dissociate when connections are turned off or reduced in number. This reversible property makes physical gel an ideal candidate for drug delivery or intelligent materials responsive to physical stimuli such as pH, temperature, or radiation (Petka et al., 1998; Shen et al., 2006).

Besides these traditional methods, connections can also be introduced via topological constraints. For example, in a concentrated solution of long polymers, polymer chains are strongly entangled; if the concentration is high enough, the topological joints can support a macroscopic network within the time scale of chain reptation. This is demonstrated by the elastic response of these systems. The open ends of polymers can also be closed to form rings, then these rings can interconnect with each other to form the so-called "Olympic" gel (Raphaël et al., 1997). This type of gel has permanent, but non-local junctions, and these junctions are topological in nature, therefore their property should resemble irreversible polymer gels; furthermore, as the junctions are non-local, this kind of material should have even better elasticity than crosslinked networks.

1.2 Gelation

Gelation is the formation of gel out of uniform solutions, which is usually marked by a transition from liquid-like behavior to solid-like behavior, for example, finite elastic modulus. Both physical gelation and chemical gelation have generated considerable interest in statistical physicists.

Sol-gel transition is a natural example of percolation (Stauffer et al., 1982), which is characterized by the emergence of a macroscopic cluster. The gelation point is identified as the critical point of

percolation, which is characterized by a threshold bond (or site) occupancy probability. If more bonds are occupied than the critical value, the system is percolated (in the gel phase), with an emergent macroscopic network and small clusters; below the critical threshold, only finite clusters are present and the system is in the sol phase. Near the threshold, physical properties including the probability distribution of finite clusters are universal and can be calculated from the percolation model.

In the classical model by Flory and Stockmayer (see Flory, 1953), the crosslinked network (e.g., vulcanized rubber) is assumed to be an infinitely large branched tree (without cycles), which is the mean-field limit of the percolation model (i.e., percolation on a Cayley tree). The Flory-Stockmayer model can be solved analytically and makes good predictions regarding the gelation point and elastic properties. Furthermore, as each crosslinker (multi-functional unit) is surrounded by many monomers, cycle structures are rare, therefore the Flory-Stockmayer model is accurate even near the critical threshold (de Gennes, 1979). Later, Coniglio et al. (1979, 1982) modified the model to account for the presence of solvent molecules. In this "site-bond correlated percolation" model, lattice sites are occupied by monomers as well as solvent molecules and a bond can be formed between neighbor monomers only. In addition, enthalpic monomer-monomer interactions are introduced as near-neighbor correlations. In this model there is a sol-gel transition as well as a phase coexistence as in normal polymer solutions due to the enthalpic interaction. The sol-gel transition intersects the phase coexistence at a tricritical point which depends on the solvent property (see Tanaka et al., 1979).

The "site-bond correlated percolation" model provides a natural extension to reversible gelation: permanent links can be replaced by reversible monomer interactions and gelation can be defined as a "transient" percolation of these reversible connections. Based on this model, Tanaka and co-workers (Tanaka, 1989, 1990; Tanaka and Matsuyama, 1989; Tanaka and Stockmayer, 1994) extended the model by Coniglio et al. (1982) to study the thermodynamics of reversible gelation. The polymer solution is treated following the mean-field theory of Flory and Huggins (Flory, 1953) and the reversible gelation is treated as a micellation. Later on, Semenov, Rubinstein and co-workers (Semenov et al., 1995b; Semenov and Rubinstein, 1998a) studied a similar model, but with different assumptions on the infinite cluster in the gel phase. Both models predict similar phase diagrams to those observed in Tanaka et al. (1979), but the different assumptions for the post-gel regime, which result in different cluster-size distributions, also lead to different predictions of the thermodynamic nature of gelation. Tanaka's theory predicted that reversible gelation is a third-order thermodynamic transition while Rubinstein's theory suggested that it is not a thermodynamic transition at all. The assumption for the post-gel regime in a reversible gel phase essentially depends on the nature of gelation and the life-time of the infinite cluster. Is the real gel phase is indeed reversible as implied by the Rubinstein model? Or does it signal some new kind of transition which resembles critical

percolation? Is the reversible gel more like a big micelle, or is it similar to a percolated network? What defines gelation in a percolation network with reversible connections?

Although the definition of irreversible gel as a macroscopic network is unambiguous and results in successful predictions, the percolation picture raises questions in the case of reversible gelation. In particular, how to consistently account for the enthalpic monomer interactions and the emergence of a macroscopic network is not obvious at all. Actually, the recent work by Zilman and Safran (2002) on self-assembled networks revealed that in a system of self-assembling chains, the percolation transition is purely topological, with no thermodynamic signature or dynamic crossover. This is clearly at odds with experimental characterization of reversible gels by their solid-like dynamic properties, which distinguish them from the liquid-like sol phase. Furthermore, the simulation results by Kumar and co-workers (Kumar and Panagiotopoulos, 1999; Kumar and Douglas, 2001) showed that for associating polymers with weak connections (associating energy comparable to k_BT), gelation is characterized by a change of dynamic properties, which marks a distinct transition line from the percolation transition. All these facts suggest that we should abandon the percolation picture, but build a model of reversible gelation from the microscopic monomer interactions.

1.3 Features of reversible gelation and relations to the glass transition

In a reversible gel, the network structure can transform through the breaking and rebuilding of connections. Therefore the dynamic property of the gel phase has a liquid-like behavior in addition to solid elasticity, this is especially evident in the long time limit. In real applications gelation is usually defined as when the system exhibits a finite elastic modulus at low frequency range (generally $1\text{Hz} \sim 10^3\text{Hz}$).

Semenov and Rubinstein (1998b) used a scaling argument to study the dynamic responses of the reversible gel phase based on the Zimm dynamics in the semi-dilute regime. The dynamic properties of the gel phase (but not the sol phase, i.e., below the gelation point) depend on the lifetime and the number of reversible junctions. In addition they also calculated the frequency dependence of dynamic modulus and the scaling of viscosity away from the gelation point. Their predictions reflect their assumptions that the reversible gel phase consists of transient network structures and the dynamics of the system is governed by the dissociation of individual junctions but not of the mesoscopic clusters.

However, recent experiments and simulations have shown that the gelation process shares many similarities with the glass transition, and the gel phase is usually characterized by static inhomogeneities with ergodicity breaking; in particular, the dynamic properties depend on small-scale relaxations as well as relaxations at the mesoscopic scale.

Segrè et al. (2001) studied reversible gelation in a weakly attractive colloidal system using light scattering. For all samples with high volume fractions ($> 8\%$), the static light scattering profile exhibits a peak at a finite wave number, implying percolation in the system with a finite correlation length. However, not all the samples are truly solid-like. In those samples at larger volume fractions ($> 11\%$), the scattering profile is stable, and the sample is non-ergodic; for samples at relatively lower volume fractions ($< 11\%$), the speckles around the peak of the scattering profile are not static, but fluctuate with time, reflecting cluster diffusions in the system. The scattering profiles of all these samples are roughly identical, suggesting that similar structures are present in both ergodic and non-ergodic samples; but the relaxation time in non-ergodic samples is infinite, while for quasi-ergodic samples it is large but finite (the scattering profile remains constant for several days). Comparing these behaviors to the glass transition, we see the following features: First, the non-ergodic samples resemble amorphous glasses, which behave like a normal solid but do not have periodic micro-structures. Second, gelation is similar to the glass transition as it is a *smooth* transition occurring over a volume fraction range, instead of at a threshold value, and both transitions are accompanied by a crossover in dynamic responses. In addition, the final decay of the dynamic light-scattering function of the system is similar to that observed in structural glasses, characterized by a power-law divergence. The intermediate scattering functions even satisfy the same scaling form as predicted by the mode coupling theory for the glass transition (Götze, 1989).

Shibayama and co-workers (Ikkai and Shibayama, 1999; Shibayama et al., 2000) studied the sol-gel transition in a reversible system consisting of poly(vinyl alcohol), Congo red (PVA/CR), and water. They found that some speckles (random fluctuations in the scattered intensity) in the time average light scattering intensity appear exclusively in the gel state, and disappear when the temperature is increased or the concentration is lowered across the gelation point. These speckling patterns indicate the existence of frozen inhomogeneities, which implies non-ergodicity in the system. In addition, the slow mode in time intensity correlation measured by dynamic light scattering is well fit by a stretched exponential form for the sol phase, and a power law for the gel phase. Similar results have been discovered in the gelatin system (Ren and Sorensen, 1993). These features are similar to the β and α relaxations observed in glasses and predicted by the mode-coupling theory (Götze, 1989).

Kumar and co-workers (Kumar and Panagiotopoulos, 1999; Kumar and Douglas, 2001) conducted Monte Carlo simulations on the phase behavior and gelation of reversibly associating polymers. Their results showed that at high temperatures (the sticker attraction energy comparable to k_BT), the "gel" structure characterized by geometric percolation (connected network) does not possess the characteristic rheological properties of a gel, e.g., elasticity at short time scales. Instead, the change of dynamic properties occurs near the so-called "clustering transition," which leads to an abrupt increase in cluster lifetimes over a small temperature range. This transition is similar to vitrification

in glass-forming liquids. Furthermore, the diffusivity data fit well with the Vogel-Fulcher form, which is known to describe the relaxation in fragile glasses.

The above results show that (1) reversible gels are characterized by the breaking of ergodicity (static inhomogeneities); (2) relaxations in the system near gelation are quite similar to those in supercooled liquids near the glass transition, usually characterized by a power low for the glassy state and a stretched-exponential function for the viscous liquid state; (3) in the "weak" interaction case (association energy comparable to k_BT), physical gelation is characterized by a dynamic transition, usually occurring after the geometric percolation.

The similarity between reversible gelation and glass transition is also evident from the microscopic perspective. Consider the solution of associating polymers. At low concentration, polymers associate to form micelles; as concentration increases, more micelles are formed with larger aggregation number, and finally these micelles overlap with each other to form a macroscopic network connected by associating polymers. Gelation should resemble the microphase order-disorder transition in the associating polymer solution. However, as these micelles have different sizes, and moreover, the micelles from associating polymers are "soft" rather than "rigid," their packing may be random and share similarities with random close packing of spheres and the jamming transition, both of which are believed to occur in certain glass transitions. These microscopic similarities between polymer gels and soft (fragile) glasses are also reflected on their similar mechanical responses, including non-equilibrium relaxations and partial breaking of ergodicity.

Here we propose that reversible gelation is essentially related to the microphase transition in the system, and can be viewed as a "glass transition" alternative to the ordering transition, or, put in other words, a transition from the disordered liquid phase to a solid-like state with random structures that may be still slowly evolving. The central idea in studying the glass transition is the free energy landscape, which is introduced to separate physical relaxations at different length and time scales. In this picture, gelation or glass transition is characterized by ergodicity breaking in the system, which results in solid-like responses; but the system has liquid-like micro-structures, and therefore can still evolve. We hope this new paradigm for reversible gelation could yield better insights into their thermodynamic nature.

In Chapter 2 we study the thermodynamics of associating polymer solutions and work out the mean-field phase diagram in this system. We recover the phase diagram as observed in Tanaka et al. (1979) and obtained in the papers by Coniglio et al. (1982), Tanaka (1989), and Semenov and Rubinstein (1998a), but the gelation line is identified as the microphase transition spinodal with no *a priori* assumption of the network. We may tentatively conclude that gelation is related to this microphase transition, at least in the mean-field sense. In Chapter 3 we adapt the replica approach by Schmalian, Wolynes, and co-workers (Westfahl et al., 2001; Schmalian and Wolynes, 2000) and study the phase diagram in the system of diblock copolymer melts. Even though diblock

copolymer melt is essentially different from associating polymer solutions, they both have the feature of microphase transition. In fact, it is believed that in copolymer solutions with non-selective solvents, the microphase transition is likened to the ordering transition in copolymer melt with "diluted" monomer interactions (Fredrickson and Leibler, 1989). Therefore our conclusion regarding the glass transitions in diblock copolymer melts remains qualitatively correct for the gelation in associating polymer solutions. Revealing the possibility of glass transitions in diblock copolymer melts also supports our conjecture that gelation is the glass-transition alternative to the ordering transition in associating polymer solutions.

Chapter 2

Mean field theory and the spinodal lines

In Chapter 1, we discussed the physical properties of reversible gel and the gelation of associating polymers. At the macroscopic level, reversible polymer gel is characterized by solid-like elasticity at high frequencies as well as liquid-like relaxations at long time scales. On the other hand, static inhomogeneities are frozen in the microscopic structures of the gel phase (Ikkai and Shibayama, 1999; Shibayama et al., 2000).

We noted that gelation in the solution of associating polymers is related to the microphase transition in copolymer systems. (For a discussion of experimental observations in diblock copolymer melts, see Chapter 3.) However, in contrast to the order-disorder transition, reversible gels do not have well-developed periodicity in the micro-structures. Therefore gelation to order-disorder transition resembles glass transition to crystallization; reversible gels share similar features as supercooled liquids, which exhibit non-equilibrium relaxations and breaking of ergodicity.

In this chapter we study the thermodynamics of the solution of A-B-A triblock copolymers, where the A monomers are associating. This system is the most widely studied model for reversible gelation (Tanaka and Matsuyama, 1989; Tanaka and Stockmayer, 1994; Ishida and Tanaka, 1997; Semenov et al., 1995a,b; Semenov and Rubinstein, 1998a,b). We adopt two mean-field approaches. First, density functional calculations can provide snapshots of the micro-structures of the solution under microphase transition. We hope to confirm our conjecture that across the microphase order-disorder transition, random structures with finite wave lengths are possible; such structures provide natural candidates for the gel phase[1]. Unfortunately we were not able to obtain enough numerical results to support our conjecture, therefore this part is only a summary of the theoretical model. Second, we construct the mean-field phase diagram through a quadratic expansion of the free energy (effective potential) from the Edwards Hamiltonian. The phase diagram shows both binodal coexistence

[1] Wolynes and co-workers (Singh et al., 1985; Hall and Wolynes, 1987) used density functional calculations to study the phase transition in an inhomogeneous hard-sphere liquid and found aperiodic structures as a more stable phase compared to the disordered liquid phase, which suggested aperiodic structures as natural candidates for the glass phase.

between polymer-rich and polymer-poor solution phases, and a spinodal transition associated with the microphase transition. Comparing the phase diagram to experimental observations by Tanaka et al. (1979), we may conclude that the gelation is an incomplete microphase transition which manifests the underlying spinodal instability. In Chapter 3 we further demonstrate that the competition between microscopic monomer interactions and this spinodal instability at a finite length scale comparable to the polymer size, results in a glass transition, which supports our conjecture that gelation is an alternative random microphase transition to the order-disorder transition. In addition, the glass transition lines approach the microphase spinodal in the mean field limit (as chain lengths go to infinite); this result underscores the close relationship between gelation and the mean-field microphase spinodal.

2.1 Self-consistent field theory

Since the successful predictions of the ordered structures in diblock copolymer melts (Matsen and Schick, 1994), self-consistent mean field theory has been widely used to study the phase diagrams in diblock and multi-block copolymer systems, and polymer blends. Many results are summarized in the reviews by Schmid (1998) and by Fredrickson et al. (2002). Further extensions such as the dynamic density functional theory by Fraaije et al. (1997) and Uneyama and Doi (2005) allow systematic studies of the phase separation kinetics in these systems.

Self-consistent field (SCF) theories approximate systems with many-body interactions as non-interacting particles under effective fields. The external fields are determined self-consistently from the microscopic Hamiltonian in a mean-field approximation. Since the order parameter is a density distribution or a function variable, density functional calculations enable us to sample the whole space of density distributions, in particular, to find the free energy minima with irregular microscopic structures. [See Fraaije et al. (1997), or the reviews, Schmid (1998) and Fredrickson et al. (2002), for examples of irregular morphologies.]

SCF provides a natural way to probe the microscopic structures of associating polymer solutions, which in many aspects are similar to copolymer melts. But applying it to polymer solutions needs some caution. Depending on the solvent selectivity and the concentration of polymer segments, the polymer chain can be significantly stretched or collapsed: in this scenario the random phase approximation underlying the SCF theory breaks down. However, at the gelation point, polymer chains overlap with each other, therefore the solution is in the semi-dilute or concentrated regime: the correlation length is much smaller than the chain size and concentration fluctuations only renormalize the microscopic "monomer size" and "monomer interactions"; at the level of polymer aggregates, we expect density distributions to look similar as in a mean-field theory, and qualitative features of the mean field theory should be preserved. In fact, SCF theory has been shown to be qualitatively

valid in phase diagram calculations even when significant chain stretching is observed (Almdal et al., 1990). In addition, as long as the polymer concentration is far away from the critical point, long-range density fluctuations are not important and mean field approximation is valid; an analysis of fluctuation effects in the spirit of Fredrickson and Helfand (1987) is presented in the next chapter.

2.1.1 Microscopic Hamiltonian of polymer mixtures

A continuum Gaussian chain with length N in an external field $V(\mathbf{r})$ is described by the Edwards Hamiltonian (Doi and Edwards, 1986)

$$h_0[\mathbf{R}(t)] = \frac{3k_{\mathrm{B}}T}{2Nb^2}\int_0^1 \left[\left(\frac{\partial \mathbf{R}(t)}{\partial t}\right)^2 + V(\mathbf{R}(t))\right] \mathrm{d}t \tag{2.1}$$

where $\mathbf{R}(t)$ maps the configuration of the polymer ($0 \le t \le 1$ is a parametrization of the polymer chain), and Nb^2 is mean square end-to-end distance.

To account for monomer interactions, we introduce the density operators $\hat{\phi}_\alpha(\mathbf{r})(\hat{\phi}_{\mathrm{A}}, \hat{\phi}_{\mathrm{B}}, \hat{\phi}_{\mathrm{S}})$

$$\begin{aligned} \hat{\phi}_{\mathrm{A,B}}(\mathbf{r}) &= \sum_{m=1}^{n_{\mathrm{p}}} \int_0^1 \delta\left(\mathbf{r} - \mathbf{R}_{\mathrm{m}}(t)\right) \delta_{\mathrm{A,B}}(t)\mathrm{d}t, \\ \hat{\phi}_{\mathrm{S}}(\mathbf{r}) &= \sum_{n=1}^{n_{\mathrm{s}}} \delta\left(\mathbf{r} - \mathbf{r}_n\right). \end{aligned} \tag{2.2}$$

Here $\mathbf{R}_{\mathrm{m}}$ labels the spatial conformation of the m-th polymer chain; $\mathbf{r}_{\mathrm{n}}$ is the position of the nth solvent molecule; $\delta_{\mathrm{A,B}}(t)$ is used to label the A or B block, e.g., $\delta_{\mathrm{A}}(t) = 1$ if the segment at t is A and $\delta_{\mathrm{B}}(t) = 1 - \delta_{\mathrm{A}}(t)$. The spatial positions of solvent molecules and polymer chains are completely described by $\{\mathbf{R}_{\mathrm{m}}(t), \mathbf{r}_{\mathrm{n}}\}$.

The two-body interactions are given by[2]

$$\sum_{\alpha\beta} \varepsilon_{\alpha\beta}\hat{\phi}_\alpha\hat{\phi}_\beta = \sum_{\alpha\neq\beta} \chi_{\alpha\beta}\hat{\phi}_\alpha\hat{\phi}_\beta + \frac{1}{2}(\varepsilon_{\mathrm{AA}}\hat{\phi}_{\mathrm{A}} + \varepsilon_{\mathrm{BB}}\hat{\phi}_{\mathrm{B}} + \varepsilon_{SS}\hat{\phi}_S), \tag{2.3}$$

where

$$\chi_{\alpha\beta} = \varepsilon_{\alpha\beta} - \frac{1}{2}\left(\varepsilon_{\alpha\alpha} + \varepsilon_{\beta\beta}\right).$$

The last term in (2.3) can be dropped as $\varepsilon_{\alpha\alpha}$ reflect constant shifts of the external fields, or self-energy contributions, which do not affect the interaction free energy.

Besides the two-body enthalpic interactions, we also need to account for the incompressibility or the excluded volume effect. Strict incompressibility can be inserted by adding a delta function (ρ is

[2]Here the summation is over each pair once.

the average bulk density),

$$\prod_{\mathbf{r}} \delta \left[\sum_{\alpha} \hat{\phi}_{\alpha}(\mathbf{r}) - \rho \right]$$

to the partition function. Alternatively, we can assume a virial expansion ("soft" incompressibility)

$$c_1 \hat{\phi}_{\mathrm{p}}^2 + c_2 \hat{\phi}_{\mathrm{p}}^3,$$

where $\hat{\phi}_{\mathrm{p}} = \hat{\phi}_{\mathrm{A}} + \hat{\phi}_{\mathrm{B}}$ is the total density of polymer segments, and c_1 and c_2 are positive constants.

The total Hamiltonian of the system is

$$\begin{aligned} \frac{H}{k_{\mathrm{B}}T} = \sum_{m=1}^{n_{\mathrm{p}}} \frac{3}{2Nb^2} \int_0^1 \left[\left(\frac{\partial \mathbf{R}_{\mathrm{m}}(t)}{\partial t} \right)^2 + V(\mathbf{R}_{\mathrm{m}}(t)) \right] \mathrm{d}t \\ + \frac{1}{k_{\mathrm{B}}T} \int \left[\sum_{\alpha\beta} \varepsilon_{\alpha\beta} \hat{\phi}_{\alpha}(\mathbf{r}) \hat{\phi}_{\beta}(\mathbf{r}) + c_1 \hat{\phi}_{\mathrm{p}}(\mathbf{r})^2 + c_2 \hat{\phi}_{\mathrm{p}}(\mathbf{r})^3 \right] \mathrm{d}\mathbf{r}. \end{aligned} \tag{2.4}$$

The strict incompressibility will result in an osmotic pressure term which we will discuss in the derivation of self-consistent equations.

2.1.2 Partition function and self-consistent equations

2.1.2.1 Partition function

In the canonical ensemble with n_{p} polymers and n_{s} solvent molecules, the classical partition function is ($\beta = 1/k_{\mathrm{B}}T$)

$$Z(n_{\mathrm{p}}, n_{\mathrm{s}}) = \int \mathcal{D}[\mathbf{R}_{\mathrm{m}}] \mathcal{D}[\mathbf{r}_{\mathrm{n}}] e^{-\beta H} \prod_{\mathbf{r}} \delta \left[\hat{\phi}_{\mathrm{A}}(\mathbf{r}) + \hat{\phi}_{\mathrm{B}}(\mathbf{r}) + \hat{\phi}_{\mathrm{S}}(\mathbf{r}) - \rho \right]. \tag{2.5}$$

Here $\mathcal{D}$ stands for functional integration (or path integral) over the configurations. And in a grand canonical ensemble where the chemical potential of polymer chains and solvents are given by μ_{p} and μ_{s}, we have[3]

$$\Xi(\mu_{\mathrm{p}}, \mu_{\mathrm{s}}) = \sum_{n_{\mathrm{p}}=0}^{\infty} \sum_{n_{\mathrm{s}}=0}^{\infty} \frac{\exp(\beta \mu_{\mathrm{p}} n_{\mathrm{p}} + \beta \mu_{\mathrm{s}} n_{\mathrm{s}})}{n_{\mathrm{s}}! n_{\mathrm{p}}!} Z(n_{\mathrm{p}}, n_{\mathrm{s}}). \tag{2.6}$$

To proceed, we introduce collective variables (functions) $\phi_{\alpha}(\mathbf{r})$, their conjugate fields $W_{\alpha}(\mathbf{r})$, and an osmotic pressure $\Pi(\mathbf{r})$ to get rid of the operator fields $\hat{\phi}_{\alpha}$. Insert

$$\int \mathcal{D}\phi_{\alpha} \delta(\phi_{\alpha} - \hat{\phi}_{\alpha}) \propto \int \mathcal{D}\phi_{\alpha} \int \mathcal{D}W_{\alpha} \exp\left[iW_{\alpha} \left(\phi_{\alpha} - \hat{\phi}_{\alpha} \right) \right] = \text{const.}$$

[3] In Wood and Wang (2002) the chemical potential of the polymer segments is assumed instead of that of the polymer chains.

into the partition function, we get

$$Z(n_{\rm p},n_{\rm s})=\frac{1}{\mathcal{N}}\int\mathcal{D}\phi_\alpha\int\mathcal{D}W_\alpha\int\mathcal{D}\Pi\exp\left\{-\beta H_1[\phi_\alpha]+iW_\alpha\phi_\alpha+i\int\Pi(\mathbf{r})\left[\sum_\alpha\phi_\alpha(\mathbf{r})-\rho\right]\mathrm{d}\mathbf{r}\right\}$$
$$\int\mathcal{D}\left[\mathbf{R}_{\rm m}\right]\int\mathcal{D}\left[\mathbf{r}_n\right]\exp\left\{-\beta H_0[\mathbf{R}_{\rm m},\mathbf{r}_{\rm n}]-iW_\alpha\hat{\phi}_\alpha\right\} \tag{2.7}$$
$$=\mathcal{N}^{-1}\int\mathcal{D}\phi_\alpha\exp\left[-\beta H_1(\phi_\alpha)-\beta F_0(\phi_\alpha)\right]; \tag{2.8}$$
$$\beta F_0(\phi_\alpha)=-\ln\int\mathcal{D}W_\alpha\mathcal{D}\Pi\exp\left\{iW_\alpha\phi_\alpha+i\int\Pi(\mathbf{r})\left[\sum_\alpha\phi_\alpha(\mathbf{r})-\rho\right]\mathrm{d}\mathbf{r}\right\}Z[iW_\alpha]; \tag{2.9}$$
$$Z[iW_\alpha]=\int\mathcal{D}\left[\mathbf{R}_{\rm m}\right]\int\mathcal{D}\left[\mathbf{r}_n\right]\exp\left\{-\beta H_0[\mathbf{R}_{\rm m},\mathbf{r}_{\rm n}]-iW_\alpha\hat{\phi}_\alpha\right\}=e^{-G_0(W_\alpha)} \tag{2.10}$$

where repeated indices imply integration over space, as well as summations over the same index,

$$W_\alpha\hat{\phi}_\alpha=\sum_\alpha\int W_\alpha(\mathbf{r})\hat{\phi}_\alpha(\mathbf{r})\mathrm{d}\mathbf{r}.$$

Physically ϕ_α and W_α correspond to the density distributions and their conjugate external fields, like the magnetic moment and the magnetic field, or the volume and the pressure in the liquid-gas system. $Z[iW_\alpha]$ gives the partition function of the imaginary system of non-interacting molecules under external fields iW_α (the imaginary unit i is introduced only for mathematical convenience), G_0 is the Gibbs free energy of this imaginary system, and F_0 is its Legendre transform, or the Helmholtz free energy in terms of the density fields ϕ_α.

$Z[iW_\alpha]$ can be calculated for arbitrary polymer systems using the random phase approximations. See Leibler (1980), Ohta and Kawasaki (1986), and de la Cruz (1991). $F_0[\phi_\alpha]$ can be expanded as a power series of ϕ_α, and the physical free energy $F=-\ln Z$ can in principle be calculated perturbatively. In the next section we shall derive the expansion of F up to quadratic order.

We note that in general the random phase approximation that assumes polymer chains to be ideal does not apply to polymer solutions as the polymer chains are swollen. Therefore our model applies to associating A-B-A polymers in a theta solvent for the middle block B, and a poor solvent for end block A. Alternatively we can interpret microscopic parameters as renormalized by chain swelling.

2.1.2.2 Self-consistent equations

In this section we derive the self-consistent equations from a saddle point approximation for the partition function in (2.7). Minimizing the exponential term with respect to ϕ_α, W_α, and Π we have

$$\frac{\delta}{\delta\phi_{\rm A}\left(\mathbf{r}\right)},\frac{\delta}{\delta\phi_{\rm B}\left(\mathbf{r}\right)},\frac{\delta}{\delta\phi_{\rm S}\left(\mathbf{r}\right)}=0\quad\Rightarrow$$

$$iW_{\mathrm{A}}(\mathbf{r})+i\Pi(\mathbf{r})=\beta\left[\varepsilon_{\mathrm{AB}}\phi_{\mathrm{B}}(\mathbf{r})+\varepsilon_{\mathrm{AS}}\phi_{\mathrm{S}}(\mathbf{r})+\varepsilon_{\mathrm{AA}}\phi_{\mathrm{A}}(\mathbf{r})+2c_1\phi_{\mathrm{p}}(\mathbf{r})+3c_2\phi_{\mathrm{p}}^2(\mathbf{r})\right]; \tag{2.11a}$$

$$iW_{\mathrm{B}}(\mathbf{r})+i\Pi(\mathbf{r})=\beta\left[\varepsilon_{\mathrm{AB}}\phi_{\mathrm{A}}(\mathbf{r})+\varepsilon_{\mathrm{BS}}\phi_{\mathrm{S}}(\mathbf{r})+\varepsilon_{\mathrm{BB}}\phi_{\mathrm{B}}(\mathbf{r})+2c_1\phi_{\mathrm{p}}(\mathbf{r})+3c_2\phi_{\mathrm{p}}^2(\mathbf{r})\right]; \tag{2.11b}$$

$$iW_{\mathrm{S}}(\mathbf{r})+i\Pi(\mathbf{r})=\beta\left[\varepsilon_{\mathrm{AS}}\phi_{\mathrm{A}}(\mathbf{r})+\varepsilon_{\mathrm{BS}}\phi_{\mathrm{B}}(\mathbf{r})+\varepsilon_{\mathrm{SS}}\phi_{\mathrm{S}}(\mathbf{r})\right]; \tag{2.11c}$$

$$\frac{\delta}{\delta\Pi\left(\mathbf{r}\right)}=0\Rightarrow\phi_{\mathrm{A}}\left(\mathbf{r}\right)+\phi_{\mathrm{B}}\left(\mathbf{r}\right)+\phi_{\mathrm{S}}\left(\mathbf{r}\right)=\rho; \tag{2.11d}$$

$$\frac{\delta}{\delta W_{\mathrm{S}}\left(\mathbf{r}\right)}=0\Rightarrow i\phi_{\mathrm{S}}\left(\mathbf{r}\right)=-\frac{\delta\ln Z(iW_\alpha)}{\delta W_{\mathrm{S}}(\mathbf{r})}; \tag{2.11e}$$

$$\frac{\delta}{\delta W_{\mathrm{A}}\left(\mathbf{r}\right)},\frac{\delta}{\delta W_{\mathrm{B}}\left(\mathbf{r}\right)}=0\Rightarrow i\phi_{\mathrm{A,B}}\left(\mathbf{r}\right)=-\frac{\delta\ln Z(iW_\alpha)}{\delta W_{\mathrm{A,B}}(\mathbf{r})}. \tag{2.11f}$$

To complete the set of equations we need to evaluate the partition function

$$Z(iW_\alpha)=Z_{\mathrm{p}}(iW_{\mathrm{A}},iW_{\mathrm{B}})\cdot Z_{\mathrm{s}}(iW_{\mathrm{S}}).$$

For solvent molecules we neglect their internal degrees of freedom,

$$Z_{\mathrm{s}}(iW_{\mathrm{S}})=\int\mathcal{D}[\mathbf{r}_{\mathrm{n}}]_{n=1,2,\cdots n_{\mathrm{s}}}\exp\left[-i\int W_{\mathrm{S}}\left(\mathbf{r}\right)\hat{\phi}_{\mathrm{S}}\left(\mathbf{r}\right)\mathrm{d}\mathbf{r}\right]=q_{\mathrm{s}}^{n_{\mathrm{s}}}, \tag{2.12}$$

where

$$q_{\mathrm{s}}=\int\exp\left[-iW_{\mathrm{S}}(\mathbf{r})\right]\mathrm{d}\mathbf{r}.$$

For polymer chains

$$Z_{\mathrm{p}}(iW_{\mathrm{A}},iW_{\mathrm{B}})=q_{\mathrm{p}}^{n_{\mathrm{p}}}, \tag{2.13}$$

where q_{p} is the partition function of a single polymer chain in external fields W_α. Details of the derivations of Z_{p} and its derivatives w.r.t. W_α are given in Appendix 2.A.1.

The self-consistent equations are

$$W_{\mathrm{A}}\left(\mathbf{r}\right)=\beta\left(\varepsilon_{\mathrm{AA}}\phi_{\mathrm{A}}+\varepsilon_{\mathrm{AB}}\phi_{\mathrm{B}}+\varepsilon_{\mathrm{AS}}\phi_{\mathrm{S}}+2c_1\phi_{\mathrm{p}}+3c_2\phi_{\mathrm{p}}^2\right), \tag{2.14a}$$

$$W_{\mathrm{B}}\left(\mathbf{r}\right)=\beta\left(\varepsilon_{\mathrm{BB}}\phi_{\mathrm{B}}+\varepsilon_{\mathrm{AB}}\phi_{\mathrm{A}}+\varepsilon_{\mathrm{BS}}\phi_{\mathrm{S}}+2c_1\phi_{\mathrm{p}}+3c_2\phi_{\mathrm{p}}^2\right), \tag{2.14b}$$

$$W_{\mathrm{S}}\left(\mathbf{r}\right)=\beta\left(\varepsilon_{\mathrm{SS}}\phi_{\mathrm{S}}+\varepsilon_{\mathrm{AS}}\phi_{\mathrm{A}}+\varepsilon_{\mathrm{BS}}\phi_{\mathrm{B}}\right); \tag{2.14c}$$

$$\phi_{\mathrm{S}}\left(\mathbf{r}\right)=n_s\left[\int\exp(-W_{\mathrm{S}}(\mathbf{r}))\mathrm{d}\mathbf{r}\right]^{-1}\exp\left(-W_{\mathrm{S}}\right), \tag{2.14d}$$

$$\phi_{\mathrm{A}}\left(\mathbf{r}\right)=Nn_{\mathrm{p}}\left[\int q(\mathbf{r},1)\mathrm{d}\mathbf{r}\right]^{-1}\int_0^1\theta_{\mathrm{A}}(t)q\left(\mathbf{r},t\right)q^*\left(\mathbf{r},1-t\right)\mathrm{d}t, \tag{2.14e}$$

$$\phi_{\mathrm{S}}\left(\mathbf{r}\right)=Nn_{\mathrm{p}}\left[\int q(\mathbf{r},1)\mathrm{d}\mathbf{r}\right]^{-1}\int_0^1\theta_{\mathrm{B}}\left(t\right)q\left(\mathbf{r},t\right)q^*\left(\mathbf{r},1-t\right)\mathrm{d}t; \tag{2.14f}$$

where $\phi_{\mathrm{p}}=\phi_{\mathrm{A}}+\phi_{\mathrm{B}}$, N is total the number of segments in each chain[4], and n_{p} and n_{s} are the

[4]For convenience we have assumed the monomer volume to be b^3.

number of polymer chains and solvent molecules, respectively. q and q^* are the once-integrated Green's functions to be obtained from solving the following diffusion equations

$$\left(\frac{\partial}{\partial t} - \frac{Nb^2}{6}\nabla^2_{\mathbf{r}} + N\sum_\alpha \theta_\alpha(t)\, W_\alpha(\mathbf{r})\right) q(\mathbf{r},t) = 0, \tag{2.15}$$

$$\left(\frac{\partial}{\partial t} - \frac{Nb^2}{6}\nabla^2_{\mathbf{r}} + N\sum_\alpha \theta_\alpha(1-t)\, W_\alpha(\mathbf{r})\right) q^*(\mathbf{r},t) = 0, \tag{2.16}$$

$$q(\mathbf{r},0) = q^*(\mathbf{r},0) = 1.$$

$\theta_\alpha(t)$ are labels for the different blocks. For a triblock copolymer with the structure $10A-80B-10A$, $\theta_\alpha(t)$ is defined as

$$\theta_{\mathrm{A}}(t) = \begin{cases} 1 & 0 \le t \le 0.1 \text{ or } 0.9 \le t \le 1 \\ 0 & 0.1 < t < 0.9 \end{cases} \tag{2.17}$$

$$\theta_{\mathrm{B}}(t) = 1 - \theta_{\mathrm{A}}(t).$$

The diffusion equations can be solved using the Crank-Nicholson scheme or the spectral method, as explained in Appendix 2.A.

2.2 Free energy expansion

In Section 2.1.1 we write the Hamiltonian of the polymer system and by introducing collective fields ϕ_α and W_α we get the free energy functions $G_0(W_\alpha)$ and $F_0(\phi_\alpha)$, as in Eqs. (2.10) and (2.9). Here we derive the perturbative expansion of F_0 and G_0 as a power series of the ϕ_α and W_α. From the quadratic term we find the mean field spinodal transition lines from the Helmholtz free energy F_0. The higher-order terms (many-body interactions) are necessary if we want to study the effects of fluctuations.

First we calculate $G_0(W_\alpha)$. From now on we replace iW_α by W_α. Note that

$$G_0(W_\alpha) = -k_{\mathrm{B}}T \ln Z(W_\alpha) = -\frac{1}{\beta}\ln \int \mathcal{D}\hat{\phi}_\alpha \exp\left(-\beta H_0 - W_\alpha \hat{\phi}_\alpha\right), \tag{2.18}$$

which admits an expansion into power series of W_α and connected correlation functions:

$$\begin{aligned} G_0(W_\alpha) - G_0(W_\alpha = 0) &= -\frac{1}{\beta}\sum_m \frac{1}{m!}\int \mathrm{d}\mathbf{x}_1 \mathrm{d}\mathbf{x}_2 \cdots \mathrm{d}\mathbf{x}_{\mathrm{m}} \\ &\quad \sum_\alpha G^{(\mathrm{m})}_{\alpha_1\alpha_2\cdots\alpha_{\mathrm{m}}}(\mathbf{x}_1,\mathbf{x}_2,\cdots,\mathbf{x}_{\mathrm{m}}) W_{\alpha_1}(\mathbf{x}_1) W_{\alpha_2}(\mathbf{x}_2)\cdots W_{\alpha_{\mathrm{m}}}(\mathbf{x}_{\mathrm{m}}) \\ &= -\frac{1}{\beta}\sum_{\mathrm{m}} \frac{1}{\mathrm{m}!} G_{\alpha_1\alpha_2\cdots\alpha_{\mathrm{m}}} W_{\alpha_1} W_{\alpha_2}\cdots W_{\alpha_{\mathrm{m}}}. \end{aligned} \tag{2.19}$$

From now on we will adopt the summation convention with integration over space.

The connected correlation functions $G^{(\mathrm{m})}$

$$G_c^{(\mathrm{m})}(\mathbf{x}_1,\mathbf{x}_2,\cdots,\mathbf{x}_\mathrm{n}) = \left.\frac{(-1)^\mathrm{m}\beta\delta^\mathrm{m}G_0(W_\alpha)}{\delta W(\mathbf{x}_1)\delta W(\mathbf{x}_2)\cdots\delta W(\mathbf{x}_\mathrm{n})}\right|_{W_\alpha=0} = \left\langle\hat{\phi}(\mathbf{x}_1)\hat{\phi}(\mathbf{x}_2)\cdots\hat{\phi}(\mathbf{x}_\mathrm{m})\right\rangle_c \tag{2.20}$$

can be calculated using the propagator of Gaussian chains; details are given in Appendix 2.B.1.

$F_0(\phi_\alpha)$ is the Legendre transform of $G_0(W_\alpha)$, which satisfies

$$F_0(\phi_\alpha) - G_0(W_\alpha) = -\frac{1}{\beta}\phi_\alpha W_\alpha = -\frac{1}{\beta}\int \phi_\alpha(\mathbf{x})W_\alpha(\mathbf{x})\mathrm{d}\mathbf{x}, \tag{2.21}$$

where ϕ_α are the averages of operators $\hat{\phi}_\alpha$ under external fields W_α, defined as

$$\phi_\alpha = \frac{\beta\delta G_0(W_\alpha)}{\delta W_\alpha} = \left\langle\hat{\phi}_\alpha\right\rangle_{W_\alpha}, \tag{2.22}$$

and we have

$$W_\alpha = -\frac{\beta\delta F_0(\phi_\alpha)}{\delta\phi_\alpha}. \tag{2.23}$$

It is known that in the expansion of $F_0(\phi_\alpha)$,

$$F_0(\varphi_\alpha+\bar{\phi}_\alpha) - F_0(\bar{\phi}_\alpha) = \frac{1}{\beta}\sum_{\mathrm{m}>1}\Gamma^{(\mathrm{m})}_{\alpha_1\alpha_2\cdots\alpha_\mathrm{m}}\varphi_{\alpha_1}\varphi_{\alpha_2}\cdots\varphi_{\alpha_\mathrm{m}}, \tag{2.24}$$

the vertex functions are related to the *amputated* connected correlation functions (Zinn-Justin, 2002):

$$\Gamma^{(2)}_{\alpha\beta}(\mathbf{x}_1,\mathbf{x}_2) = S_{\alpha\beta}(\mathbf{x}_1,\mathbf{x}_2) = \left[G_c^{(2)}(\mathbf{x}_1,\mathbf{x}_2)\right]^{-1}_{\alpha\beta}; \tag{2.25a}$$

$$\Gamma^{(3)}_{\alpha\beta\gamma}(\mathbf{x}_1,\mathbf{x}_2,\mathbf{x}_3) = -G^{(3)}_{\mathrm{amp}}(\mathbf{x}_1,\mathbf{x}_2,\mathbf{x}_3); \tag{2.25b}$$

$$\Gamma^{(4)}_{\alpha\beta\gamma\delta}(\mathbf{x}_1,\mathbf{x}_2,\mathbf{x}_3,\mathbf{x}_4) = -G^{(4)}_{\mathrm{amp}}(\mathbf{x}_1,\mathbf{x}_2,\mathbf{x}_3,\mathbf{x}_4) + \int G^{(3)}_{\mathrm{amp}}(\mathbf{x}_1,\mathbf{x}_2,\mathbf{y})G_c^{(2)}(\mathbf{y},\mathbf{z})G^{(3)}_{\mathrm{amp}}(\mathbf{z},\mathbf{x}_3,\mathbf{x}_4)\mathrm{d}\mathbf{y}\mathrm{d}\mathbf{z} + 2 \text{ permutations}; \tag{2.25c}$$

where

$$G^{(n)}_{\mathrm{amp}}(\mathbf{x}_1,\mathbf{x}_2,\cdots,\mathbf{x}_\mathrm{n}) = \int \mathrm{d}\mathbf{y}_1\mathrm{d}\mathbf{y}_2\cdots\mathrm{d}\mathbf{y}_n G^{(\mathrm{n})}_{\alpha'_1\alpha'_2\cdots\alpha'_\mathrm{n}}(\mathbf{y}_1,\mathbf{y}_2,\cdots\mathbf{y}_\mathrm{n}) S_{\alpha_1\alpha'_1}(\mathbf{x}_1,\mathbf{y}_1)S_{\alpha_2\alpha'_2}(\mathbf{x}_2,\mathbf{y}_2)\cdots S_{\alpha_\mathrm{n}\alpha'_\mathrm{n}}(\mathbf{x}_\mathrm{n},\mathbf{y}_\mathrm{n}). \tag{2.26}$$

The interacting free energy of the interacting system is

$$F(\phi) = H_1(\phi) + F_0(\phi). \tag{2.27}$$

At high temperatures ($\beta \ll 1$), the system is uniform and the free energy is minimized at $\phi = \bar{\phi}$. As the temperature decreases, the enthalpic interactions dominate over the entropic mixing term, and the system tends to phase separate. This is signaled by the instability at the quadratic expansion of the free energy with respect to perturbations of the order parameter $\varphi = \phi - \bar{\phi}$, i.e., the Hessian matrix attains negative eigen values. This defines the spinodal limit.

Up to quadratic order F is given by (See Appendix 2.B.2 for the derivation)

$$F^{(2)} = V \sum_{\mathbf{q}} \left[S^{-1}(q) - f(\beta\varepsilon) \right] \varphi_\alpha(\mathbf{q}) \varphi_\alpha(-\mathbf{q}) \tag{2.28}$$

where $S^{-1}(q)$ is the inverse structure factor, $\beta\varepsilon$ are the interaction parameters, $\varphi_\alpha(\mathbf{q})$ is the Fourier transform of $\varphi_\alpha(\mathbf{x})$, and φ_α^* is the complex conjugate of φ_α. $S^{-1}(q)$ is dependent on the chain composition and the bulk average volume fraction of polymers. To find the spinodal limit, we minimize $S^{-1}(q)$ and find the value $\beta\varepsilon$ such that $f(\beta\epsilon) \geq \min_q S^{-1}(q)$.

The wave vector q_m that minimizes $S^{-1}(q)$ gives the inverse of the correlation length of the phase separated structure. In the microphase transition, $q_\mathrm{m} \sim N^{-1/2}$, thus the correlation length is comparable to the chain length. In the macrophase phase separation, $q_\mathrm{m} = 0$. In the solution of associating triblock copolymers, both spinodals are present.

2.3 Results and discussion

First we look at the spinodal lines in the solution of associating triblock copolymers. For simplicity we assume that the only associating interaction is $\varepsilon_{\mathrm{AA}} = e_\mathrm{A} < 0$, the solvent molecules and B segments are assumed to be non-interacting.

In Figure 2.1 on page 20 we show the spinodal lines in the solution of associating polymers with composition 3A-4B-3A with different chain lengths: $N = 20, 40, 100$. The spinodal for the macrophase separation is shown in red, with a critical point; the spinodal for microphase transition is shown in blue. The phase diagram is very similar to the experimental results obtained for gelatin solution by Tanaka et al. (1979) and theoretical calculations by Tanaka (1989) and by Semenov and Rubinstein (1998a).

From Appendix 2.B.2 we find that the critical point in the binodal coexistence is given by

$$\frac{e_\mathrm{A}^*}{k_\mathrm{B}T} = \frac{1}{4f_\mathrm{A}^2(1-\phi_\mathrm{p})} + \frac{1}{4f_\mathrm{A}^2\phi_\mathrm{p}N},$$

which is of order $O(1)$, and the microphase spinodal satisfies $e_\mathrm{A} \sim N^{-1}$. Therefore increasing the chain length results in a large shift of the microphase spinodal, but only affects the macrophase spinodal weakly. The scaling $e \sim N^{-1}$ is also obtained by Tanaka et al. (1979) for the gelation line,

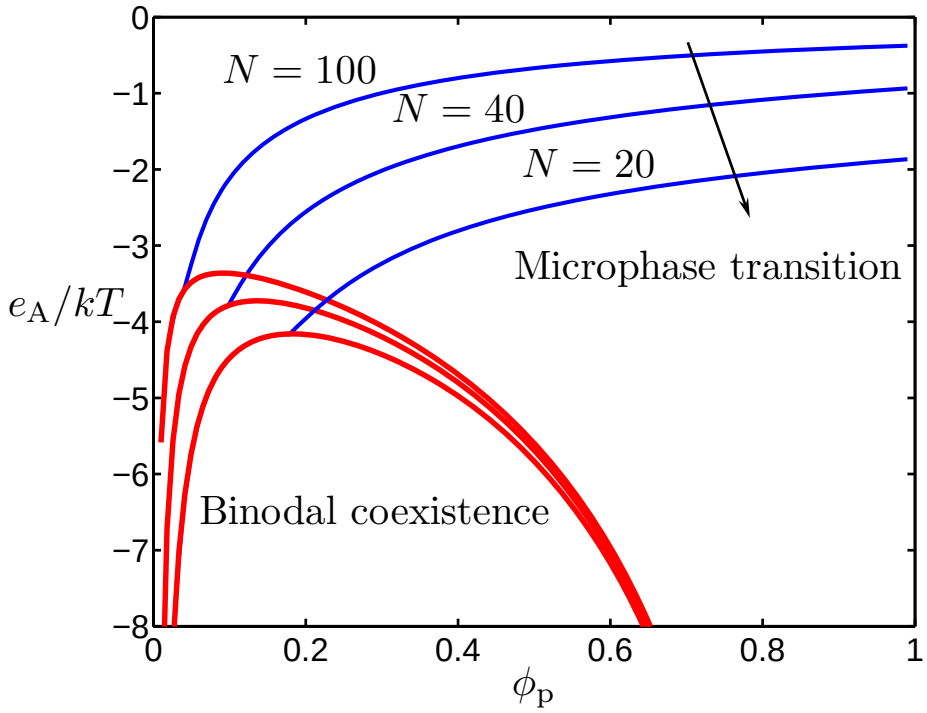

Figure 2.1: Spinodal lines for the microphase transition and the macrophase separation in solutions of associating polymers. The fraction of associating A block is 0.3 on each end of the triblock copolymer. Results are shown for associating polymers with three kuhn lengths ($N = 20$, $N = 40$ and $N = 100$). The red lines are the spinodal for the macrophase separation, with a critical point; the blue lines are the microphase spinodal with instability at wave vector $q_m > 0$.

while our result has no *a priori* assumption of the appearance of the gel phase. This coincidence suggests that gelation has the same thermodynamic signature as the microphase transition.

We notice that as chain length increases, the intersection point between the two spinodals is shifted to the left, suggesting that the solution is unstable with respect to the microphase transition for lower polymer concentrations. Therefore the solution of associating polymers with longer chains should form a gel at lower concentrations. This is expected both from the microscopic mechanism of self-assembly and from the thermodynamics of polymer solutions.

We also point out that the microphase spinodal does not terminate at the intersection, but continues below the binodal coexistence. Mathematically this implies a discontinuous jump in the quadratic coefficient a in the structure factor

$$S^{-1}(q) = q^4 - aq^2 + b.$$

This is different from the mean field Lifshitz point where a continuously decreases to zero. This might be an artifact of the mean field approximation, and fluctuation effects should drive the confluent

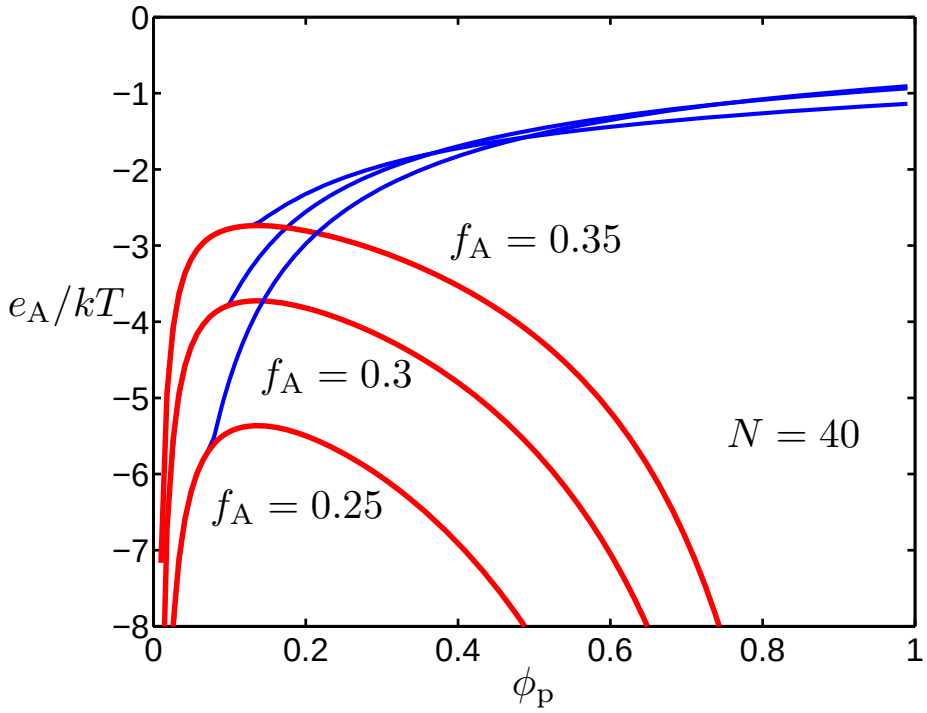

Figure 2.2: Spinodal lines in the solution of associating polymers with chain length $N = 40$ and different end-block fractions, $f_{\rm A} = 0.25, 0.3, 0.35$. The meaning of the curves are the same as in Fig. 2.1.

point to a Lifshitz tri-critical fixed point.

In Fig. 2.2 we plot the spinodal lines for associating polymers with fixed length ($N = 40$) at three different end-block fractions: $f_{\rm A} = 0.25, 0.3, 0.35$. Compared to Fig. 2.1 we see that increasing the end-block fraction has a big effect on the macrophase spinodal, but does not affect the microphase spinodal very much. This can be understood from the driving force for the phase transition in each case. In the macrophase separation, the driving force is mainly the enthalpic interactions, therefore increasing the fraction of A blocks can enhance the tendency for phase separation into A-rich and A-poor phases. On the other hand, for the microphase transition, the A blocks serve as connection while the B blocks are the linkers. Because of volume incompressibility, the local density of A segments is about the same for all chain compositions, therefore as long as the monomer interaction between A segments is strong enough, they will form aggregated structures dispersed in the B matrix. The driving force for this microphase transition is not only enthalpic, but also entropic, due to the presence of B linker. In fact, as shown in Figure 2.3 on page 22, if we further increase the end fraction to "unrealistic" high values $f_{\rm A} = 0.45$, we see that the microphase spinodal is shifted to even larger $e_{\rm A}$. In particular we observe that increasing the polymer concentration can dissolve the gel instead of triggering gelation as for lower end-block fractions. This corresponds to the "inversion" of the

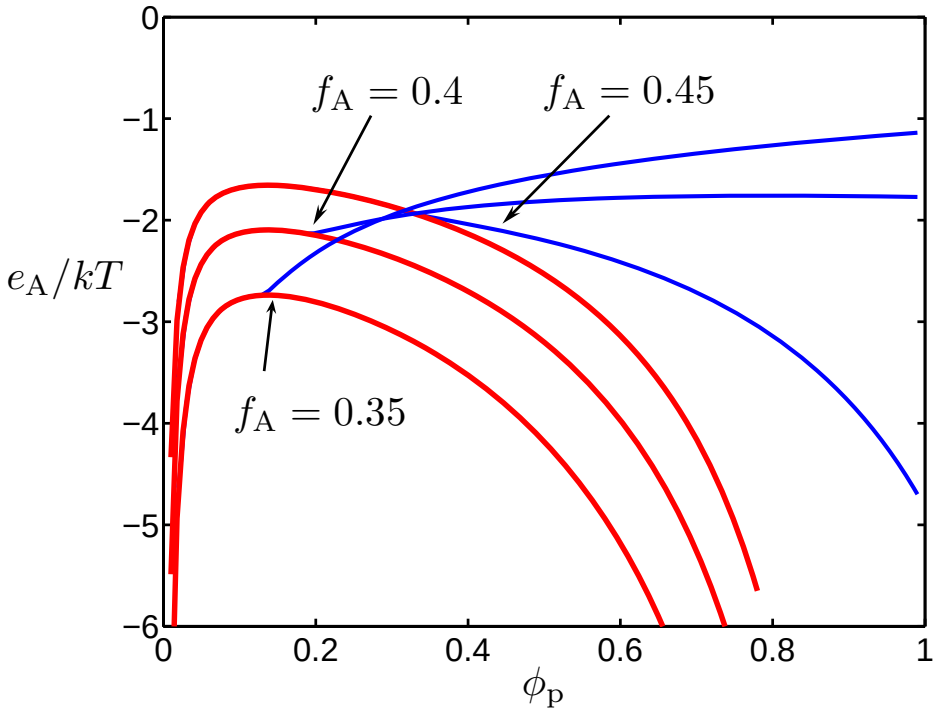

Figure 2.3: Spinodal lines in the solution of associating polymers with large end blocks. The chain length is $N = 40$ and results are shown for end fractions $f_A = 0.35, 0.4, 0.45$.

microphase structures from the A dispersed phase to the B dispersed phase, and clearly reflects the self-assembly nature of the transition.

We also note that for $f_A = 0.25$ the microphase spinodal intersects the binodal spinodal to the left of the critical point, implying the possibility of two co-existing microphases with different polymer concentrations. This is also found by Semenov and Rubinstein (1998a) for the gelation of associating polymers. Our results suggest that such a coexistence is due to the competition between short-range monomer interactions and the self-assembly of copolymers at the mesoscopic polymer length scale.

Figure 2.4 on page 23 shows the critical wave vector q_m associated with the microphase spinodal. The correlation length $\xi \sim q_m^{-1}$. From the two blue curves we see that for long chains or at high concentrations, the polymer chains are less swollen, as is expected from less screening. From the three curves with different compositions at $N = 40$ we see that the structure is more swollen for larger end-block fractions when the polymer concentration is high, but at low densities the trend is reversed. This probably reflects the entropic effect in the self-assembly, and can be easily tested in experimental measurements.

Finally in Figure 2.5 on page 24 we plot the microphase spinodal curves in a solution with virial

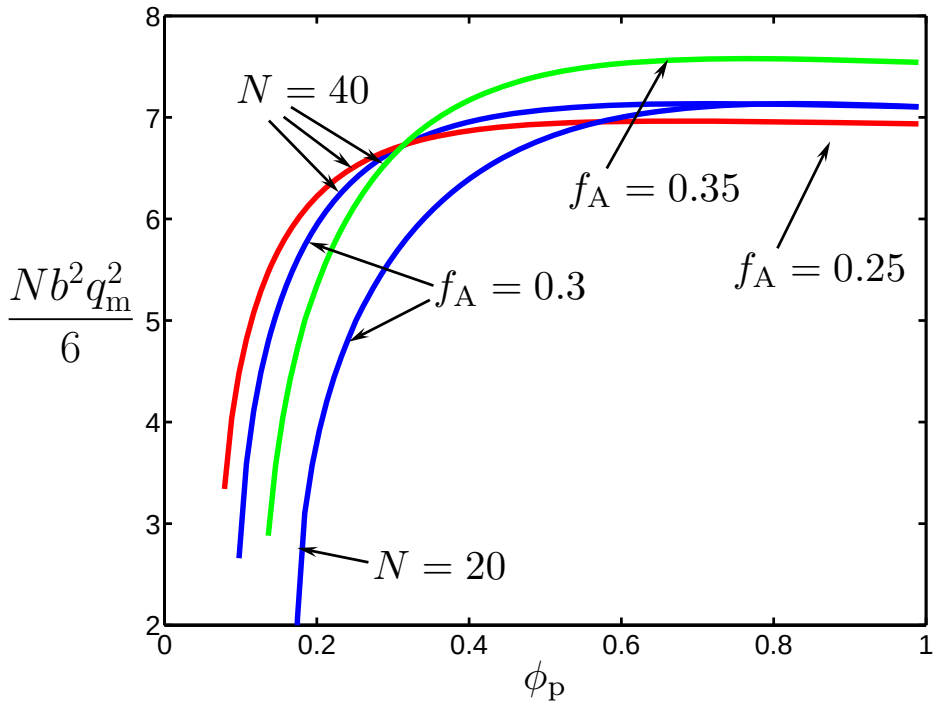

Figure 2.4: Critical wave vector in the solution of associating polymers. We present the results for three end block fractions, $f_{\rm A} = 0.25, 0.3, 0.35$ with chain length $N = 40$, and one curve $f_{\rm A} = 0.3$ for $N = 20$.

type expansion instead of volume incompressibility. The macrophase spinodals are not shown as they are similar to the previous cases. These results show similar features as for the model with strict volume incompressibility.

2.4 Conclusion

To summarize, from analysis of a simple system for reversible gelation—triblock associating polymer solutions—we find that such systems exhibit microphase transitions which share many similar features with the reversible gelation. We find that this transition is rather insensitive to the chain composition as compared to the chain length or associating energy. This reflects the nature of this transition, which is due to the interplay between short-range monomer aggregation and long-range polymer extension.

Although our work is carried out for triblock copolymer solutions, qualitative features should hold in other associating polymer systems, such as multi-block or even diblock copolymers: There should always be a microphase spinodal due to the segregation between A and B monomers. And these systems could exhibit gelation under certain conditions.

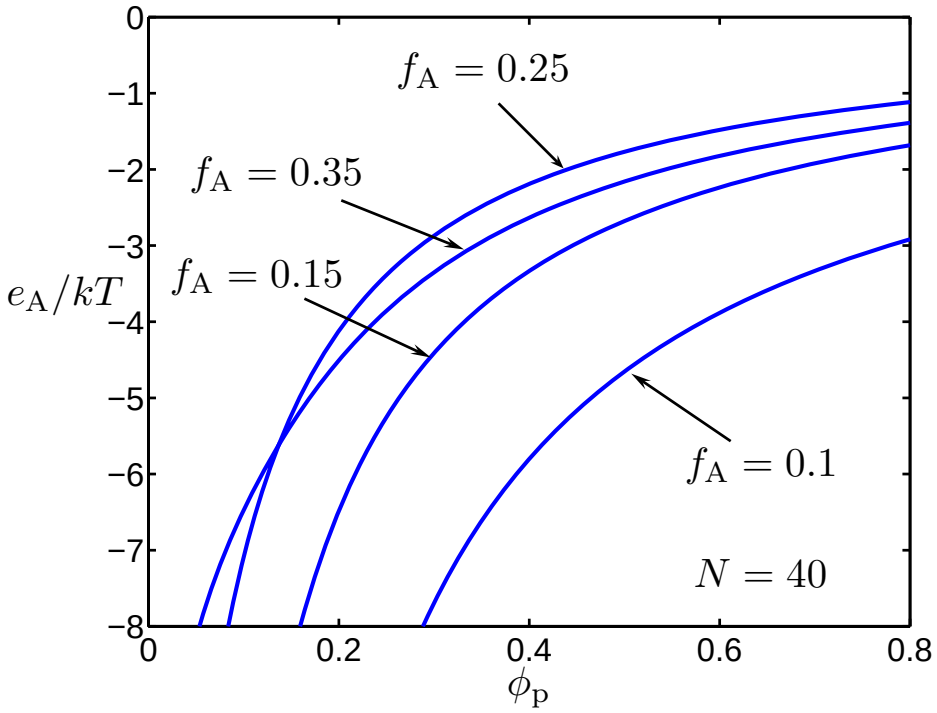

Figure 2.5: Microphase spinodal calculated using the virial-type expansion instead of strict volume incompressibility. The chain length is $N = 40$ with $c_1 = 1k_BT$ and $c_2 = 6k_BT$. Results are shown for $f_A = 0.1, 0.15, 0.25, 0.35$.

Our calculations suggest that one can start from the basic microscopic model to study the thermodynamics of gelation, without *a priori* assumptions of the gel phase. But the nature of reversible gelation, like the glass transition, is different from conventional phase transitions, and calls upon new theoretical tools. In the next chapter, which is adapted from our published paper, we analyze the possibility of glass transitions associated with this microscopic spinodal.

Appendix 2.A Self-consistent field calculation

2.A.1 Calculations of the partition functions of non-interacting polymers in external fields

In this subsection we solve the partition function $Z(iW_\alpha)$ as defined in Eq. (2.10). First we replace iW_α by W_α, it will turn out that thus defined W_α are real. From Eq. (2.12) we have

$$Z_s(iW_S) = \int \mathcal{D}[\mathbf{r}_n]_{n=1,2,\cdots n_s} \exp\left[-\int W_S(\mathbf{r})\,\hat{\phi}_S(\mathbf{r})\,d\mathbf{r}\right]$$

$$= \int \mathcal{D}[\mathbf{r}_{\mathrm{n}}] \exp\left[- \int W_{\mathrm{S}}(\mathbf{r}) \sum_{n=1}^{n_{\mathrm{s}}} \delta(\mathbf{r} - \mathbf{r}_{\mathrm{n}}) \, \mathrm{d}\mathbf{r} \right] = \left[\int e^{-W_{\mathrm{S}}(\mathbf{r})} \mathrm{d}\mathbf{r} \right]^{n_{\mathrm{s}}} = q_{\mathrm{s}}^{n_{\mathrm{s}}}. \tag{2.29}$$

We still need to calculate the single chain partition function q_{p}.

Using the Green's function for Gaussian chains (Doi and Edwards, 1986) we can express the partition function q_{p} as

$$q_{\mathrm{p}} = \int G(\mathbf{r}, \mathbf{r}'; N),$$

where $G(\mathbf{r}, \mathbf{r}'; N)$ satisfies

$$\left[\frac{\partial}{\partial N} - \frac{b^2}{6} \nabla_{\mathbf{r}}^2 + W(\mathbf{r}) \right] G(\mathbf{r}, \mathbf{r}'; N) = \delta(\mathbf{r} - \mathbf{r}'). \tag{2.30}$$

To calculate q_{p}, we only need $q(\mathbf{r}, l)$, the once-integrated Green's function (propagator) (see Wood and Wang, 2002; Tzeremes et al., 2002; Drolet and Fredrickson, 1999; Fredrickson et al., 2002)

$$q(\mathbf{r}, l) = \int G(\mathbf{r}, \mathbf{r}'; l) \mathrm{d}\mathbf{r}',$$

which satisfies the same diffusion equation as $G(\mathbf{r}, \mathbf{r}')$

$$\left[\frac{\partial}{\partial l} - \frac{b^2}{6} \nabla_{\mathbf{r}}^2 + \sum_{\alpha} \delta_{\alpha}(l) W_{\alpha}(\mathbf{r}) \right] q(\mathbf{r}, l) = 0, \tag{2.30$'$}$$

but with the following initial condition:

$$q(\mathbf{r}, 0) = 1.$$

$q^*(\mathbf{r}, l)$, the conjugate of q, satisfies

$$\left[\frac{\partial}{\partial l} - \frac{b^2}{6} \nabla_{\mathbf{r}}^2 + \sum_{\alpha} \delta_{\alpha}(N - l) W_{\alpha}(\mathbf{r}) \right] q^*(\mathbf{r}, l) = 0 \tag{2.30$''$}$$

with the same initial condition. We can rescale l by $t = l/N$, $0 \leq t \leq 1$, then the equations become

$$\left[\frac{\partial}{\partial t} - \frac{Nb^2}{6} \nabla_{\mathbf{r}}^2 + N \sum_{\alpha} \delta_{\alpha}(t) W_{\alpha}(\mathbf{r}) \right] q(\mathbf{r}, t) = 0$$

$\delta_{\mathrm{A,B}}(t)$ are defined the same as in Eq. (2.17). And

$$q_{\mathrm{p}} = \int q(\mathbf{r}, 1) \, \mathrm{d}\mathbf{r} = \int q^*(\mathbf{r}, 1) \mathrm{d}\mathbf{r}. \tag{2.31}$$

2.A.2 Grand canonical ensemble calculation

We have obtained the grand canonical partition function in Section 2.1.2 as

$$\begin{aligned}\Xi\left(\mu_{\mathrm{p}},\mu_{\mathrm{s}}\right) &= \sum_{n_{\mathrm{p}}=0}^{\infty}\sum_{n_{\mathrm{s}}=0}^{\infty}\frac{\exp\left(\beta\mu_{\mathrm{p}}n_{\mathrm{p}}+\beta\mu_{\mathrm{s}}n_{\mathrm{s}}\right)}{n_s!n_p!}Z(n_{\mathrm{p}},n_{\mathrm{s}}),\\ &= \frac{1}{\mathcal{N}}\int\mathcal{D}\phi_\alpha\int\mathcal{D}W_\alpha\int\mathcal{D}\Pi\\ &\qquad \exp\left\{-\beta H_1[\phi_\alpha]+W_\alpha\phi_\alpha+\Pi\left(\sum_\alpha\phi_\alpha-\rho\right)+e^{\mu_{\mathrm{s}}}q_{\mathrm{s}}+e^{\mu_{\mathrm{p}}}q_{\mathrm{p}}\right\}.\end{aligned} \tag{2.32}$$

where μ_{p} and μ_{s} are the chemical potential of the polymers and the solvents.

In the grand canonical ensemble, Eq. (2.14) is replaced by

$$\frac{\delta}{\delta W_{\mathrm{S}}\left(\mathbf{r}\right)}=0 \quad \Rightarrow \phi_{\mathrm{S}}=e^{\beta\mu_{\mathrm{s}}-W_{\mathrm{S}}}; \tag{2.33a}$$

$$\frac{\delta}{\delta W_{\mathrm{A,B}}\left(\mathbf{r}\right)}=0 \quad \Rightarrow \phi_{\mathrm{A,B}}\left(\mathbf{r}\right)=\exp\left(\beta\mu_{\mathrm{p}}\right)\int_0^1\theta_{\mathrm{A,B}}(t)q\left(\mathbf{r},t\right)q^*\left(\mathbf{r},1-t\right)\mathrm{d}t; \tag{2.33b}$$

$$\frac{\delta}{\delta\Pi(\mathbf{r})}=0 \quad \Rightarrow \sum_\alpha\phi_\alpha(\mathbf{r})=\rho; \tag{2.33c}$$

$$\frac{\delta}{\delta\phi_\alpha(\mathbf{r})}=0 \quad \Rightarrow W_\alpha(\mathbf{r})=\frac{\beta\partial H_1(\phi_\alpha)}{\partial\phi_\alpha}. \tag{2.33d}$$

If we use the virial expansion instead of strict incompressibility we have the following SCF equations ($\varepsilon_{\alpha\beta}$ and c_1, c_2 are given in unit of $k_{\mathrm{B}}T$):

$$W_{\mathrm{A}}\left(\mathbf{r}\right)=\varepsilon_{\mathrm{AA}}\phi_{\mathrm{A}}(\mathbf{r})+\varepsilon_{\mathrm{AB}}\phi_{\mathrm{B}}\left(\mathbf{r}\right)+\varepsilon_{\mathrm{AS}}\phi_{\mathrm{S}}\left(\mathbf{r}\right)+2c_1\phi_{\mathrm{p}}(\mathbf{r})+3c_2\phi_{\mathrm{p}}^2(\mathbf{r}), \tag{2.34a}$$

$$W_{\mathrm{B}}\left(\mathbf{r}\right)=\varepsilon_{\mathrm{BB}}\phi_{\mathrm{B}}(\mathbf{r})+\varepsilon_{\mathrm{AB}}\phi_{\mathrm{A}}\left(\mathbf{r}\right)+\varepsilon_{\mathrm{BS}}\phi_{\mathrm{S}}\left(\mathbf{r}\right)+2c_1\phi_{\mathrm{p}}(\mathbf{r})+3c_2\phi_{\mathrm{p}}^2(\mathbf{r}), \tag{2.34b}$$

$$W_{\mathrm{S}}\left(\mathbf{r}\right)=\varepsilon_{\mathrm{SS}}\phi_{\mathrm{S}}(\mathbf{r})+\varepsilon_{\mathrm{AS}}\phi_{\mathrm{A}}\left(\mathbf{r}\right)+\varepsilon_{\mathrm{BS}}\phi_{\mathrm{B}}(\mathbf{r}); \tag{2.34c}$$

$$\phi_{\mathrm{A}}=\exp\left(\beta\mu_{\mathrm{p}}\right)\int_0^1\theta_{\mathrm{A}}(t)q\left(\mathbf{r},t\right)q^*\left(\mathbf{r},1-t\right)\mathrm{d}t, \tag{2.34d}$$

$$\phi_{\mathrm{B}}=\exp\left(\beta\mu_{\mathrm{p}}\right)\int_0^1\theta_{\mathrm{B}}\left(t\right)q\left(\mathbf{r},t\right)q^*\left(\mathbf{r},1-t\right)\mathrm{d}t, \tag{2.34e}$$

$$\phi_{\mathrm{S}}=\exp\left(\beta\mu_{\mathrm{s}}-W_{\mathrm{S}}\right). \tag{2.34f}$$

Finally the grand potential is

$$G=-k_{\mathrm{B}}T\ln\Xi=H_1(\phi_\alpha)-e^{\beta\mu_{\mathrm{p}}}q_{\mathrm{p}}-e^{\beta\mu_{\mathrm{s}}}q_{\mathrm{s}}-W_\alpha\phi_\alpha. \tag{2.35}$$

In the grand canonical calculation we want to fix the concentration of the polymers in the reservoir instead of by their total density, therefore only one chemical potential is independent. We can take $\mu_{\mathrm{s}}=0$ for convenience and choose μ_{p} as in a uniform polymer solution with given volume fraction

of polymer segments, which can be calculated from Eqs. (2.35) and (2.34).

The canonical free energy of the system is

$$F(\phi_\alpha) = H_1(\phi_\alpha) - k_{\mathrm{B}}T\left(W_\alpha\phi_\alpha + n_{\mathrm{p}}\ln q_{\mathrm{p}} + n_{\mathrm{s}}\ln q_{\mathrm{s}}\right). \tag{2.36}$$

2.A.3 Numerical solution of the SCF equations

To implement numerical solutions of the self-consistent equations (2.14) or (2.34), we first note that the inputting parameters are $\varepsilon_{\alpha\beta}$, c_1 and c_2, N, f_α, and μ_{p} in the grand canonical ensemble, and $\varepsilon_{\alpha\beta}$, c_1 and c_2, N, f_α, and the average concentrations $\bar{\phi}_{\mathrm{p}}$ and $\bar{\phi}_{\mathrm{s}}$ in the canonical ensemble. f_α are the fractions of different blocks in each chain.

We adopt the following iteration scheme (Drolet and Fredrickson, 2001; Tzeremes et al., 2002):

1. The initial density distributions $\phi_\alpha^{(0)}(\mathbf{r})$ are generated by adding a tiny fluctuation to the uniform distribution, the conjugate fields $W_\alpha^{(0)}(\mathbf{r})$ are calculated from the first 3 equations of Eqs. (2.14) or (2.34);

2. For a set of $W_\alpha^{(\mathrm{i})}(\mathbf{r})$, $\phi_\alpha^{(\mathrm{i}')}(\mathbf{r})$ are obtained using the remaining 3 equations, and $W_\alpha^{(\mathrm{i}')}(\mathbf{r})$ are calculated from $\phi_\alpha^{(\mathrm{i}')}(\mathbf{r})$ using the first 3 equations;

3. $W_\alpha^{(\mathrm{i})}$ are updated by:

$$W_\alpha^{(\mathrm{i}+1)} = W_\alpha^{(\mathrm{i})} + y_1\Delta W_\alpha^{(\mathrm{i})} + y_2\Delta\phi_\alpha^{(\mathrm{i})}, \tag{2.37}$$

$$\Delta W_\alpha^{(\mathrm{i})} = W_\alpha^{(\mathrm{i}')} - W_\alpha^{(\mathrm{i})}, \tag{2.38}$$

$$\Delta\phi_\alpha^{(\mathrm{i})} = \phi_\alpha^{(\mathrm{i}')} - \phi_\alpha^{(\mathrm{i})}. \tag{2.39}$$

4. $\phi_\alpha^{(\mathrm{i}+1)}$ are updated for $W_\alpha^{(\mathrm{i}+1)}$ from the last 3 equations and step (ii) and step (iii) are repeated.

To calculate the Green's functions (the N factor has been adsorbed into $W(\mathbf{r})$):

$$q(\mathbf{r},0) = 1, \left(\frac{\partial}{\partial t} - \frac{Nb^2}{6}\nabla_{\mathbf{r}}^2 + W_\alpha(\mathbf{r})\right) q(\mathbf{r},t) = 0, \tag{2.40}$$

first we rescale $\mathbf{r}$ by $R_{\mathrm{g}} = \left(Nb^2/6\right)^{1/2}$, and the solution can be formally written as

$$q(\mathbf{r}, t+\mathrm{d}t) = \exp\left[\left(\nabla^2 - W(\mathbf{r})\right)\mathrm{d}t\right] q(\mathbf{r},t). \tag{2.41}$$

From the Baker-Hausdorff operator identity (Tzeremes et al., 2002),

$$\exp(\hat{A})\exp(\hat{B}) = \exp\left\{\hat{A} + \hat{B} - \frac{1}{2}[\hat{A},\hat{B}] + \cdots\right\},$$

Eq. (2.41) can be written as

$$q\left(\mathbf{r}, t+\mathrm{d}t\right)=\exp\left(-\frac{\mathrm{d}t}{2}W\left(\mathbf{r}\right)\right)\exp\left(\mathrm{d}t\nabla^{2}\right)\exp\left(-\frac{\mathrm{d}t}{2}W\left(\mathbf{r}\right)\right)q\left(\mathbf{r}, t\right), \tag{2.42}$$

which is accurate to $\mathrm{d}t^2$. Eq. (2.42) can be numerically implemented by Fourier transform,

$$q\left(\mathbf{r}, t+\mathrm{d}t\right)=\exp\left(-\frac{\mathrm{d}t}{2}W\left(\mathbf{r}\right)\right)\mathcal{F}^{-1}\left\{\exp\left(-\mathrm{d}t\mathbf{k}^{2}\right)\mathcal{F}\left[\exp\left(-\frac{\mathrm{d}t}{2}W\left(\mathbf{r}\right)\right)q\left(\mathbf{r}, t\right)\right]\right\}; \tag{2.43}$$

$\mathcal{F}$ denotes the Fourier transform, which can be implemented using fast Fourier transform. The fast Fourier transform (FFT) automatically ensures the periodic boundary conditions.

In the simulation we need to specify the size and discretization of the system. If we choose the discretization lattice to be 64×64 and the size of the system to be $6.4R_g\times6.4R_g$, then we can resolve the density profile to $\sim 0.1R_g$ (R_g is the radius of gyration of the polymer). In our simulations we use square lattices and resolve the density profile to $0.1\sim0.2R_g$.

2.A.4 Analysis of the iteration scheme

Self-consistent equations for polymer systems are highly non-linear and it is notoriously difficult to obtain convergent solutions. Here we briefly analyze possible steepest descent schemes to solve the self-consistent equations.

In Section 2.1 and Section 2.2 we have obtained the mean field free energy potential $F[\phi_\alpha]$:

$$F=-\ln\int\mathcal{D}\phi_\alpha\mathcal{D}W_\alpha\exp\left(-\beta H_1[\phi_\alpha]+W_\alpha\phi_\alpha-G[W_\alpha]\right). \tag{2.44}$$

Taking the saddle point we have

$$\frac{\delta F}{\delta W_\alpha}=0,\frac{\delta F}{\delta\phi_\alpha}=0.$$

From

$$\frac{\delta F}{\delta W_\alpha}=0$$

we obtain

$$\phi_\alpha=\frac{\delta G[W_\alpha]}{\delta W_\alpha}=\Phi(W_\alpha). \tag{2.45}$$

Therefore in terms of ϕ_α, the saddle point free energy is

$$F^*[\phi_\alpha]=H_1[\phi_\alpha]-\Phi^{-1}[\phi_\alpha]\phi_\alpha+G[\Phi^{-1}(\phi_\alpha)]. \tag{2.46}$$

The gradient of F^* against ϕ_α is

$$\frac{\delta F^*[\phi_\alpha]}{\delta \phi_\alpha} = \frac{\partial H_1[\phi_\alpha]}{\partial \phi_\alpha} - \Phi^{-1}(\phi_\alpha). \tag{2.47}$$

Φ^{-1} or Φ can be expanded as an asymptotic series of ϕ_α or W_α as done in the free energy expansion in Section 2.2, but we do not have close-form expressions. Therefore it is inconvenient to implement steepest descent or Langevin type dynamics in the ϕ field.

Alternatively we can first take

$$\frac{\delta F}{\delta \phi_\alpha} = 0,$$

and we have

$$W_\alpha = \frac{\partial H_1[\phi_\alpha]}{\partial \phi_\alpha} = \mathcal{W}(\phi_\alpha). \tag{2.48}$$

Then

$$F^*[W_\alpha] = H_1[\mathcal{W}^{-1}(W_\alpha)] - \mathcal{W}^{-1}(W_\alpha)W_\alpha + G[W_\alpha], \tag{2.49}$$

and the free energy gradient is

$$\frac{\delta F^*[W_\alpha]}{\delta W_\alpha} = \Phi(W_\alpha) - \mathcal{W}^{-1}(W_\alpha). \tag{2.50}$$

In most cases we do have a close form expression for $\mathcal{W}^{-1}$ or $\mathcal{W}$ from Eq. (2.48), therefore in principle we could do a steepest ascent on W_α fields. But to ensure that the steepest descent on the free energy landscape is well-behaved, we have to input the extra constraint that

$$\frac{\delta^2 F^*[W_\alpha]}{\delta W_\alpha \delta W_\beta}$$

is negative/non-positive definite. This is generally true for the first term $\Phi(W_\alpha)$. For $\mathcal{W}^{-1}$ this imposes an extra constraint on H_1 such that

$$\frac{\delta^2 H[\phi_\alpha]}{\delta \phi_\alpha \delta \phi_\beta}$$

is positive definite. But we know that **this is not the case!** Therefore the solutions to the self-consistent equations of interest to us (for H_1 with double minima) are not the extrema in W_α fields, but saddle points. It is tempting to use the "string method" to be discussed in the Chapter 5 in Part II, which is an efficient method to locate extremum as well as saddle points on the free energy landscape, or to adapt the cell dynamics approach by Bahiana and Oono (1990).

Appendix 2.B Free Energy Expansion

2.B.1 Calculation of the connected correlation functions

From Eq. (2.20), we have

$$G^{(\mathrm{m})}_{\alpha_1\alpha_2\cdots\alpha_\mathrm{m}}(\mathbf{x}_1,\mathbf{x}_2,\cdots,\mathbf{x}_\mathrm{m}) = \left\langle \hat{\phi}_{\alpha_1}(\mathbf{x}_1)\hat{\phi}_{\alpha_2}(\mathbf{x}_2)\cdots\hat{\phi}_{\alpha_\mathrm{m}}(\mathbf{x}_\mathrm{m})\right\rangle_c .$$

From now on we shall adopt the short-hand label $\mathbf{m}$ for $\mathbf{x}_m$. To calculate these correlation functions, note that the system consists of n non-interacting polymer chains, therefore

$$G^{(\mathrm{m})}_{\alpha_1\alpha_2\cdots\alpha_\mathrm{m}}(\mathbf{1},\mathbf{2},\ldots\mathbf{m}) = n g^{(\mathrm{m})}_{\alpha_1\alpha_2\cdots\alpha_\mathrm{m}}(\mathbf{1},\mathbf{2},\ldots\mathbf{m}), \tag{2.51}$$

where g is the connected correlation function for a single chain, which is the joint probability distribution $P_{\alpha_1\alpha_2\cdots\alpha_\mathrm{m}}(\mathbf{1},\mathbf{2},\ldots\mathbf{m})$, i.e., the probability that at $\mathbf{r}_1$ there is an α_1 segment, at $\mathbf{r}_2$ there is an α_2 segment, etc.

We first study $P_{i_1 i_2\cdots i_m}(\mathbf{1},\mathbf{2},...\mathbf{m})$ which is the joint probability that there is the i_1th segment at $\mathbf{r}_1$, i_2th segment at $\mathbf{r}_2$, etc. Because the Gaussian chain (Brownian motion) is Markovian, we can express $P_{i_1 i_2\cdots i_m}(\mathbf{1},\mathbf{2},...\mathbf{m})$ using the transition probabilities (two-point propagators):

$$P_{i_1 i_2\cdots i_m}(\mathbf{1},\mathbf{2},\ldots\mathbf{m}) = P_{i_1}(\mathbf{1})P_{i_1 i_2}(\mathbf{1},\mathbf{2})P_{i_2 i_3}(\mathbf{2},\mathbf{3})\cdots P_{i_{m-1} i_m}(\mathbf{m}-\mathbf{1},\mathbf{m}) \tag{2.52}$$

where

$$P_{i_1}(\mathbf{1}) = \frac{1}{V}$$

is the probability that the first segment is located at position $\mathbf{r}_1$, and

$$P_{i_1 i_2}(\mathbf{1},\mathbf{2}) = \left(\frac{3}{2\pi\left|i_2-i_1\right|b^2}\right)^3 \exp\left[-\frac{3\left|\mathbf{r_2}-\mathbf{r}_1\right|^2}{2\left|i_2-i_1\right|b^2}\right] \tag{2.53}$$

is the propagator of a Gaussian chain from $\mathbf{r}_1$ to $\mathbf{r_2}$ with capacity $(i_2-i_1)b^2$.

To evaluate $P_{i_1 i_2\cdots i_m}$, it is convenient to use the characteristic function of $P_{i_1 i_2}(\mathbf{1},\mathbf{2})$

$$P_{i_1 i_2}(\mathbf{q}) = \int e^{i\mathbf{q}\cdot\mathbf{r}} P_{i_1 i_2}(\mathbf{r})\mathrm{d}\mathbf{r} = \exp\left[\frac{-\left|i_2-i_1\right|b^2\mathbf{q}^2}{6}\right]. \tag{2.54}$$

We now go on to evaluate $g_{i_1 i_2\cdots i_m}$.

$$\begin{aligned} g_{i_1 i_2}(\mathbf{q}_1,\mathbf{q}_2) &= \int e^{i(\mathbf{q}_1\cdot\mathbf{r}_1+\mathbf{q}_2\cdot\mathbf{r}_2)} P_{i_1}(\mathbf{1})P_{i_1 i_2}(\mathbf{r}_2-\mathbf{r}_1)\mathrm{d}\mathbf{r}_1\mathrm{d}\mathbf{r}_2 \\ &= \frac{1}{V}\delta(\mathbf{q}_1+\mathbf{q}_2)P_{i_1 i_2}(\mathbf{q}_2); \end{aligned} \tag{2.55}$$

$$g_{i_1 i_2 i_3}(\mathbf{q}_1,\mathbf{q}_2,\mathbf{q}_3) = \int e^{i(\mathbf{q}_1\cdot\mathbf{r}_1+\mathbf{q}_2\cdot\mathbf{r}_2+\mathbf{q}_3\cdot\mathbf{r}_3)} P_{i_1}(\mathbf{1}) P_{i_1 i_2}(\mathbf{r}_2-\mathbf{r}_1) P_{i_2 i_3}(\mathbf{r}_3-\mathbf{r}_2)\mathrm{d}\mathbf{r}_1\mathrm{d}\mathbf{r}_2\mathrm{d}\mathbf{r}_3$$
$$= \frac{1}{V}\delta(\mathbf{q}_1+\mathbf{q}_2+\mathbf{q}_3) P_{i_1 i_2}(\mathbf{q}_1) P_{i_2 i_3}(\mathbf{q}_3); \tag{2.56}$$

$$g_{i_1 i_2 i_3 i_4}(\mathbf{q}_1,\mathbf{q}_2,\mathbf{q}_3,\mathbf{q}_4) = \int \mathrm{d}\mathbf{r}_1\mathrm{d}\mathbf{r}_2\mathrm{d}\mathbf{r}_3\mathrm{d}\mathbf{r}_4 e^{i(\mathbf{q}_1\cdot\mathbf{r}_1+\mathbf{q}_2\cdot\mathbf{r}_2+\mathbf{q}_3\cdot\mathbf{r}_3+\mathbf{q}_4\cdot\mathbf{r}_4)}$$
$$P_{i_1}(\mathbf{1}) P_{i_1 i_2}(\mathbf{r}_2-\mathbf{r}_1) P_{i_2 i_3}(\mathbf{r}_3-\mathbf{r}_2) P_{i_3 i_4}(\mathbf{r}_4-\mathbf{r}_3)$$
$$= \frac{1}{V}\delta(\mathbf{q}_1+\mathbf{q}_2+\mathbf{q}_3+\mathbf{q}_4) P_{i_1 i_2}(\mathbf{q}_1) P_{i_2 i_3}(\mathbf{q}_1+\mathbf{q}_2) P_{i_3 i_4}(\mathbf{q}_4). \tag{2.57}$$

The connected correlation functions $G_{\alpha_1\alpha_2\cdots\alpha_\mathrm{m}}(\mathbf{q}_1,\mathbf{q}_2,\ldots\mathbf{q}_\mathrm{m})$ are obtained via

$$G_{\alpha_1\alpha_2\cdots\alpha_\mathrm{m}}(\mathbf{q}_1,\mathbf{q}_2,\ldots\mathbf{q}_\mathrm{m}) = \int_{\alpha_1}\mathrm{d}i_1\int_{\alpha_2}\mathrm{d}i_2\cdots\int_{\alpha_\mathrm{m}}\mathrm{d}i_\mathrm{m} G_{i_1 i_2 i_3\cdots i_\mathrm{m}}(\mathbf{q}_1,\mathbf{q}_2,\ldots\mathbf{q}_\mathrm{m}). \tag{2.58}$$

The integral is over different blocks α_i.

2.B.2 Spinodal limit

We now study the system of associating A-B-A triblock copolymers in a theta solution for B but poor solution for A. The spinodal limit is defined as when the uniform phase becomes unstable. To calculate the spinodal transition lines we expand the free energy of the solution to the leading (quadratic) order.

The monomer interactions are assumed to be $\varepsilon_{\mathrm{AA}} = -e_\mathrm{A}$, $\varepsilon_{\alpha\beta} = 0$ otherwise. From Eqs. (2.24) and (2.27) the quadratic term in the free energy expansion is

$$\frac{F^{(2)}\{\varphi_\alpha+\bar{\phi}_\alpha\}-F^{(2)}\{\bar{\phi}_\alpha\}}{k_\mathrm{B}T} = \frac{1}{2}\int \mathrm{d}\mathbf{x}_1\mathrm{d}\mathbf{x}_2\varphi_\alpha(\mathbf{x_1})G^{-1}_{\alpha\beta}(\mathbf{x_1},\mathbf{x_2})\varphi_\beta(\mathbf{x_2}) + H_1^{(2)}, \tag{2.59}$$

where

$$H_1^{(2)} = -\frac{1}{2}e_\mathrm{A}\int\varphi_\mathrm{A}^2(\mathbf{x})\mathrm{d}\mathbf{x} + c_1\int\left(\varphi_\mathrm{A}(\mathbf{x})+\varphi_\mathrm{B}(\mathbf{x})\right)^2\mathrm{d}\mathbf{x} + 3c_2\int\left(\varphi_\mathrm{A}(\mathbf{x})+\varphi_\mathrm{B}(\mathbf{x})\right)^2\bar{\phi}_\mathrm{p}\mathrm{d}\mathbf{x}. \tag{2.60}$$

$\bar{\phi}_\alpha$ is the bulk average density of component α; $\bar{\phi}_\mathrm{p} = \bar{\phi}_\mathrm{A}+\bar{\phi}_\mathrm{B}$, is the bulk average density of polymer segments.

$F^{(2)}$ can be expressed in terms of $\varphi_\alpha(\mathbf{q})$,

$$F^{(2)} = Vk_\mathrm{B}T\sum_{\mathbf{q}}$$
$$\left[\frac{1}{2}\varphi_\alpha(\mathbf{q})G^{-1}_{\alpha\beta}(\mathbf{q},-\mathbf{q})\varphi_\beta(-\mathbf{q}) - \frac{e_\mathrm{A}}{2}\varphi_\mathrm{A}(\mathbf{q})\varphi_\mathrm{A}(-\mathbf{q}) + c_1\varphi_\mathrm{p}(\mathbf{q})\varphi_\mathrm{p}(-\mathbf{q}) + 3c_2\varphi_\mathrm{p}(\mathbf{q})\varphi_\mathrm{p}(-\mathbf{q})\bar{\phi}_\mathrm{p}\right], \tag{2.61}$$

where $\varphi_\mathrm{p} = \varphi_\mathrm{A}+\varphi_\mathrm{B}$.

$G_{\alpha\beta}$ can be obtained from Eqs. (2.55) and (2.58). Here we assume that each A block has $N_{\rm A}$ segments and the midblock has $N_{\rm B}$ segments. Then

$$G_{\alpha\beta} = \frac{n}{V}\begin{pmatrix} 2N_{\rm A}^2(D(x_{\rm A})+E(x_{\rm A})) & 2N_{\rm A}N_{\rm B}H(x_{\rm A},x_{\rm B}) \\ 2N_{\rm A}N_{\rm B}H(x_{\rm A},x_{\rm B}) & N_{\rm B}^2 D(x_{\rm B}) \end{pmatrix} = \frac{n}{V}Q_{\alpha\beta} \tag{2.62}$$

where $N_{\rm A}$ is the length of the first A block, and

$$x_\alpha = \frac{N_\alpha q^2 b^2}{6},$$

$$D(x) = \frac{x-1+e^{-x}}{x^2},$$

$$E(x) = \frac{e^{-x}(1-e^{-x})^2}{x^2},$$

$$H(x_{\rm A},x_{\rm B}) = \frac{(1-e^{-x_{\rm A}})(1-e^{-x_{\rm B}})}{x_{\rm A}x_{\rm B}}.$$

Next we minimize $F^{(2)}$ with respect to $\varphi_{\rm B}(\mathbf{q})$ or $\varphi_{\rm B}(-\mathbf{q})$,

$$\varphi_{\rm B}(\mathbf{q}) = \frac{N\left[Q^{-1}\right]_{\rm AB} + 6c_2\bar{\phi}_{\rm p}^2 + 2c_1\bar{\phi}_{\rm p}}{-6c_2\bar{\phi}_{\rm p}^2 - 2c_1\bar{\phi}_{\rm p}} - N\left[Q^{-1}\right]_{\rm BB}\varphi_{\rm A}(\mathbf{q}). \tag{2.63}$$

$[Q]^{-1}_{\alpha\beta}$ is the inverse of $[Q]_{\alpha\beta}$

$$[Q]^{-1}_{\alpha\beta}[Q]_{\beta\gamma} = \delta_{\alpha\gamma}.$$

Substitute Eq. (2.63) back into Eq. (2.61), and we obtain

$$\begin{aligned}\beta F^{(2)} &= \frac{V}{2}\sum_{\mathbf{q}}\left\{\frac{N}{\bar{\phi}_{\rm p}}\left[\frac{(Q_{\rm BB}+2Q_{\rm AB}+Q_{\rm AA})\left(2c_1\bar{\phi}_{\rm p}+6c_2\bar{\phi}_{\rm p}^2\right)-N}{\left(6c_2\bar{\phi}_{\rm p}^2+2c_1\bar{\phi}_{\rm p}\right)(Q_{\rm AA}Q_{\rm BB}-Q_{\rm AB}^2)-NQ_{\rm AA}}\right]-\beta e_{\rm A}\right\}\varphi_{\rm A}(\mathbf{q})\varphi_{\rm A}(-\mathbf{q}) \\ &= \frac{V}{2}\sum_{\mathbf{q}}\left[S^{-1}(q)-\beta e_{\rm A}\right]\varphi_{\rm A}(\mathbf{q})\varphi_{\rm A}(-\mathbf{q}).\end{aligned} \tag{2.64}$$

In the strict incompressible case, $S^{-1}(q)$ is given by

$$S^{-1}(q) = \frac{N^3D(x)+N^2(1-\bar{\phi}_{\rm p})/\bar{\phi}_{\rm p}}{\bar{\phi}_{\rm p}(Q_{\rm AA}Q_{\rm BB}-Q_{\rm AB}^2)+(1-\bar{\phi}_{\rm p})NQ_{\rm AA}}.$$

Note that the Q functions are dependent on q. The term in the square bracket attains a minimum at $q_{\rm m}$ and at $q=0$. Once $\beta e_{\rm A}$ exceeds this minimum, the free energy becomes unstable with respect to perturbations at $q_{\rm m}$. This gives the spinodal limit. At $q=q_{\rm m}$, $e_{\rm A}\sim N^{-1}$ gives the spinodal limit of a microscopic phase transition; while at $q=0$, $e_{\rm A}\sim N^0$ corresponds to the spinodal limit of the macroscopic phase separation.

Chapter 3

Random isotropic structures and possible glass transitions in diblock copolymer melts

This chapter is reprinted from our paper, C.-Z. Zhang and Z.-G. Wang *Phys. Rev. E***73**, 031804 (2006).

3.1 Introduction

Block copolymers are macromolecules built with blocks of chemically distinct monomers. Melts of block copolymers are attractive from both theoretical and experimental standpoints, as they undergo microphase transitions and produce diverse ordered microstructures (Hamley, 1998, 2004; Bates and Fredrickson, 1990, 1999).

The simplest block copolymer is the AB diblock copolymer made of two types of monomers A and B. Below the order-disorder transition (ODT) temperature, a diblock-copolymer melt can exhibit rich mesophases (Bates et al., 1994), including body-centered-cubic (bcc), hexagonally ordered cylinder (hex), lamellar (lam), and several bicontinuous (e.g., gyroid) structures. Experimentally these structures have been identified using transmission electron microscopy (TEM) (Bates et al., 1982; Gido and Thomas, 1994), small-angle neutron scattering (SANS) (Bates et al., 1982, 1990; Almdal and Bates, 1992), and dynamic mechanical measurements (Bates et al., 1990; Rosedale and Bates, 1990; Almdal and Bates, 1992). Theoretically these structures are well described by the self-consistent mean-field theory (Matsen and Schick, 1994; Matsen and Bates, 1996).

Generally these periodically ordered structures are expected to be the thermodynamically equilibrium states (Bates et al., 1990). However, they are difficult to attain either in experiments (Bates et al., 1990) or in computer simulations (Fraaije et al., 1997). Bates and co-workers (Bates and Fredrickson, 1990; Bates et al., 1990) found that quenching a nearly symmetric diblock-copolymer melt without a symmetry-breaking external field, such as reciprocal shearing, generally results in

isotropic, locally microphase-separated structures with a characteristic length scale of the radius of gyration of the polymer. In addition, such structures were also obtained (as a rule) in dynamic-density-functional calculations (Fraaije et al., 1997; Maurits and Fraaije, 1997; Hamley, 1998). The ordering kinetics in these random structures are very slow, suggesting that they are metastable states corresponding to free-energy minima. It is therefore quite possible that the ordered phases, though energetically favored, are not easily reached due to the kinetic trapping caused by the presence of a large number of metastable free-energy minima. These metastable states correspond to the locally microphase-separated states without long-range order.

Dynamic mechanical measurements by Bates and co-workers (Bates et al., 1990; Almdal and Bates, 1992) on melts of both symmetric, lamellae-forming, and asymmetric, hex-forming PE–PEP [partially deuterated poly(ethylene-propylene)–poly(ethylethylene)] copolymers revealed that the system may be frozen in random structures upon a deep quench. Comparing the quenched sample with the slowly supercooled sample and the shear-ordered sample, they found that the quenched sample exhibits very slow relaxations and extraordinarily large elastic moduli at low frequencies; but the supercooled sample behaves more like the disordered melt continuously extended to below the ODT temperature. Balsara and co-workers (Balsara et al., 1998; Kim et al., 2001) studied the grain structure of asymmetric, hex-forming PI-PS (polyisoprene–polystyrene) melt by light scattering, SANS, and rheological measurements. Similar to the findings of Bates et al. (1990), they found that upon a deep quench, randomly microphase-separated structures are obtained, which do not appear to evolve towards the equilibrium structure with long-range order within the time scales of the experiments. Besides these, Pochan et al. (1996) found randomly oriented wormlike cylinder structures in an I_2S [polyisoprene(I)-polystyrene(S)] star copolymer system.

The above results suggest that the ordering process in block-copolymer melts follow a two-step mechanism: a fast step in which unlike monomers locally phase separate into random, macroscopically isotropic structures with domains of the size of a single polymer, followed by a domain coarsening (or growth) step in which local defects in the random microstructures anhilate and long-range order is developed. The second step is generally much slower than the first and most likely involves activated processes. Therefore a rapid deep quench can result in randomly microphase-separated structures that are kinetically trapped and unable to develop long-range order within normal laboratory time scales.

This two-step mechanism is, in fact, consistent with the thermodynamic two-step scenario implicit in the Fredrickson-Helfand (FH) fluctuation theory for diblock-copolymer melts (Fredrickson and Helfand, 1987), which only applies to symmetric or nearly symmetric copolymers. Instead of the featureless background as assumed in the random-field-approximated structure factor of Leibler (Leibler, 1980), the FH theory suggests that when the temperature approaches the ODT, the disordered state is a fluctuating, heterogeneous structure consisting of locally A- and B-rich domains,

which then orders into periodic mesophases upon further cooling.

The most dramatic manifestation of the first step is the existence of disordered-spherical-micelle state in highly asymmetric copolymer melts, which almost has the appearance of a distinct phase between the featureless disordered phase and the bcc-ordered phase (Adams et al., 1994, 1996; Schwab and Stühn, 1996; Kim et al., 1999; Han et al., 2000; Sota et al., 2003; Choi et al., 2003; Wang et al., 2002). The micelle state was first predicted by Semenov (1989). Recently Dormidontova and Lodge (2001) extended the Semenov theory by including the translational entropy of the disordered spherical micelles and predicted a phase diagram that is in qualitative agreement with experiments. More recently, Wang et al. (2005) examined the nature of the disordered spherical micelles and their connection to concentration fluctuations using the self-consistent-field theory. Taking a nucleation perspective, these authors showed that the disordered micelles are large, localized concentration fluctuations through a thermally activated process.

In this work, we study the metastable states consisting of random structures in block-copolymer melts and address the possibility of glass transition using a thermodynamic replica approach. This approach was first proposed by Monasson (1995) and subsequently employed by a number of authors in studying structural glass transitions (Mézard and Parisi, 2000; Coluzzi et al., 2000; Schmalian and Wolynes, 2000; Westfahl et al., 2001; Wu et al., 2004). In this framework, the onset of glassiness is identified with broken ergodicity (Palmer, 1982), which occurs as a result of the appearance of an exponentially large number of metastable free-energy minima (Nussinov et al., 1999). The broken ergodicity is manifested through a nonvanishing long-time correlation (here manifested as the cross replica correlation function), whose first appearance defines the onset temperature of glassiness $T_{\rm A}$ (also called the dynamic glass transition temperature (Westfahl et al., 2001; Monasson, 1995)). An equivalent Kauzmann temperature $T_{\rm K}$ as in molecular liquids (Debenedetti and Stillinger, 2001) can also be defined as signaling the complete vitrification of the random structures.

The possibility of glass transitions in bicontinuous microemulsions—a system closely related to diblock copolymers—was recently examined by Wu et al. (2002), using both a dynamic mode-coupling theory and the thermodynamic replica approach. There authors have also studied glass transitions in the Coulomb-frustrated-magnet model using the replica method with a self-consistent-screening approximation (Schmalian and Wolynes, 2000; Westfahl et al., 2001) and, more recently, a local-field calculation (Wu et al., 2004). Both the microemulsion and the Coulomb-frustrated-magnet systems belong to the general class of models first proposed by Brazovskii (1975), featuring the existence of low-energy excitations around some finite wave number $q_{\rm m}$ and the formation of microphase-separated structures with length scales $\sim 1/q_{\rm m}$ at low temperatures. These studies showed that as a result of the large degeneracy in ground states (Nussinov et al., 1999), a glass transition can occur when the ratio of the correlation length of the system to the modulation length $2\pi/q_{\rm m}$ exceeds some critical value. Similar conclusions were also obtained by Grousson et al. (2002a)

using the mode-coupling theory.

Our work follows a similar approach to that employed by Schmalian and co-workers (Schmalian and Wolynes, 2000; Westfahl et al., 2001). However, we perform calculations specifically for the block-copolymer system by taking advantage of the natural smallness parameter (the inverse of the scaled degree of polymerization, $\bar{N}$); this allows us to study how the glass transitions are affected by increasing the chain length of the polymer when the system gradually approaches the mean-field limit. An important conclusion of our work is that in the limit of infinitely long chains, both the onset of glassiness and the Kauzmann temperature coincide with the mean-field spinodal of the disordered phase. Therefore the spinodal is the mean-field signature for the glass transition in the block copolymer system; the same conclusion is likely to hold in general for microphase-separating systems. Another feature of our work is the inclusion of the order-disorder transition in the phase diagram. This is important because it places the glass transition in proper relationship to the ordering transition. We find that, for symmetric, lam-forming copolymers, the glass-transition temperatures are below the ODT temperature, while for asymmetric, sphere-forming copolymers, the onset of glassiness can precede the ODT into the bcc phase. On a technical point, we propose a method for incorporating fluctuations due to the cubic interaction in the Brazovskii model, using a renormalization scheme motivated by the $1/n$ expansion of the n-vector model in critical phenomena. The effects of these fluctuations have not been addressed in any of the previous studies (Fredrickson and Helfand, 1987; de la Cruz, 1991; Dobrynin and Erukhimovich, 1991; Barrat and Fredrickson, 1991; Fredrickson and Binder, 1989) on block-copolymer systems. We find that in the leading-order approximation these fluctuations stabilize both the bcc phase and the glassy state.

3.2 Model and solution

3.2.1 Model description

We consider the melt of AB diblock copolymers of degree of polymerization $N = N_{\mathrm{A}} + N_{\mathrm{B}}$ and block composition $f = N_{\mathrm{A}}/N$. The monomer volume v and Kuhn length B are taken to be equal for both monomers. We describe the thermodynamics of the system using the random-field-approximated (RPA) free energy functional with local approximations for the cubic and quartic interactions (Leibler, 1980; Ohta and Kawasaki, 1986; Fredrickson and Helfand, 1987) as the Hamiltonian

$$\mathcal{H}[\phi] = \frac{1}{Nv}\left[\frac{1}{2}\int \frac{d^3q}{(2\pi)^3}\phi(-q)\gamma_2(q,-q)\phi(q) + \frac{\gamma_3}{3!}\int d^3x\phi(x)^3 + \frac{\gamma_4}{4!}\int d^3x\phi(x)^4\right], \qquad (3.1)$$

where the order parameter $\phi \equiv \rho_{\mathrm{A}}(x)v - f$ is the density deviation from the mean value. Throughout the paper we take $k_{\mathrm{B}}T = 1$ except for our discussion of the thermodynamic approach to the glass

transition in Section 3.2.3. To simplify the notation, we use plain letters (x, q, etc.) to denote position and wave vectors; when the plain letter is used to denote the magnitude of the wave vector (wave number), the context should make it clear.

Near the mean-field spinodal $\gamma_2(q,-q)$ can be approximated as

$$\gamma_2(q,-q) = \frac{c^2}{4}\left(q^2Nb^2 - q_{\mathrm{m}}^2Nb^2\right)^2 + 2\left(\chi N\right)_{\mathrm{S}} - 2\chi N,$$

where χN is the Flory-Huggins interaction parameter between A and B blocks, $(\chi N)_S$ is its value at the spinodal, and c is a parameter independent of N. $(\chi N)_{\mathrm{S}}$, c, and q_{m} are functions of f and N, which can be calculated using the RPA theory of Leibler (1980). Note that Eq. (3.1) as a Hamiltonian is applicable to a broad class of copolymer systems, including multiblock copolymers (de la Cruz, 1991) and copolymer/homopolymer blends (Kielhorn and Muthukumar, 1997), where the dependence on chain architectures, block compositions, and volume fractions of copolymers can be incorporated into the parameters $(\chi N)_{\mathrm{S}}$, q_{m}, etc. Therefore our results on diblock-copolymer systems should be qualitatively applicable to these systems as well.

The degree of polymerization, N, plays the role of Ginzburg parameter, which controls the magnitude of fluctuations (Fredrickson and Helfand, 1987). To highlight this feature, we non-dimensionalize the lengths and wave numbers by the ideal end-to-end distance of the polymer: $\bar{x} \equiv x/(\sqrt{N}b)$, $\bar{q} \equiv q\sqrt{N}b$, $\bar{q}_{\mathrm{m}} \equiv q_{\mathrm{m}}\sqrt{N}b$, and concurrently rescale the order parameter as $\bar{\phi}(\bar{x}) \equiv \phi(x)c\bar{q}_{\mathrm{m}}$, $\bar{\phi}(\bar{q}) \equiv \phi(q)c\bar{q}_{\mathrm{m}}/(\sqrt{N}b)^3$. Now the Hamiltonian [Eq. (3.1)] becomes

$$\begin{aligned}\mathcal{H}[\phi] &= \frac{\sqrt{N}b^3}{v}\left[\frac{1}{2}\int\frac{d^3\bar{q}}{(2\pi)^3}g(\bar{q})^{-1}\bar{\phi}(\bar{q})\bar{\phi}(-\bar{q}) + \frac{\eta}{3!}\int d^3\bar{x}\bar{\phi}(\bar{x})^3 + \frac{\lambda}{4!}\int d^3\bar{x}\bar{\phi}(\bar{x})^4\right] \\ &= \bar{N}^{1/2}H[\bar{\phi}],\end{aligned} \tag{3.2}$$

where

$$g(\bar{q})^{-1} = \frac{1}{4\bar{q}_{\mathrm{m}}^2}\left(\bar{q}^2 - \bar{q}_{\mathrm{m}}^2\right)^2 + \tau_0\bar{q}_{\mathrm{m}}^2, \tag{3.3}$$

$$\tau_0 = \frac{2\left(\chi N\right)_{\mathrm{S}} - 2\chi N}{c^2\bar{q}_{\mathrm{m}}^4}, \tag{3.4}$$

$$\eta = \frac{\gamma_3}{c^3\bar{q}_{\mathrm{m}}^3}, \tag{3.5}$$

$$\lambda = \frac{\gamma_4}{c^4\bar{q}_{\mathrm{m}}^4}. \tag{3.6}$$

The scaled couplings η and λ are, respectively, the same as $N\Gamma_3$ and $N\Gamma_4$ defined by Fredrickson and Helfand (1987). For notational simplicity, we drop the overbars on the variables and the order parameter henceforth.

We point out that, although the parameters in Eq. (3.2) are written in molecular terms, this

model is best interpreted as phenomenological. The random-phase approximation used in deriving the Hamiltonian, the approximation of higher-order interactions as spatially local, and the truncation at quartic order in the order-parameter expansion—all introduce inaccuracies whose effects are difficult to evaluate (Kudlay and Stepanow, 2003). In particular, the order-parameter expansion to quartic order is not justified for strongly asymmetric block compositions as chain stretching effects become important and the weak-segregation assumption no longer holds (Almdal et al., 1990). However, we note that taking Eq. (3.2) as the Hamiltonian, one can reproduce the experimental phase diagram of microphase transitions qualitatively at all compositions, including the disordered spherical-micelle states at very asymmetric compositions, as the state-of-the-art self-consistent-field theory. Therefore while the quantitative accuracy of our theory may not be reliable, we expect that most of our predictions should be qualitatively correct. Such an expectation is further boosted by the general success of the Fredrickson-Helfand theory [also using Eq. (3.2) as the Hamiltonian] in capturing many key features of the physics of diblock-copolymer melts at length scales comparable to or larger than the size of the polymer chain.

In addition, studying glass transitions in the system described by Eq. (3.2) is of intrinsic theoretical value, as Eq. (3.2) corresponds to the weak-coupling limit of the Brazovskii model. Therefore our results elucidate the physics of systems in the Brazovskii class in this limit.

Finally we notice that the parameter $\bar{N}^{1/2} \equiv N^{1/2}b^3/v$ (henceforth referred to as the "chain length") is a natural combination emerging in any study of the fluctuation effects in polymer melts, which gives the number of other chains within the spatial extension of a single polymer chain (Fredrickson and Helfand, 1987; Wang, 2002). $\bar{N}$ plays a role similar to $1/\hbar$ in quantum field theory (Cornwall et al., 1974)—controlling the magnitude of fluctuations. In the limit of $\bar{N} \to \infty$, mean-field behavior is recovered. For systems with large but finite $\bar{N}$ we can apply a systematic loop expansion using $1/\bar{N}^{1/2}$ as the smallness parameter.

The presence of the $\bar{N}^{1/2}$ factor in front of the Hamiltonian also has important consequences on the free-energy barriers separating the multiplicity of free-energy minima. In the mean-field approximation, we expect that the free-energy barriers should be proportional to this factor. For long polymer chains, the barriers can be much larger than the thermal energy, resulting in slow relaxations between the metastable states and from these states to the lower free energy ordered phases. This justifies the application of the energy-landscape theory of glass transitions in polymer systems.

3.2.2 Ordered states and order-disorder transition

Our current understanding of the effects of fluctuations on the ODT in block-copolymer melts is largely based on the Brazovskii-Leibler-Fredrickson-Helfand (BLFH) theory (Brazovskii, 1975; Leibler, 1980; Fredrickson and Helfand, 1987). This theory uses the self-consistent Brazovskii ap-

proximation (a Hartree-type approximation) for the quartic interaction and ignores fluctuations due to the cubic interaction. Therefore, strictly speaking, it is only valid for symmetric or nearly symmetric block copolymers where cubic interaction is small (see our discussions at the end of this subsection). Here we extend this theory to include the leading-order one-loop correction from the cubic interaction, which accounts for the fluctuation effects due to asymmetry in the copolymer composition. This improved theory should give more accurate predictions on the ODT in asymmetric copolymer melts (and other asymmetric systems) and, more important, enables a consistent comparison with the glass transition in the same system, where the cubic term is shown to play a dominant role.

As in previous weak-segregation theories (Leibler, 1980; Fredrickson and Helfand, 1987), we adopt the single-mode approximation for the periodic microphases, representing the density wave by

$$\varphi(x) = a \sum_j \left[\exp(iQ_j \cdot x) + \exp(-iQ_j \cdot x)\right], \tag{3.7}$$

where A is the magnitude of the density wave and $Q_j (1 \le j \le n)$ are the first set of vectors on the reciprocal lattice of the periodic structure of the ordered microphases (Leibler, 1980; Fredrickson and Helfand, 1987). Now we introduce the fluctuation field around the minimum, $\psi(x) = \phi(x) - \varphi(x)$, and perform an expansion of the Hamiltonian $H[\phi]$ in Eq. (3.2) around φ. The fluctuation part of $H[\phi]$ is

$$\begin{aligned}
\Delta H[\psi;\varphi] &= H[\psi+\varphi] - H[\varphi] \\
&= \frac{1}{2}\int \frac{d^3q}{(2\pi)^3}\psi(-q)g(q)^{-1}\psi(q) + \frac{\eta}{3!}\int d^3x\psi(x)^3 + \frac{\lambda}{4!}\int d^3x\psi(x)^4 \\
&\quad + \frac{\eta}{2}\int \frac{d^3q_1 d^3q_2 d^3q_3}{(2\pi)^9}\psi(q_1)\psi(q_2)\varphi(q_3)\delta^3(q_1+q_2+q_3) \\
&\quad + \frac{\lambda}{4!}\int \frac{d^3p_1 d^3p_2 d^3p_3 d^3p_4}{(2\pi)^{12}}\delta^3(p_1+p_2+p_3+p_4) \\
&\qquad [4\psi(p_1)\psi(p_2)\psi(p_3)\varphi(p_4) + 6\varphi(p_1)\varphi(p_2)\psi(p_3)\psi(p_4)]\,.
\end{aligned} \tag{3.8}$$

The linear term of ψ vanishes because φ is at the minimum of the Hamiltonian. For the quadratic term we only keep the dominant isotropic part

$$D(q)^{-1} = g(q)^{-1} + n\lambda a^2, \tag{3.9}$$

which is defined as the shifted bare propagator.

The free energy (effective potential) of the microphase-separated system is given by

$$F[\varphi] = -\bar{N}^{-1/2} \ln \left\langle \exp\left\{-\bar{N}^{1/2} H[\phi]\right\}\right\rangle$$

$$= H[\varphi] - \bar{N}^{-1/2} \ln \left\langle \exp\left\{ -\bar{N}^{1/2} \Delta H[\psi;\varphi] \right\} \right\rangle . \tag{3.10}$$

Here the free energy is scaled by $\bar{N}^{-1/2}$ such that the mean-field part $H[\varphi]$ is independent of $\bar{N}$ and reduces to the Leibler free energy (Leibler, 1980). The second term in Eq. (3.10) contains corrections due to the fluctuation part of the Hamiltonian (Eq. (3.8)). In the one-loop approximation we have

$$F[\varphi] = H[\varphi] + \frac{1}{2\bar{N}^{1/2}} \mathtt{Tr} \ln \mathcal{G}_{\mathrm{H}}^{-1} - \frac{\lambda}{8\bar{N}} \left[\int \frac{d^3q}{(2\pi)^3} \mathcal{G}_{\mathrm{H}}(q) \right]^2 - \frac{\eta^2}{12\bar{N}} \int \frac{d^3p d^3q}{(2\pi)^6} \mathcal{G}_{\mathrm{H}}(p) \mathcal{G}_{\mathrm{H}}(q) \mathcal{G}_{\mathrm{H}}(-q-p), \tag{3.11}$$

where $\mathcal{G}_{\mathrm{H}}(q)$ is the Hartree-renormalized propagator determined from

$$\mathcal{G}_{\mathrm{H}}(q)^{-1} = D(q)^{-1} + \frac{\lambda}{2\bar{N}^{1/2}} \int \frac{d^3k}{(2\pi)^3} \mathcal{G}_{\mathrm{H}}(k). \tag{3.12}$$

Our one-loop approximation is slightly different from the conventional diagrammatic expansion; details are discussed in Appendix 3.B.

Under this approximation the renormalized correlation function is given by

$$\begin{aligned} \mathcal{G}(q)^{-1} &= \left\{ \frac{\delta^2 F[\varphi]}{\delta\varphi(q)\delta\varphi(-q)} \right\}^{-1} \\ &= \mathcal{G}_{\mathrm{H}}(q)^{-1} - \frac{\eta^2}{2\bar{N}^{1/2}} \int \frac{d^3k}{(2\pi)^3} \mathcal{G}_{\mathrm{H}}(k) \mathcal{G}_{\mathrm{H}}(q-k). \end{aligned} \tag{3.13}$$

In the replica calculation $\mathcal{G}(q)$ gives the renormalized diagonal correlation function in the replica space.

The second term in Eq. (3.13), corresponding to the one-loop cubic diagram, was absent in previous theories on the ODT, as it was shown to be subdominant to the Hartree term (the first term in Eq. (3.13)) near the mean-field ODT for asymmetric copolymers (Brazovskii, 1975; Swift and Hohenberg, 1977). The arguments for ignoring this term no longer hold for the supercooled disordered phase (below the ODT temperature), and here we need a free energy function that remains valid even below the mean-field spinodal temperature. Therefore the one-loop cubic term cannot be dropped as by Brazovskii (1975) and Fredrickson and Helfand (1987). Also in the $1/\bar{N}$ expansion employed here (equivalent to a loop expansion), the one-loop cubic term is of the same order as the Hartree term and their numerical values are comparable in the part of the phase diagram of interest, except for nearly symmetric compositions when the cubic term is small[1]. Furthermore, as shown in Appendix 3.A the corresponding term is the leading term in the self-consistent equation for the cross-replica correlation function. Earlier work also showed that it is the leading term that generates long-time correlations in the mode-coupling theory for glass transitions (Kirkpatrick and

[1] In a complementary perturbative expansion motivated by the $1/n$ expansion, this cubic diagram is subdominant to the Hatree term (see Appendix 3.B for a discussion). But their numerical values turn out to be comparable.

Thirumalai, 1989). We therefore include the one-loop cubic term in our treatment of the ODT to have a consistent comparison with glass transition.

3.2.3 Random structures and glass transition

Traditionally two different approaches have been developed to study frustrated systems with quenched disorder. The dynamic approach, most notably the mode-coupling theory (Götze, 1989), focuses on dynamic correlation functions (e.g., the Edwards-Anderson order parameter defined as the long-time spin-spin correlation function in the Ising-spin-glass model (Edwards and Anderson, 1976)) and characterizes the glassy state with non-vanishing long-time correlations and broken ergodicity. On the other hand, the equilibrium thermodynamic approach, including the density functional approach (Singh et al., 1985) and the replica approach (Mézard et al., 1987), describes glass transitions in terms of the energy-landscape features of the system (Debenedetti and Stillinger, 2001). The connection between these two approaches was explicitly demonstrated in the mean-field spin-glass models (Kirkpatrick and Wolynes, 1987; Mézard et al., 1987) where it was shown that these two approaches yield consistent predictions. We now briefly describe the essential concepts in the thermodynamic approach.

The central assumption in the thermodynamic approach is that the dynamic behavior of glass-forming systems reflects the underlying free-energy-landscape features (Adam and Gibbs, 1965; Kirkpatrick et al., 1989; Monasson, 1995; Coluzzi et al., 2000; Debenedetti and Stillinger, 2001). At high temperatures, there is only one minimum corresponding to the uniform liquid state. As temperature decreases, multiple metastable minima begin to appear that are separated by sizable activation barriers, and below some temperature T_{A}, the number of these minima becomes thermodynamically large, giving a finite contribution to the partition sum of these "disjoint" metastable states and generating extensive configurational complexity manifested in a nonvanishing configurational entropy (Kirkpatrick et al., 1989). This signals the onset of glassiness or broken ergodicity (Palmer, 1982) in the sense that within times scales of typical liquid relaxations, the system is trapped in these metastable free-energy minima; transitions between the minima, however, can still occur through activated processes (Kirkpatrick and Wolynes, 1987). Dynamically, one expects a significant slowing down of structural relaxations, often accompanied by the appearance of long plateaus in the time correlation functions (Debenedetti and Stillinger, 2001; Kirkpatrick and Thirumalai, 1989). Complete vitrification occurs at a lower temperature T_{K}, below which the system is dominated by one or less than an exponentially large number of deep free energy minima; thermodynamically, this is signaled by the vanishing of the configurational entropy. T_{K} is often termed the ideal glass transition temperature and is conceptually identified with the underlying thermodynamic glass transition at which the viscosity of the supercooled liquid diverges (Kauzmann, 1948; Adam and Gibbs, 1965; Monasson, 1995; Debenedetti and Stillinger, 2001).

Recently Monasson (1995) proposed a replica method which allows explicit implementation of the thermodynamic approach for studying structural glasses resulting from self-generated randomness. Using this method Westfahl et al. (2001) successfully predicted the glass transitions in the Coulomb-frustrated-magnet model. Here we adopt this approach to study the glass transition in block-copolymer melts.

Following Monasson (1995), we introduce an external pinning field ζ and calculate the pinned free energy of the system, $F[\zeta]$

$$F[\zeta] = -k_{\mathrm{B}}T \ln Z[\zeta] = -k_{\mathrm{B}}T \ln \int \mathcal{D}\phi \exp\left(-\frac{1}{k_{\mathrm{B}}T}\left\{\mathcal{H}[\phi] + \frac{\alpha}{2}\int d^3x \left[\phi(x) - \zeta(x)\right]^2\right\}\right), \quad (3.14)$$

where $\alpha > 0$ is the coupling between the pinning field and the order parameter. (In Eqs. (3.14)–(3.20), we reintroduce the $k_{\mathrm{B}}T$ factor in order to allow explicit temperature derivatives.) The effect of ζ is to locate the basins on the free-energy landscape. The coupling constant will be taken to be infinitesimally small at the end and serves as a convenient device for breaking ergodicity—localizing the system into separate basins. Its role is similar to that of the infinitesimal field that breaks the up-down symmetry of the Ising model below the critical temperature. One can show that the minima of $F[\zeta]$ coincide with those of the effective potential of $\mathcal{H}[\phi]$ as $\alpha \to 0$; proof is given in Appendix 3.D. Thus ζ serves as a running index for labeling different basins on the free-energy landscape, and sampling the configuration space of ζ gives information on the metastable free-energy minima (the energy minima with their location fluctuations) of the system. Therefore one can use $F(\zeta)$ as an "effective Hamiltonian" for the metastable free energy minima and compute the "quenched-average" free energy

$$\bar{F} = \frac{\int \mathcal{D}\zeta F[\zeta] \exp\left\{-F[\zeta]/k_{\mathrm{B}}T\right\}}{\int \mathcal{D}\zeta \exp\left\{-F[\zeta]/k_{\mathrm{B}}T\right\}}. \quad (3.15)$$

If the system is fully ergodic, one can verify that $\bar{F}$ is equal to the equilibrium free energy

$$F = -k_{\mathrm{B}}T \ln \int \mathcal{D}\phi \exp\{-\mathcal{H}[\phi]/k_{\mathrm{B}}T\}$$

in the thermodynamic limit as $\alpha \to 0^+$. However, when ergodicity is broken $\lim_{\alpha\to 0^+} \bar{F}$ can be different from F. Their difference

$$\bar{F} - F = TS_{\mathrm{c}} \quad (3.16)$$

defines the configurational entropy that measures the configurational complexity due to an exponentionally large number of metastable states (Monasson, 1995; Westfahl et al., 2001; Mézard et al., 1987; Palmer, 1982). In the thermodynamic approach, S_{c} jumps discontinuously from zero to an extensive finite value at T_{A}, implying broken ergodicity due to disjoint metastable states; S_{c} decreases upon further cooling and vanishes at T_{K}, when the system becomes completely vitrified.

To calculate S_c it is convenient to introduce the "replicated" free energy

$$F_m = -\lim_{\alpha\to 0^+} \frac{k_B T}{m} \ln \int \mathcal{D}\zeta \exp\left\{-\frac{m}{k_B T} F[\zeta]\right\} = -\lim_{\alpha\to 0^+} \frac{k_B T}{m} \ln \int \mathcal{D}\zeta Z[\zeta]^m = -\frac{k_B T}{m} \ln Z_m, \tag{3.17}$$

where T/m is introduced as the effective temperature conjugate to $F[\zeta]$. $\bar{F}$ and S_c are obtained from Eq. (3.17) straighforwardly as

$$\bar{F} = \left.\frac{\partial(mF_m)}{\partial m}\right|_{m=1}, \tag{3.18}$$

$$S_c = -\left.\frac{\partial F_m}{\partial(T/m)}\right|_{m=1} = \frac{1}{T}\left.\frac{\partial F_m}{\partial m}\right|_{m=1}. \tag{3.19}$$

When m is an integer, Z_m in Eq. (3.17) can be simplified by introducing m copies of ϕ and integrating out the ζ field, which gives

$$Z_m = \lim_{\alpha\to 0^+} \int \mathcal{D}\phi_a \exp\left\{-\frac{1}{k_B T}\sum_{a=1}^{m} \mathcal{H}[\phi_a] - \frac{\alpha}{2mk_B T} \sum_{1\le a<b\le m}^{m} \int d^3x \left[\phi_a(x) - \phi_b(x)\right]^2\right\}, \tag{3.20}$$

where a, b are replica indices. Eq. (3.20) has the same form as the replicated partition function for a random system with quenched disorder (Mézard et al., 1987), although here we are interested in the physical limit corresponding to $m = 1$.

To characterize the physical states of the system, we introduce the (renormalized) correlation functions $\mathcal{G}(q) = \langle\phi_A(q)\phi_A(-q)\rangle$ and $\mathcal{F}(q) = \langle\phi_A(q)\phi_B(-q)\rangle_{a\neq b}$. $\mathcal{G}(q)$ is the normal physical correlation function of the system, whereas $\mathcal{F}(q)$ measures the correlation between different replicas. It has been shown that $\mathcal{F}(q)$ is equivalent to the long-time correlation function in the conventional mode-coupling approach (Monasson, 1995; Westfahl et al., 2001; Kirkpatrick and Thirumalai, 1989). At high temperatures the system is ergodic, and in the limit $\alpha \to 0^+$ different replicas are not coupled; thus, $\mathcal{F}(q) = 0$. When ergodicity is spontaneously broken, different replicas become coupled even in the limit $\alpha \to 0^+$, and $\mathcal{F}(q) \neq 0$. Using $\mathcal{F}(q)$ as the order parameter for ergodicity breaking, we can define the onset of glassiness T_A as the temperature when there first appears a solution with $\mathcal{F}(q) \neq 0$. T_A defined in this way coincides with the dynamic-transition temperature in mean-field—spin-glass models characterized by the appearance of drastically slow dynamic relaxation (Monasson, 1995; Westfahl et al., 2001).

To obtain the replica free energy defined by Eq. (3.17), we adopt the self-energy approach (Cornwall et al., 1974) and express the effective potential F_m as a functional of bare and renormalized correlation functions

$$F_m[\mathbf{G}] = \frac{1}{m}\left\{\frac{1}{2}\mathtt{Tr}\ln\mathbf{G}^{-1} + \frac{1}{2}\mathtt{Tr}\left(\mathbf{D}^{-1}\mathbf{G}\right) - \Gamma_2[\mathbf{G}]\right\}. \tag{3.21}$$

Here $\mathbf{D}$ and $\mathbf{G}$ are bare and renormalized correlation functions, with

$$\mathbf{G} = (\mathcal{G} - \mathcal{F})\,\mathbf{I} + \mathcal{F}\mathbf{E}, \tag{3.22}$$

where $E_{ab} = 1$ and $I_{ab} = \delta_{ab}$. (Henceforth we use bold face uppercase letters ($\mathbf{G}$, $\mathbf{D}$, $\mathbf{\Sigma}$) for the matrices of functions in the replica space, plain uppercase letters with subscript indices (G_{ab}, D_{ab}, etc.) for the matrix elements. $\mathcal{G}$ and $\mathcal{F}$ are reserved for the renormalized diagonal (physical) and cross-replica correlation functions respectively.)

D_{ab} is the replica-symmetric bare correlation function, $D_{ab}(q) = g(q)\delta_{ab}$, with $g(q)$ given from Eq. (3.3)

$$q_{\mathrm{m}}^{-2} g(q)^{-1} = \frac{1}{4}\left(\frac{q^2}{q_{\mathrm{m}}^2} - 1\right)^2 + \tau_0.$$

The self-energy functions Σ_{ab} are defined by

$$\mathbf{\Sigma} = \mathbf{G}^{-1} - \mathbf{D}^{-1} \tag{3.23}$$

and obtained through variation of F_m:

$$\mathbf{\Sigma} = -\frac{2\delta\Gamma_2[\mathbf{G}]}{\delta\mathbf{G}}. \tag{3.24}$$

$\Gamma_2[\mathbf{G}]$ contains all two-particle-irreducible (2PI) diagrams, which are evaluated perturbatively. Detailed calculations are given in Appendix 3.A.

Taking the inverse of $\mathbf{G}$ defined in Eq. (3.22), we find that the self-energy from Eq. (3.23) takes the form

$$\Sigma_{ab} = (\Sigma_{\mathcal{G}} - \Sigma_{\mathcal{F}})\delta_{ab} + \Sigma_{\mathcal{F}}, \tag{3.25}$$

where

$$\Sigma_{\mathcal{G}}(q) = \mathcal{G}(q)^{-1} - g(q)^{-1}, \tag{3.26}$$

$$\Sigma_{\mathcal{F}}(q) = \mathcal{G}(q)^{-1} - \frac{1}{\mathcal{G}(q) - \mathcal{F}(q)}. \tag{3.27}$$

Assuming that the momentum dependence of self-energy functions $\Sigma_{\mathcal{G}}(q)$ and $\Sigma_{\mathcal{F}}(q)$ is negligible compared with $g(q)$, we can approximate the renormalized diagonal correlation function as

$$q_{\mathrm{m}}^{-2}\mathcal{G}(q)^{-1} \approx \frac{1}{4}\left(\frac{q^2}{q_{\mathrm{m}}^2} - 1\right)^2 + \tau_0 + \Sigma_{\mathcal{G}}(q_{\mathrm{m}})q_{\mathrm{m}}^{-2} \equiv \frac{1}{4}\left(\frac{q^2}{q_{\mathrm{m}}^2} - 1\right)^2 + r. \tag{3.28}$$

And the off-diagonal correlation function $\mathcal{F}(q)$ takes the form

$$\mathcal{F}(q) = \mathcal{G}(q) - \frac{1}{\mathcal{G}(q)^{-1} - \Sigma_{\mathcal{F}}(q)} \tag{3.29}$$

$$\approx \frac{q_{\rm m}^{-2}}{\frac{1}{4}\left(\frac{q^2}{q_{\rm m}^2}-1\right)^2 + r} - \frac{q_{\rm m}^{-2}}{\frac{1}{4}\left(\frac{q^2}{q_{\rm m}^2}-1\right)^2 + r - q_{\rm m}^{-2}\Sigma_{\mathcal{F}}(q_{\rm m})} \tag{3.30}$$

$$\equiv \frac{q_{\rm m}^{-2}}{\frac{1}{4}\left(\frac{q^2}{q_{\rm m}^2}-1\right)^2 + r} - \frac{q_{\rm m}^{-2}}{\frac{1}{4}\left(\frac{q^2}{q_{\rm m}^2}-1\right)^2 + s}. \tag{3.31}$$

Equations. (3.23) and (3.24) give the self-consistent equations for $\mathcal{G}$ and $\mathcal{F}$ (algebraic equations for r and s in our case). Solving these equations we obtain a normal replica-symmetric solution with $r = s$ and a replica-symmetry-broken solution with $r < s$ below the dynamic-transition temperature $T_{\rm A}$ (corresponding to some $(\chi N)_{\rm A}$ in our diblock-copolymer model).

The configurational entropy is obtained from Eqs. (3.19) and (3.21) to be

$$\frac{S_{\rm c}}{k_{\rm B}} = -\frac{1}{2}\int \frac{d^3q}{(2\pi)^3}\left[\ln\left(1 - \frac{\mathcal{F}(q)}{\mathcal{G}(q)}\right) + \frac{\mathcal{F}(q)}{\mathcal{G}(q)}\right] - \frac{\partial}{\partial m}\left(\frac{\Gamma_2}{m}\right)\bigg|_{m=1}. \tag{3.32}$$

One indeed finds that $S_{\rm c}$ becomes extensive below $T_{\rm A}$ and decreases to zero at $T = T_{\rm K} < T_{\rm A}$; $T_{\rm K}$ determines the Kauzmann temperature or the thermodynamic glass transition defined above.

3.3 Results and discussion

3.3.1 Glass transition

Glass transitions in the Coulomb-frustrated-magnet model have been addressed by several groups in recent years (Nussinov et al., 1999; Grousson et al., 2001, 2002a,b; Schmalian and Wolynes, 2000; Westfahl et al., 2001; Geissler and Reichman, 2004; Nussinov, 2004; Wu et al., 2004). These studies establish that in this model glass transitions are possible and could be kinetically favored. However, all these studies focus on the strong-coupling regime, and except in Wu et al. (2004), the asymmetric cubic interaction has been ignored. The block-copolymer system we are studying belongs to the same universality class as the Coulomb-frustrated-magnet—both are examples of the Brazovskii model. But for long chains our system corresponds to the weak-coupling regime of the Brazovskii model. Furthermore, the presence of the cubic interaction, reflecting compositional asymmetry in the copolymer, is the rule rather than exception. It has a strong effect on the ODT and the glass transition, as we will discuss in this work.

We start with the glass transition. Figure 3.1 shows the transition lines for two chain lengths $\bar{N} = 10^4$ and $\bar{N} = 5\times10^4$. The dotted line represents the mean-field spinodal; dashed lines represent the Kauzmann temperature (or the thermodynamic glass transition temperature) $T_{\rm K}$ (Westfahl

et al., 2001)). The dynamic glass transition temperature $T_{\rm A}$ is found to be close to the Kauzmann temperature $T_{\rm K}$ on the scale of this figure in both cases, so we do not present $T_{\rm A}$ here and only include it in Figs. 3.2 and 3.3. In the energy-landscape theory of glass transitions, $T_{\rm A}$ signals the onset of glassy behavior (e.g., slow dynamics), whereas $T_{\rm K}$ represents the limit of supercooling below which the system becomes vitrified (Debenedetti and Stillinger, 2001). (Note that we use the term "temperature" even though the phase diagram is presented in terms of the Flory-Huggins interaction parameter χN; the actual temperature can be determined from the temperature dependence of χN.) These results show that in diblock-copolymer melts, glass transitions occur at finite temperatures at any chain composition f. The narrow gap between $T_{\rm A}$ and $T_{\rm K}$ suggests that the system becomes vitrified right after the onset of glassiness. Furthermore, as the chain length increases, both $T_{\rm A}$ and $T_{\rm K}$ transitions approach the mean-field spinodal. This latter result is consistent with our anticipation that a large number of inhomogeneous metastable free-energy minima emerge as the system approaches the mean-field spinodal.

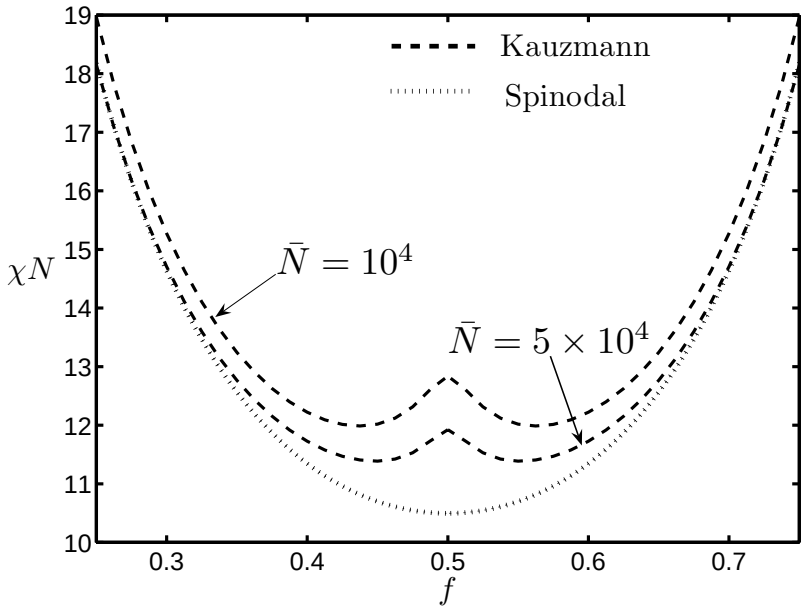

Figure 3.1: Glass transitions in diblock-copolymer melt. Dashed lines are for the Kauzmann temperature and the dotted line for the mean-field spinodal. The upper dashed line is for chain length $\bar{N} = 10^4$; the lower one for $\bar{N} = 5 \times 10^4$. Since $T_{\rm A}$ and $T_{\rm K}$ are very close, only the $T_{\rm K}$ transition is shown here.

Figure 3.1 also shows the full crossover from nearly symmetric copolymer, whose glass transitions are dominated by the quartic coupling, to highly asymmetric copolymer dominated by the cubic coupling. (We again remind the reader that the results for highly asymmetric block compositions should only be taken as qualitatively but not quantitatively valid.) For symmetric or

nearly symmetric copolymer, it is well known (Ling et al., 1981; Fredrickson and Helfand, 1987) that the mean-field spinodal is destroyed by fluctuations and the disordered phase is always locally stable. Also the transition from the disordered phase to the lam phase is a first-order transition with rather complicated (and probably slow) kinetics (Hohenberg and Swift, 1995; Fredrickson and Binder, 1989). Therefore a deep quench without annealing can result in the trapping of the system in randomly microphase-separated structures; these structures represent the glassy state captured here. This scenario is consistent with the experimental observations of Bates et al. (1990), where they studied the mechanical properties of three different samples: a rapidly quenched sample, a slowly supercooled sample, and a shear-oriented sample. By analogy to molecular liquids, these three samples can be likened to the glassy state, the supercooled-liquid state, and the ordered crystalline state, respectively. The quenched sample in this study exhibits solidlike responses at low frequencies while the supercooled sample has typical liquidlike responses.

We notice that in going from symmetric to asymmetric compositions on either side, the transition lines exhibit a minimum. This is attributed to the crossover from the quartic-coupling dominant to the cubic-coupling dominant regime. As we will discuss later, the cubic term considerably stabilizes the glassy state and enlarges the region of glassy state in the phase diagram. This results in the initial drop of χN values at the transitions as f deviates from 0.5.

For very asymmetric copolymers, mean-field theory predicts a first-order transition into ordered spherical phases (face-centered cubic (fcc) or bcc) at χN smaller than the mean-field spinodal $(\chi N)_{\mathrm{S}}$ (Matsen and Bates, 1996). However, experiments show that between the featureless disordered phase and the ordered bcc phase, there exists an intervening disordered-micelle state (Adams et al., 1994, 1996; Schwab and Stühn, 1996; Kim et al., 1999; Han et al., 2000; Sota et al., 2003; Choi et al., 2003; Wang et al., 2002; Semenov, 1989; Dormidontova and Lodge, 2001). In a self-consistent-field calculation, it was shown (Wang et al., 2005) that the micelles are formed via a thermally activated process, with a free energy barrier vanishing at the mean-field spinodal. Therefore, if the system is quickly quenched to the vicinity of the spinodal, micelles will proliferate all over the sample; the jamming of these micelles causes their translational diffusion to be so slow that long-range order cannot be developed.

The interplay between the glass transition and the ODT is complicated. We will present some tentative results in the next subsection. But here we simply note that, in contrast to the symmetric case where glass transitions occur at $\chi N > (\chi N)_{\mathrm{S}}$ (or below the mean-field spinodal temperature), for asymmetric copolymer glass transitions can occur at $\chi N < (\chi N)_{\mathrm{S}}$ (or above the mean-field spinodal temperature). We attribute this to the fact that different arrangements of micelles could generate a large number of metastable states, which significantly stabilize the glassy state.

As highlighted in Eq. (3.2), the chain length $\bar{N}$ controls the magnitude of nonlinear fluctuations and, hence, the deviation from mean-field behavior that is recovered in the limit $\bar{N} \to \infty$. Figure 3.2

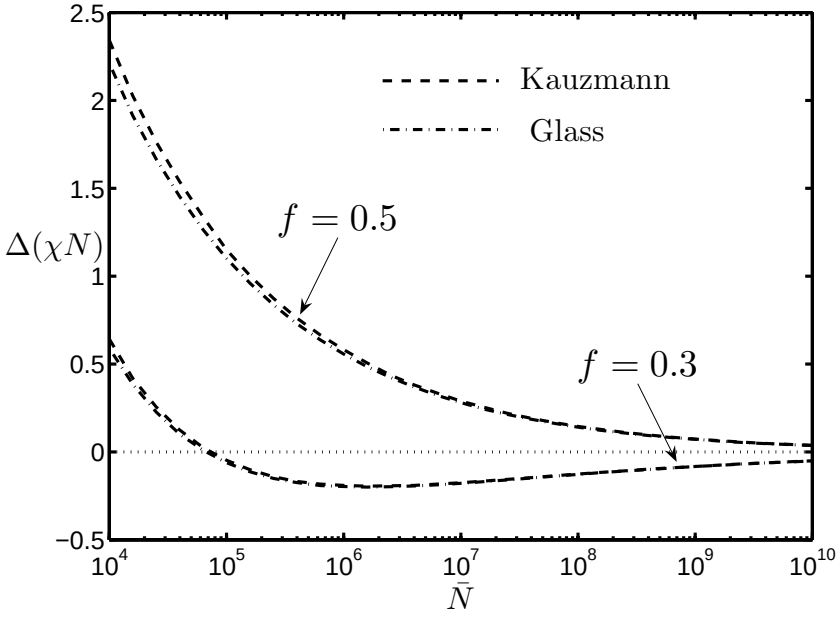

Figure 3.2: Chain-length dependence of glass transitions. Plot of $\Delta(\chi N) \equiv \chi N - (\chi N)_{\rm S}$ against $\bar{N}$. Dashed lines are for the Kauzmann temperature, and dash-dotted lines are for the onset of glassiness. Upper dashed and dash-dotted lines are for the symmetric copolymer, and lower ones for the asymmetric copolymer with $f = 0.3$.

shows the chain-length dependence of the glass transition temperatures [measured by $(\chi N)_{\rm A}$ and $(\chi N)_{\rm K}$, respectively] relative to the mean-field spinodal for symmetric and asymmetric ($f = 0.3$) copolymer melts. It is clear that in both cases the glass transitions (both $T_{\rm A}$ and $T_{\rm K}$) approach the mean-field spinodal as $\bar{N}$ goes to infinity (though from different directions in symmetric and asymmetric cases), implying that in this limit the mean-field spinodal is the true stability limit of the disordered phase (with respect to either ordered or randomly phase-separated structures). In other words, the mean-field spinodal is ultimately responsible for the appearance of random structures, and thus is the mean-field signature for the glass transition. This general conclusion is likely to be universal to the class of models with continuous degeneracy in the ground states, such as the Brazovskii model (see Nussinov, 2004 for other models of the same class). We note that the connection between the spinodal and the glass transition was also implied in an earlier study by Bagchi et al. (1983) of the Lennard-Jones liquid, where the authors conjectured that the liquid spinodal corresponds to the state of random close packing in an equivalent hard-sphere system.

We now discuss the chain-length dependence of the gap between glass transitions and the spinodal, $(\chi N)_{\rm A} - (\chi N)_{\rm S}$ and $(\chi N)_{\rm K} - (\chi N)_{\rm S}$. By a simple scaling analysis given in Appendix 3.C, we find that both should scale as $\bar{N}^{-0.3}$ for symmetric copolymer. This is consistent with the analysis of Wu et al. (2004) if we substitute the $\bar{N}$ dependence of the parameters into their scaling relation. Our

more accurate numerical calculations confirm this result, as shown in Fig. 3.3, where the first-order transition into lam phase is also included for comparison.

For asymmetric copolymers, the results are more complicated: for short chains, both $(\chi N)_{\rm A}$ and $(\chi N)_{\rm K}$ are larger than the spinodal value $(\chi N)_S$; as $\bar{N}$ increases, the transition lines first shift downward below the spinodal line, which indicates a possible crossover; then, for even larger $\bar{N}$, the transitions gradually approach the spinodal and eventually collapse to the spinodal as $\bar{N} \to \infty$. In this latter limit, we find, using the scaling analysis outlined in Appendix 3.C, that $(\chi N)_{\rm S} - (\chi N)_{\rm A,K} \sim \bar{N}^{-1/4}$. We attribute the nonmonotonic dependence on $\bar{N}$ to the crossover from the quartic-coupling dominant to cubic-coupling dominant regime as the chain length increases. Generally for asymmetric copolymers, quartic coupling dominates for short chains and the glass-transition lines are located above the spinodal (or below the spinodal temperature); for long chains, the opposite holds.

We close this subsection with a brief discussion of the dynamics of the system. For the Coulomb-frustrated-magnet model, by invoking the entropy-droplet picture, Wolynes and co-workers (Xia and Wolynes, 2000; Westfahl et al., 2001) predicted that the system should exhibit relaxations similar to fragile liquids (Angell, 1995), characterized by the Vogel-Fulcher behavior, with a relaxation time $\tau \propto \exp[A/(T - T_K)]$ between T_A and T_K, and diverging at the Kauzmann temperature $T_{\rm K}$. This prediction was disputed by Geissler and Reichman (2004), who performed dynamic Monte Carlo simulations of the Brazovskii model without the cubic interaction. They found that as the system approaches the glass-transition temperature predicted by the mode-coupling theory, the relaxation time indeed increases dramatically, but does not show characteristics of fragile liquids. Schmalian et al. (2003) subsequently argued that the failure to find the expected dynamic behavior could be a result of the mode-coupling approximation which overestimates the transition temperature. Here we note that the simulations by Geissler and Reichman (2004) were performed at temperatures above the ODT temperature, but our calculations show that in the absence of the cubic interaction, the onset of glassiness always occurs below the ODT temperature, at least in the weak-coupling regime. Therefore simulations at lower temperatures (below the ODT temperature) are necessary in order to elucidate the dynamic behavior of this model.

For block-copolymer melts, the situation is even more complicated. The Hamiltonian given by Eq. (3.1) is a coarse-grained description of the system that focuses on the physics at length scales comparable to or larger than the size of the polymer. Therefore we expect the validity of our analysis to be limited to this range of length scales. The configurational entropy $S_{\rm c}$ defined above only measures the number of configurations of chain aggregrates in the locally phase-separated structures, but does not account for different chain conformations within each aggregrate. Indeed, above the glass-transition temperature of the *monomer*, polymer chains remain liquidlike even though the system acquires solidlike behavior at the microstructural scale (at high frequencies). Chain diffusion also provides an additional mechanism for relaxations. Therefore, to accurately describe the dynamic

relaxations in block-copolymer melts, one has to consider relaxations both at the microstructural scale and of individual chains.

3.3.2 Glass transition vs order-disorder transition

Our analysis in the previous subsection shows that the glass transition is possible in diblock-copolymer melts and is related to the underlying mean-field spinodal of the disordered phase, which is responsible for the proliferation of inhomogeneous metastable states. However, the ODT also occurs in the neighborhood of the spinodal. Thus a full understanding of the glass transition in this system must address the relationship between these two transitions.

In molecular liquids the glass transition always takes place in the supercooled state—below the melting (freezing) temperature. However, in diblock-copolymer melts, the structural entities forming the random structures are themselves molecular aggregates formed through self-assembly, the number and size of which depend on the temperature of the system. Therefore the relationship between the glass transition and the ODT is not obvious.

Microphase transitions in block-copolymer systems have been extensively studied, both theoretically and experimentally (Bates and Fredrickson, 1990; Hamley, 1998). In previous theories only the Hartree term arising from the quartic interaction was retained; fluctuations due to the cubic interaction were ignored. However, our analysis in the previous subsection shows that fluctuations due to the cubic interaction play an essential role in the glass transitions in asymmetric diblock copolymers, at least for long chains[2]. Moreover, as discussed in Section 3.2.2, the leading cubic diagram is of the same order in $\bar{N}$ as the Hartree term, and their numerical magnitudes are comparable. Therefore we need to include fluctuations due to the cubic term in our studies to have a consistent comparison between the ODT and the glass transition.

In this subsection, we compare the transitions into the ordered phase and into the glassy state. We have chosen to study symmetric ($f = 0.5$) and highly asymmetric $f \sim 0.1$ copolymers, as our perturbative methods are better controlled in these two limits (dominated by the quartic and cubic nonlinear interactions, respectively).

Figure 3.3 shows the chain length dependence of the transitions for symmetric copolymers; it can be considered as a generalized phase diagram. The solid line delineates the equilibrium phase boundary between the disordered phase and the ordered lam phase. For a given $\bar{N}$, as temperature decreases ($\Delta(\chi N)$ increases), the equilibrium state of the system will change from the disordered phase through a weakly first-order transition to the lam phase. However, since the nucleation kinetics is generally slow and complicated (Fredrickson and Binder, 1989; Hohenberg and Swift, 1995), if the system is supercooled to avoid the nucleation of lam phase, the system will remain in a metastable

[2]In the system of short chains the situation is ambiguous as the higher-order diagrammatic terms neglected in our analysis could become important.

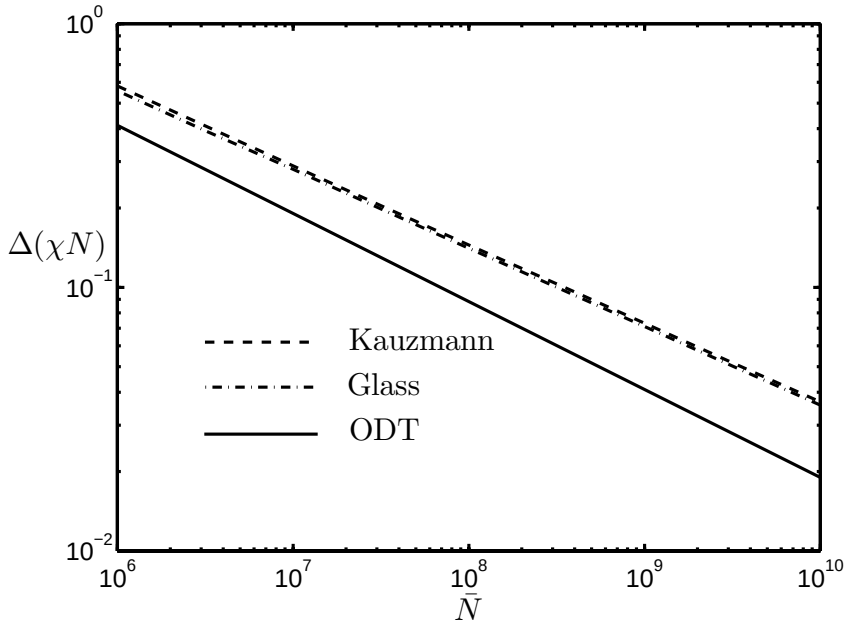

Figure 3.3: Glass transition vs ODT in symmetric copolymer melts. Dashed and dash-dotted lines have the same meanings as in Fig. 3.2; the solid line represents the ODT into the lamellar phase.

disordered state below the ODT temperature. Upon further cooling to the temperature $T_{\rm A}$ shown as the dash-dotted line, the system enters the glassy regime. The region bounded by this line and the Kauzmann line (the dashed line) defines the dynamic range within which glass transition can take place (Monasson, 1995; Schmalian and Wolynes, 2000). Although the lam phase has the lowest free energy at low temperatures, once a system is supercooled below $T_{\rm K}$, it becomes essentially frozen and incapable of reaching the more stable lam state. The narrow gap between the onset of glassiness and the Kauzmann temperature implies that the glass transition in block copolymer melts will be fairly sharp.

In symmetric copolymer melts we observe the scaling of $(\chi N)_{\rm ODT} - (\chi N)_{\rm S} \sim \bar{N}^{-1/3}$ as predicted by Fredrickson and Helfand (1987). For the onset of glassiness, $(\chi N)_{\rm A} - (\chi N)_{\rm S}$ scales as $\bar{N}^{-0.3}$, which agrees well with our approximate scaling analysis given in Appendix 3.C. Our results show that for symmetric copolymers, the ODT always occurs before the glass transitions (i.e., at temperatures above the glass transitions). While one might argue that this conclusion could be due to the particular choice of diagrams in our perturbative calculation, we find that this scaling with $\bar{N}$ remains unchanged when a different approximation scheme, the self-consistent-screening approximation, is used[3]. In addition, our results are also consistent with the local-field calculations by Wu et al. (2004), as will be discussed later in this subsection. Since $(\chi N)_{\rm ODT} - (\chi N)_{\rm S}$ decays more rapidly with $\bar{N}$ than both $(\chi N)_{\rm A} - (\chi N)_{\rm S}$ and $(\chi N)_{\rm K} - (\chi N)_{\rm S}$, for sufficiently large $\bar{N}$, we always

[3]C.-Z. Zhang and Z.-G. Wang (unpublished).

have $(\chi N)_{\mathrm{ODT}} < (\chi N)_{\mathrm{A,K}}$. Therefore, at least in the long-chain limit, our conclusion that the glass transition occurs below the ODT temperature should be valid, regardless of the approximations in the calculation.

Figure 3.4 shows various transitions for highly asymmetric copolymers around $f = 0.1$. Here again T_{A} is not shown as it is very close to T_{K} on the scale of the figures. In the case of $\bar{N} = 10^7$, the glass-transition lines are located below the ODT, i.e., the glass transition temperatures are above the ODT temperature. In other words, glass transitions can precede the ordering transition into the bcc phase. This unusual behavior is quite different from what happens in molecular fluids, where the glass transition always occurs below the freezing (ordering) temperature. In the case of longer chains with $\bar{N} = 10^8$, the ODT occurs before the glass transitions; this is the expected behavior in the asymptotic limit $\bar{N} \to \infty$, since in this limit the glass-transition lines approach the mean-field spinodal whereas the ODT into the bcc phase takes place at a finite distance below the spinodal (Matsen and Bates, 1996).

The chain-length dependence of the glass transitions relative to the ODT for asymmetric diblock copolymers is qualitatively similar to the critical micelle temperature in the same system. It is shown (Wang et al., 2005) that disordered micelles can appear in large numbers before the ordering transition only for not-too-long chains; for very long chains, the ODT will set in before the disordered micelles reach a considerable concentration, essentially precluding the disordered micelles from being a distinct intervening phase between the featureless disordered state and the ordered (fcc or bcc) phases. Since micelles are likely to be the structural entities in the glassy asymmetric copolymer melts, the connection between the micelle formation and the glass transition is worth further investigation.

As discussed in Section 3.3.1, the cubic interaction stabilizes the glassy state. We attribute this stabilizing effect to the additional complexities in the configurational space caused by the cubic term. This effect is closely related to the effect of the cubic interaction on the ODT. Theoretical analysis shows that the presence of the cubic term can considerably reduce the free energy of ordered microstructures with three-fold symmetries. This is consistent with the fact that there are more stable ordered phases in asymmetric diblock copolymers. If we visualize the random structures as polycrystals with local but no long-range order, then the increased variety of mesophase structures will increase the complexity in the configuration space[4], which can explain the stabilization of the glassy state in asymmetric copolymers.

As a final technical point, we compare our treatment of the cubic term with that by Wu et al. (2004). There the authors used a local-field approximation, in which a momentum-independent self-energy is solved variationally by mapping the Brazovskii Hamiltonian (as given by Eq. (3.2))

[4]For a discussion on the possible differences between polycrystalline phases and structural glasses in this context, see Wu et al. (2004).

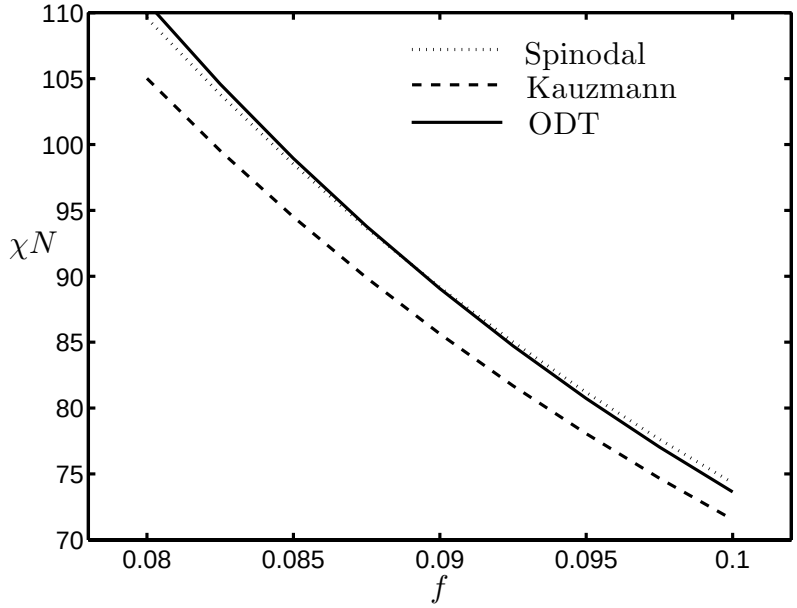

(a) $\bar{N} = 10^7$

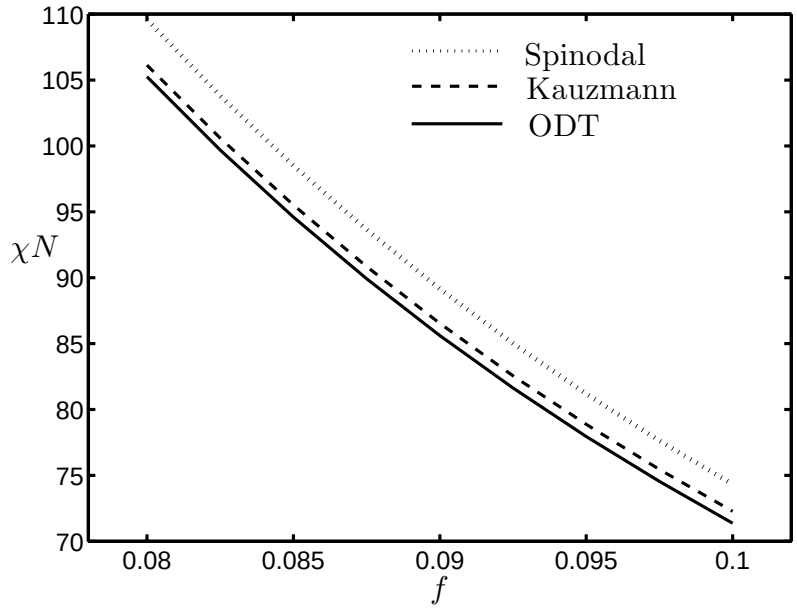

(b) $\bar{N} = 10^8$

Figure 3.4: Glass transition vs ODT in very asymmetric copolymer. (a) $\bar{N} = 10^7$, from above: mean-field spinodal (dotted line), ODT (solid line), and Kauzmann temperature (dashed line). (b) $\bar{N} = 10^8$, from above: mean-field spinodal (dotted line), Kauzmann temperature (dashed line), and ODT (solid line)

to a reference nonlinear but local Hamiltonian. Within this approximation, it was found that the cubic interaction considerably stabilizes the glassy state and the glass transition can occur at temperatures above the mean-field spinodal temperature; these results coincide with ours. However, for certain choices of parameters in the weak-coupling regime, this local-field treatment could result in a nonmonotonic relation between the correlation length and the temperature. We believe this unphysical behavior is probably due to overestimating the fluctuation effects due to the cubic term in their treatment.

3.4 Conclusions

To conclude, using the thermodynamic replica formalism we have shown that at low temperatures, diblock-copolymer melts can exist as randomly microphase-separated structures, in addition to the thermodynamically stable periodic structures. This transition is essentially a glass transition in which the supercooled liquid gradually gets vitrified. We have identified the temperature range over which this glass transition can occur, which is bordered by the onset of glassiness (or the dynamic glass transition) temperature from above and the Kauzmann (thermodynamic glass transition) temperature from below. For symmetric diblock copolymers, the glass transition takes place below the temperature of the ODT into the lam phase. However, for asymmetric diblock copolymers, the glass transition can precede the ordering transition, which is an unusual feature that probably reflects the self-assembly nature of the system. This study leads us to naturally identify the quenched samples of block copolymers in some previous experimental works as the glassy state of the system. Given the slow phase transition kinetics in copolymer systems, we expect such glassy structures to be quite common in these systems without externally imposed aligning fields.

As in any theories on polymer mixtures (Fredrickson and Helfand, 1987; Wang, 2002), the scaled degree of polymerization, $\bar{N}$, serves as a Ginzburg parameter which allows us to systematically examine the approach to mean-field behavior as $\bar{N} \to \infty$. An important conclusion is that in the limit of infinitely long chains, the glass transitions collapse to the mean-field spinodal, suggesting that the mean-field spinodal is ultimately responsible for the proliferation of inhomogeneous free-energy minima and can be used as the mean-field signature for the glass transition.

That a glass transition occurs at the mean-field spinodal in the limit of $\bar{N} \to \infty$ can also be understood using the following dynamical argument. Since the Hamiltonian has an overall factor of $\bar{N}^{1/2}$, in the mean-field approximation, we expect the free energy barriers between the metastable states to be proportional to this factor. For very long chains, these barriers can be very large. Since proliferation of the metastable minima appears at the spinodal (Nussinov, 2004), upon a quench below the spinodal, the system will first go to these metastable states with overwhelming probability because of their large number, and transitions from these metastable states should be

very slow. Note that it is the barriers from these metastable states to the (more stable) ordered phases and between the metastable states themselves, rather than the nucleation barrier from the uniform disordered phase to the ordered phases, that are relevant to the glass transition. Hence, for example, in symmetric diblock copolymers, even though the transition from the disordered to lamellar phase approaches second order in the limit $\bar{N} \to \infty$ (where the nucleation barrier vanishes (Fredrickson and Binder, 1989)), our theory predicts a glass transition that coincides with the ODT, which is the spinodal in this limit.

Studying diblock-copolymer melt as a specific example of the Brazovskii model, we find that the cubic interaction significantly increases the stability of the glassy state as well as the bcc phase, and causes qualitative changes in the scaling relations with the chain length. We conjecture that this stabilizing effect is due to increased configurational complexity as a result of more free-energy minima due to the presence of the cubic term.

Appendix 3.A Perturbative expansion of the effective potential with broken symmetries

In this appendix we present the details of our perturbative calculation of the free energy defined in Eq. (3.17). The general expansion of the effective potential for a system with broken symmetry was derived by Cornwall et al. (1974). Here we omit the details of that derivation but give the result

$$\Gamma[\varphi, \mathbf{G}] = I[\varphi] + \frac{1}{2}\mathtt{Tr}\ln \mathbf{G}^{-1} + \frac{1}{2}\mathtt{Tr}\left(\mathbf{D}^{-1}\mathbf{G}\right) - \Gamma_2[\mathbf{G}; \Delta H]. \tag{3.33}$$

Here φ is the order parameter in the ordered phase, $I[\varphi]$ is the mean-field free energy (in our case the Leibler free energy), $\Delta H[\psi; \varphi]$ is the shifted Hamiltonian (see Eq. (3.8)), $\mathbf{D}$ is the shifted bare propagator defined as

$$D_{ab}(q) = \frac{\delta^2 \Delta H[\varphi]}{\delta\varphi_{\mathrm{A}}(q)\delta\varphi_{\mathrm{B}}(-q)}, \tag{3.34}$$

and $\mathbf{G}$ is the renormalized propagator. As noted before, we reserve boldface uppercase letters for matrices of correlation functions and use the corresponding plain ones when referring to the matrix element. The second term ($\mathtt{Tr}\ln$) in Eq. (3.33) is the one-loop correction and the last term, Γ_2 contains higher-order corrections, including all 2PI diagrams generated by the vertices in the shifted Hamiltonian ΔH with the renormalized propagator $\mathbf{G}$. The third term ensures the consistency of the expansion in terms of the renormalized propagator.

It has been shown by Cornwall et al. (1974) that $\Gamma[\varphi, \mathbf{G}]$, as defined in Eq. (3.33), is stationary with respect to both φ and $\mathbf{G}$. Therefore one can derive the self-energy equations through a variation

of Eq. (3.33), which gives

$$\frac{\delta\Gamma[\mathbf{G}]}{\delta\mathbf{G}} = 0 \Rightarrow \mathbf{\Sigma} = \mathbf{G}^{-1} - \mathbf{D}^{-1} = -\frac{2\delta\Gamma_2[\mathbf{G}]}{\delta\mathbf{G}}. \tag{3.35}$$

In the field-theory description of diblock-copolymer melts (Eq. (3.2)), $\bar{N}^{-1/2}$ serves as a smallness parameter, which enables a straightforward loop expansion for $\Gamma_2[\mathbf{G}]$. To the leading two-loop order (one-loop order in the self-energy), one has three terms

$$\Gamma_2^{(1)} = -\frac{\lambda}{8\bar{N}} \sum_a \int \frac{d^3q_1 d^3q_2}{(2\pi)^6} G_{aa}(q_1) G_{aa}(q_2), \tag{3.36a}$$

$$\Gamma_2^{(2)} = \frac{\eta^2}{12\bar{N}} \sum_{a,b} \int \frac{d^3q_1 d^3q_2}{(2\pi)^6} G_{ab}(q_1) G_{ab}(q_2) G_{ab}(-q_1-q_2), \tag{3.36b}$$

$$\Gamma_2^{(3)} = \frac{\lambda^2}{12\bar{N}} \sum_{a,b} \int \frac{d^3q_1 d^3q_2 d^3q_3}{(2\pi)^9} \varphi_{\rm A}(q_1) G_{ab}(-q_2) G_{ab}(-q_3) G_{ab}(q_1+q_2+q_3) \varphi_{\rm B}(-q_1), \tag{3.36c}$$

corresponding to the diagrams shown in Figs. 3.5(a), (b), and 5(c) respectively. In the glassy state, translational symmetry breaking does not occur; therefore, $\varphi = 0$, $D_{ab}(q) = g(q)\delta_{ab}$, and $\Gamma_2^{(3)}$ vanishes. Note that $\Gamma_2^{(1)}$ is the Hartree term which only generates a momentum-independent self-energy in the diagonal part of $\mathbf{G}$; $\Gamma_2^{(2)}$ generates an off-diagonal self-energy which enables a nontrivial solution with broken replica symmetry. For symmetric copolymer, the cubic coupling is zero; therefore, to find possible solutions with broken replica symmetry we need to include the off-diagonal term of second order,

$$\Gamma_2^{(4)} = \frac{\lambda^2}{48\bar{N}^{3/2}} \sum_{a,b} \int \frac{d^3q_1 d^3q_2 d^3q_3}{(2\pi)^9} G_{ab}(q_1) G_{ab}(q_2) G_{ab}(q_3) G_{ab}(-q_1-q_2-q_3), \tag{3.36d}$$

corresponding to the three-loop diagram as shown in Fig. 3.5(d). To study the crossover from very asymmetric to symmetric copolymer, we keep $\Gamma_2^{(4)}$ in the off-diagonal renormalization for asymmetric copolymer as well.

From Eqs. (3.35) and (3.36) we obtain the self-energy

$$\begin{aligned}\Sigma_{ab}(k) = {} & \frac{\lambda}{2\bar{N}^{1/2}} \int \frac{d^3q}{(2\pi)^3} G_{aa}(q)\delta_{ab} - \frac{\eta^2}{2\bar{N}^{1/2}} \int \frac{d^3q}{(2\pi)^3} G_{ab}(q) G_{ab}(k-q) \\ & - \frac{\lambda^2}{6\bar{N}} \int \frac{d^3q d^3p}{(2\pi)^6} G_{ab}(q) G_{ab}(p) G_{ab}(k-p-q).\end{aligned} \tag{3.37}$$

The three terms on the right-hand side corresponde to Figs. 3.5(e), (f), and (g), respectively.

Under the one-step replica-symmetry-breaking (1-RSB) ansatz, $G_{ab}(q) = [\mathcal{G}(q) - \mathcal{F}(q)]\,\delta_{ab} +$

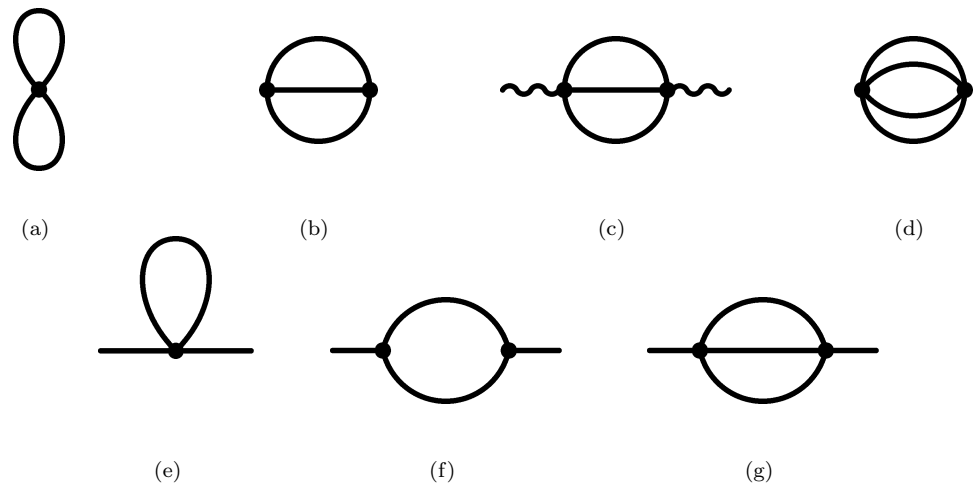

Figure 3.5: Feynman diagrams: (a)–(d) Loop diagrams in Γ_2. (e)–(g) Self-energy diagrams. In the diagrams thick solid lines represent the renormalized propagator $\mathbf{G}$ and wiggly lines represent the external leg of the order parameter $\varphi(q)$. We use a slightly different perturbative expansion for the diagonal renormalization, as explained in Appendix 3.B.

$\mathcal{F}(q)$, and Γ_2 has three terms from Eqs. (3.36a), (3.36b), and (3.36d)

$$\Gamma_2^{(1)} = -\frac{m\lambda}{8\bar{N}}\left(\int \frac{d^3q}{(2\pi)^3}\mathcal{G}(q)\right)^2, \tag{3.38a}$$

$$\Gamma_2^{(2)} = \frac{\eta^2}{12\bar{N}}\left[m\int \frac{d^3q_1 d^3q_2}{(2\pi)^6}\mathcal{G}(q_1)\mathcal{G}(q_2)\mathcal{G}(-q_1-q_2) + m(m-1)\int \frac{d^3q_1 d^3q_2}{(2\pi)^6}\mathcal{F}(q_1)\mathcal{F}(q_2)\mathcal{F}(-q_1-q_2)\right], \tag{3.38b}$$

$$\Gamma_2^{(4)} = \frac{\lambda^2}{48\bar{N}^{3/2}}\left[m\int \frac{d^3q_1 d^3q_2 d^3q_3}{(2\pi)^9}\mathcal{G}(q_1)\mathcal{G}(q_2)\mathcal{G}(q_3)\mathcal{G}(-q_1-q_2-q_3) + m(m-1)\int \frac{d^3q_1 d^3q_2 d^3q_3}{(2\pi)^9}\mathcal{F}(q_1)\mathcal{F}(q_2)\mathcal{F}(q_3)\mathcal{F}(-q_1-q_2-q_3)\right]. \tag{3.38c}$$

Using the polarization functions $\Pi_{ab}(k)$,

$$\Pi_{ab}(k) = \int \frac{d^3q}{(2\pi)^3}G_{ab}(q)G_{ba}(k+q) = \left[\Pi_{\mathcal{G}}(k) - \Pi_{\mathcal{F}}(k)\right]\delta_{ab} + \mathcal{F}(k),$$

$$\Pi_{\mathcal{G}}(k) = \int \frac{d^3q}{(2\pi)^3}\mathcal{G}(q)\mathcal{G}(k+q), \tag{3.39a}$$

$$\Pi_{\mathcal{F}}(k) = \int \frac{d^3q}{(2\pi)^3}\mathcal{F}(q)\mathcal{F}(k+q), \tag{3.39b}$$

we can rewrite the self-energy functions (after taking $m = 1$) as

$$\Sigma_{ab} = \left(\Sigma_{\mathcal{G}} - \Sigma_{\mathcal{F}}\right)\delta_{ab} + \Sigma_{\mathcal{F}},$$

$$\Sigma_{\mathcal{G}}(k) = \frac{\lambda}{2\bar{N}^{1/2}}\int \frac{d^3q}{(2\pi)^3}\mathcal{G}(q) - \frac{\eta^2}{2\bar{N}^{1/2}}\Pi_{\mathcal{G}}(k) - \frac{\lambda^2}{6\bar{N}}\int \frac{d^3q}{(2\pi)^3}\mathcal{G}(q)\Pi_{\mathcal{G}}(q+k), \tag{3.40a}$$

$$\Sigma_{\mathcal{F}}(k) = -\frac{\eta^2}{2\bar{N}^{1/2}}\Pi_{\mathcal{F}}(k) - \frac{\lambda^2}{6\bar{N}}\int \frac{d^3q}{(2\pi)^3}\mathcal{F}(q)\Pi_{\mathcal{F}}(q+k). \tag{3.40b}$$

The configurational entropy is obtained from Eqs. (3.32) and (3.38) to be

$$S_{\rm c} = \frac{1}{T}\left.\frac{\partial F_m}{\partial m}\right|_{m=1} = S_{\rm c}^{(0)} + S_{\rm c}^{(1)},$$

$$S_{\rm c}^{(0)} = -\frac{1}{2\bar{N}^{1/2}}\int \frac{d^3q}{(2\pi)^3}\left[\ln\left(1-\frac{\mathcal{F}(q)}{\mathcal{G}(q)}\right) + \frac{\mathcal{F}(q)}{\mathcal{G}(q)}\right], \tag{3.41a}$$

$$S_{\rm c}^{(1)} = -\frac{\eta^2}{12\bar{N}}\int \frac{d^3q}{(2\pi)^3}\Pi_{\mathcal{F}}(q)\mathcal{F}(-q) - \frac{\lambda^2}{48\bar{N}^{3/2}}\int \frac{d^3q}{(2\pi)^3}\Pi_{\mathcal{F}}(q)\Pi_{\mathcal{F}}(-q). \tag{3.41b}$$

We have set $k_{\rm B}T = 1$ in the above derivations; the configurational entropy is given in unit of $k_{\rm B}$ per unit volume.

Appendix 3.B Order-disorder transition

In this appendix, we present our calculation of the ODT in diblock-copolymer melts. Our approach is different from the Brazovskii approximation (Brazovskii, 1975; Fredrickson and Helfand, 1987).

Following the derivation in Appendix 3.A, we expand the effective potential to two-loop order and keep only the diagonal terms in Eq. (3.36):

$$\Gamma[\bar{\phi}=\varphi] = F_{\rm L}(\varphi) + \frac{1}{2\bar{N}^{1/2}}\mathtt{Tr}\ln\mathcal{G}^{-1} + \frac{1}{2\bar{N}^{1/2}}\mathtt{Tr}(D^{-1}\mathcal{G}) + \frac{\lambda}{8\bar{N}}\left[\int\frac{d^3q}{(2\pi)^3}\mathcal{G}(q)\right]^2$$
$$- \frac{\eta^2}{12\bar{N}}\int\frac{d^3q}{(2\pi)^3}\mathcal{G}(q)\Pi_{\mathcal{G}}(-q) - \frac{\lambda^2}{12\bar{N}}\int\frac{d^3q_1d^3q_2}{(2\pi)^6}\varphi(q_1)\mathcal{G}(-q_2)\Pi_{\mathcal{G}}(q_1+q_2)\varphi(-q_1), \tag{3.42}$$

where $F_{\rm L}(\varphi)$ is the Leibler free energy for the ordered phase, $D(q)$ is the shifted bare propagator as given in Eq. (3.9). The Hartree approximation (similar to the Brazovskii approximation) amounts to keeping only the first four terms of Eq. (3.42), which can be justified by a renormalization-group argument (Shankar, 1994). The central idea is the following: since near the critical temperature the dominant fluctuations are those with wave numbers close to $q_{\rm m}$ at which the propagator is maximized, one can decompose the spherical shell into small "patches" and rewrite the order parameter into n components, each corresponding to one patch. In this way one can rewrite the original Hamiltonian (Eq. (3.2)) as an n-vector model. At the critical point, n goes to infinity and the Hartree approximation becomes exact. Therefore we may replace $\mathcal{G}$ by the Hartree approximation $\mathcal{G}_{\rm H}$ as defined in Eq. (3.12)

$$\mathcal{G}_{\rm H}(k)^{-1} = D(k)^{-1} + \frac{\lambda}{2\bar{N}^{1/2}}\int\frac{d^3q}{(2\pi)^3}\mathcal{G}_{\rm H}(q).$$

This gives the first three terms in Eq. (3.10).

However, here we want to study the correction due to the cubic coupling; thus, we want to include the leading-order diagram from the cubic interaction in the effective potential, as shown in Fig. 3.5(b). It can be shown that in the corresponding n-vector model as mentioned above, the Hartree term (Fig. 3.5(a)) is of order $O(n)$ and this correction term (Fig. 3.5(b)) is of order $O\left(n^{1/2}\right)$. In our numerical calculations we find these two terms to be comparable for the temperature range we are interested in. By a similar argument the last term in Eq. (3.42) is of order $O(1)$ and ignored in our calculation (the numerical value is indeed small compared with the other one-loop diagrams because of the weak first-order nature of the transition). To summarize, the free energy is given by Eq. (3.42) with the last term dropped, as is Eq. (3.11).

To find the ODT temperature, the free energy is minimized numerically with respect to the magnitude of density wave A as given in Eq. (3.7) and the ODT occurs when the free energy of the ordered phase equals the free energy of the disordered phase.

The physical correlation function is given by Eq. (3.13) and the corresponding self-energy is

$$\Sigma_{\mathcal{G}}(k) = \frac{\lambda}{2\bar{N}^{1/2}} \int \frac{d^3q}{(2\pi)^3} \mathcal{G}_{\mathrm{H}}(q) - \frac{\eta^2}{6\bar{N}^{1/2}} \int \frac{d^3q}{(2\pi)^3} \mathcal{G}_{\mathrm{H}}(q)\mathcal{G}_{\mathrm{H}}(q+k). \tag{3.43}$$

This renormalization scheme includes two parts, the first corresponding to a simple Hartree approximation and the second incorporating fluctuations from the cubic interaction using the Hartree-renormalized propagator, which is schematically shown in the following diagrammatic equations:

(3.44)

where thin lines represent the bare propagator $g(q)$, double lines represent the Hartree-renormalized propagator $\mathcal{G}_{\mathrm{H}}(q)$, and thick lines represent the physical propagator $\mathcal{G}(q)$. Equation (3.43) modifies the self-energy equation (3.40a) we derived using a straightforward loop expansion in Appendix 3.A. One can verify that this self-energy equation does not have the unphysical non-monotonic relation between temperature (manifested through χN in τ_0) and correlation length (manifested in r in $\mathcal{G}(q)$) which occurs in a naive loop expansion, and this renormalization scheme indeed gives consistent result in the known limits; e.g., when $(\chi N)_{\mathrm{S}} - \chi N \gg 1$ it reduces to the loop expansion and when $(\chi N)_{\mathrm{S}} - \chi N \sim 0$ it gives the leading-order terms in the $1/n$ expansion.

Appendix 3.C Approximate solution of the glass transition

In this last appendix we provide an approximate solution of the self-consistent equations obtained in Appendix 3.A. The diagonal and off-diagonal self-energy equations are shown in the following diagrammatic equations:

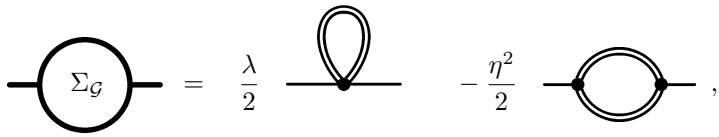

(3.45)

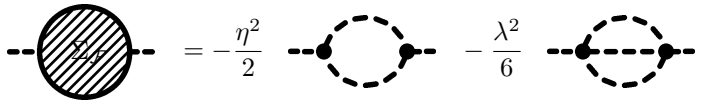

(3.46)

where dashed lines represent the renormalized off-diagonal propagator $\mathcal{F}$; thick lines and double lines represent the renormalized diagonal propagator $\mathcal{G}$ and the Hartree-renormalized propagator, respectively, the same as before.

From Eqs. (3.28) and (3.31) the renormalized propagators $\mathcal{G}$ and $\mathcal{F}$ are given by

$$\mathcal{G}(q) = \frac{4q_{\mathrm{m}}^{-2}}{\left(q^2/q_{\mathrm{m}}^2 - 1\right)^2 + 4r}, \tag{3.28$'$}$$

$$\mathcal{F}(q) = \frac{4q_{\mathrm{m}}^{-2}}{\left(q^2/q_{\mathrm{m}}^2 - 1\right)^2 + 4r} - \frac{4q_{\mathrm{m}}^{-2}}{\left(q^2/q_{\mathrm{m}}^2 - 1\right)^2 + 4s}. \tag{3.31$'$}$$

When r,s are small, the polarization functions can be approximated as

$$\Pi_{\mathcal{G}}(k) \simeq \frac{1}{4kr}, \tag{3.47a}$$

$$\Pi_{\mathcal{F}}(k) \simeq \frac{1}{4k}\left(\frac{1}{\sqrt{r}} - \frac{1}{\sqrt{s}}\right)^2, \tag{3.47b}$$

for $0 < |k| < 2$ and zero elsewhere. These are verified numerically and work well for r, s not too large ($\lesssim 0.1$). The diagrammatic terms in our calculations are found to be

$$\int \frac{d^3q}{(2\pi)^3}\mathcal{G}(q) \approx \frac{q_{\mathrm{m}}}{2\pi\sqrt{r}}, \tag{3.48a}$$

$$\int \frac{d^3q}{(2\pi)^3}\mathcal{G}(k-q)\Pi_{\mathcal{G}}(q)\Big|_{k=q_{\mathrm{m}}} \approx \frac{1}{8\pi r\sqrt{r}}, \tag{3.48b}$$

$$\int \frac{d^3q}{(2\pi)^3}\mathcal{F}(k-q)\Pi_{\mathcal{F}}(q)\Big|_{k=q_{\mathrm{m}}} \approx \frac{1}{8\pi}\left(\frac{1}{\sqrt{r}} - \frac{1}{\sqrt{s}}\right)^3, \tag{3.48c}$$

$$\int \frac{d^3q}{(2\pi)^3}\mathcal{F}(-q)\Pi_{\mathcal{F}}(q) \approx \frac{1}{8\pi}\left(\frac{1}{\sqrt{r}} - \frac{1}{\sqrt{s}}\right)^3, \tag{3.48d}$$

$$\int \frac{d^3q}{(2\pi)^3}\Pi_{\mathcal{F}}(-q)\Pi_{\mathcal{F}}(q) \approx \frac{q_{\rm m}}{16\pi^2}\left(\frac{1}{\sqrt{r}}-\frac{1}{\sqrt{s}}\right)^4. \tag{3.48e}$$

From Eqs. (3.44) and (3.28′) we have the following equations for r

$$\begin{aligned}\tau_0 &= \tau - \frac{\lambda}{4\pi\bar{N}^{1/2}q_{\rm m}\sqrt{\tau}},\\ r &= \tau - \frac{\eta^2}{8\pi\bar{N}^{1/2}q_{\rm m}^3\tau}.\end{aligned} \tag{3.49}$$

And from Eqs. (3.46) and (3.31′) we have

$$s-r = \frac{\lambda^2}{48\pi\bar{N}q_{\rm m}^2}\left(\frac{1}{\sqrt{r}}-\frac{1}{\sqrt{s}}\right)^3 + \frac{\eta^2}{8\bar{N}^{1/2}q_{\rm m}^3}\left(\frac{1}{\sqrt{r}}-\frac{1}{\sqrt{s}}\right)^2. \tag{3.50}$$

Let us look at Eq. (3.50) first. Defining $t \equiv \sqrt{r/s}$, Eq. (3.50) becomes

$$t^{-2}-1 = \frac{\lambda^2(1-t)^3}{48\pi\bar{N}q_{\rm m}^2r^{5/2}} + \frac{\eta^2(1-t)^2}{8\bar{N}^{1/2}q_{\rm m}^3r^2}. \tag{3.51}$$

This equation always has a replica-symmetric solution $t = 1$ ($\mathcal{F} = 0$). Here we are seeking a replica-symmetry-broken solution with $t < 1$. Defining the dimensionless parameters

$$\begin{aligned}A &\equiv \frac{\lambda^2}{48\pi\bar{N}q_{\rm m}^2r^{5/2}},\\ B &\equiv \frac{\eta^2}{8\bar{N}^{1/2}q_{\rm m}^3r^2},\end{aligned}$$

Eq. (3.51) becomes

$$\frac{A(1-t)^2t^2}{1+t} + \frac{B(1-t)t^2}{1+t} = 1. \tag{3.51′}$$

Numerical calculations show that when both A and B are non-negative and either $A > 23.66$ or $B > 11.09$, there is always a solution $0 < t^* < 1$. For symmetric copolymer and very asymmetric copolymer, respectively, these inequalities result in the criteria

$$r \lesssim \left(\frac{\lambda^2}{\bar{N}q_{\rm m}^2}\right)^{2/5} \sim \bar{N}^{-2/5}, \tag{3.52}$$

$$r \lesssim \left(\frac{\eta^2}{\bar{N}^{1/2}q_{\rm m}^3}\right)^{1/2} \sim \bar{N}^{-1/4}. \tag{3.53}$$

And the resulted scaling relations for τ_0 [$\propto (\chi N)_{\rm S} - \chi N$] for symmetric and asymmetric copolymers are, respectively,

$$\tau_0 \sim -\bar{N}^{-0.3}, \tag{3.54}$$

$$\tau_0 \sim \bar{N}^{-1/4}. \tag{3.55}$$

These have been verified by our numerical calculations.

Finally we look at the configurational entropy and the Kauzmann temperature. The configurational entropy is given in Eq. (3.41) and found to be

$$S_{\mathrm{c}}^{(0)} = \frac{q_{\mathrm{m}}^3\sqrt{r}}{4\pi\bar{N}^{1/2}t}(1-t)^2, \tag{3.56a}$$

$$S_{\mathrm{c}}^{(1)} \approx -\frac{\eta^2}{96\pi\bar{N}r^{3/2}}(1-t)^3 - \frac{\lambda^2 q_{\mathrm{m}}}{768\pi^2\bar{N}^{3/2}r^2}(1-t)^4. \tag{3.56b}$$

Thus for symmetric copolymer ($\eta = 0$), the Kauzmann transition is located at

$$r \sim \bar{N}^{-2/5}, \tag{3.57}$$

$$\tau_0 \sim -\bar{N}^{-0.3}. \tag{3.58}$$

And for very asymmetric copolymer ($\eta/q_{\mathrm{m}}^{3/2} \gg \lambda/q_{\mathrm{m}}$),

$$r \sim \bar{N}^{-1/4}, \tag{3.59}$$

$$\tau_0 \sim \bar{N}^{-1/4}. \tag{3.60}$$

Appendix 3.D Relationship between the pinned free energy $F[\zeta]$ and the free energy landscape of the original Hamiltonian $H[\phi]$

Here we explicitly show that the free energy $F[\zeta]$ defined in Eq. (3.14) captures the metastable free-energy minima of the Hamiltonian $H[\phi]$ as defined in Eq. (3.2). First we rewrite Eq. (3.14) as

$$F[\zeta] = -\ln \int \mathcal{D}\phi \exp\left(-\mathcal{H}'[\phi] + \alpha\zeta * \phi - \frac{\alpha}{2}\zeta * \zeta\right),$$

where $*$ is a shorthand notation for integration and

$$H'[\phi] = H[\phi] + \frac{\alpha}{2}\phi * \phi. \tag{3.61}$$

We then define the generating functional of the perturbed Hamiltonian $H'[\phi]$,

$$W[J = \alpha\zeta] = -\ln \int \mathcal{D}\phi \exp\left(-\mathcal{H}'[\phi] + J * \phi\right). \tag{3.62}$$

The effective potential $\Gamma'[\varphi]$ of the Hamiltonian $H'[\phi]$ is obtained as the Legendre transform of $W[J]$. Thus we have

$$\left.\frac{\delta W[J]}{\delta J}\right|_{J=\alpha\zeta} = -\varphi, \tag{3.63}$$

$$\Gamma'[\varphi] = W[J] + J * \varphi, \tag{3.64}$$

$$\left.\frac{\delta \Gamma'[\varphi]}{\delta \varphi}\right|_{\varphi} = J. \tag{3.65}$$

Now $W[J]$ is related to $F[\zeta]$ by

$$W[J = \alpha\zeta] = F[\zeta] - \frac{\alpha}{2}\zeta * \zeta, \tag{3.66}$$

so that for any ζ^* that minimizes $F[\zeta]$, we have

$$\left.\frac{\delta F[\zeta]}{\delta \zeta}\right|_{\zeta=\zeta^*} = \alpha \left.\frac{\delta W[J]}{\delta J}\right|_{J=\alpha\zeta^*} + \alpha\zeta^* = 0, \tag{3.67}$$

that is,

$$\zeta^* = -\left.\frac{\delta W[J]}{\delta J}\right|_{J=\alpha\zeta^*} = \varphi^*. \tag{3.68}$$

Equation (3.68) holds for any positive α, including in particular the limit $\alpha \to 0^+$. In the limit of $\alpha \to 0^+$, $H'[\phi]$ approaches $H[\phi]$ and $\Gamma'[\varphi]$ approaches $\Gamma[\varphi]$, the effective potential of the original Hamiltonian $H[\phi]$. Also $J = \alpha\zeta \to 0$, from Eq. (3.65), φ^* becomes a minimum of $\Gamma[\varphi]$. This, together with Eq. (3.68), shows that the minima of $F[\zeta]$ coincide with the minima of the effective potential $\Gamma[\varphi]$ of the orginal Hamiltonian in the limit $\alpha \to 0^+$.

Part II

Interplay of Generic Interactions and Specific Binding

Chapter 4

Thermodynamics of polymer-tethered ligand-receptor interactions between surfaces

4.1 Introduction

Cells communicate via ligand-receptor interactions (Alberts et al., 2002; Baltimore et al., 2003). Such non-covalent interactions, which are present between specific pairs of residues in proteins or polypeptides, are specific (one-to-one) and reversible (Lauffenburger and Linderman, 1993). The interplay between specific and other generic physical interactions, such as electrostatic, hydrophobic and steric interactions (Israelachvili, 1992), is crucial to the adhesion and signalling between cells and the extracellular matrix, and has been extensively studied by researchers in physiology, biochemistry, biophysics, and bioengineering (Alberts et al., 2002; Bongrand, 1999; Hammer and Tirrell, 1996; Orsello et al., 2001; Zhu et al., 2000; Baudry et al., 2004; Cuvelier et al., 2004). Understanding specific cellular interactions, especially their interplay with other generic interactions in biological processes, assists bioengineering design, such as tissue engineering and bio-specific recognition. On the other hand, artificially-designed bio-mimetic materials, such as polymersomes (Discher et al., 1999; Lin et al., 2004; Bermúdez et al., 2004; Lin et al., 2005), vesicles or liposomes (Cuvelier et al., 2004; Cuvelier and Nassoy, 2004), and substrate-supported monolayer and bilayer membranes (Sackmann, 1996; Tanaka and Sackmann, 2005) allow better characterization of the specific and non-specific interactions because of the absence of complicating factors such as chemical signaling and deformability of biological cells *in vivo* (Lawrence and Springer, 1991; Dustin et al., 1996; Finger et al., 1996; Kuo and Lauffenburger, 1993; Eniola et al., 2003).

Designing biomaterials with biocompatibility requires qualitative understanding of the ligand-receptor interactions. In the classical model of cell adhesion proposed by Bell, Dembo, and Bongrand (Bell, 1978; Bell et al., 1984; Torney et al., 1986; Dembo and Bell, 1987) (illustrated in Fig. 4.1), ligand-receptor binding is treated as a chemical equilibrium between ligand and receptor molecules, the interplay between specific binding and generic physical interactions resulting in an equilibrium constant dependent on the separation between the adhesion surfaces. The Bell model captures the qualitative features of cell adhesion and has been successful in fitting certain experimental measurements quantitatively. However, careful inspection of the theory reveals several flaws and confusions. First, the equilibrium constant in the Bell model is by definition for a chemical reaction in two dimensions (2D), which can only be inferred from measurements in bulk solutions (3D), but the relation between these two equilibrium constants is obscure and often causes confusion (Dustin et al., 1996; Orsello et al., 2001; Zhu et al., 2000). A rigorous treatment of the statistical thermodynamics of binding in a 2D system is still lacking. Second, a chemical-equilibrium treatment implicitly assumes that the ligand and receptor molecules are mobile on the surfaces, which is valid only when molecules are embedded in a fluid bilayer or membrane. In many experimental settings ligands and receptors are fixed on beads (Kuo and Lauffenburger, 1993; Eniola et al., 2003) or covalently linked (Lin et al., 2004; Bermúdez et al., 2004), therefore the chemical-equilibrium assumption fails (Martin et al.,

2006) and it is erroneous to extract the parameters of the Bell model from these measurements by fitting to a chemical equilibrium expression naively.

In many biological or engineering systems, ligand or receptor groups are tethered by polymers or polypeptides to enhance specificity (Garcia, 2006; Chen and Dormidontova, 2005) or achieve different functions (Springer, 1990, 1994). Polymer-tethering has also been a common motif in surface force measurements and single-molecule studies (Wong et al., 1997; Jeppesen et al., 2001). The polymer tether turns the short-range lock-and-key type interaction into a long-range specific interaction, which has important implications to the equilibrium as well as dynamic properties of adhesion (Martin et al., 2006; Moore and Kuhl, 2006; Moreira and Marques, 2004; Sain and Wortis, 2004), and suggests a new route to controlling the interactions between surfaces typically achieved by generic physical interactions (Israelachvili, 1992; Hiddessen et al., 2000; Carignano and Szleifer, 2003; Nap and Szleifer, 2005). To characterize the polymer-tethered ligand-receptor binding, we need to separate the contributions to the effective binding constant from molecular binding and from conformation degrees of freedom—a single phenomenological binding constant is inadequate.

In this paper we study a microscopic model of polymer-tethered ligand-receptor binding and analyze the thermodynamics of binding as well as the interactions between surfaces mediated by the ligands and receptors. We explicitly account for the degrees of freedom of the flexible polymer tether, and separate their contributions to the effective binding affinity as measured in experiments. Specific attention is paid to the quenched case, where both ligands and receptors are immobile with random distributions. In this scenario the physical free energy is the average over the random distributions of ligands and receptors ("quenched average"), and an "effective binding constant" is not applicable. In the low-density regime, the quenched system has qualitatively different thermodynamics than the annealed system. We develop an asymptotic expansion of the quenched free energy of binding in terms of the scaled molecular densities of ligands and receptors, which extends our previous analysis for the single-ligand problem (Martin et al., 2006). The leading-order contributions (which are accurate at low densities and intermediate binding strength) allow us to derive the dependence of the binding free energy and the fraction of bound molecules on the microscopic binding affinity and the tether chain lengths, which are qualitatively different from the annealed systems.

Another feature of this paper is that we distinguish between ligands and receptors with fixed densities (closed) and connected to a reservoir with fixed chemical potential (open). In the Bell model the densities of ligands and receptors are both assumed to be the bulk average values. However, both experiments (Dustin et al., 1996) and theoretical estimations (Bruinsma et al., 2000; Bruinsma and Sackmann, 2002) suggest that in the adhesion of cells or vesicles, the small contact adhesion zones have ligand-receptor bonds aggregated at much higher densities than the bulk average. In this scenario the whole non-contact area serves as a reservoir for the small adhesion zones; therefore the adhesion part should be more naturally treated as an open system with a reservoir of molecules.

The biological implications are briefly discussed in Section 4.3.2. For further discussions in relation to experiments, see Bruinsma and Sackmann (2002).

We illustrate all our calculations using the ideal-Gaussian-chain model for the polymer tether and highlight the scaling dependences on the contour chain length (kuhn length); extensions to more complicated realistic models are straightforward (Szleifer and Carignano, 1996; Chen and Dormidontova, 2005). The Gaussian model allows exact analytical calculations of the chain confinement repulsion as well as the chain stretching energy, which are the main motifs in addition to the specific binding. We find that both at the onset of binding (where ligand-receptor pairs start to form) and at the free energy minimum (bridging conformation is most stable), the surface separations scale linearly as the spatial extension of the Gaussian chain. While the equilibrium separation is found to be insensitive to the binding energy, the onset of binding is proportional to the square root of the binding energy $\sqrt{\epsilon/k_{\mathrm{B}}T}$ as was suggested by Moore and Kuhl (2006). These result in a quasi-equilibrium critical tension for breaking a tethered ligand-receptor bond that scales as $N^{-1/2}$.

This chapter extends our previous paper (Martin et al., 2006) where a discrete lattice model was used and adhesion was between a single ligand and receptors. In Section 4.2 we define the continuum model for tethered ligand-receptor binding as illustrated in Fig. 4.1, and present the theoretical analysis. For simplicity we choose to study univalent ligands and receptors with monodisperse tether lengths. In Section 4.3 we discuss the key features for the simple system corresponding to the model solved in Section 4.2, and go on to study several examples combining different types of specific and non-specific interactions based on the results in Section 4.2. We suggest some tentative guidelines for the control over the interactions between surfaces via specific binding. The main conclusions are summarized in Section 4.4 with brief discussions on relevant problems.

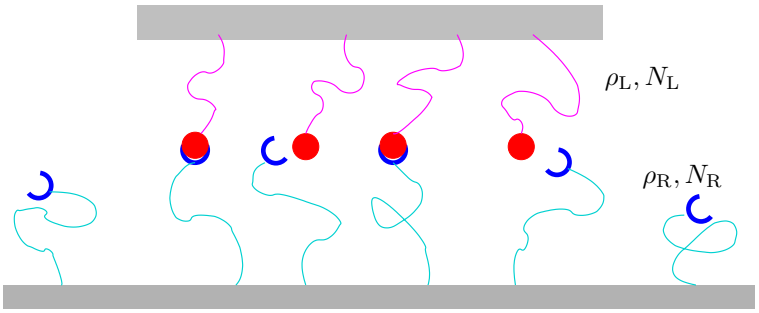

Figure 4.1: Schematic view of the model for surfaces with tethered ligands and receptors. The surfaces are separated by a distance L_z, the polymer tethers have mean square end-to-end distance $N_{\mathrm{L}}b^2$ and $N_{\mathrm{R}}b^2$, with area densities ρ_{L} and ρ_{R} for ligands and receptors, respectively; the anchoring ends are located within distance z_0 from the surface. In the Bell model, binding between ligands and receptors is treated as a chemical equilibrium with constant K dependent on the surface separation. Here we assume the binding between a ligand residue and a receptor residue to have an equilibrium constant K_0 as can be measured in a bulk solution of proteins.

4.2 Model and solution

The model is schematically shown in Fig. 4.1. Definitions of variables are given in Table. 4.1. We assume the anchoring ends on the surfaces to be non-interacting (i.e., ideal gas in 2D), and the surfaces are non-adsorbing and impenetrable for the polymer segments.

The binding (ligand and receptor) groups are located at the free ends of the polymers. The binding affinity is characterized by the equilibrium constant K_0 of the reaction

$$L + R \rightleftharpoons LR$$

in a bulk solution of ligand and receptor proteins (without the polymer tether), as is given by

$$K_0 = \frac{c_{\rm LR}}{c_{\rm L} c_{\rm R}}.$$

In our calculations all densities are molecular densities instead of molar densities.

From statistical thermodynamics we know that

$$K_0 = \frac{q'_{\rm LR}}{q'_{\rm L} q'_{\rm R}},$$

where $q'_{\rm i} = q_{\rm i}/V$ (i = L, R, or LR) is the internal part of the partition function for species i. If molecules are tethered or confined, the translation part is modified, but we can assume that the internal partition function remains the same, i.e., $q'_{\rm i}$ is unaffected by the tether. For the current model as illustrated in Fig. 4.1, the equilibrium constant in terms of the surface densities of molecules is given by

$$K = \frac{\rho_{\rm LR}}{\rho_{\rm L}\rho_{\rm R}} = \frac{q_{\rm LR}/A}{q_{\rm L}/A \cdot q_{\rm R}/A} = \frac{q'_{\rm LR}}{q'_{\rm L} q'_{\rm R}} \cdot \frac{A q^{\rm t}_{\rm LR}}{q^{\rm t}_{\rm L} q^{\rm t}_{\rm R}} = K_0 \frac{A q^{\rm t}_{\rm LR}}{q^{\rm t}_{\rm L} q^{\rm t}_{\rm R}}. \tag{4.1}$$

$q^t_{\rm i}$ are the translation part of the partition function, which are calculated in Section 4.2.2.

Throughout the paper we use $c_{\rm i}$ to denote concentrations in 3D, in unit of "number of molecules per unit volume" and $\rho_{\rm i}$ for concentrations in 2D (number of molecules per unit area). Later on we also introduce a dimensionless density $\phi_{\rm i}$ which is $\rho_{\rm i}$ multiplied by the area spanned by the tether.

4.2.1 Thermodynamics of the surface interactions

Before discussing the thermodynamics of tethered binding, we first consider the general thermodynamics for the interactions between the surfaces with polymer-tethered ligands and receptors. The total free energy of interaction ΔF is measured by the free energy at given surface separation relative to infinite separation (non-interacting). Depending on the mobility and the relative fraction of the contact area to the whole surface, each species of molecules (ligands or receptors) can be in one of three different scenarios: immobile, mobile with a fixed density, or mobile with a fixed

Table 4.1: Glossary

Variable	Definition	Dimensions or Expressions
$N_{\rm i}b^2$	mean square end-to-end distance of the polymer tether	$[{\rm L}]^2$
$x_{\rm L}(x_{\rm R})$	fraction of tether lengths	$N_{\rm L}/(N_{\rm L}+N_{\rm R})$
$m_{\rm i}$	total number of molecules for each species	–
$c_{\rm i}$	number of molecules per unit volume	$[{\rm L}]^{-3}$
$\rho_{\rm i}$	number of molecules per unit area	$[{\rm L}]^{-2}$
$\phi_{\rm i}$	scaled density in 2D	$\rho_{\rm i}Nb^2$
$c_{\rm i}^{(0)}$, $\rho_{\rm i}^{(0)}$, $\phi_{\rm i}^{(0)}$	overall densities (both bound and unbound)	same as above
L	separation between surfaces	$[{\rm L}]$
l	scaled surface separation	$L/\sqrt{N}b$
$l_0(L_0)$	position of the free energy minimum	–
$l_1(L_1)$	onset of binding	–
$q_{\rm i}$	partition function of the tethered receptor	–
$q_{\rm i}'$	internal partition function	$[{\rm L}]^{-3}$
$q_{\rm i}^{\rm t}$	partition function of the polymer tether	$[{\rm L}]^3$
F	total free energy	$k_{\rm B}T$
ΔF	interaction free energy	$k_{\rm B}T$
$F_{\rm b}, F_{\rm r}$	contribution to ΔF from *binding* and *repulsive confinement*	$k_{\rm B}T$
$\mu_{\rm i}$	reservoir chemical potential	$k_{\rm B}T$
Ξ, Q	grand partition function for open systems	–
W, p	grand potential, osmotic pressure	$k_{\rm B}T$
K_0	standard binding constant in terms of $c_{\rm i}$	$[{\rm L}]^3$
K	2D binding constant in terms of $\rho_{\rm i}$	$[{\rm L}]^2$
$(\tilde{\epsilon})\epsilon$	(effective) binding energy	$k_{\rm B}T$
A	surface area	$[{\rm L}]^2$
$A_{\rm L}^{(0)}(A_{\rm R}^{(0)})$	total area of the surface occupied by ligands (receptors)	$[{\rm L}]^2$
$G(\mathbf{r},\mathbf{r}';N)$	Green's function of the polymer chain	$[{\rm L}]^{-3}$
z_0	anchoring distance	$[{\rm L}]$
$T(T_{\rm c})$	(critical) quasi-equilibrium tension force to break a single ligand-receptor bond	$[{\rm M}][{\rm L}]^{-1}[{\rm T}]^{-2}$
$\tau_{\rm D}$, $\tau_{\rm p}$, $\tau_{\rm r}$	different time scales	$[{\rm T}]$

chemical potential (connected to a reservoir). These different scenarios are described by different thermodynamic potentials.

For mobile receptors and ligands, the Helmholtz free energy can be written as

$$F_{\rm tot} = F_{\rm L}(A_{\rm L}^{(0)} - A, m_{\rm L}^{(0)} - m_{\rm L}) + F_{\rm R}(A_{\rm R}^{(0)} - A, m_{\rm R}^{(0)} - m_{\rm R}) + F(A, m_{\rm L}, m_{\rm R}).$$

Here $A_\alpha^{(0)}$ is the total area of the surface occupied by species α, $m_\alpha^{(0)}$ is the total number of molecules, A is the contact area, m_α is the number of molecules within the contact area A, F_α is the free energy of species α in the non-contact region on the surface, and F is the free energy in the contact region.

Before the surfaces are in contact, the free energy is

$$F_{\rm tot}^{(0)} = F_{\rm L}(A^{(0)}, m_{\rm L}^{(0)}) + F_{\rm R}(A_{\rm R}^{(0)}, m_{\rm R}^{(0)}).$$

Therefore the net interaction free energy is

$$\begin{aligned}\Delta F = {} & F(A, m_{\rm L}, m_{\rm R}) + F_{\rm L}(A_{\rm L}^{(0)} - A, m_{\rm L}^{(0)} - m_{\rm L}) - F_{\rm L}(A^{(0)}, m_{\rm L}^{(0)}) \\ & + F_{\rm R}(A_{\rm R}^{(0)} - A, m_{\rm R}^{(0)} - m_{\rm R}) - F_{\rm R}(A_{\rm R}^{(0)}, m_{\rm R}^{(0)}).\end{aligned} \tag{4.2}$$

If both species have fixed densities, we can take the surface in contact to be the entire surface, and $A_\alpha^{(0)} = A$. We have

$$\Delta F = F(A, m_{\rm L}, m_{\rm R}) - F_{\rm L}(A, m_{\rm L}) - F_{\rm R}(A, m_{\rm R}); \tag{4.3a}$$

If one species is connected to a reservoir with fixed chemical potential, then the total surface area for that species can be considered infinite relative to the contact area, e.g., $A_{\rm L}^{(0)} \gg A = A_{\rm R}$, then the net free energy of interaction is

$$\begin{aligned}\Delta F &= F(A, m_{\rm L}, m_{\rm R}) - F_{\rm R}(A_{\rm R}, m_{\rm R}) - A \left.\frac{\partial F_{\rm L}}{\partial A_{\rm L}}\right|_{A_{\rm L}=A_{\rm L}^{(0)}} - m_{\rm L} \left.\frac{\partial F_{\rm L}}{\partial m_{\rm L}}\right|_{m_{\rm L}=m_{\rm L}^{(0)}} \\ &= F(A, m_{\rm L}, m_{\rm R}) - m_{\rm L}\mu_{\rm L} - [F_{\rm R}(A, m_{\rm R}) - Ap_{\rm L}].\end{aligned} \tag{4.3b}$$

$p_{\rm L} = -\partial F_{\rm L}/\partial A_{\rm L}$ is the osmotic pressure of the ligands in the reservoir. For the case where both species are mobile, the interaction free energy is

$$\Delta F = F(A, m_{\rm L}, m_{\rm R}) - m_{\rm L}\mu_{\rm L} - m_{\rm R}\mu_{\rm R} + A(p_{\rm L} + p_{\rm R}) = -A(p - p_{\rm L} - p_{\rm R}). \tag{4.3c}$$

In these two cases the appropriate thermodynamic potential is given by $F - \mu_{\rm L} m_{\rm L}$ and $F - \mu_{\rm L} m_{\rm L} - \mu_{\rm R} m_{\rm R}$, respectively, corresponding to the case of open ensemble for ligands (closed ensemble for receptors), and open ensemble for both ligands and receptors.

If one species is immobile (localized) while the other is mobile, the immobile species essentially corresponds to the closed system with fixed densities. However, if both species are immobile, the translation degrees of freedom are lost. This case is referred to as the "quenched" case. Here we assume *a priori* that the quenched average free energy is self-averaging, i.e.,

$$\frac{1}{A} \lim_{A\to\infty} F(A) = \mathcal{F} = \Big\langle F(\{\mathbf{x}_{\rm i}\}, \{\mathbf{y}_{\rm j}\}) \Big\rangle,$$

A is the total surface area; the first equation defines the average free energy in the thermodynamic limit, and the second implies that this is equivalent to the average over different distributions of the quenched molecules.

In the quenched case the binding free energy is a random variable dependent on the distribution of molecules, and its average is essentially different from the annealed cases (where either of the

species is mobile). Let us first look at the simple case when ligands and receptors are put on a lattice with no tether, i.e., binding occurs only between molecules directly facing each other, then the quenched average of the binding free energy is just

$$\langle F_{\rm b}\rangle = -\rho_{\rm L}\rho_{\rm R}\epsilon,$$

where $\rho_{\rm L}$ and $\rho_{\rm R}$ give the probability of finding a ligand/receptor molecule within a unit area, and ϵ gives the energetic gain due to binding. Clearly this is different from the chemical equilibrium in the annealed cases.

Polymer tethers enlarge the range of binding between immobile ligands and receptors, as compared to the molecular case, nonetheless, at low densities most molecules are far apart: the physics of interactions is similar to the molecular case with a scaled density. In Section 4.2.3 we develop an asymptotic expansion in this low density limit for the binding free energy, from which the density (fraction) of bound pairs can be obtained.

In the rest of this subsection we discuss the relevant thermodynamic quantities for each of the annealed cases in detail; these results are quite general and do not depend on the specific model for the tether polymer; explicit treatment of polymer tethering will be described in detail in Section 4.2.2.

4.2.1.1 Both-open system

First we examine the system where both receptors and ligands are connected to a reservoir (in a grand canonical ensemble). The free energy of interaction is related to the grand canonical partition function, which is given by

$$\Xi(\mu_{\rm L},\mu_{\rm R}) = \exp\Big[e^{\beta\mu_{\rm L}}q_{\rm L} + e^{\beta\mu_{\rm R}}q_{\rm R} + e^{\beta(\mu_{\rm L}+\mu_{\rm R})}q_{\rm LR}\Big], \tag{4.4}$$

where $\mu_{\rm L}$ and $\mu_{\rm R}$ are the chemical potentials of ligands and receptors; $q_{\rm L}$, $q_{\rm R}$, and $q_{\rm LR}$ are the partition functions of ligands, receptors, and ligand-receptor pairs.

At equilibrium the chemical potential of the bound pair $\mu_{\rm LR}$ is equal to $\mu_{\rm L}+\mu_{\rm R}$, hence we can rewrite the above equation as

$$\Xi = \exp\Big(e^{\beta\mu_{\rm L}}q_{\rm L} + e^{\beta\mu_{\rm R}}q_{\rm R} + e^{\beta\mu_{\rm LR}}q_{\rm LR}\Big). \tag{4.4$'$}$$

And from the grand potential

$$W = -k_{\rm B}T\ln\Xi = -k_{\rm B}T\left(e^{\beta\mu_{\rm L}}q_{\rm L} + e^{\beta\mu_{\rm R}}q_{\rm R} + e^{\beta\mu_{\rm LR}}q_{\rm LR}\right), \tag{4.5}$$

we can obtain the 2D concentrations of ligands, receptors, and bound pairs in equilibrium

$$\rho_{\mathrm{i}} = \frac{1}{A}\frac{\partial \ln \Xi}{\partial \beta \mu_{\mathrm{i}}} = \frac{1}{A} e^{\beta \mu_{\mathrm{i}}} q_{\mathrm{i}} = \frac{q_{\mathrm{i}}^{\mathrm{t}}}{A} e^{\beta \mu_{\mathrm{i}}} q_{\mathrm{i}}' \quad (\mathrm{i} = \mathrm{L}, \mathrm{R}, \mathrm{LR}) \tag{4.6}$$

where $q_{\mathrm{i}}^{\mathrm{t}}$ is the translation part of the partition function. From these we obtain the relation between 2D and 3D binding constant as given by Eq. (4.1)

$$K = \frac{\rho_{\mathrm{LR}}}{\rho_{\mathrm{L}} \rho_{\mathrm{R}}} = K_0 \frac{A q_{\mathrm{LR}}^{\mathrm{t}}}{q_{\mathrm{L}}^{\mathrm{t}} q_{\mathrm{R}}^{\mathrm{t}}}.$$

In Eq. (4.6) $q_{\mathrm{i}}^{\mathrm{t}}$ depends on the surface separation L_z. At infinite separation ($L_z = \infty$) no binding occurs, therefore $\rho_\alpha(\infty)$ ($\alpha = \mathrm{L}, \mathrm{R}$) are just the reservoir concentrations $\rho_\alpha^{(0)}$,

$$\rho_\alpha^{(0)} = \frac{q_\alpha^{\mathrm{t}}(\infty)}{A} e^{\beta \mu_\alpha} q_\alpha'.$$

This relates ρ_{i} at finite surface separation L_z to the reservoir concentrations $\rho_\alpha^{(0)}$ as

$$\rho_\alpha = \rho_\alpha^{(0)} \frac{q_\alpha^{\mathrm{t}}(L_z)}{q_\alpha^{\mathrm{t}}(\infty)}, \qquad (\alpha = \mathrm{L}, \mathrm{R}) \tag{4.7}$$

$$\rho_{\mathrm{LR}} = K \rho_{\mathrm{L}}^{(0)} \rho_{\mathrm{R}}^{(0)} \frac{q_{\mathrm{L}}^{\mathrm{t}}(L_z) q_{\mathrm{R}}^{\mathrm{t}}(L_z)}{q_{\mathrm{L}}^{\mathrm{t}}(\infty) q_{\mathrm{R}}^{\mathrm{t}}(\infty)}. \tag{4.8}$$

The interacting free energy per unit area is given by the difference in the grand potential as given in Eq. (4.5)

$$\begin{aligned} \frac{\Delta F(L_z)}{A k_{\mathrm{B}} T} &= \frac{W(L_z)}{A k_{\mathrm{B}} T} - \frac{W(\infty)}{A k_{\mathrm{B}} T} \\ &= -\rho_{\mathrm{L}} - \rho_{\mathrm{R}} - \rho_{\mathrm{LR}} + \rho_{\mathrm{L}}^{(0)} + \rho_{\mathrm{R}}^{(0)} \\ &= \rho_{\mathrm{L}}^0 \left[1 - \frac{q_{\mathrm{L}}^{\mathrm{t}}(L_z)}{q_{\mathrm{L}}^{\mathrm{t}}(\infty)}\right] + \rho_{\mathrm{R}}^0 \left[1 - \frac{q_{\mathrm{R}}^{\mathrm{t}}(L_z)}{q_{\mathrm{R}}^{\mathrm{t}}(\infty)}\right] - K \rho_{\mathrm{L}}^0 \rho_{\mathrm{R}}^0 \cdot \frac{q_{\mathrm{L}}^{\mathrm{t}}(L_z)}{q_{\mathrm{L}}^{\mathrm{t}}(\infty)} \frac{q_{\mathrm{R}}^{\mathrm{t}}(L_z)}{q_{\mathrm{R}}^{\mathrm{t}}(\infty)}. \end{aligned} \tag{4.9}$$

4.2.1.2 Both-closed system

In the both-closed system the total number of molecules are fixed within the contact area. The chemical equilibrium between receptors, ligands, and bound pairs implies

$$K \left(\rho_{\mathrm{L}}^{(0)} - \rho_{\mathrm{LR}}\right) \left(\rho_{\mathrm{R}}^{(0)} - \rho_{\mathrm{LR}}\right) = \rho_{\mathrm{LR}},$$

which gives

$$\rho_{\mathrm{LR}} = \frac{1}{2}\left[\rho_{\mathrm{L}}^{(0)} + \rho_{\mathrm{R}}^{(0)} + K^{-1} - \sqrt{(\rho_{\mathrm{L}}^{(0)} + \rho_{\mathrm{R}}^{(0)} + K^{-1})^2 - 4\rho_{\mathrm{L}}^{(0)} \rho_{\mathrm{R}}^{(0)}}\right]. \tag{4.10}$$

Here $\rho_{\mathrm{LR}}, \rho_{\mathrm{L}}$, and ρ_{R} are 2D concentrations of ligand-receptor pairs, free ligands, and free receptors, and $\rho_\alpha^{(0)} = \rho_\alpha + \rho_{\mathrm{LR}}$ ($\alpha = \mathrm{L}, \mathrm{R}$) give the total concentration of ligands and receptors (both free and

bound) within the contact area.

The Helmholtz free energy is related to the grand potential by a Legendre transform[1]

$$\begin{aligned}\frac{F}{k_{\mathrm{B}}T} &= -\frac{W}{k_{\mathrm{B}}T} + \sum_{\alpha=\mathrm{L,R}} \frac{\mu_\alpha}{k_{\mathrm{B}}T}\left(\rho_\alpha + \rho_{\mathrm{LR}}\right) \\ &= -\rho_{\mathrm{L}} - \rho_{\mathrm{R}} - \rho_{\mathrm{LR}} + \sum_{\alpha=\mathrm{L,R}} \left(\rho_\alpha + \rho_{\mathrm{LR}}\right) \ln \frac{\rho_\alpha A}{q^{\mathrm{t}}_\alpha q'_\alpha}. \end{aligned} \tag{4.11}$$

The interaction free energy is given by

$$\begin{aligned}\frac{\Delta F(L_z)}{Ak_{\mathrm{B}}T} &= \frac{F(L_z)}{Ak_{\mathrm{B}}T} - \frac{F(\infty)}{Ak_{\mathrm{B}}T} \\ &= \rho_{\mathrm{LR}}(L_z) - \rho_L^{(0)} \ln \frac{q^{\mathrm{t}}_{\mathrm{L}}(L_z)}{q^{\mathrm{t}}_{\mathrm{L}}(\infty)} - \rho_{\mathrm{R}}^{(0)} \ln \frac{q^{\mathrm{t}}_{\mathrm{R}}(L_z)}{q^{\mathrm{t}}_{\mathrm{R}}(\infty)} + \rho_{\mathrm{L}}^{(0)} \ln \frac{\rho_{\mathrm{L}}(L_z)}{\rho_{\mathrm{L}}^{(0)}} + \rho_{\mathrm{R}}^{(0)} \ln \frac{\rho_{\mathrm{R}}(L_z)}{\rho_{\mathrm{R}}^{(0)}}. \end{aligned} \tag{4.12}$$

One can verify that if one species is immobile while the other is mobile and both have fixed number of molecules, the only difference is the translation entropy of the immobile species, which is independent of binding. Therefore the free energy of interaction is the same as in the both mobile case.

4.2.1.3 Open-closed system

Finally we examine the case in which one surface has a fixed number of molecules while molecules on the other has a fixed chemical potential. This corresponds to the scenario in which the two surfaces have different overall sizes, e.g., a virus binding to a cell, or a versicle or bead binding to a fluid bilayer.

Assuming that receptors have a fixed overall density, we have

$$\rho_{\mathrm{LR}} = K\rho_{\mathrm{L}}(\rho_{\mathrm{R}}^{(0)} - \rho_{\mathrm{LR}}) \Rightarrow \rho_{\mathrm{LR}} = \frac{K\rho_{\mathrm{R}}^{(0)}\rho_{\mathrm{L}}}{1 + K\rho_{\mathrm{L}}}, \tag{4.13}$$

which is simply the Langmuir isotherm for an ideal gas of ligands. ρ_{L} is related to the reservoir density as in Eq. (4.6)

$$\rho_{\mathrm{L}}(L_z) = \rho_{\mathrm{L}}^{(0)} \frac{q^{\mathrm{t}}_{\mathrm{L}}(L_z)}{q^{\mathrm{t}}_{\mathrm{L}}(\infty)}.$$

The thermodynamic potential of interest is obtained from the grand potential through a Legendre transform over the fixed density and the free energy of interaction is given by

$$\frac{\Delta F}{Ak_{\mathrm{B}}T} = \rho_{\mathrm{L}}^{(0)} - \rho_{\mathrm{L}}(L_z) + \rho_{\mathrm{R}}^{(0)} \ln \frac{\rho_{\mathrm{R}}(L_z)}{\rho_{\mathrm{R}}^{(0)}} - \rho_{\mathrm{R}}^{(0)} \ln \frac{q^{\mathrm{t}}_{\mathrm{R}}(L_z)}{q^{\mathrm{t}}_{\mathrm{R}}(\infty)}. \tag{4.14}$$

[1] Note that in Eq. (4.3a) m_α refer to the total number of ligands or species within the contact area, including both free molecules and bound ones; here ρ_{i} refer to the density of the free molecules only.

This also applies to the case in which receptors are immobile, where the difference due to the translational entropy is a constant independent of binding.

The results are summarized in Table. 4.2. In the next subsection we study the effects of the polymer tether and derive the expressions of q_i^t for the Gaussian chain model. The quenched case is treated separately in Section 4.2.3.

Table 4.2: Summary of different scenarios

	ligands	receptors	ensemble	expressions
I	immobile	immobile	quenched	(4.33), (4.36)
II	fixed c	fixed c	canonical ensemble	(4.3a), (4.10), (4.12)
	fixed c	immobile		
III	fixed μ	fixed c	open-closed	(4.3b), (4.13), (4.14)
	fixed μ	immobile		
IV	fixed μ	fixed μ	grand canonical	(4.3c),(4.8), (4.9)

4.2.2 Polymer-mediated specific interactions

In this subsection we calculate the contribution of polymer tethers to the ligand-receptor interactions. Before presenting the exact analytical calculations for the Gaussian chain, we first explore the scaling behavior of the physical quantities of interest.

4.2.2.1 Scaling analysis

As mentioned above, polymer tethers have two effects: chain stretching in binding, and repulsion between the surfaces due to short-range confinement. Both effects are classic problems in polymer physics (de Gennes, 1979). A systematic scaling analysis of polymers confined between surfaces can be found in Lipowsky (1995), and Manghi and Aubouy (2003). Here we analyze the scaling of the size of the polymer tether in the presence of ligand-receptor binding. The scaling analysis is carried out for a polymer chain with Flory exponent ν, (i.e., $< R^2 > \sim N^{2\nu} b$). The Gaussian chain results follow by take $\nu = 1/2$.

When surfaces are far apart, the polymer chain is confined in a semi-infinite space, which gives the reference state for the problem. As surfaces come closer, ligand and the receptor groups at chain ends can meet and bind with each other. We assume that at this stage the two surfaces are still far apart so that the polymer chain is significantly stretched and chain confinement can be neglected, which will be justified *a posteriori*. In the strong stretching regime, the polymer chain can be viewed as a string of blobs of size ξ. Then the stretching energy is given by

$$E \sim k_B T \times \text{number of blobs} \sim \frac{N}{(\xi/b)^{1/\nu}},$$

and the equilibrium end-to-end distance is

$$L_z \sim N\xi^{1-\frac{1}{\nu}} b^{1/\nu}.$$

Therefore the stretching energy is given in terms of the end-to-end distance as

$$\frac{E}{k_{\mathrm{B}}T} \sim N\left(\frac{L_z}{Nb}\right)^{\frac{1}{1-\nu}} = \left(\frac{L_z}{N^{\nu}b}\right)^{\frac{1}{1-\nu}}. \tag{4.15}$$

When binding becomes possible, the molecular binding energy ϵ becomes comparable to the stretching energy, hence we have for the separation L_z^1 corresponding to the onset of binding

$$\left(\frac{L_z^1}{N^{\nu}b}\right)^{\frac{1}{1-\nu}} \sim \frac{\epsilon}{k_{\mathrm{B}}T} \Rightarrow L_z^1 \sim (\epsilon/k_{\mathrm{B}}T)^{1-\nu} N^{\nu} b. \tag{4.16}$$

This justifies our initial assumption that confinement is negligible in this regime.

As surfaces come very close, the polymer chains are squeezed by the surfaces into a string of blobs on a plane parallel to the surfaces, with thickness L_z. The blob size is

$$\xi \simeq L_z,$$

therefore free energy due to confinement is

$$V = k_{\mathrm{B}}T \frac{N}{(L_z/b)^{1/\nu}}. \tag{4.17}$$

Putting these two terms together with the binding energy, the overall free energy of a single ligand-receptor pair is (C_1 and C_2 are dimensionless constants)

$$\frac{F}{k_{\mathrm{B}}T} = -f\left[\frac{\epsilon}{k_{\mathrm{B}}T} - C_1\left(\frac{L_z}{N^{\nu}b}\right)^{\frac{1}{1-\nu}}\right] + C_2\frac{N}{(L_z/b)^{1/\nu}}, \tag{4.18}$$

and attains minimum at L_z^0 which is given by

$$L_z^0 \sim f^{-\nu(1-\nu)} N^{\nu} b, \tag{4.19}$$

where f is the fraction of ligand-receptor bridges per ligand-receptor pair. For $\epsilon \gg k_{\mathrm{B}}T$, $L_z^1 \gg N^{\nu}b$, hence binding overcomes stretching energy and most molecules are bound ($f \approx 1$), therefore the equilibrium separation between the surfaces is given by $L_z^0 \sim N^{\nu}b$.

The quenched case is more subtle. Assume $\epsilon \gg k_{\mathrm{B}}T$. The binding fraction of a tethered ligand is essentially the probability of finding a receptor within the "natural extension" of the ligand tether,

$\rho_{\mathrm{R}}\left\langle r_{\parallel}^2\right\rangle$. (Here "$\langle\rangle$" denotes the average over different chain conformations.) For a stretched chain, $r_{\parallel}^2$ is given by an ideal string of blobs in 2D,

$$\left\langle r_{\parallel}^2\right\rangle \simeq \frac{N}{(\xi/b)^{1/\nu}}\xi^2 \sim Nb^2\left(\frac{N}{L_z}\right)^{\frac{2\nu-1}{1-\nu}}, \tag{4.20a}$$

while for a confined chain the "natural" size of the tether parallel to the surface is that of a self-avoiding walk in 2D,

$$\left\langle r_{\parallel}^2\right\rangle \simeq \left[\frac{N}{(\xi/b)^{1/\nu}}\right]^{2\nu_2}\xi^2 \sim N^{2\nu_2}L_z^{2-2\nu_2/\nu}b^{2\nu_2/\nu}, \tag{4.20b}$$

ν_2 is the 2D Flory exponent.

For Gaussian chains, $\nu=\nu_2=1/2$, the scaling is the same in both cases, $f\sim Nb^2\rho_{\mathrm{R}}$, which is a scaled density of the receptor molecules. And we have (cf. Eq. (4.19))

$$L_z^0 \sim N^{1/2}b\left(\rho_{\mathrm{R}}Nb^2\right)^{-1/4}. \tag{4.21}$$

Hence we see that if ρ_{R} is kept constant $O(1)$, then the equilibrium occurs at a smaller surface separation compared to the annealed case. For swollen chains, $\nu\approx 3/5$ and $\nu_2=3/4$, the scaling in both scenarios (stretched and confined) also happen to be identical, and the probability for forming a ligand-receptor bridge is $f\sim\rho_{\mathrm{R}}N^{3/2}b^2(L_z/b)^{-1/2}$. The extra $L_z^{-1/2}$ factor suggests that as surfaces get closer, the polymer tether extends further in the direction parallel to the surface (since $\nu_2=3/4>\nu_3\approx 3/5$). The scaled density is given by $\rho_{\mathrm{R}}N^{3/2}b^2$, and the equilibrium separation is (cf. Eq. (4.19))

$$L_z^0 \sim bN^{15/22}\left(\rho_{\mathrm{R}}N^{3/2}b^2\right)^{-3/11} \sim N^{6/22}\rho_{\mathrm{R}}^{-3/11}. \tag{4.22}$$

Finally we can also estimate the interaction force between the surfaces due to binding. For a single bond, when the surfaces are pulled apart till the bond is broken, the total work done by the pulling force is roughly equal to the ϵ, hence we have (for binding fraction f) the average pulling force due to one ligand-receptor bond is

$$\tau \sim f\frac{\epsilon}{L_z^1-L_z^0} \sim \frac{fk_{\mathrm{B}}T}{N^{\nu}b}\left(\frac{\epsilon}{k_{\mathrm{B}}T}\right)^{\nu}. \tag{4.23}$$

4.2.2.2 Analytical calculations for the Gaussian chain

Here we carry out the exact analytical calculations for Gaussian chains. Since the internal partition functions q_{i}' is assumed to be unaffected by the polymer tether, all we need is the translation part of the partition function $q_{\mathrm{i}}^{\mathrm{t}}$ modified by the polymer tether. Using the Green's functions of the polymer

chain we can express $q_{\rm i}^{\rm t}$ as

$$q_{\rm LR}^{\rm t} = \int_{\mathbf{r}} \int_{\mathbf{r}_{\rm R},\mathbf{r}_{\rm L}} G(\mathbf{r},\mathbf{r}_{\rm R};N_{\rm R}) G(\mathbf{r},\mathbf{r}_{\rm L};N_{\rm L}) = \int_{\mathbf{r}_{\rm L},\mathbf{r}_{\rm R}} G(\mathbf{r}_{\rm L},\mathbf{r}_{\rm R};N_{\rm L}+N_{\rm R}); \tag{4.24a}$$

$$q_{\alpha}^{\rm t} = \int_{\mathbf{r}} \int_{\mathbf{r}_\alpha} G(\mathbf{r},\mathbf{r}_\alpha;N_\alpha) \qquad (\alpha = {\rm L},{\rm R}). \tag{4.24b}$$

Here $\mathbf{r}$ is the position of the ligand or receptor group in the space between the surfaces, and $\mathbf{r}_{\rm L}$ and $\mathbf{r}_{\rm R}$ are the positions of the anchoring ends of ligand or receptor tethers. Eq. (4.24) apply to any chain model for the polymer tether (as reflected in the Green's functions), as well as to both annealed and quenched cases: For annealed cases, $\mathbf{r}_{\rm L}$ ($\mathbf{r}_{\rm R}$) is restricted to the membrane whose integral is over a thin layer within distance z_0 from the surface; for the quenched case, it reduces to a summation over the positions of the immobile molecules.

For ideal Gaussian chain model, we can factorize the Green functions,

$$G(\mathbf{r}_1,\mathbf{r}_2;N) = g(\mathbf{u}_1,\mathbf{u}_2;N) h(z_1,z_2;N),$$

where $\mathbf{u}$ and z are the transverse (parallel to the surface) and the longitudinal (perpendicular to the surface) coordinates, and g and h are the transverse and the longitudinal part of the Green's functions. By translational invariance we have

$$g(\mathbf{u}_1,\mathbf{u}_2;N) = g(\mathbf{u}_1-\mathbf{u}_2;N),$$

and

$$\int_{\mathbf{u}_1,\mathbf{u}_2} g(\mathbf{u}_1,\mathbf{u}_2;N) = A \int_{\mathbf{u}} g(\mathbf{u};N).$$

For the end-anchored polymer chain we further assume that $z_0 \ll \sqrt{N}b$, and

$$\int_0^{z_0} dz h(z,z_1;N) \approx z_0 h(z_0,z_1;N) = z_0 h_0(z_1;N).$$

For small enough z_0, its value does not affect the physical quantities of interest, such as the binding constant or the free energy of interactions.

From Eq. (4.1), the binding constant is given by

$$K = K_0 \frac{A q_{\rm LR}^{\rm t}}{q_{\rm L}^{\rm t} q_{\rm R}^{\rm t}} = K_0 \frac{h_0(L_z;N_{\rm L}+N_{\rm R}) \int_{\mathbf{u}} g(\mathbf{u};N_{\rm L}+N_{\rm R})}{\int_{\mathbf{u}} g(\mathbf{u};N_{\rm L}) \int_z h_0(z;N_{\rm L}) \int_{\mathbf{u}} g(\mathbf{u};N_{\rm R}) \int_z h_0(z;N_{\rm R})}. \tag{4.25}$$

For Gaussian chains, $g(\mathbf{u})$ is a Gaussian distribution and the integration over $\mathbf{u}$ yields unity. We are left with

$$K = K_0 \frac{h_0(L_z;N_{\rm L}+N_{\rm R})}{\int_z h_0(z;N_{\rm L}) \int_z h_0(z;N_{\rm R})}. \tag{4.26}$$

The one-dimensional Green's function h_0 for a Gaussian chain confined between surfaces can be analytically solved; details are given in Appendix 4.A.

To highlight the scalings for Gaussian chains, it is convenient to rescale lengths by $\sqrt{N}b$, which is the mean square end-to-end distance. Here we choose to scale all lengths by $\sqrt{N_\mathrm{L}+N_\mathrm{R}}b = \sqrt{N}b$. (As is shown in Appendix 4.A, h_0 scales as a function of $L_z/\sqrt{N}b$.) With this rescaling the (dimensionless) receptor/ligand densities are given by

$$\phi_\alpha = \rho_\alpha N b^2, \tag{4.27}$$

with a dimensionless binding constant

$$\begin{aligned}\frac{\phi_\mathrm{LR}}{\phi_\mathrm{L}\phi_\mathrm{R}} &= \frac{K_0}{Nb^2}\frac{h_0(L_z/\sqrt{N}b)}{\int_z h_0(z/\sqrt{N_\mathrm{L}}b)\int_z h_0(z/\sqrt{N_\mathrm{R}}b)} \\ &= \frac{K_0}{(Nb^2)^{3/2}}\cdot\frac{\sqrt{N}bh_0(l)}{q^\mathrm{t}_\mathrm{L}(l)q^\mathrm{t}_\mathrm{R}(l)}.\end{aligned} \tag{4.28}$$

(Note that h_0 is of dimension [length]$^{-1}$, hence the second factor, which depends on the scaled surface separation $l = L_z/\sqrt{N}b$, is dimensionless.)

In the literature the dissociation constant K_d is frequently reported in unit of M (mol/litre) and a binding energy ϵ_0 is defined as

$$\epsilon_0 = -k_\mathrm{B}T\ln(K_\mathrm{d}/[\mathrm{M}]),$$

which is considered the binding energy measuring the intrinsic binding affinity. For most bound pairs ϵ_0 is found to be 5 to 30 $k_\mathrm{B}T$ (Moore and Kuhl, 2006). In our problem K_0 is given in terms of molecular densities, it is related to K_d as

$$K_0 = K_\mathrm{d}^{-1}N_\mathrm{a}^{-1},$$

where N_a is Avogadro's number.

Eq. (4.28) suggests that for tethered binding, we can define an effective binding energy

$$\ln\frac{\phi_\mathrm{LR}}{\phi_\mathrm{L}\phi_\mathrm{R}} = \frac{\tilde{\epsilon}(l)}{k_\mathrm{B}T} = \frac{\epsilon+\Delta\epsilon(l)}{k_\mathrm{B}T}, \tag{4.29}$$

$$\epsilon = k_\mathrm{B}T\ln\frac{K_0}{(Nb^2)^{3/2}}, \tag{4.30}$$

$$\Delta\epsilon(l) = k_\mathrm{B}T\ln\frac{\sqrt{N}bh_0(l)}{q_\mathrm{L}(l)q_\mathrm{R}(l)}. \tag{4.31}$$

$\Delta\epsilon(l)$ measures the energetic cost due to stretching of the polymer tether; while ϵ accounts for the

binding affinity excluding chain stretching. ϵ is related to ϵ_0 as

$$\epsilon = \epsilon_0 + \ln \frac{10^{-3}\mathrm{m}^3}{(Nb^2)^{3/2}N_\mathrm{a}}. \tag{4.32}$$

For tether lengths in the normal range $Nb \sim 10$nm while $b \sim 0.1$nm, the second term is of order 0.1. One can use either ϵ_0 or ϵ as a measure of the binding affinity in the tethered case; we adopt ϵ for convenience in the discussion of different energetic contributions to the binding.

4.2.3 Immobile receptors and ligands: low-density limit

Since the quenched case (both receptors and ligands are immobile) is qualitatively different from the annealed case, we discuss it in detail in this subsection.

As mentioned above, in this case the physical quantities of interest are averaged over the quenched distributions of the molecules. We assume the quenched distribution is uniform for each molecule on the surface, namely the probability that a particular molecule is found at $\mathbf{r}$ satisfies

$$p(\mathbf{r}_\alpha = \mathbf{r}) = \frac{1}{A}\mathrm{d}^2\mathbf{r}.$$

For each species (ligand or receptor), we assume that the distribution of molecules correspond to a particular realization of the grand canonical distribution controlled by a chemical potential μ,[2] then the probability distribution of samples with given number of molecules n in an area A is given by

$$p(n) = \frac{1}{Q}\frac{\lambda^n q^n}{n!},$$

where $\lambda = e^{\beta\mu}$ and the normalization (grand partition function) is

$$Q = \sum_n \frac{\lambda^n q^n}{n!} = \exp(\lambda q).$$

Hence for the ligand-receptor system, the quenched average free energy is given by

$$\bar{F} = \sum_{m_\mathrm{L}, m_\mathrm{R}} p(m_\mathrm{L}) p(m_\mathrm{R}) \left\langle F(m_\mathrm{L}, m_\mathrm{R}) \right\rangle. \tag{4.33}$$

The chemical potential is related to the (thermodynamic average) number density of molecules as

$$\rho_\alpha^{(0)} = \frac{1}{A}\frac{\partial \ln Q}{\partial \mu_\alpha} = \frac{\lambda_\alpha q_\alpha}{A}. \tag{4.34}$$

[2]Here we temporarily omit the subscript α for convenience.

Putting this back into Eq. (4.33) we have

$$\begin{aligned}\bar{F} &= \frac{1}{e^{A\rho_{\rm L}^{(0)}+A\rho_{\rm R}^{(0)}}}\sum_{m_{\rm L},m_{\rm R}}\frac{(A\rho_{\rm L}^{(0)})^{m_{\rm L}}(A\rho_{\rm R}^{(0)})^{m_{\rm R}}}{m_{\rm L}!m_{\rm R}!}\left\langle F(m_{\rm L},m_{\rm R})\right\rangle \\ &= A\left[\mathcal{F}^{(1,1)}\rho_{\rm L}^{(0)}\rho_{\rm R}^{(0)}+\mathcal{F}^{(1,2)}\rho_{\rm L}^{(0)}{\rho_{\rm R}^{(0)}}^2+\mathcal{F}^{(2,1)}{\rho_{\rm L}^{(0)}}^2\rho_{\rm R}^{(0)}+\cdots\right].\end{aligned} \tag{4.35}$$

(Note that we have reserved $\bar{F}$ for the "grand canonical average" and $\langle F(m_{\rm L},m_{\rm R})\rangle$ can be regarded as the "canonical average" free energy with given number of molecules, $m_{\rm L}$ and $m_{\rm R}$. It is easy to see that the largest term in the series in Eq. (4.35) has $m_{\rm L}=A\rho_{\rm L}^{(0)}$ and $m_{\rm R}=A\rho_{\rm R}^{(0)}$, therefore in the thermodynamic limit, the canonical average $< F >$ should be equal to the grand canonical average $\bar{F}$.) In Appendix 4.B we present the calculations for $\mathcal{F}^{(n,m)}$ up to $n=2,m=2$. The binding fraction is most conveniently obtained by taking the derivative of F with respect to $\beta\epsilon$ (or $\ln K$).

Despite that the expansion is asymptotic, the leading-order results are usually qualitatively accurate well beyond the range of densities in which the series is convergent, and here we present the results

$$\bar{F}=\bar{F}_{\rm b}(\text{binding})+F_{\rm r}(\text{repulsion})$$

$$\bar{F}_{\rm b}=-A\rho_{\rm L}^{(0)}\rho_{\rm R}^{(0)}\int_{\mathbf{u}}\ln\left\{1+\frac{3}{2\pi}\exp\left[\beta\tilde{\epsilon}(l)-\frac{3u^2}{2Nb^2}\right]\right\}, \tag{4.36a}$$

$$F_{\rm r}=-Ak_{\rm B}T\left[\rho_{\rm L}^{(0)}\ln\frac{q_{\rm L}^{\rm t}(L_z)}{q_{\rm L}^{\rm t}(\infty)}+\rho_{\rm R}^{(0)}\ln\frac{q_{\rm R}^{\rm t}(L_z)}{q_{\rm R}^{\rm t}(\infty)}\right], \tag{4.36b}$$

$$\bar{\rho}_{\rm LR}=\frac{2\pi}{3}Nb^2\ln\left(1+\frac{3}{2\pi}e^{\beta\tilde{\epsilon}}\right)\rho_{\rm L}^{(0)}\rho_{\rm R}^{(0)}. \tag{4.36c}$$

4.3 Results and discussion

In this section we discuss the key features of binding between polymer-tethered ligands and receptors, and the overall interactions between surfaces mediated by these polymers. To focus on the key aspects of the problem without complications due to other interactions we assume the ideal-Gaussian-chain model. As discussed at the end of Section 4.2.2, after rescaling by the ideal end-to-end distance of the polymer tether, we obtain the dimensionless quantities as listed in Table 4.3 (cf. Table. 4.1 for definitions of the variables).

Table 4.3: Scaled variables

surface separation	$l=L_z/\sqrt{N}b$
densities	$\phi_{\rm i}=\rho_{\rm i}Nb^2$
binding affinity	$\epsilon=k_{\rm B}T\ln\left[K_0/(Nb^2)^{3/2}\right]$
tether fraction	$x_\alpha=N_\alpha/(N_{\rm L}+N_{\rm R})$, $(\alpha={\rm L},{\rm R})$

Before the discussion, it is informative to estimate the values of these parameters. The aver-

age number of ligand/receptor molecules is $10^5 \sim 10^7$ per cell, and the average area of a cell is $10^{-7} \sim 10^{-6}\text{cm}^2$: these give the average area densities of receptors/ligands $\rho \sim 10^{12}/\text{cm}^2$. The average tether length (contour length) of integrins and selectins on lymphocyte cells is of order 10nm (Springer, 1990), which is comparable to the estimation in the Bell papers (Bell, 1978; Bell et al., 1984; Torney et al., 1986). Assuming the monomer size b to be $\sim 10^{-8}$cm we find

$$\phi \sim 10^{12} \cdot 10^{-6} \cdot 10^{-8} = 10^{-2},$$

which gives the overall (dimensionless) density of molecules on the cell surface. In other cases (e.g., a cell adhering to a large surface) where the adhesion zone is an open system (a small part of the whole surface), we estimate that $\phi \sim O(1)$ within the focal zone, and $\phi \sim 0.001$ outside the contact area (the reservoir) due to depletion of ligands and receptors.

The binding constant K_0 can be obtained from the dissociation constant K_d. In Dustin et al. (1996) the dissociation constant was found to be $K_\text{d} = 6\mu M$, and the binding constant is $K_0 = (K_\text{d} N_\text{a})^{-1} \approx 10^{-16}\text{cm}^3$, which corresponds to a binding energy (in unit of $k_\text{B}T$)

$$\ln \frac{K_0}{(Nb^2)^{3/2}} \approx \ln 10^5 \approx 12$$

in our definition. Bell et al. (1984) estimated the 2D binding constant to be $K^{2\text{D}} \sim 10^{-8}\text{cm}^2$, which gives a binding energy

$$\frac{\epsilon}{k_\text{B}T} = \ln \frac{K^{2\text{D}}}{(Nb^2)} \approx \ln 10^6 \approx 14$$

in our definition. Moore and Kuhl (2006) compiled a list of experimentally measured physical parameters of ligand-receptor binding and it was quoted that the average binding energy ϵ_0 (cf. Eq. (4.32)) of all available ligand-receptor pairs is about $15k_\text{B}T$. The numerical values of ϵ_0 and ϵ are comparable; in our calculations we take ϵ to be $10k_\text{B}T$ or $15k_\text{B}T$.

In the discussions we proceed as follows. In Section 4.3.1 we study the effects of polymer tether on specific binding and non-specific repulsion. In particular we examine the dependence of binding on the tether fractions x_L and x_R. In Section 4.3.2, we discuss in detail the interactions between surfaces mediated by ligand-receptor binding. We consider the following cases for the receptors and ligands: I. Quenched (both ligands and receptors are immobile); II. "Both closed" (either ligands or receptors are mobile, but both with fixed densities); III. "Open-closed" (ligands are connected to a reservoir, and receptors have a fixed density (either mobile or immobile), or vice versa); IV. "Both open" (both ligands and receptors are connected to a reservoir). Hereafter we will refer to these different scenarios as "case I" to "case IV."

We focus on the free energy of interaction and the average number of bound pair per ligand/receptor ("binding fraction"). In particular we discuss features including the dependences

of the equilibrium separation and the minimum free energy on the binding energy and the molecular densities; scaling relations are tested by analytical calculations. In addition we also study the equilibrium force-extension curve between the surfaces. Finally in Section 4.3.3, we study several systems combining different types of specific and non-specific interactions, including ligand-receptor pairs with different tether lengths or binding affinities, and additional repelling polymers between surfaces.

4.3.1 Effects of the polymer tether on specific binding and non-specific interactions

From Eqs. (4.29) and (4.62) we see that the binding affinity in both quenched and annealed cases is measured by the separation-dependent effective binding energy

$$\frac{\tilde{\epsilon}(l)}{k_{\rm B}T} = \frac{\epsilon}{k_{\rm B}T} + \ln \frac{\sqrt{N}bh_0(l)}{q_{\rm L}^{\rm t}(l)q_{\rm R}^{\rm t}(l)}.$$

Since ϵ is only weakly dependent on the chain length (cf. Table. 4.3), the dependence in the binding affinity is primarily contained in the scaled surface separation $l = L_z/\sqrt{N}b$ in the second term. In Appendix 4.A.1 we have worked out the close-form expressions for the second term in the asymptotic limits of large and small separations

$$\frac{\tilde{\epsilon}(l) - \epsilon}{k_{\rm B}T} \simeq \begin{cases} \ln \dfrac{\pi^2}{8l} & (l \ll 1), \\ \ln \left[3\sqrt{6\pi} l^2 e^{-3l^2/2} \sqrt{x_{\rm L} x_{\rm R}}\right] & (l \gg 1). \end{cases} \tag{4.37}$$

The effective binding constant (for the annealed case) is given by

$$K = \frac{\rho_{\rm LR}}{\rho_{\rm L}\rho_{\rm R}} = Nb^2 e^{\beta\tilde{\epsilon}(l)},$$

and from Eqs. (4.37) this becomes

$$K \propto \begin{cases} \dfrac{K_0}{l\sqrt{N}b} = \dfrac{K_0}{L_z} & (l \ll 1), \\ \dfrac{K_0}{\sqrt{N}b} l^2 e^{-3l^2/2} & (l \gg 1). \end{cases} \tag{4.38}$$

Bell and co-workers (Bell, 1978; Bell et al., 1984; Torney et al., 1986) suggested that the 2D binding constant should be related to the 3D binding constant as

$$K = \frac{K_0}{L_z}.$$

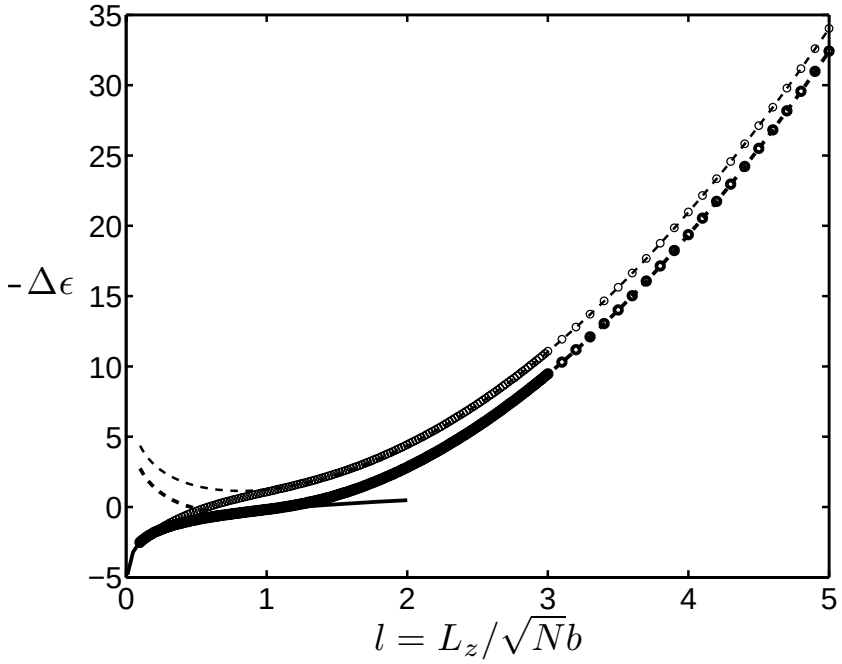

Figure 4.2: The contribution to the effective binding energy due to tether stretching: $-\Delta\epsilon = \epsilon - \tilde{\epsilon}(l)$. Here $-\Delta\epsilon$ is given in unit of $k_{\rm B}T$ and plotted against scaled surface separation $l = L_z/\sqrt{N}b$. Dash lines and the solid line are results from the asymptotic expressions in the limits $l \gg 1$ and $l \ll 1$, respectively; circles are from exact solutions. The thick dash line and circles are for equal tether lengths ($x_{\rm L} = x_{\rm R} = 0.5$), and the thin line and circles for a tether length ratio of $1 : 99$. In all calculations the total tether length $N = N_{\rm L} + N_{\rm R}$ is kept constant.

Our calculation establishes that this is valid only when surfaces are close enough, i.e., the surface separation is less than the ideal size of the tethered ligand-receptor bridge. When surfaces are far separate, the second expression implies a large stretching energy cost. Therefore one should be careful when inferring 2D binding constant from the 3D experimental data[3].

In Fig. 4.2 we plot $-\Delta\epsilon = \epsilon - \tilde{\epsilon}(l)$ in units of $k_{\rm B}T$ against the scaled surface separation $l = L_z/\sqrt{N}b$. (Here $-\Delta\epsilon$ can be interpreted as the free energy cost due to tether stretching.) We choose two different tether length ratios ($x_{\rm L}$): the thick lines and circles represent the case with equal tether lengths, $x_{\rm L} = x_{\rm R} = 0.5$; while the thin lines and circles are for the case with $x_{\rm L} = 0.01$ (equivalent to $x_{\rm R} = 0.01$ by symmetry). Here the circles represent results from exact solutions, dash lines are from the approximate expressions for large separations and the solid line is for small separations (in the latter case the results only depend on the total tether length and are identical in both cases).

For the whole range of surface separations the approximate expressions work remarkably well. In particular, the stretching energy cost is given by $3l^2/2$ to the leading-order, as was given by scaling

[3]In real situations the polymer tethers are probably not Gaussian, however, our scaling analysis (cf. Section 4.2.2.1) showed that the stretching regime and the confinement regime are qualitatively different, therefore it is impossible to have one expression valid for these different regimes.

arguments (de Gennes, 1979). We can define the onset of binding l_1 as where $\tilde{\epsilon} \gtrsim 0$, whence the density of bound pairs starts to increase significantly. Assuming that at l_1 the polymer tether is stretched, we can estimate l_1 as (from the asymptotic expression in the strong stretching limit)

$$l_1 = \frac{L_z}{\sqrt{N}b} \sim \sqrt{\epsilon/k_{\rm B}T} > 1, \tag{4.39}$$

which justifies our assumption *a posteriori*. Therefore for $\epsilon \gg k_{\rm B}T$, the tether chains are considerably stretched when ligand-receptor bridges start to form.

From Fig. 4.2 we also see that with total tether length $N = N_{\rm L} + N_{\rm R}$ fixed, binding is optimal if ligand and receptor tether lengths are equal; the difference between different tether ratios vanishes at small surface separations as can be inferred from Eq. (4.37). The $3k_{\rm B}T$ difference is purely an entropic effect, and allows the fine tuning of the binding affinity at intermediate or large surface separations without affecting the short-range behavior. This feature is especially relevant near the onset of binding, where $\tilde{\epsilon} \approx 0$, and a small difference in $\Delta\epsilon$ can result in a large change in l_1.

Another contribution from the polymers is the repulsion between surfaces due to the confinement of polymer segments. Figure 4.3 shows the dependence of the repulsive free energy on the surface separation for a single polymer with ideal end-to-end distance Nb^2.

From Appendix 4.A.1 we have obtained[4]

$$\frac{F_{\rm r}}{k_{\rm B}T} \simeq \begin{cases} -\ln\dfrac{4z_0}{l\sqrt{N}b} + \dfrac{\pi^2}{6l^2} & l \ll 1, \\ \\ -\ln\dfrac{4z_0}{\sqrt{N}b} - \ln\dfrac{\sqrt{6}}{4\sqrt{\pi}} & l \gg 1. \end{cases} \tag{4.40}$$

The constant in the limit $l \gg 1$ gives the free energy of confining a single Gaussian chain in half space, while the result for $l \ll 1$ scales as $1/l^2$, as is inferred from scaling arguments.

While the stretching energy cost flattens off at small surface separations, the repulsive free energy ($\sim 1/l^2$) increases sharply and dominates over the binding energy. On the other hand the stretching energy grows as l^2 at large separations and prohibits binding at large l. The net effect results in a total free energy minimum attained around $l = 1$, with low stretching energy and not too strong repulsion due to confinement. Next we discuss the total interaction due to tethered binding in different physical scenarios.

[4]In Fig. 4.3 we have substracted out the first term in Eqs. (4.40) involving the anchoring distance z_0, which is a constant for given chain length.

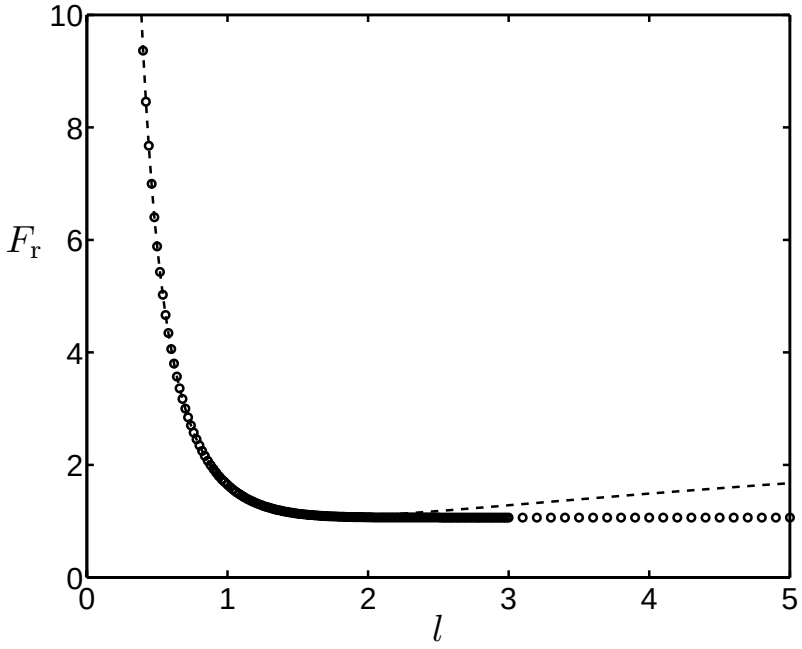

Figure 4.3: The free energy of confining a polymer between parallel surfaces. Circles are results from exact solutions and the dash line is from the asymptotic expression for $l \ll 1$.

4.3.2 Interactions between surfaces mediated by ligand-receptor binding

In this subsection we study 4 different scenarios according to the different mobilities of the species: case I (quenched), case II (both closed), case III (open-closed), and case IV (both open). The expressions for the density of bound molecules and the free energy of interactions are given by (cf. Table. 4.2) Eqs. (4.36) for the quenched case (case I), Eqs. (4.10) and (4.12) for the both-closed system (case II), Eqs. (4.13) and (4.14) for the open-closed system (case III), and Eqs. (4.8) and (4.9) for the both-open system (case IV).

While the quenched case applies to interacting surfaces with immobile molecules unambiguously, the different annealed cases can be difficult to distinguish. In particular we note that if one species is mobile, the thermodynamics is the same whether the other species with a fixed density are immobile or mobile. In reality a closed system (as in case II or case III) is best associated with surfaces with uniformly distributed molecules, such as lipid bilayers supported on flat substrates. An open system, on the other hand, corresponds to an inhomogeneous system with partial contact, such as flexible membranes or lipid bilayers supported on spherical particles. In these cases the non-contact part of the surface serves as a reservoir for the part in contact. Some typical examples of each cases are listed in Table. 4.3.2.

Here we focus on two quantities. The binding fraction f is defined as the number of bound

Table 4.4: Examples of different cases

Case I (quenched)	polymersomes, solid substrates, colloidal particles with attached polymers
Case II (both closed)	substrate-supporting lipid bilayers and monolayers
Case III (open-closed)	flexible membranes interacting with surfaces covered by immobile molecules
Case IV (both open)	flexible membranes, spherical vesicles

molecules divided by the number of molecules:

$$f = \frac{\rho_{\mathrm{LR}}}{\min(\rho_{\mathrm{L}}^{(0)}, \rho_{\mathrm{R}}^{(0)})};$$

the free energy per molecule is defined by

$$F(l) = \frac{\Delta F}{A \min(\rho_{\mathrm{L}}^{(0)}, \rho_{\mathrm{R}}^{(0)})},$$

which measures the strength of binding interactions between ligands and receptors. The definition of $F(l)$ coincides with the definition by Bell et al. (1984), and also allows a comparison with the single-chain calculation in our previous paper (Martin et al., 2006). To avoid ambiguity we choose $\rho_{\mathrm{L}}^{(0)} = \rho_{\mathrm{R}}^{(0)} = \rho$ ($\phi_{\mathrm{L}}^{(0)} = \phi_{\mathrm{R}}^{(0)} = \phi^{(0)}$) in our calculations. If both species are connected to a reservoir, then the density of bound pairs ρ_{LR} can be significantly higher than the reservoir densities $\rho_{\mathrm{L}}^{(0)}$ or $\rho_{\mathrm{R}}^{(0)}$; in this case f and F lose the meaning of "binding fraction" or "free energy per ligand or receptor," but purely serve as a comparison to the other cases (I, II, and III).

First we compare the different annealed cases (II, III, IV) where molecules are mobile. In Fig. 4.4, we show results for case II (thin lines) and case III (thick lines) with densities $\phi_{\mathrm{L}}^{(0)} = \phi_{\mathrm{R}}^{(0)} = 0.01$. The binding energy is taken to be $\epsilon = 10 k_{\mathrm{B}} T$ and equal tether lengths for ligands and receptors are assumed. We see that for $l \geq 0.5$, both cases are similar. In case III the binding fraction f saturates at a larger surface separation than in case II. In particular, near $l = 1$ the binding fraction is close to unity even for a lower reservoir density $\phi^{(0)} = 0.001$ (results not shown here). This indicates that molecules in the reservoir can be attracted into the system and bind with their counterparts; near the equilibrium bound state, the density of bound pairs is insensitive to the average density of ligands or receptors in the reservoir, but is determined from the binding constant and the (maximum) fixed density—this is consistent with the experimental observations by Dustin et al. (1996).

As surfaces come closer ($l < 1$), molecules start to feel the repulsion from the surfaces and are squeezed out from the contact area. At very small $l (< 0.5)$, the confinement repulsion dominates, and in case III even bound pairs are broken and molecules are pushed out into the reservoir; accordingly f drops to zero. In this regime of case III, the total interaction energy is the sum of the confinement free energy of the molecules remaining in the system and the osmotic pressure from the reservoir.

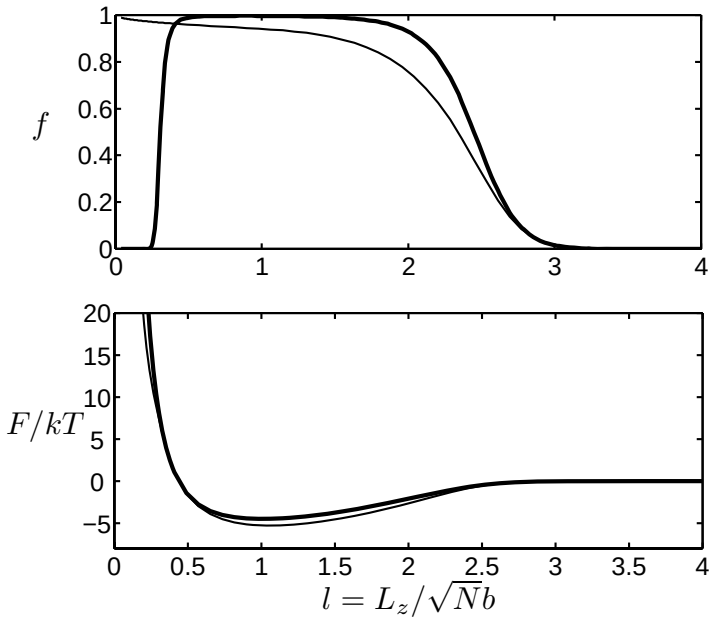

Figure 4.4: Comparison of case II ("both closed" system) and case III ("open-closed" system). The binding fraction f and the interaction free energy F are plotted against the scaled surface separation $l = L_z/\sqrt{N_{\rm L}+N_{\rm R}}b$. Thin solid lines are results for case II with $\phi^{(0)} = \rho_{\rm L}^{(0)}(N_{\rm L}+N_{\rm R})b^2 = 0.01$, ($\rho_{\rm L}^{(0)} = \rho_{\rm R}^{(0)}$); thick lines are for case III with the same densities. All calculations are for a binding energy $\epsilon = 10k_{\rm B}T$ and equal tether lengths.

We see that the free energy of interaction is always lower compared with case II due to the extra degrees of freedom of the species connected to a reservoir.

In Fig. 4.5 we compare case III ("open-closed") and case IV ("both open"). The binding energy is $\epsilon = 10k_{\rm B}T$, and all the densities are $\phi_{\rm L}^{(0)} = \phi_{\rm R}^{(0)} = 10^{-3}$. Here thin lines are for case III and thick lines for case IV; the dot line in Fig. 4.5(a) is the density of free (unbound) molecules with a reservoir. (From Eq. (4.13) if the reservoir densities are equal, the density of free molecules is the same in case III and case IV.) In both cases we see that as surfaces approach each other, free molecules are pushed out, while the densities of bound molecules hit a maximum near $l = 1$, close to the free energy minimum. But in the "both-open" system, we see a great enhancement of the local densities since both types of molecules can flow into the system due to binding attraction. As surfaces come even closer, both receptors and ligands are pushed out, the free energy in the "both open" system flattens off at $F = 2k_{\rm B}T$, which is the total osmotic pressure from the reservoir.

Next we compare the annealed case (case II) and the quenched case (case I) and discuss the features of binding in more detail.

Figure 4.6 shows F and f for case I (quenched) and case II (both closed) with scaled densities $\phi_{\rm L}^{(0)} = \phi_{\rm R}^{(0)} = 0.01$: the solid lines are results for case II; for the quenched case, the dash lines are results from the leading-order density expansion [$O(\phi_{\rm L}\phi_{\rm R})$], and circles are from expansions up to quartic order[$O(\phi^4)$]. To ensure accuracy of the density expansion, we choose a modest binding

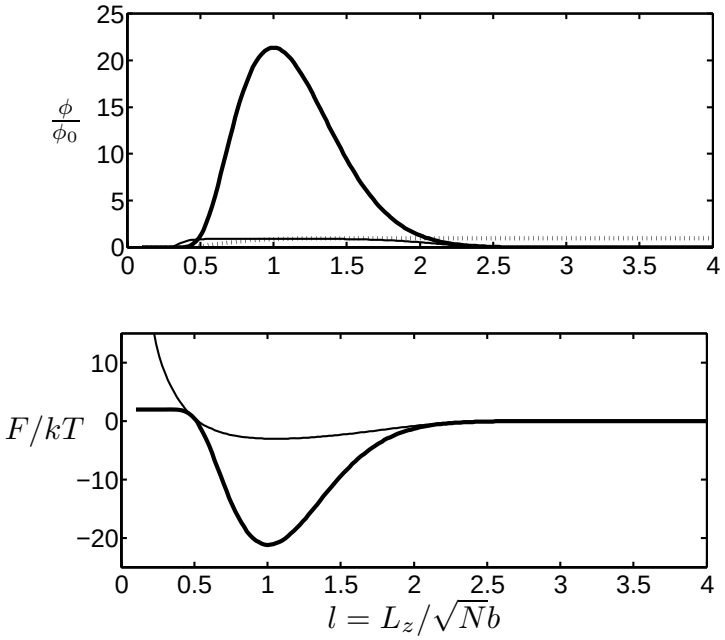

Figure 4.5: Comparison of case III ("open-closed") and case IV ("both open"). In either case all densities are chosen to be $\phi^{(0)} = 10^{-3}$. Upper figure shows densities of molecules relative to the reservoir density: the dot line represents the relative density of free molecules, thin and thick solid lines represent the relative densities of bound pairs for case III and case IV. Lower figure: Total free energy of interaction for case III (thin solid line) and case IV (thick solid line). The molecular binding energy is $\epsilon = 10k_{\rm B}T$.

energy $\epsilon = 10k_{\rm B}T$.

In both cases, we see that the binding fraction f starts to increase around $L_z/\sqrt{N}b = 3.5$, which corresponds to the onset of binding. At the onset of binding, very few bound ligand-receptor pairs are sparsely distributed and the situation is similar to isolated non-interacting ligand-receptor pairs, therefore the scaling dependence of l_1 on ϵ should be identical to that for a single ligand-receptor pair, $l_1 = L_z^1/\sqrt{N}b \sim \sqrt{\epsilon/k_{\rm B}T}$, as discussed previously. Indeed this scaling estimate gives $l_1 \approx 3.2$ for the Gaussian chain model, quite close to the exact results[5].

In the annealed case, as surfaces come closer, the binding fraction first increases rapidly and then gradually approaches unity, whence most molecules are bound. In the latter regime the separation between the surfaces is comparable to the size of the connected polymer tether, and ligand and receptor groups can reach anywhere between the surfaces with almost equal probability—put in other words, their densities are almost uniform in the space between the surfaces. This implies that the 2D binding constant K is related to the 3D constant K_0 as $K = K_0/L_z$. On the other hand, as surfaces come even closer the polymers start to feel stronger confinement from the surfaces, which contributes a repulsive free energy scaling as $1/l^2$ for Gaussian chains. The balance between

[5]Of course, for very strong binding $\beta\epsilon \gg 1$, we have $l_1 \gg 1$ and the Gaussian chain model becomes inaccurate. In this regime the finite extensibility of the polymer chain should be accounted for.

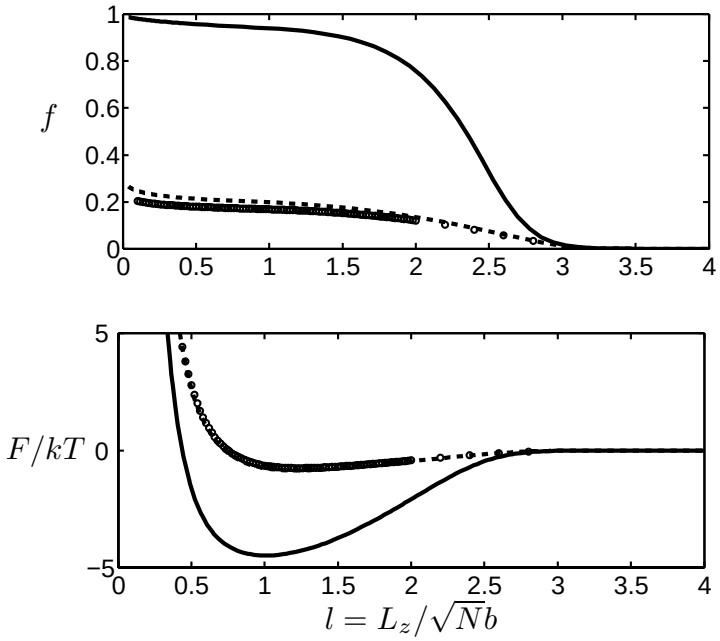

Figure 4.6: Comparison of case I ("quenched") and case II ("both closed"). Solid lines are for case II (mobile ligands and receptors with fixed densities), and dash lines are for case I (immobile ligands and receptors) from leading-order density expansion; Circles are results for the quenched case from second-order density expansion. The binding energy is $\epsilon = 10k_{\rm B}T$ and both ligands and receptors have a density $\phi^{(0)} = 0.01$.

the attractive binding and the repulsive confinement leads to a free energy minimum at $l_0 \approx 1$. Single-bound-pair scaling applies here as well because in this regime most molecules are bound, hence $f \approx 1$. For weaker binding such that the binding fraction has a substantial dependence on l, the equilibrium separation l_0 will also depend on ϵ, as will be discussed below.

We now investigate the quenched case. As discussed in Section 4.2.1, the free energy is averaged over the random distributions of the molecules. The generic repulsion due to confinement is independent of the relative positions of ligands and receptors; the quenched average is only invoked for the binding part. By the convexity of the free energy,

$$F_{\rm q} = -k_{\rm B}T\Big\langle \ln Q \Big\rangle \geq -k_{\rm B}T \ln\Big\langle Q \Big\rangle = F,$$

i.e., the quenched average is always larger than the annealed average. Hence the bound state in a quenched system has a higher free energy, and binding is less probable compared to the annealed case.

At least two factors contribute to the reduced tendency of binding between immobile molecules at low densities[6]. First, at low densities the anchoring ends of ligands and receptors are far apart, therefore the tether chains have to be laterally stretched for ligands and receptors to bind. This

[6]At high densities the quenched case should approach the annealed case.

lateral stretching adds an extra energetic cost to binding, and is only dependent on the densities and the tether lengths of the molecules. Another effect is due to the local inhomogeneity in molecule distributions[7]: due to fluctuations in the quenched distributions, locally there could be more ligands than receptors or vice versa, and the excess ones have no counterparts nearby, and remain unbound; while in the annealed case, these molecules can move around to locate their counterparts.

In the Gaussian chain model, the polymer chain is infinitely extensible. We can estimate the average number of molecules within an"accessible" distance as[8]

$$\rho R^2 = \rho N b^2 \epsilon / k_{\rm B}T = \phi\epsilon/k_{\rm B}T,$$

where the binding energy gain ϵ enables the tether to stretch farther to form a bridge. This gives an estimate for the maximal binding fraction, $f \lesssim \phi\epsilon/k_{\rm B}T$, which is attained when surfaces are very close. For reasonable values of ϵ with small ϕ it is always less than unity[9].

We also note that the asymptotic density expansion is accurate if the surface densities $\phi_{\rm L}, \phi_{\rm R}$ are small and binding energy is not too big. Since the density expansion is carried out around the no binding state, an empirical criterion is given by $\phi\epsilon/k_{\rm B}T < 1$, corresponding to the "weak" binding scenario. We see that the leading-order expansion is fairly accurate compared with the higher-order expansion (up to $O(\phi^4)$). Since we are mostly interested in the low-density regime when the quenched case and the annealed cases are most different, we shall use the leading-order result throughout the rest of the paper. From the leading-order expansion we have

$$\bar{\rho}_{\rm LR} \propto \rho_{\rm L}^{(0)} \rho_{\rm R}^{(0)} N b^2 \tilde{\epsilon},$$

this should be distinguished from the conventional binding equilibrium,

$$\rho_{\rm LR} \propto (\rho_{\rm L}^{(0)} - \rho_{\rm LR})(\rho_{\rm R}^{(0)} - \rho_{\rm LR}) e^{\beta\tilde{\epsilon}}.$$

In general there is no well-defined binding constant for the quenched case, especially when higher order terms $O(\phi^3)$ and $O(\phi^4)$ are relevant.

To summarize the binding favorability in different scenarios, we have

Both open $\gg$ open-close $\gtrsim$ both close $>$ quenched.

The difference is the entropic effect due to flexible polymers as well as to the diffusion of molecules in the reservoir. To better illustrate the difference between these cases, we plot in Fig. 4.7 the free

[7]This is briefly commented on by Moreira et al. (2003).

[8]When the surface separation is large, ϵ should be replaced by $\tilde{\epsilon}$ to account for the stretching energy.

[9]For finitely extensible chains, as in our previous paper (Martin et al., 2006), there is a strict upper bound set by the average number of molecules within the maximal extension in the limit of $\beta\epsilon \to \infty$, which is completely determined by the molecular density and maximal tether extension.

energy of binding and the binding fraction against the density of one species (receptors or ligands) while keeping the other fixed $\phi^{(0)} = 0.01$ (F and f is normalized to this fixed density). We see that for the quenched case the free energy and binding fraction increases almost linearly with the density, the slope is small, reflecting the restricted availability of binding molecules. In case II and case III where the maximum density of bound pairs is set by the fixed density of one species, as the density of the other species increases, f first increases exponentially but then approaches saturation. In case IV, the increase is linear all the way with a much larger slope that is proportional to K (cf. Eqs. (4.8) and (4.9)); this reflects a positive feedback effect: increasing the density of one species automatically attracts more molecules of the other species from the reservoir.

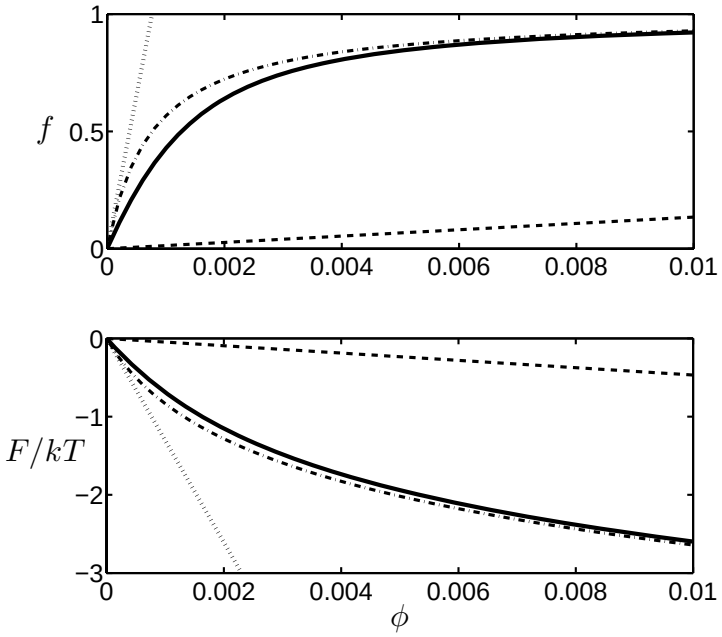

Figure 4.7: Dependence of the binding fraction and the free energy on the density of molecules for case I (dash line), II (solid line), III (dash dot line), and IV (dot line). The binding energy is $\epsilon = 10k_{\mathrm{B}}T$; receptors and ligands have equal tether lengths, one species has a fixed density $\phi^{(0)} = 0.01$, while the other has a varying density. The free energy and the binding fraction are calculated for a fixed surface separation $l = 1$ ($L_z = \sqrt{N}b$), which is near the equilibrium position (cf. Fig. 4.8).

Next we focus on the features related to the equilibrium separation l_0 and the equilibrium (minimum) free energy. From our scaling analysis in Section 4.2.2, for Gaussian chains the interaction free energy (per bound pair) can be written as

$$\frac{F}{k_{\mathrm{B}}T} \approx -f\left(\frac{\epsilon}{k_{\mathrm{B}}T} - C_1 l^2\right) + \frac{C_2}{l^2}.$$

The first term gives the total stretching and binding energy, while the second term measures the repulsion due to confinement. Assuming that f has a weaker dependence on l compared with the

stretching energy and the confinement repulsion[10], we obtain the equilibrium separation as

$$l^0 \approx f^{-1/4},$$

and the minimum free energy

$$\frac{F_{\min}}{k_{\rm B}T} \approx -f\frac{\epsilon}{k_{\rm B}T} + C_3 f^{1/2}.$$

The only dependence of l_0 on the binding energy is contained in f. From previous discussions we have seen that for reasonably large binding energy, f is close to unity near the equilibrium position in the annealed cases, therefore in these scenarios we expect l_0 to reach a constant if $\epsilon/k_{\rm B}T \gg 1$, this is indeed true as shown from in Fig. 4.8.

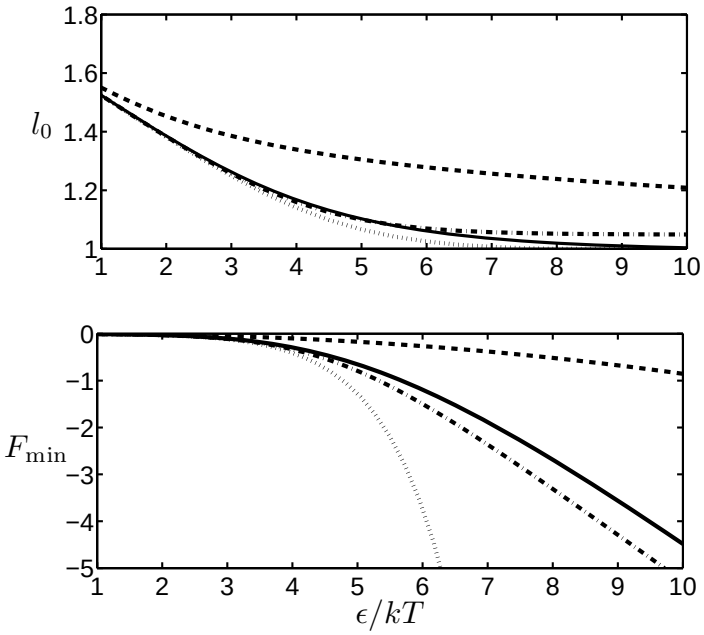

Figure 4.8: The dependence of the equilibrium separation and free energy on the molecular binding energy for case I (dash line), II (solid line), III (dash dot line), and IV (dot line). Ligands and receptors have equal tether length, with densities $\phi^{(0)} = 0.01$.

In Fig. 4.8 we plot l_0 and the equilibrium free energy for different binding energies. Broken lines represent the quenched case, solid lines for case II (both closed), dash-dot lines for case III (open-closed), and dot lines for case IV (both open). The receptors and ligands have equal tether lengths, with equal density $\phi_{\rm L}^{(0)} = \phi_{\rm R}^{(0)} = 0.01$. We observe that for the annealed cases in which the binding fractions reach unity in the strong binding regime, l_0 approaches 1, where the total energy due to stretching and confinement is minimized. In the free energy plot, we see that in case II and case III, for large ϵ the free energy curves approach linear with slope 1, reflecting that in this regime

[10]Indeed $f \sim 1$ near the equilibrium separation in case II and case III, $\partial f/\partial L \simeq 0$ in case IV, and in the quenched case $f \propto \epsilon$ with a logarithmic dependence when $l \simeq 1$.

most molecules are bound ($f \approx 1$); in the both-open system, the free energy has an exponential increase due to the incoming molecules from the reservoirs.

On the other hand the quenched case is essentially different. From above we have the estimate that $f \leq \phi\epsilon/k_{\rm B}T$, therefore $f \ll 1$ for the range of ϵ we choose. Naive estimate for l_0 gives $l_0 \sim f^{-1/4} \sim \epsilon^{-1/4} > 1$, which would be true only if f is independent of l. Even though the latter assumption does not hold in this regime, the qualitative trends still hold: we indeed observe that l_0 is bigger than in the annealed cases and decreases as ϵ increases.

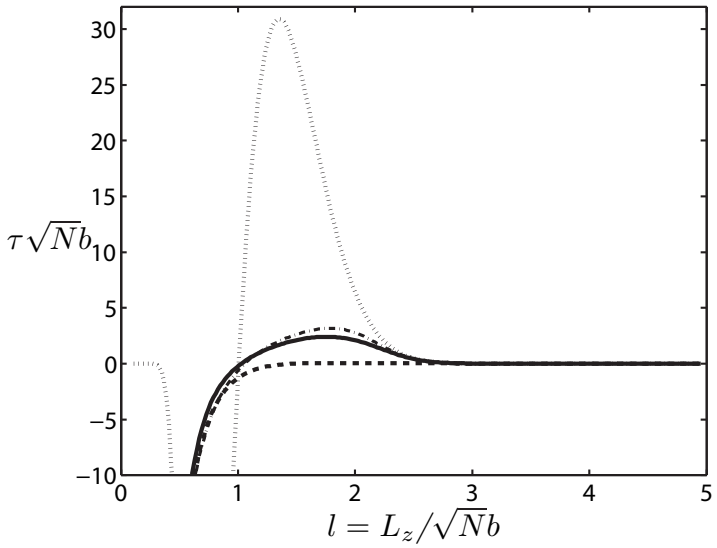

Figure 4.9: The force-extension curve for case I (dash line), II (solid line), III (dash-dot line), and IV (dot line). The binding energy is $\epsilon = 10k_{\rm B}T$ and the molecular densities are $\phi_{\rm L}^{(0)} = \phi_{\rm R}^{(0)} = 0.01$.

Finally from the interaction potential we calculate the equilibrium force defined as

$$\tau = \frac{\partial F}{\partial L_z}.$$

τ measures the force between the surfaces at a given surface separation in a quasi-equilibrium state. (We adopt the convention that τ is positive if the surfaces are attracting each other, i.e., one needs to exert force to pull the surfaces apart.) In Fig. 4.9 we plot $\tau\sqrt{N}b$ against the scaled surface separation l. If we neglect the weak dependence of ϵ on N, this is a scaling plot for $\tau\sqrt{N}b$ against l. One immediately sees that τ scales as $N^{-1/2}$ against the tether length, reflecting the finite range of binding attraction mediated by the polymer tether. The maximum in the force-extension curve corresponds to the critical pulling force above which the bond will be broken even in the quasi-equilibrium state (without fluctuations), which gives an upper bound of the bridging force (Moore

and Kuhl, 2006). From scaling arguments we would expect

$$\tau_{\rm c} \sim \frac{f\beta\epsilon}{l_1 - l_0} \sim f\left(\frac{\epsilon}{k_{\rm B}T}\right)^{1/2} N^{-1/2}.$$

For tether length $\sqrt{N}b \sim 3$nm and $\rho \sim 10^{-1}\text{nm}^{-2}$, $1k_{\rm B}T$ in Fig. 4.9 corresponds to a force per unit area 3.7 N/m^2. Therefore the critical stresses in different cases are 2N/m^2 (case I), 15N/m^2 (case II, III), and 100N/m^2 (case IV). The values are comparable to the results reported by Moore and Kuhl (2006), but larger than their values which are around $4\text{N}/m^2$. However, the polymer tether is significantly stretched in the experiments by Moore and Kuhl (2006) therefore the Gaussian chain approximation is invalid. In this strong stretching regime, the critical tension is approximately

$$\tau_{\rm c} \sim \frac{f\epsilon/k_{\rm B}T}{l_1 - l_0} \sim f\left(\frac{\epsilon}{k_{\rm B}T}\right) N^{-1}.$$

In summary, the interactions between surfaces due to ligands and receptors include the generic repulsion due to confinement and the specific attraction due to binding. The magnitude of the binding attraction is determined by the microscopic binding affinity, the tether lengths, and the molecular densities, through an effective binding constant and the scaled molecular densities. The net effect of binding attraction and confinement repulsion results in a free energy minimum at a surface separation comparable to the ideal size of a tethered bridge.

When one or both species are connected to a reservoir, molecules can be attracted into or pushed out of the system according to the interaction potential. Qualitatively different is the case when molecules are immobile. The free energy cost due to lateral stretching makes binding much less probable, resulting in a binding fraction considerably less than unity.

We further notice that in all these cases, the onset of binding (where the binding fraction starts to increase considerably) appears to be identical, reflecting the binding energy ϵ as a universal measure of binding strength; while the equilibrium bound state, which is dependent on the saturated density of bound molecules, differs in the various scenarios due to entropic effects (diffusion of molecules). The dependences of the equilibrium separation and the minimum free energy can be qualitatively explained using the scaling relations.

Since our results are based on equilibrium analysis but real systems or processes are usually non-equilibrium in nature, it is natural to ask in what situations these conclusions hold. Let's take the surface force measurement (Wong et al., 1997; Jeppesen et al., 2001) as an example. Here we observe three physical time scales, corresponding to the binding reaction ($\tau_{\rm r}$), the diffusion of the polymer tether (or the ligand/receptor group) in solution ($\tau_{\rm p}$), and the trans-membrane diffusion of polymers ($\tau_{\rm D}$). In addition there is the time scale corresponding to the relative speed at which surfaces are approaching or departing from each other (τ). Moore and Kuhl (2006) found that the polymer

diffusion time $\tau_{\rm p}$ (Zimm time) is roughly 1μs, and the binding reaction time $\tau_{\rm r}$ is typically several nanoseconds. The diffusivity of the protein across the membrane was quoted in Dustin et al. (1996) and Cuvelier et al. (2004) to be $10^{-8} \sim 10^{-9}{\rm cm}^2/{\rm s}$, which gives a time scale of $\tau_{\rm D} \sim (\rho D)^{-1} \sim 1$ms for the rearrangement of molecular distributions. Therefore we have

$$\tau_{\rm D} \gg \tau_{\rm p} \gg \tau_{\rm r}.$$

Generally $\tau \gg \tau_{\rm r}$, and it is always valid to treat the binding reaction as an equilibrium. If the surfaces approach very fast such that $\tau < \tau_{\rm p}$, then the diffusion of the polymer tether is relevant and this is the scenario analyzed by Moreira et al. (2003) and Moreira and Marques (2004) using reaction-diffusion theory. If the surfaces approach slow enough such that $\tau > \tau_{\rm D}$, then the system is essentially governed by the equilibrium thermodynamics and all our results should hold; if $\tau_{\rm D} > \tau > \tau_{\rm p}$, the system is in the quenched scenario as the diffusion of the molecules across the membrane is too slow to be treated as annealed.

Moreira et al. (2003), Moreira and Marques (2004), and Moore and Kuhl (2006) discussed the relevance of the approaching speed to the interacting force between the surfaces and the dependence of the fraction of bonds on the surface separation. For the dependence of the onset of binding (their "binding range") on the binding affinity, they found the same result as ours, $l_1 \propto \sqrt{\epsilon/k_{\rm B}T}$, which sets an upper bound in the dynamic measurements where surfaces approach at a finite speed; for the dependence on the tether length, our result suggests $l_1 \sim \sqrt{\epsilon/k_{\rm B}T}N^{\nu}b$, which agrees with their experimental results for long tethers[11]; for short tethers the finite extensibility of the tether should change the scaling dependence. The breaking of the bond is more subtle and is best put in a dynamic context (Evans and Ritchie, 1999; Sain and Wortis, 2004). But as discussed by Moore and Kuhl (2006), the equilibrium force gives an upper bound on the bridging force or the breaking force as long as the approaching or separating speed is not faster than the relaxation of the polymer segments. And our prediction that $\tau \sim \epsilon^{1/2}/N^{\nu}$ should hold for long chains in this regime. Thermal fluctuations will even lower the threshold for breaking the bond, as was considered by Sain and Wortis (2004).

The distinct time scales of motion result in different physical scenarios. For example, the diffusion of ligand and/or receptor groups is governed by the diffusion of the polymer tether as well as the diffusion of the anchoring end in the membrane. But the diffusion in the bilayer is much slower compared to the diffusion of polymer segments in the solution, therefore tethered ligands and receptors can locate their counterparts more easily and result in faster adhesion dynamics compared with the adhesion without tether, as was observed by Cuvelier and Nassoy (2004). In addition the polymer tether increases the range of binding, which admits larger membrane deformations compared with the case of molecular binding: such membrane fluctuations lower the energy barrier

[11] Moreira et al. (2003) and Moreira and Marques (2004) did not do a scaling plot.

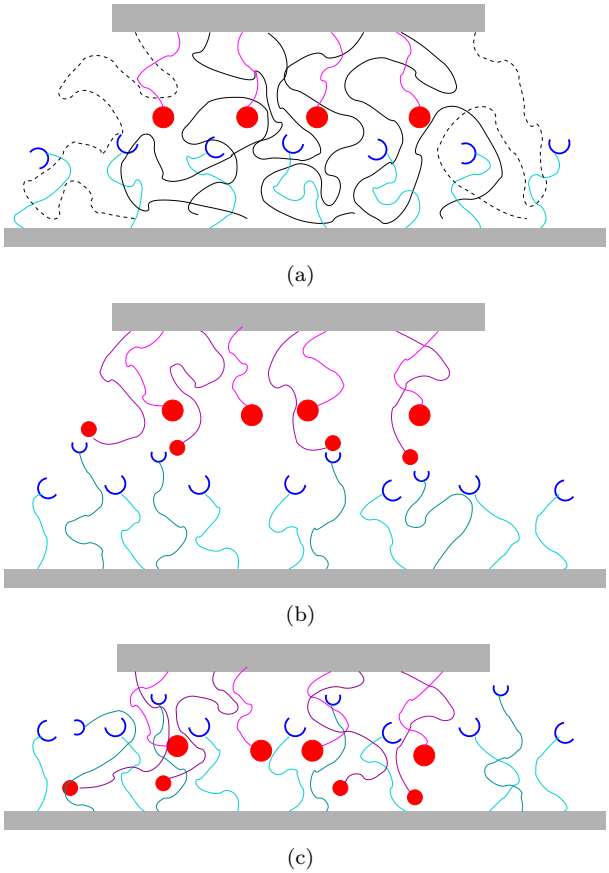

Figure 4.10: Schematic views of the models to be discussed in Section 4.3.3.1 (a), Section 4.3.3.2 (b), and Section 4.3.3.3(c). When molecules with different lengths are present, we usually scale the densities by the length of the (shorter) tethered ligand-receptor bridge, and refer to the molecular densities of other species relative to the density of ligands or receptors.

of adhesion and stabilize the bound state. These two effects qualitatively explain the experimental findings by Cuvelier and Nassoy (2004), although quantitative treatments require an analysis of the adhesion dynamics, which is beyond the scope of our current paper.

4.3.3 Composite interaction potential from specific binding and non-specific interactions

In previous subsections we discuss the interactions between surfaces mediated by polymer-tethered ligand-receptor binding. Real biological processes, however, usually involve many different types of ligand-receptor interactions, with different binding affinities or tether lengths. (See Springer (1990) for a snapshot of different proteins involved in immunological responses.) Even in a simple cell adhesion, the polysaccharide layer on the cell surface introduces additional repulsion between the cell surface and the external surface. This repulsive layer effectively prevents non-specific and preserves specific adhesion.

Here we study the overall interaction potential between the surfaces mediated by several specific and non-specific interactions. We neglect non-specific intra- and intermolecular interactions, such as the excluded volume, and focus on the features of specific interactions and generic repulsion. From these examples we try to illustrate the different features associated with each interacting species and provide some general principles for the design and control of surface interactions.

4.3.3.1 Cell adhesion revisited

Bell and co-workers (Bell, 1978; Bell et al., 1984; Torney et al., 1986) first proposed that cell adhesion is a net result of specific ligand-receptor binding and non-specific steric repulsion due to repelling molecules on the cell surface. Here we re-examine this model and study the dependence of the interaction potential on measurable and controllable molecular parameters, which can guide bioengineering design of artificial surfaces that can trigger cell adhesion. Specifically we treat the binding molecules as polymer-tethered ligands and receptors and the repelling polymers as linear Gaussian chains confined between surfaces [12]. The model is schematically shown in Fig. 4.10(a).

Figure 4.11 shows the composite interaction potential due to ligand-receptor binding and steric repellers. In Fig. 4.11(a) the system belongs to case III (open-closed system) and we plot the cases with mobile repellers (dash line) and immobile repellers (thick solid line). The interaction potential due to ligand-receptor interactions alone is shown for comparison (thin solid line).

The repeller polymer has length $N_{\rm r} = 16(N_{\rm L} + N_{\rm R})$, hence the repulsion is present at

$$L_z \sim \sqrt{N_{\rm r}}b = 4\sqrt{N_{\rm L} + N_{\rm R}}b \gtrsim \sqrt{\beta\epsilon}\sqrt{N_{\rm L} + N_{\rm R}}b,$$

which is slightly larger than the separation at the onset of binding. When repellers are mobile, the repulsive potential flattens off at small separation, implying that they are squeezed out (or "redistributed" in Bell's terminology). This introduces a modest barrier (osmotic pressure) that is proportional to the density of repellers; the length of repellers only affects the range of repulsion, not the barrier height. When repellers are immobile, the short-range repulsion scales as $N_{\rm r}b^2/L_z^2$ and presents a strong repulsion. Accordingly the equilibrium bound state is shifted towards larger surface separations with shallower free energy minimum, due to the strong repulsion at small surface separations.

In Fig. 4.11(b), we examine the case when both receptors and ligands are connected to a reservoir with densities $\phi^{(0)} = 0.005$ and with immobile repeller polymers at different densities. Contrary to the case of receptors/ligands with fixed densities, the equilibrium separation is shifted very little, although the free energy minimum becomes shallower if not vanishing. This suggests a way to adjust

[12] Simple scaling tells us that the short-range repulsion due to confinement of Gaussian chains scales as $\sim Nb^2/L_z^2$, Nb^2 being the mean square end-to-end distance of the polymer and L_z the spatial confinement size. In the Bell model, the repulsion is assumed to scale as $\propto (L_z)^{-1}$; this would correspond to stretched polymers in the brush regime. Extension to this scenario can be straightforwardly implemented via self-consistent calculation.

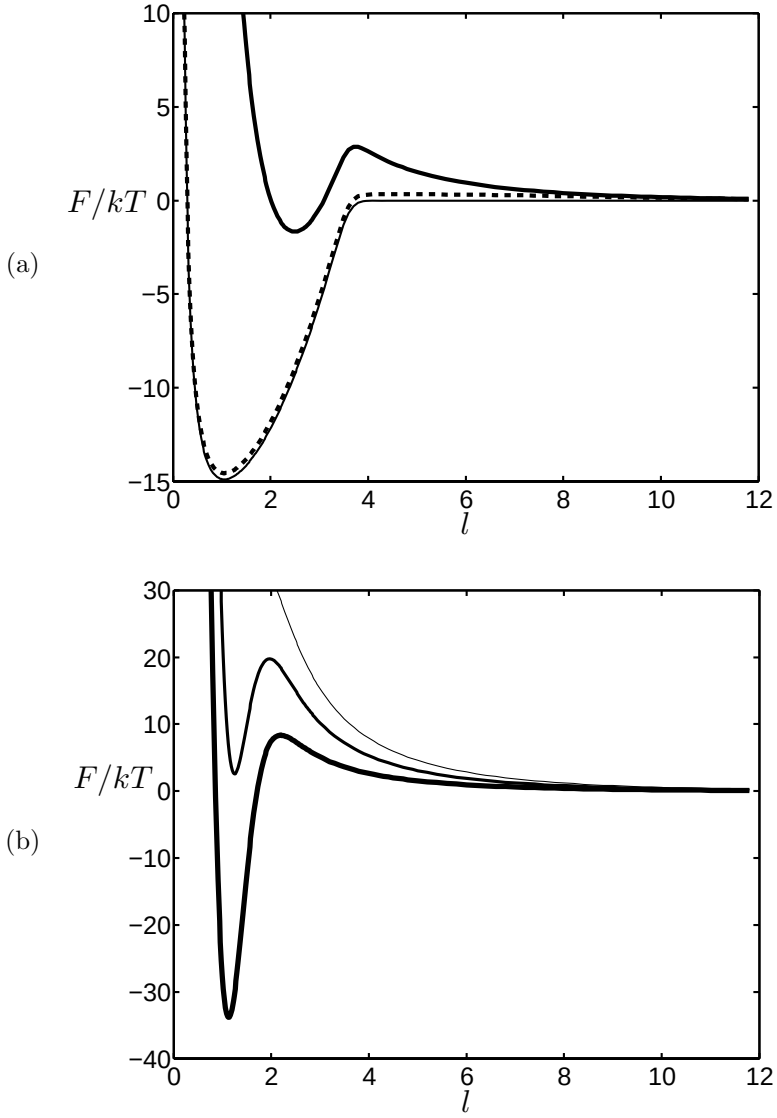

Figure 4.11: The interaction between surfaces mediated by ligand-receptor binding and repulsive polymers. The ligand-receptor binding has a binding energy $\epsilon = 15k_{\rm B}T$. The length of repelling polymers is $N_{\rm r} = 16(N_{\rm L}+N_{\rm R})$. In (a) the densities of ligands and receptors are $\rho^{(0)}(N_{\rm L}+N_{\rm R})b^2 = 1$ and the repeller density is $\rho_{\rm r} = \rho^{(0)}/3$. The dash line is for mobile repellers and the thick solid line for immobile repellers; the thin line is for the bare ligand-receptor system without repellers. (b) Receptors and ligands are both in open system (case IV) with reservoir densities $\rho^{(0)}(N_{\rm L}+N_{\rm R})b^2 = 0.005$, the binding energy is the same as in (a); from above the densities of repelling polymers are: $\rho_{\rm r} = \rho^{(0)}$ (thinnest), $\rho_{\rm r} = 2\rho^{(0)}/3$ (moderate), and $\rho_{\rm r} = \rho^{(0)}/3$ (thick).

the depth of the free energy of the bound state independent of its location, as compared to the case in Fig. 4.11(a) where the two are correlated.

Recently Bruinsma et al. (2000) studied the adhesion between a large versicle and a lipid bilayer when both receptors and repellers are present. They observed that tightly bound regions with higher densities of receptors coexist with loosely bound states with lower densities, and receptors

slowly aggregate to the tightly bound regions (focal adhesion zone). This coexistence was argued to result from a double-well inter-membrane potential separated by a barrier induced by the repeller molecules. The authors further pointed out that the repellers are better characterized as mobile with a given chemical potential so that they can be pushed out in the tightly bound regions.

In our model we do not account for the long-range physical interactions or membrane deformations, which result in the loosely bound minimum described in the Bruinsma paper. Otherwise our analysis qualitatively agrees with their observations. In addition we point out that since the growth of the contact area is slow, initially the adhesion zone should be viewed as an open system of receptors with the loosely bound part serving as the reservoir. This was also observed by Dustin et al. (1996). The attraction inside the focal contact is significantly higher than that predicted from the overall density on the surface, which can overcome the barrier due to immobile repellers; such a process would be impossible if the binding molecules were uniformly distributed as in a closed ensemble.

Finally we point out that due to the barrier between the bound and the unbound state, even in flat geometries the adhesion process should be a first-order transition (Bruinsma and Sackmann, 2002; Weikl et al., 2002). Therefore the presence of a considerable barrier is adequate to prevent non-specific adhesion even though the bound minimum still exists. In this case the growth of the adhesion contact is through nucleation, which is most likely mediated by membrane fluctuations. We will study this interplay between membrane fluctuations and ligand-receptor interactions in Chapter 5.

4.3.3.2 Bidisperse ligand-receptor binding

Introducing long repelling polymers can generate a barrier from the unbound to the bound state, thus preventing unwanted binding or adhesion between the surfaces. If, instead of purely repelling polymers, we introduce longer-tethered ligands and receptors, then these molecules act as a "barrier" to the shorter-tethered binding, but on the other hand generate another minimum at a larger surface separation. Properly adjusting the binding affinities and tether lengths of these two ligand/receptor pairs gives us extra freedom in controlling the strength and range of the attraction between the surfaces.

Here we consider a system with two ligand-receptor pairs with different tether lengths and affinities, as schematically represented in Fig. 4.10(b). The interaction potentials are shown in Fig. 4.12. The shorter-tethered ligand/receptor pair has a larger binding energy $\epsilon = 15k_{\mathrm{B}}T$ and higher density $\phi_1^{(0)} = 1$, and we assume them to be an "open-closed" system to mimic cell-substrate interactions. The longer-tethered one has a smaller binding energy $\epsilon = 5k_{\mathrm{B}}T$ and smaller density $\rho_2^{(0)} = 0.5\rho_1^{(0)}$ (note that this is the molecular density instead of the scaled density ϕ) and we assume both of them to be in a closed system.

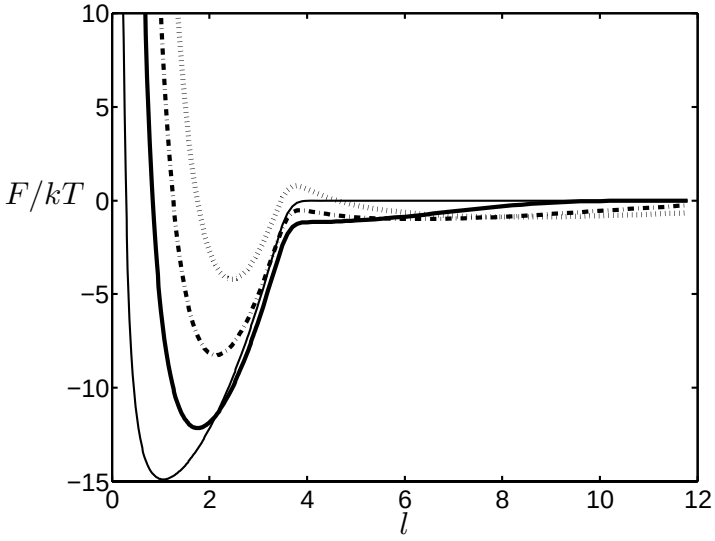

Figure 4.12: The interaction potential resulting from binary ligand-receptor interactions. Ligands and receptors have equal densities as their counterparts. The short-tethered ligand-receptor pairs have $\epsilon_1 = 15k_{\rm B}T$, and $\phi_1^{(0)} = 1$, and the system belongs to case III (open-closed). The thin line represents the interaction potential of this system alone. The long-tethered ligand-receptor pairs have weaker binding energy $\epsilon_2 = 5k_{\rm B}T$, with fixed densities (case II) $\rho_2^{(0)} = 0.5\rho_1^{(0)}$. Both ligand-receptor pairs have equal lengths for ligand and receptor tether. From above, the lengths of the longer tethers are: $N_2 = 64N_1$ (dot line), $N_2 = 36N_1$ (dash-dot line), and $N_2 = 16N_1$ (thick solid line).

Since the long-tethered molecules introduce a barrier to the short-tethered binding and generate a new free energy minimum at larger separation, the superimposed interaction potential should take a double-well shape. In Fig. 4.12 the dot line represents the case with tether ratio $N_2/N_1 = 64$, the dash-dot line for $N_2/N_1 = 36$, and the thick solid line for $N_2/N_1 = 16$; the thin solid line is for the system with short-tethered ligands and receptors only, the same as in Fig. 4.11(a). For the range of tether lengths we studied, we see that the minimum due to the short-tethered binding is shifted to larger separations with higher free energies, similar to Fig. 4.11(a).

When the length of the long-tethered bridge is much larger than that of the short-tethered one (dot line), we observe two minima separated by a positive barrier. If the long tether is of intermediate size (dash-dot line), we still observe two separate minima, but the barrier between them is small and negative; for comparable tether lengths (thick solid line), the two minima merge with a larger range of attraction. These results demonstrate that by adjusting the relative length ratio one can qualitatively control the shape of the interaction potential from single well to double well.

Understanding the interactions due to binary ligand-receptor binding is both relevant to surface engineering and to our understanding of biological systems. In a colloidal suspension with particles interacting via a double-well potential, we expect structures with competing length scales of ordering

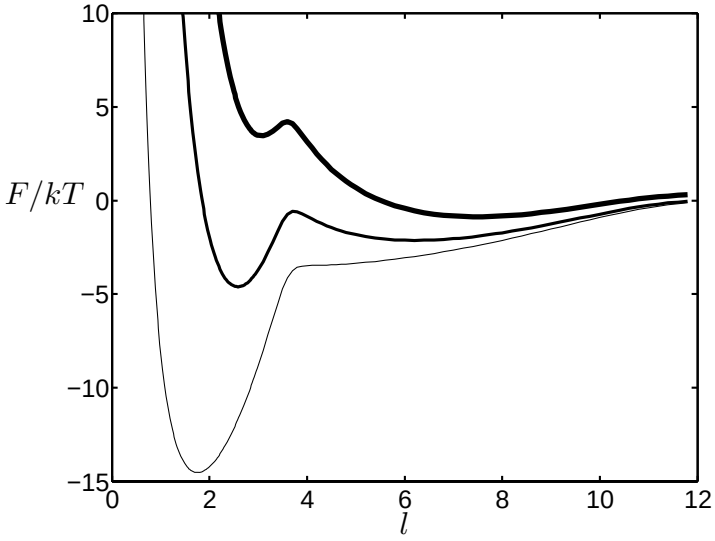

Figure 4.13: Interaction between surfaces with two different ligand-receptor interactions and repelling polymers. For short-tethered ligands/receptors we have $\epsilon_1 = 15k_{\rm B}T$, and $\phi_1^{(0)} = 1$; for the long-tethered ligands/receptors we have $\epsilon_2 = 10k_{\rm B}T$, $\rho_2^{(0)} = 0.5\rho_1^{(0)}$, and $N_2 = 16N_1$. Ligand and receptor tether lengths are equal for both types. And the short-tethered binding is assumed to belong to case III (open-closed) and the long one to case II (both closed). The lengths of the immobile repelling polymers are $N_{\rm r} = 36N_1$ (thickest line) and $N_{\rm r} = 16N_1$ (intermediate) with density $\rho_{\rm r} = \rho_1^{(0)}/3$.

with complicated symmetries, as well as colloidal gels with local but no long-range order[13]. On the other hand, it is known that in the rolling of leukocyte cells (Lawrence and Springer, 1991; Springer, 1994), the longer but weaker selectin ligands mediate rolling of the cells, while the shorter but stronger integrin receptors result in the final strong adhesion; the interplay between longer-tethered ligands and shorter-tethered ligands is key to the successful immunological response (Qi et al., 2001). For stable rolling, the double-well shape interaction potential might be crucial.

4.3.3.3 Attempt at a synthesis

From the above examples we have seen two ways to adjust the interaction potential between surfaces: (1) introduce a barrier from the unbound to the bound state by adding longer repelling polymers; (2) shift the equilibrium separation and the minimum free energy and allow different minima to appear by combining ligand-receptor pairs of different lengths.

Let's summarize the main results in these two cases. To introduce a barrier to the bound state, mobile repellers introduce a less noticeable barrier and smaller shift to the equilibrium separation compared with immobile repellers; with immobile repellers increasing the density or the chain length of the repeller molecules can both increase the barrier height, but the latter will also result in a larger range of repulsion. When a different type of ligand/receptor pairs with longer tethers is introduced,

[13]See Hiddessen et al. (2000) for some examples using single ligand-receptor pairs.

depending on the tether lengths, the system can show two free energy minima separated by a large barrier (large tether-length difference), two minima separated by a small barrier (intermediate tether-length difference), or one minimum only (comparable tether lengths). Adjusting the density of each type of ligand/receptor molecules allows us to control the relative stability of the minima due to each ligand-receptor pair.

Combining these two methods allows us to control the subtle features of the interaction potential. Here we just give one example to illustrate how the relative stability of the minima in a bidisperse ligand-receptor system can be controlled by introducing repellers of different lengths. In Fig. 4.13 the thin line represents the system with bidisperse ligand/receptor molecules with parameters: $\epsilon_1 = 15k_{\rm B}T$, $\phi_1^{(0)} = 1$, and $\epsilon_2 = 10k_{\rm B}T$, $N_2 = 16N_1$, $\rho_2^{(0)} = 0.5\rho_1^{(0)}$. Comparing Fig. 4.13 with Fig. 4.12, we see that although the binding energy for the longer-tethered ligand/receptor molecules is larger, the qualitative features are identical, hence changing the binding energy has little effect on the shape of the interaction potential. However, by introducing immobile repeller molecules with a fixed density $\rho_{\rm r} = \rho_1^{(0)}/3$ but different lengths, we can qualitatively control the interaction potential. In both cases we see two separate minima. For long repellers ($N_{\rm r} = 36N_1$, thickest line) the stable one is at the larger separation, corresponding to the longer-tethered binding, and the repellers generate a barrier to the bound state. In the case of short repellers ($N_{\rm r} = 16N_1$) the stable bound state is at the smaller separation and there is no barrier from unbound to the longer-tethered bound state.

Clearly one can introduce more species into the system to adjust the individual features independently. Because of the specificity of ligand-receptor binding, each type of ligand-receptor binding is independent of others, and the total interaction potential is the superposition of all ligand-receptor pairs, which provides a diverse and powerful way to engineer surface interactions.

4.4 Conclusion

We have studied a continuum microscopic model for polymer-tethered ligand-receptor interactions between surfaces and analyzed the thermodynamics of interactions between the surfaces, which essentially consist of a repulsion due to the confinement of polymers at small surface separations, and an attractive binding at intermediate range of separations mediated by the polymer tether. The generic short-range repulsion due to confinement can be calculated or estimated from scaling analysis for a given chain model. For the tethered binding we find an effective binding constant that relates the density of bound pairs to those of ligands and receptors.

The binding constant has contributions from a microscopic binding affinity between the ligand and the receptor group, which is independent of the surface separation or tether lengths, and a tether stretching energy, which reflects the conformation change of the polymer tethers due to binding. At small surface separations, the 2D binding constant is independent of the tether length, and can

be related to the 3D binding constant by $K^{2D} = K^{3D}/\text{surface separation}$, but at large surface separations the stretching energy is important. The attractive binding and the repulsion due to confinement result in an equilibrium separation between the surfaces corresponding to the minimum of the total interaction free energy.

For the overall interactions between surfaces, we study the different scenarios when binding molecules have different mobilities. Specifically ligands and receptors can be immobile, mobile with a fixed density, or mobile with a fixed chemical potential. These different scenarios correspond to binding between objects with different geometries or different molecular embeddings. Binding is least probable in the case when both species are immobile. On the other hand, in the cases with open ensembles, molecules are attracted into or pushed out of the system due to the net interaction, resulting in a lower free energy. In particular, for the case with ligands in a closed system and receptors in an open system, the maximum density of bound ligand-receptor pairs is determined by the fixed density of ligands, and is insensitive to the reservoir density, as is observed in experiments.

We illustrate our calculations using an ideal-Gaussian-chain model. Simple scaling arguments yield that the onset of binding (adhesion range) scales as $L_z^1 \sim \sqrt{\epsilon/k_B T}\sqrt{N}b$, and the equilibrium separation scales as $L_z^0 \sim \sqrt{N}b$. These results agree well with the exact solutions. We also infer that the quasi-equilibrium critical tension as obtained from the equilibrium force-extension curve should scale as $N^{-1/2}$ for the Gaussian tether. These scaling dependences should also hold for non-Gaussian chain models by replacing the $N^{1/2}$ factor with the characteristic size of the polymer chain (N^{ν}).

Finally we demonstrate that by combining different types of ligand-receptor interactions and non-specific repeller molecules, one can achieve precise control over the interaction potential between surfaces. Specific examples include introducing a barrier between the unbound and the bound state and introducing multiple minima and controlling the range and magnitude of each minimum. These results suggest possible strategies for bioengineering design with better specificity and for a diverse control of surface interactions using specific interactions.

Appendix 4.A Polymer confined between two surfaces

In this appendix we present in detail the calculations of the partition function of a polymer confined between surfaces with hard wall boundary conditions. We shall discuss two examples: Gaussian chains with infinite extensions and rigid rods with finite extensions.

4.A.1 Gaussian chain

First we consider Gaussian chains. The Green's function of a free Gaussian chain is governed by the partial differential equation (Doi and Edwards, 1986)

$$\left(\frac{\partial}{\partial N} - \frac{b^2}{6}\nabla^2\right) G(\mathbf{r}, \mathbf{r}_0; N) = \delta^3(\mathbf{r} - \mathbf{r}_0)\delta(N). \tag{4.41}$$

The non-adsorbing (hard wall) boundary conditions are

$$G(\mathbf{r}, \mathbf{r}_0; N) = 0 \text{ if } \mathbf{r} \text{ or } \mathbf{r}_0 \text{ is at the boundary.} \tag{4.42}$$

The general result is

$$G(\mathbf{r}, \mathbf{r}_0; N) = g(x, x_0; N)g(y, y_0; N)g(z, z_0; N); \tag{4.43}$$

$$g(x, x_0; N) = \frac{2}{L_x} \sum_{1 \le p \le \infty} \sin\left(\frac{p\pi x}{L_x}\right) \sin\left(\frac{p\pi x^0}{L_x}\right) \exp\left(-\frac{p^2\pi^2 N b^2}{6L_x^2}\right), \tag{4.44}$$

and similar results for $g(y, y_0; N)$ and $g(z, z_0; N)$. Here (L_x, L_y, L_z) is the size of the box containing this polymer.

In our system the x and y directions are infinite, hence $g(x, x_0; N)$ and $g(y, y_0; N)$ are Gaussian [$\mathbf{u} = (x, y)$]:

$$g(\mathbf{u}; N) = \frac{3}{2\pi N b^2} e^{-\frac{3u^2}{2Nb^2}}. \tag{4.45}$$

In the z direction $g(z, z_0; N)$ is confined between 0 and L_z with hard-wall boundary conditions. The general expansion for $g(z, z_0; N)$ is

$$\begin{aligned} g(z, z_0; N) &= \sum_{-\infty \le k_z \le \infty} a(k_z) e^{ik_z(z_0 - z)} e^{-k_z^2 N b^2/6} \\ &= \sum_{0 \le k_z \le \infty} a(k_z) \left[\cos(k_z z_0)\cos(k_z z) + \sin(k_z z_0)\sin(k_z z)\right] e^{-k_z^2 N b^2/6}. \end{aligned}$$

To satisfy the Dirichlet boundary condition, we should choose $\sin(k_z z_0)\sin(k_z z)$; if we want a reflective boundary condition we should use $\cos(k_z z)\cos(k_z z_0)$.

For the non-adsorbing boundary condition we have

$$g(z,z_0;N)=\frac{2}{L_z}\sum_p \sin\frac{p\pi z}{L_z}\sin\frac{p\pi z_0}{L_z}\exp\left(-\frac{Nb^2p^2\pi^2}{6L_z^2}\right). \tag{4.46}$$

In our problem, one end of the polymer is anchored at z_0 very close to the surface, therefore the Green's function is given by

$$h_0(z;N)=\frac{2z_0}{L_z^2}\sum_p p\pi\sin\frac{p\pi z}{L_z}\exp\left(-\frac{Nb^2p^2\pi^2}{6L_z^2}\right) \tag{4.46$'$}$$

to first order in z_0/L_z.

The partition function is given by

$$q_z=\int_0^{L_z}dzh_0(z;N)=\frac{4z_0}{L_z}\sum_{p=1,3,5,\ldots}e^{-p^2\pi^2/6l^2}, \tag{4.47}$$

and is approximated by

$$q_z=\begin{cases}\dfrac{4z_0}{L_z}e^{-\pi^2/6l^2} & l\ll 1,\\ \dfrac{\sqrt{6}z_0}{\sqrt{\pi Nb^2}} & l\gg 1.\end{cases} \tag{4.48}$$

Similarly for $h_0(L_z)$, the partition function of a ligand-receptor bridge we have[14]

$$\begin{aligned}h_0(L_z;N_{\rm L}+N_{\rm R}):=h_0(L_z-z_0;N_{\rm L}+N_{\rm R})&=\frac{2}{L_z}\sum_p(-1)^{p+1}\sin\frac{p\pi z_0}{L_z}\sin\frac{p\pi z_0}{L_z}e^{-(p\pi)^2/6l^2}\\ &\approx\frac{2z_0^2}{L_z^3}\sum_p(-1)^{p+1}(p\pi)^2e^{-(p\pi)^2/6l^2}\\ &=-\frac{2z_0^2}{L_z^3}\sum_p\cos p\pi(p\pi)^2e^{-(p\pi)^2/6l^2}.\end{aligned} \tag{4.49}$$

$h_0(L_z;N)$ can be approximated by

$$\begin{cases}\dfrac{2z_0^2\pi^2}{L_z^3}e^{-\pi^2/6l^2} & l\ll 1,\\ 18\sqrt{\dfrac{6}{\pi}}\dfrac{z_0^2}{(Nb^2)^{3/2}}l^2e^{-3l^2/2} & l\gg 1.\end{cases} \tag{4.50}$$

Assembling the terms together we have

$$e^{\tilde{\epsilon}(l)-\epsilon}=\sqrt{N}b\cdot\frac{h_0(L_z;N_{\rm L}+N_{\rm R})}{\int_0^{L_z}dzh_0(z;N_{\rm L})\int_0^{L_z}dzh_0(z;N_{\rm R})}$$

[14]Since $h_0(L_z)$ vanishes, we define it to be $h_0(L_z-z_0)$, as is shown later, for our interest this will not cause ambiguity.

$$\approx \frac{1}{8l} \frac{\sum_p (-1)^{p+1} (p\pi)^2 e^{-(p\pi)^2/6l^2}}{\left[\sum_{p=2k-1} \exp\left(-\frac{N_\mathrm{L}}{N_\mathrm{L}+N_\mathrm{R}} \frac{p^2\pi^2}{6l^2}\right)\right] \cdot \left[\sum_{p=2k-1} \exp\left(-\frac{N_\mathrm{R}}{N_\mathrm{L}+N_\mathrm{R}} \frac{p^2\pi^2}{6l^2}\right)\right]}, \tag{4.51}$$

and the asymptotic limits are

$$\begin{cases} \dfrac{\pi^2}{8l} & l \ll 1, \\ 3\sqrt{6\pi} l^2 e^{-3l^2/2} \dfrac{\sqrt{N_\mathrm{L} N_\mathrm{R}}}{N_\mathrm{L} + N_\mathrm{R}} & l \gg 1. \end{cases} \tag{4.52}$$

4.A.2 Rigid rod and variants

Here we study models with finite extensibility. First we consider a spherical chain model, in which the distribution of the free end is uniform within the hemisphere of radius R and zero outside. R can be identified as the contour length of the polymer, or as an approximation to the Gaussian chain model, identified with the mean square end-to-end distance of the Gaussian chain. For this model the Green function of the polymer with one end fixed at the origin is given by

$$G(r, \theta, \phi; N) = \frac{3r^2 \sin\theta}{2\pi R^3}, \tag{4.53}$$

and the partition function is

$$q = \begin{cases} 1 & L_z \geq R, \\ \frac{1}{3}\left[\frac{3L_z}{R} - \left(\frac{L_z}{R}\right)^3\right] & L_z < R. \end{cases} \tag{4.54}$$

Slightly different is the model of a freely rotating rod, corresponding to a short polymer whose contour length is smaller than the persistence length. The Green function is

$$G(\mathbf{r}, \mathbf{r}_0; R) = \frac{1}{2\pi R^2} \delta\left(\frac{|\mathbf{r} - \mathbf{r}_0|}{R} - 1\right). \tag{4.55}$$

R is the rod length, which is equal to the contour length of the polymer. For this model, the partition function is

$$q = \begin{cases} \frac{L_z}{R} & L_z < R, \\ 1 & L_z \geq R. \end{cases} \tag{4.56}$$

The Green's function for the tether chain with two connected rods is conveniently represented by the length of the arc from the intersection circle of the two hemispheres spanned by the rod ends that is confined between the surfaces. The expression can be worked out, but is quite lengthy. Two examples are shown in Figure 4.14 on page 108.

For ligand and receptor tethers we have $R_{\mathrm{L,R}} = N_{\mathrm{L,R}} b$, and the combined tether length is

$G(r, L_z; N_{\mathrm{L}} = N_{\mathrm{R}})$

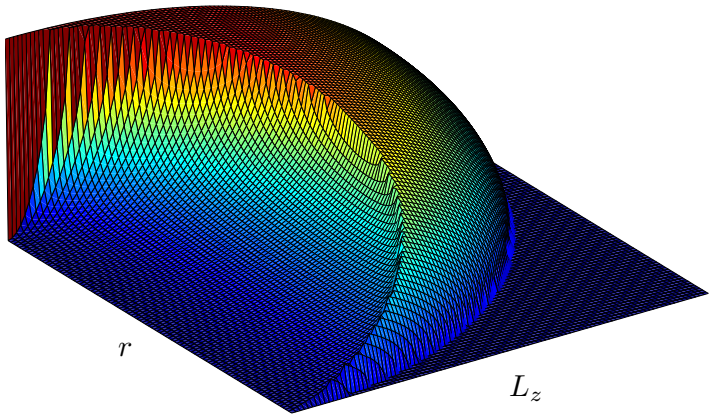

$G(r, L_z; N_{\mathrm{L}} = 1.5N_{\mathrm{R}})$

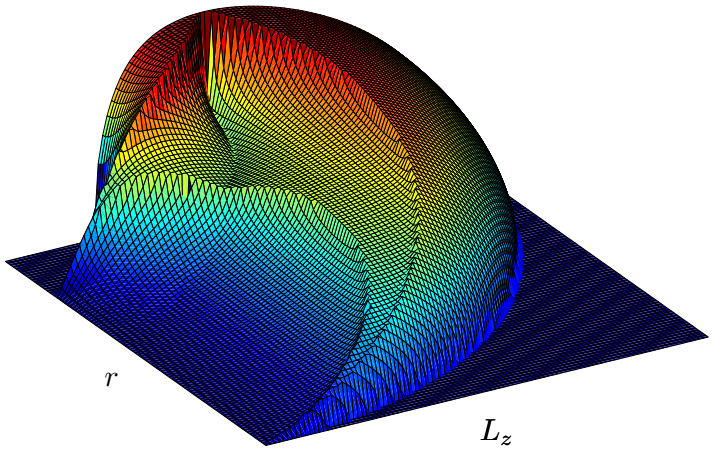

Figure 4.14: Green's function of joined rods

$(N_{\mathrm{L}} + N_{\mathrm{R}})b$. Let us define the scaled densities

$$\phi_{\mathrm{L,R}} = \rho_{\mathrm{L,R}} N^2 b^2.$$

From Eqs. (4.24), the binding constant is given by

$$\begin{aligned} K =& \frac{\rho_{\mathrm{LR}}}{\rho_{\mathrm{L}}\rho_{\mathrm{R}}} = \frac{K_0 A \int_{\mathbf{r}_{\mathrm{L}},\mathbf{r}_{\mathrm{R}}} G_{\mathrm{LR}}(\mathbf{r}_{\mathrm{L}},\mathbf{r}_{\mathrm{R}})}{\int_{\mathbf{r}}\int_{\mathbf{r}_{\mathrm{L}}} G(\mathbf{r},\mathbf{r}_{\mathrm{L}};N_{\mathrm{L}})\int_{\mathbf{r}}\int_{\mathbf{r}_{\mathrm{R}}} G(\mathbf{r},\mathbf{r}_{\mathrm{R}};N_{\mathrm{R}})} \\ =& \frac{K_0}{q_{\mathrm{L}}q_{\mathrm{R}}}\int G_{\mathrm{LR}}(\mathbf{r};N_{\mathrm{L}},N_{\mathrm{R}})\mathrm{d}^2\mathbf{r}. \end{aligned} \tag{4.57}$$

G_{LR} is the partition function of a ligand-receptor bridge. In the quenched case we have (cf. Appendix 4.B for the definition of $w(\mathbf{r})$)

$$w(\mathbf{r}) = \frac{K_0 G_{\mathrm{LR}}(\mathbf{r};N_{\mathrm{L}},N_{\mathrm{R}})}{q_{\mathrm{L}}q_{\mathrm{R}}}. \tag{4.58}$$

We immediately recognize from the finite extensibility that in these models binding is present only if $L_z \le (N_{\mathrm{L}}+N_{\mathrm{R}})b$. In addition, if molecules are immobile, binding is less probable compared with Gaussian chains. For the rigid-rod model, consider a ligand and a receptor with lateral separation $\mathbf{r}$, a necessary but not sufficient condition for binding to be possible is

$$|N_{\mathrm{L}}-N_{\mathrm{R}}|b \le \sqrt{\mathbf{r}^2+L_z^2} \le (N_{\mathrm{L}}+N_{\mathrm{R}})b.$$

When surfaces come too close, binding becomes less probable.

Appendix 4.B Low-density expansion for the quenched problem

For an immobile ligand anchored at $\mathbf{r}_{\mathrm{L}}$ and a receptor at $\mathbf{r}_{\mathrm{R}}$, the ratio of the Boltzmann factor of the bound state to that of the unbound state is given from Eqs. (4.24) and (4.25) to be

$$w(\mathbf{r}_{\mathrm{L}},\mathbf{r}_{\mathrm{R}}) = \frac{q_{\mathrm{LR}}}{q_{\mathrm{L}}q_{\mathrm{R}}} = \frac{K_0 q^{\mathrm{t}}_{\mathrm{LR}}}{q^{\mathrm{t}}_{\mathrm{L}}q^{\mathrm{t}}_{\mathrm{R}}} = \frac{K_0 h(L_z) g(\mathbf{r}_{\mathrm{L}}-\mathbf{r}_{\mathrm{R}};N_{\mathrm{L}}+N_{\mathrm{R}})}{q_{\mathrm{L}}(L_z)q_{\mathrm{R}}(L_z)}. \tag{4.59}$$

Note that since molecules are immobile, the integration over $\mathbf{r}_{\mathrm{L}}$ or $\mathbf{r}_{\mathrm{R}}$ is removed; but the translational invariance implies that $w(\mathbf{r}_1,\mathbf{r}_2) = w(\mathbf{r}_1-\mathbf{r}_2)$. Using $w(\mathbf{u})$ we can easily write down the first few terms of $F(m_{\mathrm{L}},m_{\mathrm{R}})$ (cf. Eq. (4.35)):

$$\begin{aligned} -\beta F(1,1) &= \ln[1+w(\mathbf{x}_1-\mathbf{y}_2)] + \ln q_{\mathrm{L}} + \ln q_{\mathrm{R}}, \\ -\beta F(1,2) &= \ln q_{\mathrm{L}} + 2\ln q_{\mathrm{R}} + \ln[1+w(\mathbf{x}_1-\mathbf{y}_1)+w(\mathbf{x}_1-\mathbf{y}_2)], \\ -\beta F(2,2) &= 2\ln q_{\mathrm{L}} + 2\ln q_{\mathrm{R}} + \ln\left[1+w(\mathbf{x}_1-\mathbf{y}_1)+w(\mathbf{x}_1-\mathbf{y}_2)+w(\mathbf{x}_2-\mathbf{y}_1)+w(\mathbf{x}_2-\mathbf{y}_2)\right. \\ &\qquad \left. + w(\mathbf{x}_1-\mathbf{y}_1)w(\mathbf{x}_2-\mathbf{y}_2)+w(\mathbf{x}_1-\mathbf{y}_2)+w(\mathbf{x}_2-\mathbf{y}_1)\right]. \end{aligned}$$

Here $\mathbf{x}_{\mathrm{i}}$ and $\mathbf{y}_{\mathrm{j}}$ are positions of ligands and receptors, respectively.

Assuming that receptors and ligands are randomly distributed on the surfaces and for any receptor or ligand, its position distribution is independent of the others, we have the quenched average

$$\left\langle F(\mathbf{x}_1, \mathbf{x}_2, \cdots, \mathbf{x}_m, \mathbf{y}_1, \mathbf{y}_2, \cdots, \mathbf{y}_n)\right\rangle = \frac{1}{A^{i+j}} \int_{\{\mathbf{x}_\mathrm{i}\},\{\mathbf{y}_\mathrm{j}\}} F(\{\mathbf{x}_\mathrm{i}\},\{\mathbf{y}_\mathrm{j}\}),$$

Evaluating these averages is straighforward, which gives

$$-\beta \left\langle F(1,1)\right\rangle = \ln q_\mathrm{L} + \ln q_\mathrm{R} + \frac{1}{A}\int_{\mathbf{u}} \ln[1+w(\mathbf{u})], \tag{4.60a}$$

$$-\beta \left\langle F(1,2)\right\rangle = \ln q_\mathrm{L} + 2\ln q_\mathrm{R} + \frac{1}{A^2}\int_{\mathbf{u}_1,\mathbf{u}_2} \ln[1+w(\mathbf{u}_1)+w(\mathbf{u}_2)], \tag{4.60b}$$

$$-\beta \left\langle F(2,1)\right\rangle = 2\ln q_\mathrm{L} + \ln q_\mathrm{L} + \frac{1}{A^2}\int_{\mathbf{u}_1,\mathbf{u}_2} \ln[1+w(\mathbf{u}_1)+w(\mathbf{u}_2)], \tag{4.60c}$$

$$-\beta \left\langle F(1,m)\right\rangle = \ln q_\mathrm{L} + m\ln q_\mathrm{R} + \frac{1}{A^m}\int_{\mathbf{u}_1,\cdots\mathbf{u}_m} \ln[1+\sum_m w(\mathbf{u}_m)], \tag{4.60d}$$

$$\begin{aligned}-\beta \left\langle F(2,2)\right\rangle = {} & 2\ln q_\mathrm{L} + 2\ln q_\mathrm{R} + \frac{1}{A^3}\int_{\mathbf{u}_1,\mathbf{u}_2,\mathbf{v}_1} \ln[1+w(\mathbf{u}_1)+w(\mathbf{u}_2)+w(\mathbf{u}_1+\mathbf{v})+w(\mathbf{u}_2+\mathbf{v}) \\ & + w(\mathbf{u}_2)w(\mathbf{u}_1+\mathbf{v}) + w(\mathbf{u}_1)w(\mathbf{u}_2+\mathbf{v})].\end{aligned} \tag{4.60e}$$

Substituting these back into Eq. (4.35) we have

$$\begin{aligned}-\beta\bar{F}^{(1,1)} &= \frac{1}{e^{A\rho_\mathrm{L}+A\rho_\mathrm{R}}} \sum_{m_\mathrm{L}\geq 1, m_\mathrm{R}\geq 1} \frac{(A\rho_\mathrm{L})^{m_\mathrm{L}}(A\rho_\mathrm{R})^{m_\mathrm{R}}}{m_\mathrm{L}!m_\mathrm{R}!}\frac{m_\mathrm{L}m_\mathrm{R}}{A}\int_{\mathbf{u}}\ln[1+w(\mathbf{u})] \\ &= A\rho_\mathrm{L}\rho_\mathrm{R}\int_{\mathbf{u}}\ln[1+w(\mathbf{u})] \\ &= A\rho_\mathrm{L}\rho_\mathrm{R}\mathcal{F}^{(1,1)};\end{aligned} \tag{4.61a}$$

$$\begin{aligned}-\beta\bar{F}^{(1,2)} &= \frac{1}{e^{A(\rho_\mathrm{L}+\rho_\mathrm{R})}} \sum_{m_\mathrm{L}\geq 1, m_\mathrm{R}\geq 2} \frac{(A\rho_\mathrm{L})^{m_\mathrm{L}}(A\rho_\mathrm{R})^{m_\mathrm{R}}}{m_\mathrm{L}!m_\mathrm{R}!} m_\mathrm{L}^1 m_\mathrm{R}^2 \\ &\quad \left\{\frac{1}{A^2}\int_{\mathbf{u}_1,\mathbf{u}_2}\ln[1+w(\mathbf{u}_1)+w(\mathbf{u}_2)] - \frac{2}{A}\int_{\mathbf{u}}\ln[1+w(\mathbf{u})]\right\} \\ &= \frac{A\rho_\mathrm{L}\rho_\mathrm{R}^2}{2}\int_{\mathbf{u}_1,\mathbf{u}_2}\{\ln[1+w(\mathbf{u}_1)+w(\mathbf{u}_2)] - \ln[1+w(\mathbf{u}_1)] - \ln[1+w(\mathbf{u}_2)]\} \\ &= \frac{A\rho_\mathrm{L}\rho_\mathrm{R}^2}{2}\mathcal{F}^{(1,2)};\end{aligned} \tag{4.61b}$$

$$-\beta\bar{F}^{(1,m)} = \frac{A\rho_\mathrm{L}\rho_\mathrm{R}^m}{m!}\left\{\int_{\mathbf{u}_1,\mathbf{u}_2,\cdots\mathbf{u}_m}\ln\left[1+\sum_i w(\mathbf{u}_i)\right] - \sum_{1\leq k<m} A^{m-k}\mathrm{C}_m^k\mathcal{F}^{(1,k)}\right\}; \tag{4.61c}$$

$$\begin{aligned}-\beta\bar{F}^{(2,2)} = {} & \frac{A\rho_\mathrm{L}^2\rho_\mathrm{R}^2}{4}\left(\int_{\mathbf{u}_1,\mathbf{u}_2,\mathbf{v}}\ln\Big[1+w(\mathbf{u}_1)+w(\mathbf{u}_2)+w(\mathbf{u}_1+\mathbf{v})+w(\mathbf{u}_2+\mathbf{v})\right. \\ & \left. + w(\mathbf{u}_1)w(\mathbf{u}_2+\mathbf{v}) + w(\mathbf{u}_2)w(\mathbf{u}_1+\mathbf{v})\Big]\right. \\ & - 4A\int_{\mathbf{u}_\mathrm{L},\mathbf{u}_\mathrm{R}}\Big\{\ln\big[1+w(\mathbf{u}_1)+w(\mathbf{u}_2)\big] - \ln[1+w(\mathbf{u}_1)] - \ln[1+w(\mathbf{u}_2)]\Big\}\end{aligned}$$

$$- 4A^2 \int_{\mathbf{u}} \ln[1 + w(\mathbf{u})]\Big) \tag{4.61d}$$
$$= \frac{A\rho_{\mathrm{L}}^2\rho_{\mathrm{R}}^2}{4}\mathcal{F}^{(2,2)}.$$

For Gaussian chains, the quantity $w(\mathbf{r})$ can be rewritten as

$$w(\mathbf{u}) = \frac{K_0 h_0(l)}{q_{\mathrm{L}}(l)q_{\mathrm{R}}(l)} g(\mathbf{u}; N_{\mathrm{L}} + N_{\mathrm{R}}) = \frac{3}{2\pi}\exp\left[\beta\tilde{\epsilon}(l) - \frac{3u^2}{2Nb^2}\right], \tag{4.62}$$

where the effective binding energy $\tilde{\epsilon}$ is defined above as in Eq. (4.29) and the second term accounts for lateral stretching. From Eq. (4.62) we see that (a) the effective binding energy has a similar dependence on the surface separation as in the annealed case as reflected in $\tilde{\epsilon}$; (b) each integral over $\mathbf{u}$ gives a factor of Nb^2, hence

$$\mathcal{F}^{(n,m)} \propto (Nb^2\beta)^{n+m-1},$$

and we see that in Eq. (4.61) the real expansion parameter is $\phi = \rho N b^2$. (Similarly one can verify that in the case of rigid rods, the expansion is in terms of $\phi = \rho N^2 b^2$.) For large binding energy $\beta\tilde{\epsilon}$, each integral over the scaled $\mathbf{u}$ also contributes a factor of $\beta\tilde{\epsilon}$, therefore the asymptotic density expansion is valid only if

$$\beta\tilde{\epsilon}\phi \ll 1.$$

The density of bound pairs is obtained by taking the derivative of $\bar{F}$ against $\ln w$. At leading order the binding fraction can be expressed in a close form:

$$f^{(1,1)} = \int_{\mathbf{u}} \frac{\mathrm{d}}{\mathrm{d}\ln w}\ln(1+w) = \int_{\mathbf{r}} \frac{w(\mathbf{u})}{1 + w(\mathbf{u})}, \tag{4.63}$$

which for Gaussian chain with

$$w(\mathbf{u}) \propto e^{-\frac{3u^2}{2}},$$

becomes

$$f^{(1,1)} = 2\pi\int_0^\infty \frac{w(0)e^{-\frac{3u^2}{2}}}{1 + w(0)e^{-\frac{3u^2}{2}}} u\mathrm{d}u = \frac{2\pi}{3}\ln(1 + w(0)) = \frac{2\pi}{3}\ln(1 + w(0)). \tag{4.64}$$

Appendix 4.C Exact results for the single-chain quenched problem

Consider the problem of one ligand with randomly anchored receptors, the quenched average quantities include the free energy

$$-\frac{\Delta F}{kT} = \left\langle \ln\left[1+\sum_{\mathbf{r}}\sigma(\mathbf{r})w(\mathbf{r})\right]\right\rangle_{\{\sigma\}},$$

and the binding fraction

$$f = \left\langle \frac{\sum_{\mathbf{r}}\sigma(\mathbf{r})w(\mathbf{r})}{1+\sum_{\mathbf{r}}\sigma(\mathbf{r})w(\mathbf{r})}\right\rangle_{\{\sigma\}},$$

both of which involve

$$\Sigma = \sum_{\mathbf{r}}\sigma(\mathbf{r})w(\mathbf{r}).$$

$\sigma(\mathbf{r})$ labels the occupation of each lattice site, namely $\sigma(\mathbf{r}) = 1$ if the lattice site is occupied and 0 otherwise. Σ is a random variable with mean

$$E[\Sigma] = \rho e^{\beta\epsilon}\int g(\mathbf{r})\mathrm{d}^2\mathbf{r}.$$

The only problem is to find the distribution of Σ. Let's calculate the characteristic function of Σ.

4.C.1 Ideal solution model

Here we assume that each lattice site has a probability ϕ to be occupied. The partition function of non-interacting system is

$$Q = (1+e^{\mu})^A,$$

with

$$\phi = \frac{e^{\mu}}{1+e^{\mu}}.$$

Further we assume that lattice sites are decoupled, i.e., they are independent. The characteristic function of one site is

$$\varphi_{\sigma}(t) = 1-\phi+\phi e^{it}. \tag{4.65}$$

Then for

$$\Sigma = \sum_{\mathbf{r}}\sigma(\mathbf{r})w(\mathbf{r}),$$

we have

$$\varphi_\Sigma(t) = \prod_{\mathbf{r}} \left(1 - \phi + \phi e^{itw(\mathbf{r})}\right) = \exp\left[\sum_{\mathbf{r}} \log\left(1 - \phi + \phi e^{itw(\mathbf{r})}\right)\right]. \tag{4.66}$$

In the continuum model, the summation can be replaced by an integral,

$$\varphi_\Sigma(t) = \exp\left[\frac{1}{a^2}\int \log\left(1 - \phi + \phi e^{itw(x,y)}\right) \mathrm{d}x\mathrm{d}y\right].$$

Assuming that $\phi \ll 1$, we can approximate the exponent by

$$\frac{\phi}{a^2}\int_{-\infty}^{\infty} dx \int_{-\infty}^{\infty} dy \left(e^{itg(x,y)} - 1\right).$$

This is in fact the —

4.C.2 Ideal lattice gas model

In the ideal lattice gas model, the lattice distribution variable satisfies the Poisson distribution

$$P(\sigma = n) = \frac{e^{-\phi}\phi^n}{n!},$$

$$\varphi_\sigma(t) = \exp\left(e^{it}\phi - \phi\right).$$

Then for

$$\Sigma = \sum_{\mathbf{r}} w(\mathbf{r})\sigma(\mathbf{r}),$$

we have

$$\varphi_\Sigma(t) = \exp\left[\phi \sum_{\mathbf{r}} \left(e^{itw(\mathbf{r})} - 1\right)\right].$$

Alternatively one can define

$$\Sigma = \sum_{\mathbf{r}} w(\mathbf{r}) \sum_i \delta(\mathbf{r} - \mathbf{r}_i),$$

where $\mathbf{r}_i$ are the positions of the receptors. Ignoring the maximum occupancy constraint, as the receptors position distributions are independent, we have

$$\varphi_\Sigma = \prod_{\mathbf{r}} \left(1 - \frac{a^2}{A} + \frac{a^2}{A} e^{itg(\mathbf{r})}\right)^n = \exp\left[n \sum_{\mathbf{r}} \ln\left(1 - \frac{a^2}{A} + \frac{a^2}{A} e^{itw(\mathbf{r})}\right)\right] \tag{4.67}$$

$$\simeq \prod_{\mathbf{r}} \exp\left[\frac{na^2}{A}\left(e^{itw(\mathbf{r})} - 1\right)\right] \simeq \exp\left[\rho \int \left(e^{itw(\mathbf{r})} - 1\right) \mathrm{d}\mathbf{r}\right]. \tag{4.68}$$

The "$\simeq$" becomes "=" in the thermodynamic limit $A \to \infty$ and in the continuum limit $a^2 \to 0$.

We know that $w(\mathbf{r})$ is Gaussian, and can be written as[15]

$$w(x,y) = \exp\left(\beta\epsilon - \frac{x^2+y^2}{Nb^2}\right) = g(x,y)e^{\beta\epsilon}.$$

We can drop the $\exp(\beta\epsilon)$ term as it is a constant, and

$$\begin{aligned}
\varphi_\Sigma(t) =& \exp\left[\rho\int_{-\infty}^{\infty}\mathrm{d}x\int_{-\infty}^{\infty}\mathrm{d}y\left(e^{itw(x,y)}-1\right)\right] \\
=& \exp\left\{\rho Nb^2\int_{-\infty}^{\infty}\mathrm{d}u\int_{-\infty}^{\infty}\mathrm{d}v\left[\exp\left(ite^{\beta\epsilon-(u^2+v^2)}\right)-1\right]\right\} \\
=& \exp\left\{\rho Nb^2\sum_{m\geq 1}\frac{1}{m!}\int_{-\infty}^{\infty}\mathrm{d}u\int_{-\infty}^{\infty}\mathrm{d}v\left[ie^{\beta\epsilon}te^{-(u^2+v^2)}\right]^m\right\} \\
=& \exp\left[\pi\rho Nb^2\sum_{m\geq 1}\frac{(it)^m e^{m\beta\epsilon}}{m\cdot m!}\right] = \exp\left\{\pi\rho Nb^2\int_0^{e^{\beta\epsilon}t}\frac{e^{ix}-1}{x}\mathrm{d}x\right\}.
\end{aligned} \tag{4.69}$$

The probability distribution of $e^{-\beta\epsilon}\Sigma$ is given by

$$f_{e^{-\beta\epsilon}\Sigma}(x) = \frac{1}{2\pi}\int_{-\infty}^{\infty}e^{-itx}\varphi_\Sigma(t)\mathrm{d}t = \frac{1}{2\pi}\int_{-\infty}^{\infty}\exp\left[-itx+\Phi\int_0^t\frac{e^{iu}-1}{u}\mathrm{d}u\right]\mathrm{d}t \tag{4.70}$$

$$= \frac{1}{\pi}\int_0^{\infty}\exp\left[-\Phi\int_0^t\frac{1-\cos u}{u}\mathrm{d}u\right]\cos\left(-tx+\Phi\int_0^t\frac{\sin u}{u}\mathrm{d}u\right)\mathrm{d}t. \tag{4.71}$$

We note that $\int_0^t \frac{\sin x}{x}dx$ is an odd function of t while $\int_0^t \frac{\cos u-1}{u}du$ is an even function of t.

If $\Phi \gg 1$, then the integral has most contribution from $t \ll 1$

$$1-\cos u = \frac{u^2}{2} - \frac{u^4}{4!} + \frac{u^6}{6!} + \cdots$$

$$\int_0^t\frac{1-\cos u}{u}\mathrm{d}u \approx \frac{t^2}{4} - \frac{t^4}{96} + \cdots$$

$$\int_0^t\frac{\sin u}{u}\mathrm{d}u \approx t - \frac{t^3}{18} + \cdots$$

[15] In general we have

$$\varphi_A(t) = \exp\left[\phi\sum_{n\geq 2}\frac{i^n t^n}{n!}W_n\right]$$

where

$$W_n = \sum_{\mathbf{r}} w(\mathbf{r})^n$$

and the probability distribution of A is

$$\begin{aligned}
f_A(x) =& \frac{1}{2\pi}\int_{-\infty}^{\infty}e^{-itx}\varphi_A(t)dt = \frac{1}{2\pi}\int_{-\infty}^{\infty}dt\exp\left[-itx+\phi\sum_{n\geq 2}\frac{i^n t^n}{n!}W_n\right] \\
=& \frac{1}{\pi}\int_0^{\infty}\exp\left[\phi\sum_{n=2k}^{k\geq 1}\frac{(-)^k t^{2k}}{n!}W_n\right]\cos\left(-tx+\phi\sum_{n=2k+1}^{k\geq 1}\frac{(-)^k t^{2k+1}}{n!}W_n\right).
\end{aligned}$$

$$f_{e^{-\beta\epsilon}\Sigma}(x) \approx \frac{1}{\pi}\int_0^\infty \exp\left[-\frac{\Phi t^2}{4}\right]\cos\left[-tx+\Phi\left(t-\frac{t^3}{18}\right)\right]\mathrm{d}t. \tag{4.72}$$

The extra t^3 term is kept as the leading-order correction to Gaussian distribution of Λ.

If $\Phi \ll 1$, then the exponent can be expanded as a power series—we have

$$\begin{aligned}\varphi_{e^{-\beta\epsilon}\Sigma}(t) =& \exp\left\{\Phi\int_0^t \frac{e^{iu}-1}{u}\mathrm{d}u\right\}\\ \approx& 1+\Phi\int_0^t\frac{e^{iu}-1}{u}\mathrm{d}u \simeq 1-\Phi\ln\frac{t}{\delta}+\Phi\int_\delta^t\frac{e^{iu}}{u}\mathrm{d}u.\end{aligned} \tag{4.73}$$

Let's choose $\delta = te^{-R^2/Nb^2}$. Then this equation becomes

$$\begin{aligned}\varphi_{e^{-\beta\epsilon}\Sigma}(t) \simeq& 1-\frac{\Phi R^2}{Nb^2}+\Phi\int_{e^{-R^2/Nb^2}t}^t\frac{e^{iu}}{u}\mathrm{d}u\\ =& 1-\rho\pi R^2+\rho\int_0^R \exp\left(ite^{-r^2}\right)r\mathrm{d}r.\end{aligned} \tag{4.74}$$

This corresponds to a uniform distribution of receptors within a circle with radius R. We see that if $\Phi \ll 1$ then each ligand essentially sees only one receptor and the perturbative expansion in Appendix 4.B is accurate in this regime.

Appendix 4.D Multi-chain quenched problem in the high-density limit

As seen in Appendix 4.C, in the high-density limit, the single-chain quenched problem approaches the annealed case. Will the same conclusion hold for the multi-chain problem?

Assume the area densities of receptors and ligands to be ρ_R and ρ_L. And we simplify $w(\mathbf{u})$ to be a step function, i.e.,

$$w(\mathbf{u}) = \begin{cases} e^{\beta\epsilon} & u < u^*,\\ 0 & u \geq u^*.\end{cases} \tag{4.75}$$

Now within a area $S = \pi(u^*)^2$ all ligands and receptors can bind with each other. Assume that $\rho_\mathrm{i}^0(u^*)^2 \gg 1$, the average number of molecules within S is roughly Gaussian and peaked at $\rho_\mathrm{i}^0(u^*)^2$. Also assume that $\epsilon \gg 1$, therefore as many molecules are bound as possible. The only difference between the quenched case and the annealed case is in their entropy. The partition function for each quenched sample satisfies

$$Q(\{\mathbf{r}_\mathrm{L}\},\{\mathbf{r}_\mathrm{R}\}) > (q^*)^{A/(u^*)^2}, \tag{4.76}$$

q^* is the partition sum within S, whose entropic term is approximately

$$q^* \simeq \frac{[\rho_{\rm L}^0 (u^*)^2]![\rho_{\rm R}^0 (u^*)^2]!}{\left[\rho_{\rm L}(u^*)^2\right]!\left[\rho_{\rm R}(u^*)^2\right]!\left[\rho_{\rm LR}(u^*)^2\right]!} = \frac{\phi_{\rm L}^0!\phi_{\rm R}^0!}{\phi_{\rm L}!\phi_{\rm R}!\phi_{\rm LR}!}. \tag{4.77}$$

In the annealed case the change in the entropic part of the free energy is

$$\frac{\Delta f_s}{kT} = \phi_{\rm L}\ln\phi_{\rm L} + \phi_{\rm R}\ln\phi_{\rm R} + \phi_{\rm LR}\ln\phi_{\rm LR} + \phi_{\rm LR} - \phi_{\rm L}^0\ln\phi_{\rm L}^0 - \phi_{\rm R}^0\ln\phi_{\rm R}^0. \tag{4.78}$$

Therefore one concludes that the quenched free energy within S

$$< f >\leq f.$$

On the other hand, we know that $< f >\geq f$ by definition, therefore this suggests that $< f >= f$ in the thermodynamic limit.

This result follows from the fact that within S the fluctuation in the quenched distribution is negligible, hence the quenched system is essentially "annealed" within S; therefore their free energies are equal, as the free energy $< f >$ is self-averaging.

Chapter 5

Dynamics of membrane adhesion mediated by receptor interactions

5.1 Introduction

Cell adhesion is crucial to many biological processes, including cell differentiation and division, signal transduction, and immunological responses (Alberts et al., 2002; Berg et al., 2002; Springer, 1990). Many different interactions are involved in adhesions *in vivo*: lock-and-key type interactions between proteins (Lauffenburger and Linderman, 1993), force-induced signaling, reorganization of actin filaments and the cortex (Lipowsky, 1995), and various generic physical forces (Nelson et al., 2004). Despite the complexity of these interactions, researchers have been successful in explaining many experimental observations from thermodynamic and physico-chemical analysis, and many features of cell adhesion can be qualitatively understood from basic physical principles (Bell, 1978; Bell et al., 1984; Torney et al., 1986; Coombs et al., 2004; Flyvbjerg et al., 1997; Zukerman and Bruinsma, 1995; Lipowsky, 1996; Bruinsma et al., 2000; Boulbitch et al., 2001; Bruinsma and Sackmann, 2002; Sackmann and Bruinsma, 2002; Sackmann and Goennenwein, 2006).

In contrast to adhesion mediated by generic interactions such as the van der Waals or electrostatic forces, biological adhesions are induced by specific binding between proteins with complementary domains, i.e, receptors and ligands. Other interactions provide different regulation mechanisms to fortify (e.g., cytoskeleton reorganization) or destabilize (e.g., repeller molecules) the adhesion contact. While adhesion receptors play the major role and are extensively studied, de-adhesion forces are crucial to ensure *specificity* of the adhesion (Bruinsma et al., 2000; Bruinsma and Sackmann, 2002). The interplay between attractive specific and (usually repulsive) non-specific forces is a recurring theme in cell adhesion, and provides delicate control over the adhesion–de-adhesion process in cell migration and immunological response.

While receptors and their ligands have been the focus of biological studies over the past decades, the physical carrier of these proteins—the cell membrane—has been extensively studied by physicists and biophysicists since the fluid-mosaic model was proposed by Mitchell and Nicholson. Membranes are composed of self-assembled lipid molecules and form vesicles in aqueous solutions of typical sizes up to 10 μm. The physics of fluid or solid membranes are well studied and summarized by Peliti (1994), Nelson et al. (2004), and Safran (1994). In particular the interactions between flexible membranes have been studied by Lipowsky and co-workers (Peliti and Leibler, 1985; Lipowsky and Leibler, 1986; Lipowsky, 1994, 1995).

Recent advances in bioengineering techniques have enabled studies of adhesion between biomimetic membranes mediated by specific and non-specific interactions. Sackmann and co-workers (Sackmann, 1996; Tanaka and Sackmann, 2005) have designed self-assembled vesicles and monolayers supported by a polymer cushion to mimic cell membranes and the extracellular matrix; in the membranes they incorporated specific proteins (to mimic ligand-receptor binding), glycolipids (to mimic the glycocalyx), as well as other additives to stabilize the vesicles. This system provides the first

biomimetic system incorporating key elements in cell adhesion and allows systematic studies of the dynamics and mechanics of adhesion without complications due to other factors present in biological cells.

Based on *in vitro* experiments using biomimetic vesicles, Sackmann, Bruinsma, and co-workers (Bruinsma et al., 2000; Bruinsma and Sackmann, 2002; Sackmann and Goennenwein, 2006) found that cell adhesion is controlled by a double-well potential: a weak-adhesion state at a large surface separation due to generic van der Waals interactions between lipids, and a strong-adhesion state at a small surface separation due to ligand-receptor binding; membrane undulation and glycolipid depletion induce repulsive forces that constitute the barrier between the two minima. The adhesion process proceeds in three steps (Albersdörfer et al., 1997; Kloboucek et al., 1999; Boulbitch et al., 2001; Sackmann and Bruinsma, 2002). First, small adhesion contacts are formed which are most likely induced by membrane undulations; such a process is an activated process with a nucleation barrier larger than 10 $k_{\rm B}T$. Following nucleation, receptors diffuse into the adhesion contacts and contact area grows accompanied by a depletion of repellers (glycolipids), this is the growth step. Finally, after receptors are depleted, the adhesion contacts evolve like coarsening in a phase separation: the number of adhesion contacts decreases and various small focal contacts are formed with high densities of receptors, accompanied by a possible decrease in the total area of contact. The whole process is likened to the wetting transition (Bruinsma and Sackmann, 2002) and phenomenological parameters like the surface tension, the spreading pressure, and the contact angle can be measured and related to underlying parameters, including the mechanical properties of the membrane and the molecular parameters of receptors (Bruinsma et al., 2000; Simson et al., 1998; Boulbitch et al., 2001).

The conformations of adhered membranes are recorded *in situ* by reflection interference contrast microscopy (RICM) (Rädler and Sackmann, 1993; Rädler et al., 1995), which provide direct experimental measurements of the formation and growth of adhesion plaques. However, RICM is unable to resolve adhesion contacts smaller than 300 nm (Boulbitch et al., 2001), therefore cannot give direct support for the nucleation process. On the other hand, scaling arguments and Monte Carlo studies (Lipowsky, 1994; Volmer et al., 1998) usually cannot yield quantitative results that are experimentally testable.

In this paper we present a systematic study of the nucleation step of the adhesion controlled by a double-well interacting potential. Following Bruinsma et al. (2000), Bruinsma and Sackmann (2002), and Sackmann and Bruinsma (2002), we assume the "minimum" model of membrane adhesion consisting of the elastic deformation energy of the flexible membrane and the double-well adhesion potential. As discussed above, this minimum model preserves the key features of cell adhesion. From a scaling analysis we find that the membrane shapes are governed by the adhesion length R_0 which is determined from the bending rigidity κ and adhesion potential; the energy barrier is controlled

by the energy scale $\sqrt{\kappa V_{\rm eff} L_0^2}$, where $V_{\rm eff}$ is the effective barrier height and L_0 is the characteristic length determined by the adhesion potential.

If $F_0 \gg k_{\rm B}T$, adhesion is a first-order transition and nucleation proceeds along the "minimum energy path" governed by the effective potential (free energy). Using the string method by E et al. (2002), we calculate the "minimum energy path" from the weakly bound state to a well-developed adhesion contact. We find that the typical energy barrier for adhesion between flexible membranes is about 20–30 $k_{\rm B}T$, corresponding to a time scale of 0.1–1000 seconds. For adhesion of cells with actin cortices, which have much larger bending modulus, the nucleation barrier is much larger and is essentially insurmountable by thermal undulations, and actin reorganization and cell signaling provide additional mechanisms for stabilizing the adhesion contact.

For F_0 comparable to $k_{\rm B}T$, we adopt a Peierls argument following Lipowsky (1994, 1995). We find that near the critical unbinding transition, adhesion is a weak first-order transition, and the adhesion dynamics depend on the shape of the irregular boundary. We show that if the potential minima have comparable depth, the adhesion dynamics are controlled by the potential depths only, and independent of the length scale of the double-well potential, which reflects the dominance of membrane undulations.

5.2 Model and solution

5.2.1 Model description

The thickness of a self-assembled monolayer or bilayer is about 10–100 nm, thus negligible compared to the spatial extension (~ 10 μm). Therefore the macroscopic behaviors of membranes are mostly determined by their geometric shapes, and to a good approximation independent of the microscopic degrees of freedom of the consistituent amphiphilic molecules. Flexible membranes as random surfaces have been extensively studied in the past decades by physicists; theoretical models and results are collected in the book edited by Nelson et al. (2004). For cell membranes or self-assembled monolayers with biological relevance, see Safran (1994) and the book edited by Lipowsky (1995); a more up-to-date review of simulation methods and other approaches is given by Müller et al. (2006).

For a single membrane that is homogeneous, smooth, and non-interacting, Canham (1970) and Helfrich (1973) proposed that up to 2nd-order derivatives with respect to the local coordinates of the membrane shape, the elastic energy of a deformed membrane is given by

$$\frac{H_{\rm e}}{k_{\rm B}T} = \int_S \left[\sigma + \frac{1}{2}\kappa \left(H - H_0\right)^2 + \bar{\kappa} K\right] {\rm d}A. \tag{5.1}$$

Here σ is the (local) surface tension conjugate to the surface area, κ and $\bar{\kappa}$ are elastic moduli known as the bending regidity and the Gaussian rigidity coupled to the mean curvature H and the Gaussian

curvature K, H_0 is the spontaneous curvature. The integral is over the whole membrane area[1].

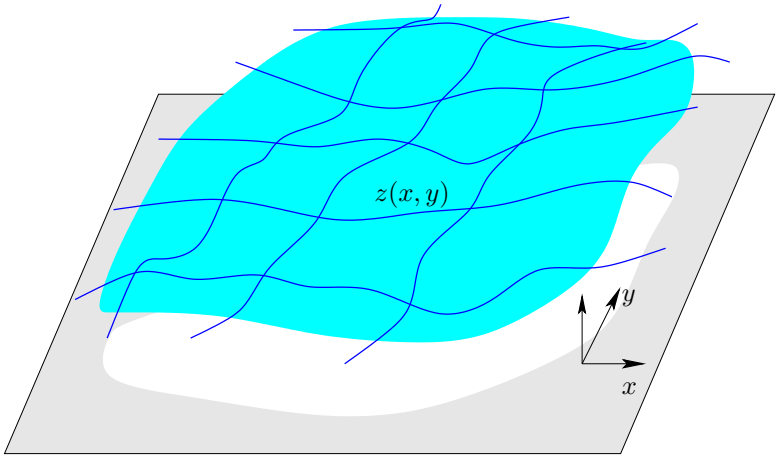

Figure 5.1: Monge representation of a near-flat membrane shape

In this paper we study the adhesion between a flexible membrane and a flat surface, corresponding to the experimental system studied by Bruinsma et al. (2000). For this model the separation between the membrane and the flat surface provides a natural representation of the membrane shape (cf. Fig. 5.1), $z = z(x, y)$, also called the Monge representation[2]. Since we focus on the initial stage of adhesion where the adhesion contact is small compared to the size of the membrane, we assume $H_0 = 0$, and in this case the Monge representation is useful. The elastic energy of the membrane is given by

$$\frac{H_\mathrm{e}}{k_\mathrm{B}T} = \int \left\{ \frac{\kappa}{2} \left[\Delta z(x, y)\right]^2 + \sigma \left[\nabla z(x, y)\right]^2 \right\} \mathrm{d}x\mathrm{d}y. \tag{5.2}$$

The elastic energy gives the "kinetic" part of the Hamiltonian, now we consider the interacting potential between the membrane and the adhering surface. Generic (non-specific) interactions, including the van der Waals interaction, electrostatic interaction, and hydration forces (see Nelson et al., 2004, Chapter 3) results in a potential V_g with a minimum around 10–100 nm (Albersdörfer et al., 1997; Bruinsma et al., 2000; Guttenberg et al., 2001). The net interaction between the surfaces mediated by receptors and repellers has been calculated in our previous paper[3]; for phenomenological treatments, see Zukerman and Bruinsma (1995), Bruinsma et al. (2000), and Weikl et al. (2002).

[1] The Helfrich Hamiltonian is the simplest renormalizable model for fluctuating membranes that satisfies Euclidean symmetry and reparametrization invariance; the functional accounts for the energy of elastic deformations from the equilibrium state with minimum area A_min and uniform curvature H_0. If the Gaussian rigidity is constant, then the Gaussian curvature term is constant for a surface with fixed topology (Euler characteristic). See Peliti (1994) and Nelson et al. (2004) for thorough discussions.

[2] In the case of adhesion between two membranes, the elastic energy is divided into two parts: one due to deformation of the "center of mass" of the binary system, the other dependent on the relative separation between the membranes; after integrating out the center of mass deformations, one can write the elastic energy dependent on the relative separation in the same form as above with the additive bending rigidity (cf. Lipowsky (1996))

$$\kappa^{-1} = \kappa_1^{-1} + \kappa_2^{-1}.$$

[3] Manuscript submitted to *Langmuir*.

The interaction potential due to receptors $V_{\rm s}$ can be generally written as a functional of the density distributions $\phi_{\rm i}(x,y)$, and $\phi_{\rm i}$ depends on the local surface separation $z(x,y)$. Here we assume that molecular transport is fast enough so that we can write $V_{\rm s}$ as a functional of the separation $z(x,y)$. Therefore the total Hamiltonian is given by [$\mathbf{r}=(x,y)$]

$$H[z(\mathbf{r}),\phi_{\rm i}(\mathbf{r})] = H_{\rm e}[z(\mathbf{r})] + V_{\rm g}[z(\mathbf{r})] + V_{\rm s}[z(\mathbf{r})]. \tag{5.3}$$

The free energy (effective potential) of the model given by (5.3) can be calculated by standard field theoretic method by integrating out fluctuations of the separation variable $z(\mathbf{r})$. These fluctuation effects have been extensively studied (Nelson et al., 2004); in particular, membrane fluctuations induce an effective repulsion which contributes to $V[z(\mathbf{r})]$. Since fluctuation effects are not our focus here, we apply a mean-field approximation and assume the free energy takes the same form as the Hamiltonian with *renormalized* elastic constants and interacting potential: these renormalized parameters are experimentally measurable; we shall consider the membrane undulation effects in Section 5.4 by scaling arguments.

With these approximations we can write the effective potential of our model as

$$\frac{F[z(\mathbf{r})]}{k_{\rm B}T} = \int \left\{ \frac{\kappa}{2} \left[\Delta z(\mathbf{r})\right]^2 + \sigma \left[\nabla z(\mathbf{r})\right]^2 + V[z(\mathbf{r})] \right\} {\rm d}^2\mathbf{r}. \tag{5.4}$$

The adhesion (interacting) potential $V(z)$ has a double-well shape (Bruinsma et al., 2000; Bruinsma and Sackmann, 2002) and is characterized by the depths of and the locations of the minima, as is schematically shown in Fig. 5.2(a). The parameters in Eq. (5.4) have been measured by Sackmann and co-workers in different systems (see Flyvbjerg et al., 1997; Simson et al., 1998; Kloboucek et al., 1999; Bruinsma and Sackmann, 2002; Sackmann, 2006; Sackmann and Goennenwein, 2006). κ is about 20 $k_{\rm B}T$ for a self-assembled bilayer, and of order 1000 $k_{\rm B}T$ for cells with actin cortices. σ is related to the so-called capillary length (Sackmann and Goennenwein, 2006)

$$R_{\rm c} = \sqrt{\kappa/\sigma},$$

which defines the length scale above which surface tension becomes important. Typical values for $R_{\rm c}$ are about 0.1–1 μm (Bruinsma et al., 2000; Sackmann and Goennenwein, 2006). Generally the size of adhesion plaques in the initial stage of adhesion is smaller than $R_{\rm c}$, therefore the bending energy dominates.

For clarity of our discussion it is convenient to scale the separation $z(\mathbf{r})$ and the radial coordinate r by natural length scales arisen from the adhesion potential and the membrane elasticity. After the general rescaling

$$r/R_0 \to r,\ l/L_0 \to l,\ z/L_0 \to z; V/V_2 \to v$$

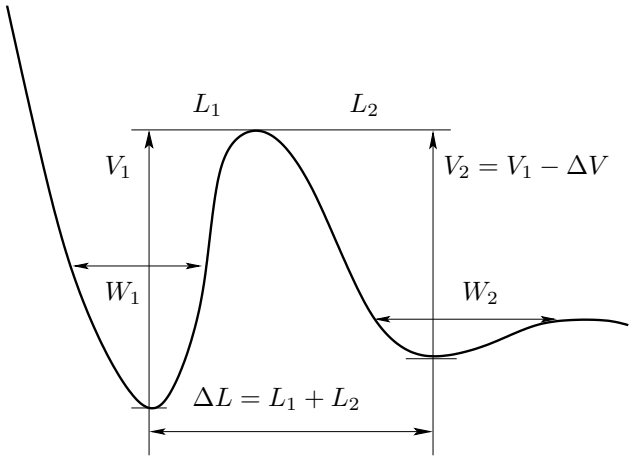

Figure 5.2: Schematic representation of the interaction potential $V(z)$. The shape of the potential is similar to that calculated from a phenomenological model proposed by Bruinsma et al. (2000). Only the part of the potential inbetween the minima are important for our calculations, and the potential is characterized by the position L_1, L_2 (fixing the barrier at the origin) and the depths W_1, W_2 of the minima. In our numerical calculations we choose the functional form for $V(z)$ such that the widths $W_1 \approx L_1$ and $W_2 \approx L_2$ for fast convergence.

the effective potential becomes

$$\frac{F[z]}{k_\mathrm{B}T} = \int_S \left[\frac{\kappa L_0^2}{2R_0^2}\left(\nabla^2 z\right)^2 + \gamma L_0^2 \left(\nabla z\right)^2 + V_2 R_0^2 v(z)\right] \mathrm{d}^2\mathbf{r}. \tag{5.5}$$

In the rigidity dominant regime, we choose

$$V_2 R_0^2 = \frac{\kappa L_0^2}{R_0^2},$$

such that the length scales are determined by the adhesion potential $V(z)$ and the bending rigidity. This leads to

$$\frac{F[z]}{k_\mathrm{B}T} = \sqrt{\kappa V_2 L_0^2} \int_S \left[\frac{1}{2}\left(\nabla^2 z\right)^2 + \frac{\Sigma}{2}\left(\nabla z\right)^2 + v(z)\right] \mathrm{d}^2\mathbf{r}, \tag{5.5$'$}$$

where

$$\Sigma = \frac{2\sigma L_0}{\sqrt{\kappa V_2}} = \frac{2R_0^2}{R_\mathrm{c}^2}, \tag{5.6}$$

$$R_0 = \left(\frac{\kappa L_0^2}{V_2}\right)^{1/4}. \tag{5.7}$$

We call R_0 the adhesion length (similar to the "persistence length" defined by Sackmann and Goennenwein (2006)), which turns out to control the interfacial width of the adhesion contact. In general $R_0 \sim 10$ nm $\ll R_\mathrm{c}$, therefore the surface tension term is unimportant.

We further notice that the combination $\sqrt{\kappa V_2 L_0^2}$ (even though L_0 is unspecified) controls the

magnitude of the free energy. If $\kappa V_2 L_0^2 \gg 1$, then the minima of $V(z)$ is separated by a large barrier (cf. Lipowsky (1995, 1994)). In this regime, thermal fluctuations are unimportant compared to the adhesion energy, and we can apply the mean-field capillary approximation.

5.2.2 Scaling analysis of the nucleation dynamics

Experimental measurements suggest that cell adhesion is a first-order transition (Albersdörfer et al., 1997; Boulbitch et al., 2001), therefore the potential minima are separated by a large barrier and adhesion should proceed via a nucleation-and-growth pathway. Here we study the nucleation dynamics in this regime using the classical capillary approximation.

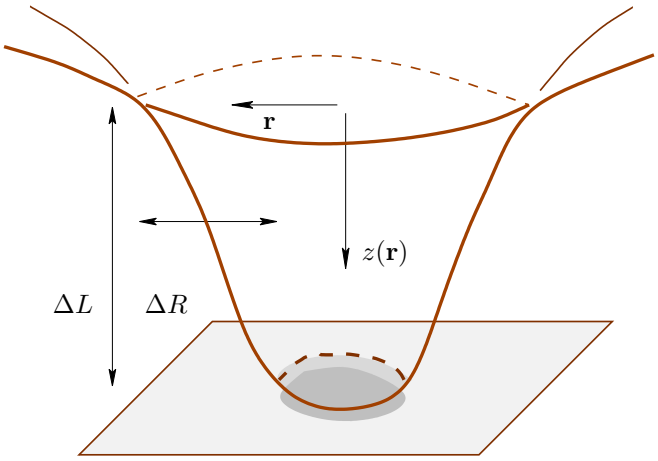

Figure 5.3: Illustration of a regular adhesion droplet

Initially the membrane is in a loosely bound state at a larger separation L_2, and the equilibrium shape is flat. Nucleation of an adhesion contact is driven by membrane undulations and results in a droplet as shown in Fig. 5.3. When thermal fluctuations are irrelevant, the boundary of the adhesion droplet is regular (a simple curve), and without loss of generality we assume the droplet to be axi-symmetric and the membrane deviation to be a function of the radius $z(r)$. If potential depths are comparable, i.e., $\Delta V \ll V_2$, the length scale L_0 associated with the adhesion potential $V(z)$ is naturally chosen to be the separation between the minima ΔL; otherwise when $\Delta V > V_2$, L_0 should be taken to be the separation of the metastable minimum (V_2) from the barrier, L_2.

In the first case, there is a well-defined adhesion "nucleus" which has size R in the interior and an interfacial area of width ΔR (cf. Fig. 5.3). The length scales are

$$L_0 = \Delta L,$$
$$R_0 = \left(\frac{\kappa \Delta L^2}{V_2}\right)^{1/4},$$

and the energy scale is

$$F_0 = \sqrt{\kappa V_2 \Delta L^2}.$$

From scaling analysis we have ($\Delta r = \Delta R/R_0, r = R/R_0$)

$$\nabla^2 z \sim \frac{L_0}{\Delta R^2}, \kappa \int (\nabla^2 z)^2 \mathrm{d}A \sim \frac{\kappa R L_0^2}{\Delta R^3}; \tag{5.8}$$

$$\int [V(z) - V(L_2)] \mathrm{d}A \sim -\pi R^2 \Delta V + \pi R \Delta R V_2. \tag{5.9}$$

Combining these two contributions we find

$$\Delta R \sim R_0 = \left(\frac{\kappa \Delta L^2}{V_2} \right)^{1/4}. \tag{5.10}$$

We recognize that the free energy is similar to that in the capillary approximation, with a line tension

$$\Gamma = \Delta R V_2 \sim \kappa^{1/4} V_2^{3/4} \Delta L^{1/2}. \tag{5.11}$$

At the critical radius $R^\ddagger$ the free energy attains maximum, and we have

$$R^\ddagger \sim \frac{V_2}{\Delta V} \Delta R = \frac{V_2}{\Delta V} \left(\frac{\kappa \Delta L^2}{V_2} \right)^{1/4} = \frac{V_2}{\Delta V} R_0, \tag{5.12}$$

$$F^\ddagger \sim \frac{V_2^2}{\Delta V} \Delta R^2 = \frac{V_2}{\Delta V} (\kappa V_2 \Delta L^2)^{1/2} = \frac{V_2}{\Delta V} F_0. \tag{5.13}$$

In the second case $V_2/\Delta V \lesssim 1$, and the radius R is comparable to the boundary width δR. The above results become

$$R \sim \delta R \sim R_0 = \left(\frac{\kappa \Delta L^2}{V_2} \right)^{1/4}, \tag{5.12$'$}$$

$$F \sim \pi R_0^2 V_2 = F_0. \tag{5.13$'$}$$

From Eqs. (5.12), (5.13) and (5.12$'$), (5.13$'$) we see that R_0 and F_0 control the length (R and ΔR) and energy (F) scales. The scaling $R^\ddagger \sim V_2^{-1/4}$ is different from classical mean-field results $R^\ddagger V^{-1/2}$ which is due to the difference in the surface energy. We note that the capillary analysis is valid only if $F_0 \gg k_\mathrm{B} T$, and thermal fluctuations are not important. In particular,

$$\kappa V_2 \Delta L^2 \approx 1 \tag{5.14}$$

marks the tricritical point where the unbinding transiton crosses over from first order to second order (Lipowsky, 1994).

5.2.3 Minimum-energy-path calculation

Under the mean field approximation (zero temperature limit), nucleation proceeds along the "minimum energy path," or the valley on the free energy landscape. We parametrize this path by a variable s and represent the path as

$$z(r,s) : s \to z(r).$$

The minimum energy path (MEP) is defined such that the tangent along the path $\nabla_s z(r,s)$ is parallel to the free energy gradient $\delta F[z]/\delta z$ at $z(r,s)$ for any s, or equivalently

$$\left(\frac{\delta F[z]}{\delta z}\right)^{\perp} = \frac{\delta F[z]}{\delta z} \cdot (\mathbf{I} - \hat{s}\hat{s}) = 0 \tag{5.15}$$
$$\hat{s} = \frac{\nabla_s z(r,s)}{\|\nabla_s z(r,s)\|}.$$

To calculate $z(r,s)$ we adopt the string method by E and co-workers (E et al., 2002), which is a modified steepest descent

$$\frac{\partial z(R,s;t)}{\partial t} = -\frac{\delta F[z]}{\delta z} \cdot (I - \hat{s}\hat{s}) + \lambda \hat{s}. \tag{5.16}$$

Here λ is a Lagrangian multiplier which is used to fix the parametrization s. The choice of λ is arbitrary, and we adopt the same parametrization as given by E et al. (2002), which requires the points be uniformly separated along the path,

$$\|\nabla_s z(r,s)\| = \text{const.}$$

which has a close form expression.

$\delta F[z]/\delta z$ is the free energy gradient

$$\frac{\delta F[z]}{\delta z} = \Delta^2 z - \Sigma \Delta z + v'(z). \tag{5.17}$$

In radial coordinates, the Laplacian is

$$\Delta \to \frac{\mathrm{d}^2}{\mathrm{d}r^2} + \frac{1}{r}\frac{\mathrm{d}}{\mathrm{d}r},$$

and

$$\Delta^2 \to \frac{\mathrm{d}^4}{\mathrm{d}r^4} + \frac{2}{r}\frac{\mathrm{d}^3}{\mathrm{d}r^3} - \frac{1}{r^2}\frac{\mathrm{d}^2}{\mathrm{d}r^2} + \frac{1}{r^3}\frac{\mathrm{d}}{\mathrm{d}r}.$$

To implement the steepest descent as described by Eq. (5.16), we proceed as follows: First we impose a circular droplet centered at $z = \Delta L$ which has a radius large enough such that letting it evolve along the free energy gradient (steepest descent) the size of the droplet grows instead of shrinking to the flat profile. After evolving for some steps the profile reaches steady growth, and

has passed the nucleation barrier, and this profile is taken as the final state $z(r, s = 1; t = 0)$, and the initial path is generated by a simple linear interpolation between $z = 0$ and $z(r, s = 1; t = 0)$. Although the final state $z(r, s = 1; t = 0)$ might not be on the minimum energy path, after iteration using Eq. (5.16), the whole path will evolve to the MEP and the maximum of the free energy corresponds to the critical "nucleus."

We adopt an explicit forward time splitting for the potential $V(z)$ and an implicit splitting for the differential operators, which ensures fast convergence[4]. Iteration stops when the maximum free energy of the reaction path $\max_s F[z(s)]$ reaches a constant and the maximum residual gradient $\max_s\{\nabla F(z)^\perp\}$ is used to test the accuracy of convergence. In the next section we discuss the numerical results.

5.3 Numerical results and discussion

In this section we discuss numerical results of the minimum-energy-path (MEP) calculations. Before the discussion we first estimate the typical length and energy scales associated with the adhesion process. The bending rigidity κ is about 20 $k_{\rm B}T$ for bilayer membranes and 1000 $k_{\rm B}T$ for cell membranes with actin cortices (Sackmann and Goennenwein, 2006; Bruinsma and Sackmann, 2002). The separation ΔL is between 5 and 50 nm, depending on the size of the receptors (Bruinsma et al., 2000; Martin et al., 2006), and we take $L_0 = 5$ nm. The barrier height V_2 is estimated to be 10^{-5} J/m^2 (Bruinsma et al., 2000). Therefore the energy scale for flexible membranes is (at $T = 300$ K)

$$F_0 = (\kappa V_2 \Delta L^2)^{1/2} \approx 1 k_{\rm B}T,$$

which indeed reflects flexibility. The lateral length scale is

$$R_0 = \sqrt[4]{\kappa \Delta L^2 / V_2} \approx 2 \text{ nm}.$$

In the case of cell membranes with actin network, F_0 increases by about 7 times and R_0 about 2.5 times. The capillary length

$$R_{\rm c} = \sqrt{\kappa/\sigma}$$

is usually of order 0.1μm (Sackmann and Goennenwein, 2006), and hence the surface tension

$$\Sigma \sim \frac{R_0^2}{R_c^2}$$

is small, and we neglect the surface tension term in our calculations except in the discussion of their effects on adhesion.

[4]See for example, the (p)reprints at `http://www.math.utah.edu/~eyre/research/methods/papers.html`.

In the following discussions quantities are represented using the scaled units. The scaled potential $V(z)$ is parametrized by the positions of the potential minima and their depth as

$$V(z) = p(z; -L_1, V_1) + p(z; L_2, V_2),$$

where $p(x; L, V)$ is given by

$$p(x; L, V) = -V\left[\left(\frac{x}{L} - 1\right)^2 - 1\right] \exp\left[-4\left(\frac{x}{L} - 1\right)^2\right]. \tag{5.18}$$

The combined potential has two minima located at $-L_1$ and L_2 with depths V_1 and V_2, and the barrier is located at $z = 0$. An example is shown in Fig. 5.4.

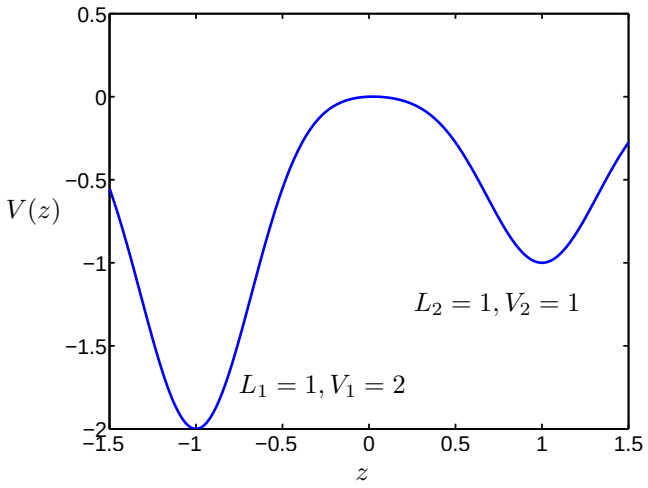

Figure 5.4: Shape of the potential $V(z)$ for $L_1 = L_2 = 1$, $V_1 = 2$, $V_2 = 1$

In Fig. 5.5 we present two representative nucleation paths. The barrier height is $V_2 = 1$, the locations of minima are $L_2 = 1$, $L_1 = 1$, and we choose two cases $V_1 = 1.3$ and $V_1 = 4$, giving potential depth difference $\Delta V = 0.3$ and 3, respectively. Figure 5.5(a) and (c) show the evolution of membrane shapes along the minimum energy path (MEP): the membrane conformation evolves in the direction of the arrow; Figure 5.5(b) and (d) give the free energy along the MEP with red circles corresponding to each membrane shape shown on the left. The red thick curves in (a) and (c) are the critical shape corresponding to the maximum free energy along the nucleation contour (saddle point).

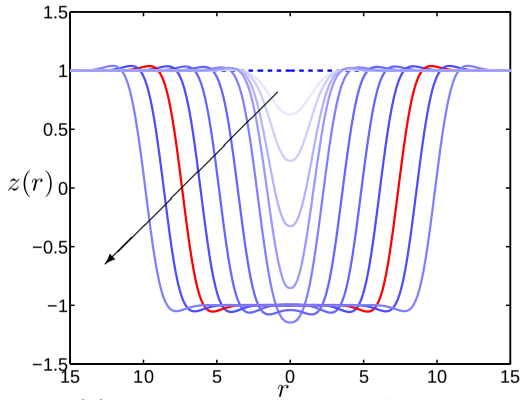

(a) Membrane shapes for $\Delta V = 0.3$

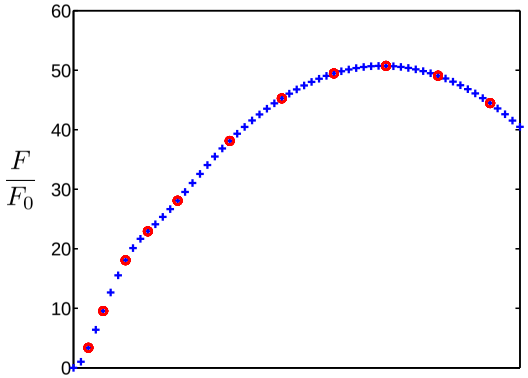

(b) Minimum energy path for $\Delta V = 0.3$

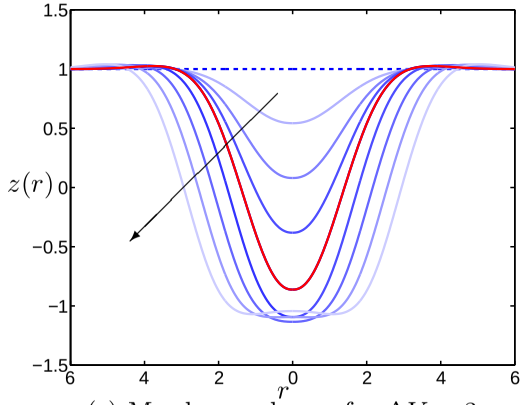

(c) Membrane shapes for $\Delta V = 3$

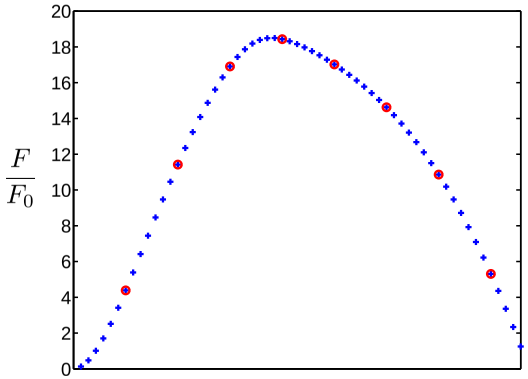

(d) Minimum energy path for $\Delta V = 3$

Figure 5.5: Evolution of the adhesion shape [(a) and (c)] and the free energy [(c) and (d)] along the minimum energy path for different adhesion potentials. Free energies of the representative shapes in (a) and (c) are shown as red circles in (b) and (d), with the red (most saturated) curve giving the critical shape corresponding to the maximum free energy along the contour. (a) and (b) are for the case when the potential depths are comparable, $V_1 = -1$ and $V_2 = -1.3$; (c) and (d) are for $V_1 = -1$ and $V_2 = -4$. In both cases the separation of the potential minima to the barrier is 1, given $\Delta L = 2$.

In the case that the barrier height is large, $\Delta V = 0.3 < V_2 = 1$, we see that the critical nucleus has a well-formed adhesion contact with radius $R^\ddagger \approx 7R_0 = 14$ nm, with an interfacial width $\delta R \approx 3R_0 = 6$ nm: this is similar to the classical nucleation scenario where capillary approximation applies. On the other hand for $\Delta V = 3 > V_2$, the critical shape has not formed an adhesion contact yet, but barely passed the barrier position $z = 0$. The free energy barrier in the second case is about 18 $k_\mathrm{B}T$ while in the first case is 51 $k_\mathrm{B}T$, the ratio is about 2.8, which is quite close to the scaling result given by $V_2/\Delta V = 1/0.3 \approx 3.33$.

To have a better understanding of the nucleation dynamics, we estimate the characteristic time scales of membrane undulations. By dimensional analysis, we have

$$\tau_\mathrm{un} \sim \eta L^3/k_\mathrm{B}T = 0.24 \text{ ns}$$

for $L = 1$ nm. For an energy barrier of 25 $k_\mathrm{B}T$ the nucleation time is

$$\tau_0 \sim \tau_\mathrm{un} e^{-F^\ddagger/kT} \sim 14 \text{ s}.$$

Therefore in the first case ($\Delta V = 3$) there is little barrier and nucleation is fast, while in the second case ($\Delta V = 0.3$) the nucleation barrier is so high that it is essentially impossible. It has been pointed out by Bruinsma et al. (2000) and by us (Martin et al., 2006) that in the initial stage of adhesion receptors form local aggregrates with very high densities, resulting in a deep potential minimum; our calculations further corroborate this assumption. On the other hand, for cellular adhesion the nucleation barrier is much higher and the reorganization of the actin cortex provides a mechanism to fortify the adhesion contact; other mechanisms such as dimerization can also be triggered by cell signaling.

Komura and Andelman (2000) studied the membrane shape near the phase boundary under lateral phase separation induced by adhesion, and found that the membrane deformation is non-monotonic near the phase boundary between coexisting phases. Our results show that this non-monotonic feature is present throughout the adhesion process. As we shall see at the end of this section, this feature is due to the bending energy term; increasing surface tension will diminish this feature.

To study the crossover between the two scenarios shown in Fig. 5.5, we plot the critical membrane shapes for different ΔV in Fig. 5.6. We notice that for $2 \leq \Delta V \leq 4$ the critical shape is almost invariant: in this regime the barrier height V_2 is small compared to the potential depth difference ΔV, and nucleation is determined by the potential near the metastable minimum at L_2. On the other hand, when ΔV is small, the critical shape has a well-developed adhesion contact with increasing radii as ΔV becomes smaller, and one can compare the critical radius and free energy with scaling results from the capillary approximation.

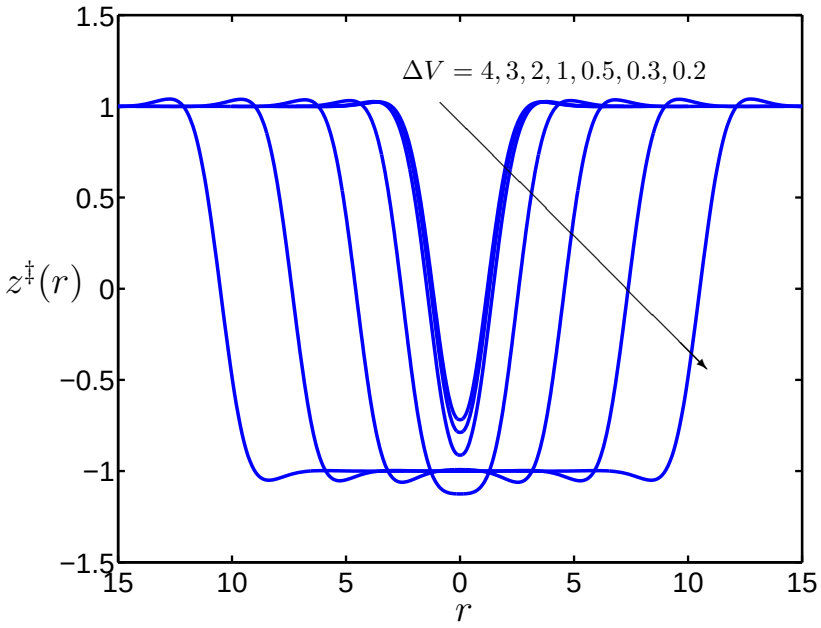

Figure 5.6: Critical membrane shapes at different potential depths. The positions of the minima are the same as in Fig. 5.5, $L_1 = L_2 = 1$. $V_2 = 1$ and $V_1 = V_2 + \Delta V$ with $\Delta V = 4, 3, 2, 1, 0.5, 0.3, 0.2$ along the arrow.

In Fig. 5.7 we plot the free energy barrier $F^{\ddagger}$ (maximum on the MEP) and the critical nucleus $R^{\ddagger}$, defined as the radius of the membrane contact within the adhesion minimum (with $z(r) < 0$). The plot is on a log-log scale. Scaling arguments imply that when $\Delta V \ll V_2$, the free energy barrier and the critical nucleus both scale as $1/\Delta V$. Numerical results indeed confirm this scaling. When $\Delta V \gg V_2$, scaling arguments suggest that ΔV is irrelevant, this trend also holds approximately.

Inspecting Fig. 5.6 we notice that critical shapes at different ΔV resemble the growth of a single adhesion contact, as in Fig. 5.5(a). Scaling analysis suggests that in the bending dominant regime the controlling length scale is $R_0 = (\kappa L_0^2/V_2)^{1/4}$, which is independent of the potential depth difference; in particular, the interfacial width $\delta R \sim R_0$. Therefore all membrane shapes look similar. Since only R_0 controls the shape of membrane deformations, we expect that the nucleation path in the conformation space is mostly determined by R_0, through the barrier height V_2, the length scale L_0 (which is proportional to ΔL here) and the bending rigidity κ; potential depth difference ΔV controls only the location of the saddle point along the nucleation path and the energy barrier.

To verify the dependence of nucleation on the minimum separation ΔL, we calculate the energy barrier $F^{\ddagger}$ and the critical radius $R^{\ddagger}$ for interacting potential $V(z)$ with potential minima having the same depths but varying locations. These results are shown in Fig. 5.8. The potential depths are fixed at $V_1 = 2$ and $V_2 = 1$ and the minima are located at $-L$ and L with L varying from 1 to 2. We see that scaling relations $R^{\ddagger} \propto \Delta L^{1/2}$ and $F^{\ddagger} \propto \Delta L$ fit well with numerical results.

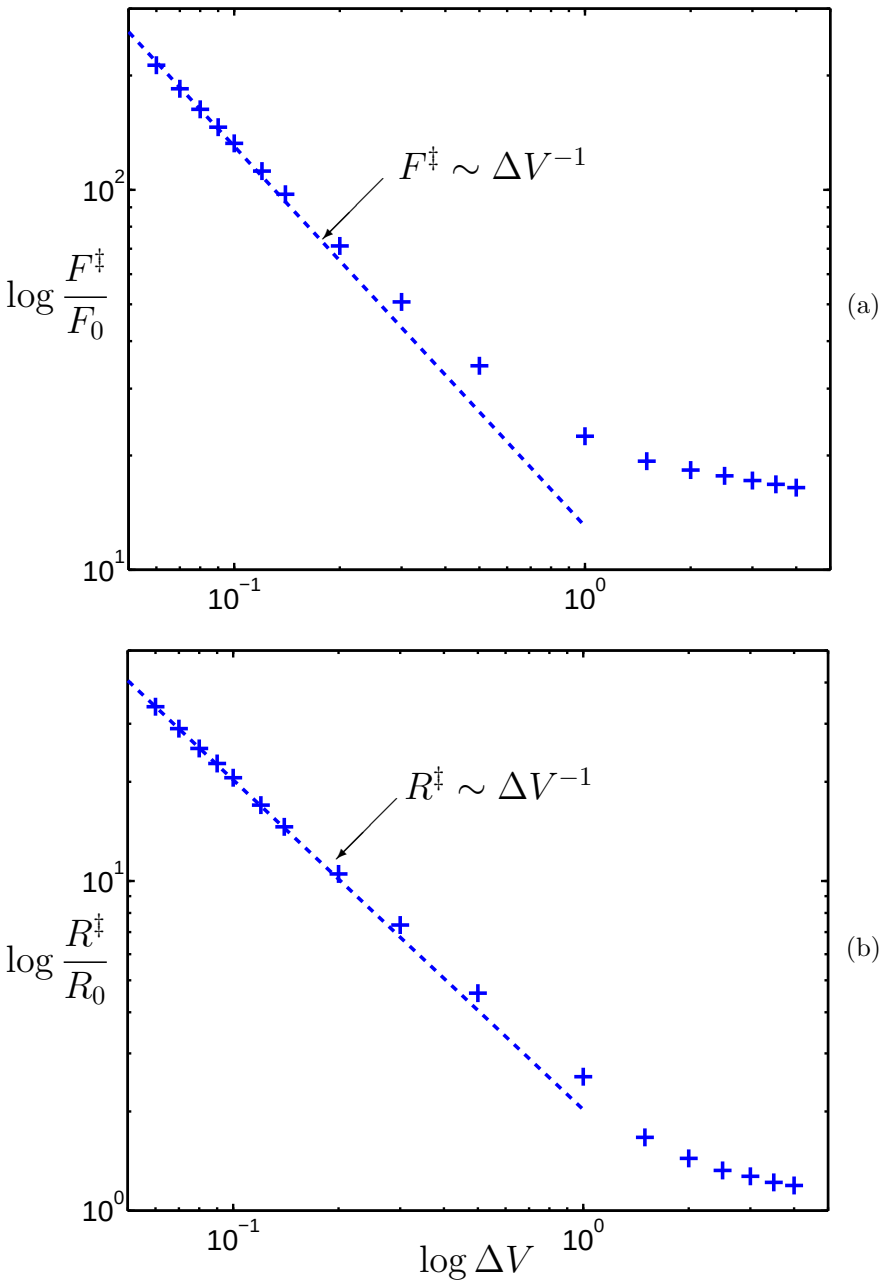

Figure 5.7: The saddle point free energy $F^\ddagger$ and the critical shape radius $R^\ddagger$ at different potential depths. The potential is identical to that in Fig. 5.6 with changing ΔV. The radius R is defined as the radial size of the contact area within the adhesion potential well: in our case the barrier is fixed at $z = 0$, therefore the radius is given by the size of the contact with $z \leq 0$.

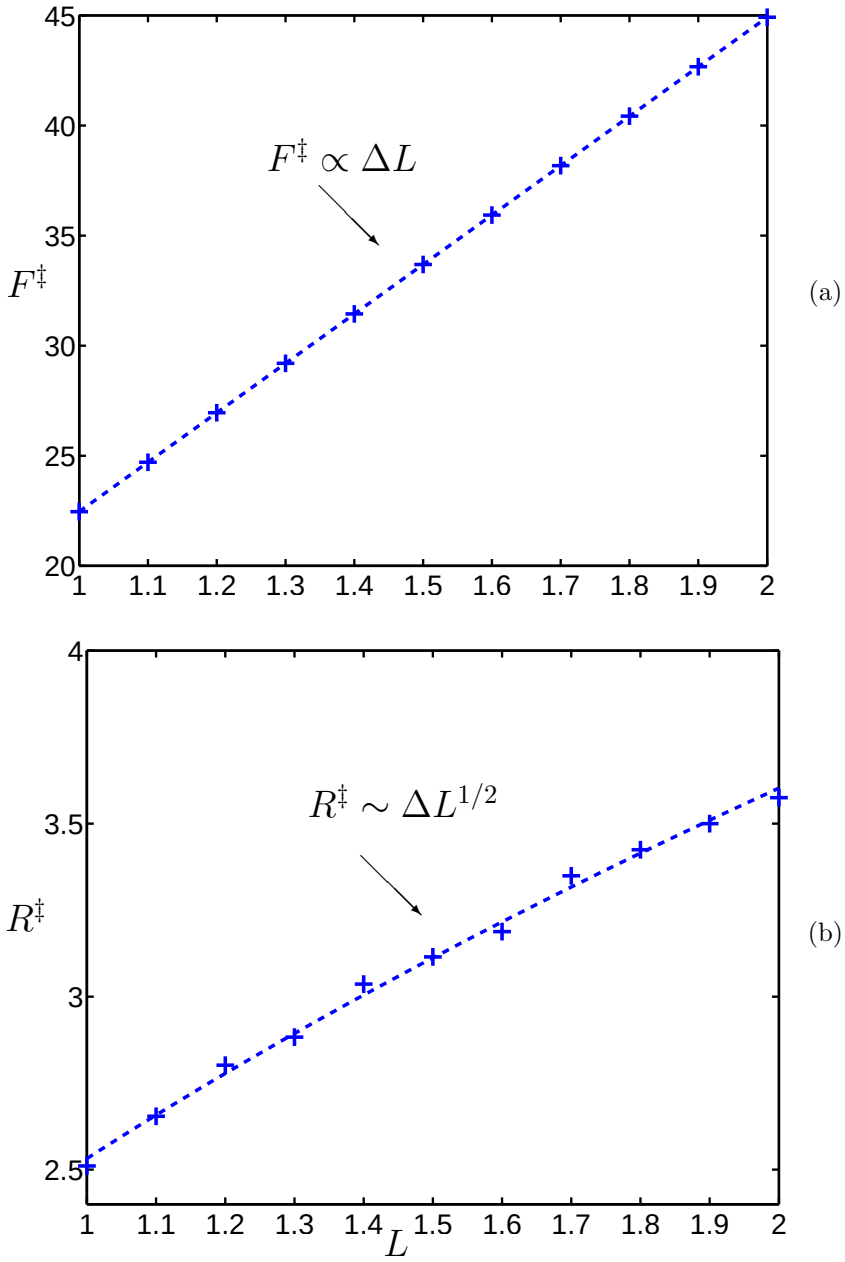

Figure 5.8: The saddle point free energy $F^\ddagger$ and the critical shape radius $R^\ddagger$ at different potential well separations. The potential wells are symmetrically positioned across the barrier with separation $\Delta L = 2L$ ranging from 2 to 4. The potential depths are fixed at $V_1 = 2$, $V_2 = 1$. Linear fits are done for $F^\ddagger$ against ΔL and $\log R^\ddagger$ against $\log \Delta L$ and show as dash lines.

Finally we study the effects of the surface tension term. Fig. 5.9(a) shows the development of an adhesion nucleus under strong surface tension $\Sigma = 3$. The potential depths are $V_1 = 2$ and $V_2 = 1$ and the minima are located at $L_1 = L_2 = 1$. Compared to the case with no surface tension, we observe that the membrane shape is flatter, and the extra surface energy increases the critical nucleus size. Fig. 5.9(b) shows the crossover of the critical membrane shape from rigidity-dominant regime to tension-dominant regime and the straighten-up of the membrane shape due to surface tension is apparent. In Fig. 5.9(c) we plot the energy barrier against the surface tension. Under a small surface tension, the size of the critical nucleus does not change much and is still determined by the adhesion length R_0, hence the extra surface area of the adhesion droplet is almost constant, and the free energy should be a linear function of the surface tension: this is also verified by numerical results.

In summary we have shown that the adhesion strength $R_0 = (\kappa \Delta L^2/V_2)^{1/4}$ controls the evolution of the membrane shape in the nucleation process, and the energy scale $F_0 = \sqrt{\kappa V_2 \Delta L^2}$ determines the nucleation barrier and the dynamics of the process. Our numerical results verify the scaling relations obtained from capillary approximations. In addition, the surface tension term flattens out the membrane shape and adds a surface energy to the energy barrier which is a linear function of the surface tension.

Our results apply to membrane adhesions mediated by any double-well adhesion potential. In particular, we note that our model also applies to the formation of the immunological synapse, which are focal contacts between a T-lymphocyte cell and an antigen-present cell (APC) (Grakoui et al., 1999). The synapse primarily consists of the T-cell receptor (TCR)–Major Histocompatibility molecule-peptide Complex (MHC) bonds and integrin (ICAM-1/LFA-1) bonds. Due to their different spatial extensions (the natural size of the integrin-ligand bond is $\sim$40nm, and is about 15nm for the TCR-MHC complex), the binary system consisting of TCR and integrin binding should exhibit a double-well interaction potential (Raychaudhuri et al., 2003). Given the high membrane bending rigidity ($\sim 400kT$) of the T-cell, our results suggest that even after the integrin bonds form an adhesion contact (surfaces are brought close to 40nm separation), nucleation of the TCR contact at normal TCR densities still exhibits a considerable barrier. Such a barrier would be impossible to overcome by thermal fluctuations. Therefore some active mechanism is likely to be involved that overcomes this barrier. Alternatively, increasing TCR expression could lower the TCR binding minimum, thereby descreasing the nucleation barrier [cf. Fig. 5.7(a)], which is the case in the synapse between a mature T-cell and APC (Qi et al., 2001). The fact that the synapses between premature T-cells (thymocytes) and the APC do not show a well-developed contact with TCR-MHC bonds could be due to either insufficient TCR bonds (Lee et al., 2003; Raychaudhuri et al., 2003), or the absence of active mechanisms to overcome the high energy barrier. Our calculations thus offer a complementary perspective to the work by Chakraborty and co-workers which did not explicitly

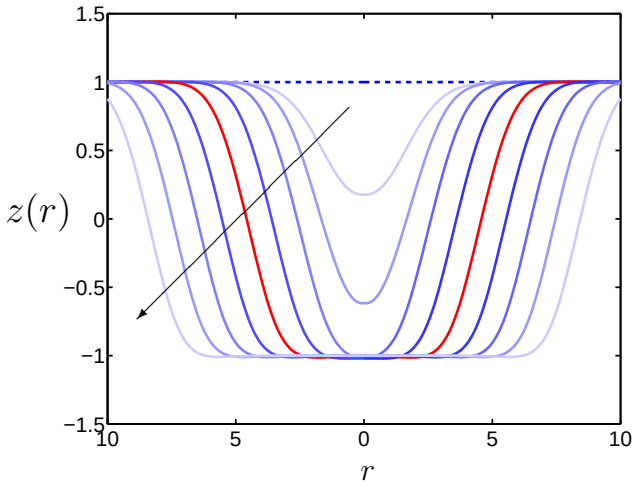

(a) Evolution of the membrane shape with $\Sigma = 3$

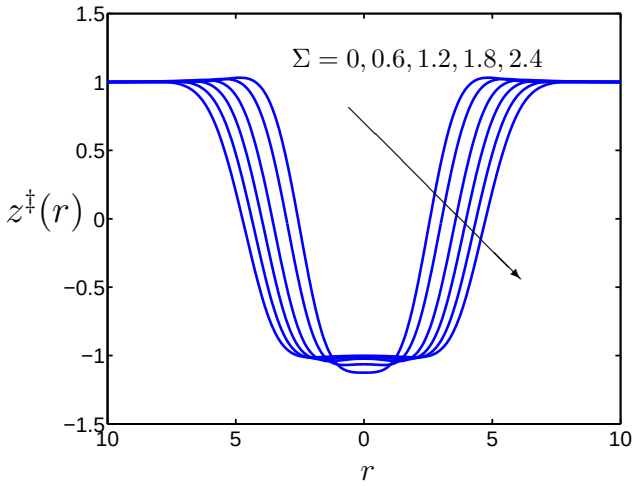

(b) Critical membrane shapes at different Σ

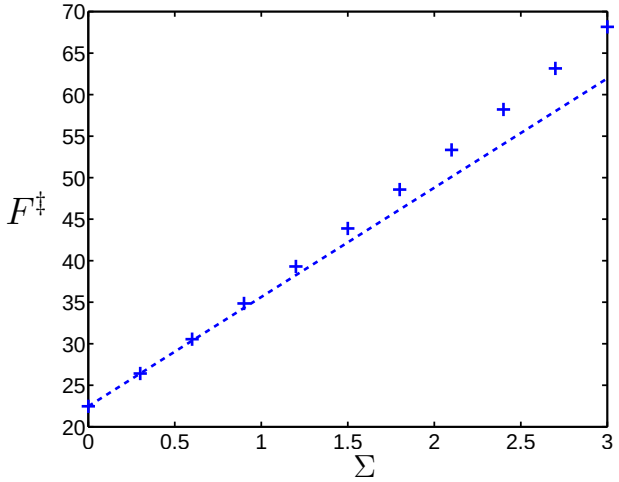

(c) Saddle point free energy at different Σ

Figure 5.9: Illustration of the effects of surface tension. The potential is parametrized by $L_1 = L_2 = 1$, $V_1 = -2$, $V_2 = 1$.

address the issue of nucleation.

5.4 The Peierls argument near the critical unbinding transition

Above we have discussed the nucleation dynamics of adhesion that is controlled by a large energy barrier. Here we study the scenario when the energy barrier is small, i.e.,

$$\kappa V_2 L_0^2 \lesssim k_{\rm B}T.$$

This is the case when the barrier is small or the membrane is very flexible. In this regime thermal fluctuations (membrane undulations) are comparable to the size of adhesion plaques, and the shape of the adhesion contact may be irregular. Our discussions follow those by Lipowsky and co-workers (Lipowsky, 1994, 1995; Lipowsky and Dimova, 2003).

Before the discussion of adhesion dynamics we first briefly discuss the interaction between the membrane surfaces due to shape undulations. For a membrane confined within a well of width W, the confinement free energy is found to be (Lipowsky, 1995)

$$\frac{V}{k_{\rm B}T} = \frac{c_1}{\kappa W^2}. \tag{5.19}$$

c_1 is a constant of order 1. This extra entropic repulsion contributes to the free energy at each minimum $c_1/\kappa W^2$, and results in an effective energy barrier $V_{\rm eff} < V_2$, the bare energy barrier that is calculated based on molecular models of ligand-receptor binding by us (Martin et al., 2006).

Taking into account the entropic contributions, we find the renormalized potential depth difference ΔV to be

$$\Delta V = \Delta V_{\rm bare} - \frac{c_1}{\kappa W_1^2} + \frac{c_1}{\kappa W_2^2}, \tag{5.20}$$

where $W_{\rm i}$ are the widths of the potential minima. $\Delta V = 0$ corresponds to the binodal phase coexistence (binding-unbinding transition).

If κ is small or the energy scale $F_0 = \sqrt{\kappa V_{\rm eff} L_0^2} \sim k_{\rm B}T$, then membrane undulations are prominent and the boundary width δR is controlled by thermal fluctuations and determined as

$$\kappa \left(\frac{L_0}{\delta R^2}\right)^2 \delta R^2 \sim 1 \Rightarrow \delta R \sim \sqrt{\kappa} L_0. \tag{5.21}$$

Here L_0 is the membrane roughness which measures the magnitude of thermal undulations. In the adhesion we can take L_0 to be the width of the metastable minimum W_2.

As we mentioned at the beginning of this section, membrane undulations induce an effective

repulsion between the surfaces; the effective barrier height is

$$V_{\rm eff} = V_2 - \frac{c_1}{\kappa W_2^2}, \tag{5.22}$$

where the 2nd term corresponds to the confinement energy of membrane undulations within the metastable minimum. The line tension is given by

$$\gamma \propto V_{\rm eff}\delta R. \tag{5.23}$$

If $\kappa V_2 W_2^2 \lesssim k_{\rm B}T$, then the line tension becomes zero and the barrier vanishes. Below we focus on the case when $\kappa V_2 W_2^2 > k_{\rm B}T$ with $V_{\rm eff} > 0$.

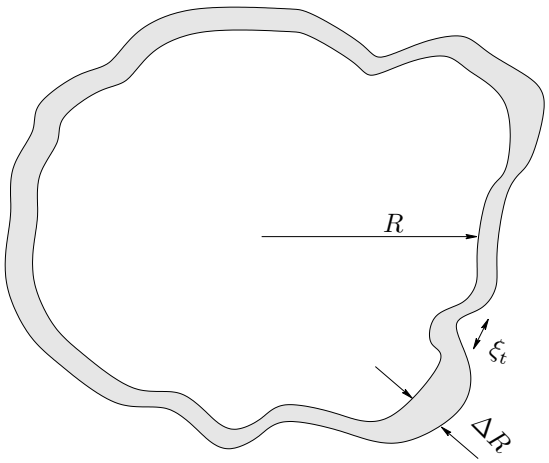

Figure 5.10: Projection of an irregular droplet

When fluctuations are prevalent, the domain boundaries between the adhesion states (corresponding to the two potential minima) are irregular, and we can apply a Peierls-type argument to account for the extra entropic contribution due to the fluctuations of the boundary shapes. Assume the boundary to be a self-avoiding walk in 2D plane (2D SAW) with Hausdorff dimension 4/3, then the perimeter of a droplet scales as

$$\mathcal{L} \sim \frac{R^{4/3}}{\xi_{\rm t}^{1/3}}, \tag{5.24}$$

where $\xi_{\rm t}$ is the "unit" step size of this self-avoiding loop (δR is the width of this loop, see Fig. 5.10). The configuration entropy of the domain boundary is given by

$$S \approx c_2 \frac{\mathcal{L}}{\xi_{\rm t}}, \tag{5.25}$$

c_2 is a universal constant.

For a string with line tension γ and width δR, the step size or persistence length scales as

$\xi_t \sim \gamma\delta R^2$, therefore the combined interface energy is given by

$$\begin{aligned}\Gamma = \gamma\mathcal{L} - S &= \left(\gamma - \frac{c_2}{\xi_t}\right)\mathcal{L} \\ &= \left(\gamma - \frac{c_2}{\gamma\delta R^2}\right)\frac{R^{4/3}}{(\gamma\delta R^2)^{1/3}}.\end{aligned} \tag{5.26}$$

We see that if $\gamma\delta R \sim 1$, i.e.,

$$\kappa V_{\text{eff}} L_0^2 \sim 1, \tag{5.27}$$

then the interface energy is of order $k_B T$ and adhesion is a second-order transition. If $\gamma\delta R \gg 1$, then

$$\Gamma \sim V_{\text{eff}}^{2/3} R^{4/3}, \tag{5.28}$$

and adhesion is a weak first-order transition. While Eq. (5.27) gives the transition from first order adhesion to second order, which should be governed by a tricritical point (Lipowsky, 1995).

For the weak first order transition that is still governed by the critical point, we can modify the capillary argument by incorporating the entropic correction. For an adhesion plaque ("nucleus"), the total free energy is

$$\begin{aligned}F &= -\pi R^2 \Delta V + \Gamma, \\ &= -\pi R^2 \Delta V + R^{4/3} V_{\text{eff}}^{2/3}.\end{aligned} \tag{5.29}$$

The critical radius is

$$R^{\ddagger} \sim V_{\text{eff}} \Delta V^{-3/2}, \tag{5.30}$$

and the free energy barrier scales as

$$F^{\ddagger} \sim \left(\frac{V_{\text{eff}}}{\Delta V}\right)^2. \tag{5.31}$$

Eqs. (5.30) and (5.31) apply to the regime when the persistence length of the boundary $\xi_t \ll R$, i.e,

$$\gamma\delta R^2 \ll R^{\ddagger} \Rightarrow \kappa \Delta V L_0^2 \ll 1. \tag{5.32}$$

This is further translated into $\Delta V \ll V_{\text{eff}}$. We note that in this regime the critical size $R^{\ddagger}$ and the energy barrier only depend on the potential depths, but not on the length scale associated with the potential $V(z)$; this is because membrane undulations are comparable to the separation between the potential minima, and the tunneling of the barrier is controlled by thermal fluctuations but not the shape of the adhesion potential.

If $\kappa\Delta V L_0^2 > \kappa V_{\text{eff}} L_0^2$, then

$$R \sim \delta R = \sqrt{\kappa} L_0 \tag{5.30$'$}$$

and the energy is given by

$$F \sim R^2 V_{\text{eff}} = \kappa V_{\text{eff}} L_0^2. \tag{5.31'}$$

Table 5.1 summarizes the scaling results in this section and in Section 5.2.2.

Rigid Membrane $\kappa V_2 L_0^2 \gg 1$		
	$V_2 \gg \Delta V$	$\Delta V \gtrsim V_2$
R	$\frac{V_2}{\Delta V}\left(\frac{\kappa \Delta L^2}{V_2}\right)^{1/4}$	$\left(\frac{\kappa L_2^2}{V_2}\right)^{1/4}$
F	$\frac{V_2}{\Delta V}\sqrt{\kappa V_2 \Delta L^2}$	$\sqrt{\kappa V_2 L_2^2}$
Flexible membrane $\kappa V_{\text{eff}} L_0^2 \gtrsim 1$		
	$V_{\text{eff}} \gg \Delta V$	$\Delta V \gtrsim V_{\text{eff}}$
R	$V_{\text{eff}}/\Delta V^{3/2}$	$\sqrt{\kappa} W_2$
F	$(V_{\text{eff}}/\Delta V)^2$	$\kappa V_2 W_2^2$

Table 5.1: Summary of scaling results

5.5 Conclusion

In this paper we have systematically studied the nucleation dynamics of membrane adhesions mediated by specific receptor binding. We distinguish between the different regimes according to the nature of the adhesion and the shape of the adhesion potential. Scaling arguments suggest that in the rigid-membrane regime when adhesion is a first-order transition, the geometry of the membrane shape is controlled by the adhesion length R_0, while the energetics is controlled by the characteristic energy $F_0 = \sqrt{\kappa V_2 L_0^2}$ —where L_0 is the length scale associated with the adhesion potential, V_2 is the barrier height, and κ is the bending rigidity. These conclusions are further verified from our numerical calculations of the minimum energy path.

When the membrane is very flexible or the barrier is small, entropic effects due to membrane undulations are important, and adhesion is a weak first-order transition controlled by the characteristic energy scale given by $F_0 = \sqrt{\kappa V_{\text{eff}} L_0^2}$. If the potential depth difference ΔV is small, the adhesion droplet still has a well-defined but irregular boundary. Applying a Peierls argument we find that the nucleation dynamics depend on the geometric dimension of the boundary of the adhesion droplet. In addition, the energy barrier and the critical nucleus size only depend on the potential depths but not their locations.

The surface tension term increases the nucleation barrier as well as the size of the critical nucleus. But we find that at a small surface tension, the shape of the nucleus is still controlled by the adhesion length R_0, which is almost unaffected by the surface tension, implying that the extra surface area

in the critical adhesion droplet is almost constant. We also show that the non-monotonic feature in the membrane shape near the phase boundary, as was first found by Komura and Andelman (2000), is due to the bending energy term and is reduced at increasing surface tension.

Bibliography

Adam, G., and Gibbs, J. H. (1965). On the temperature dependence of cooperative relaxation properties in glass-forming liquids. *J. Chem. Phys.*, 43(1):139.

Adams, J. L., Graessley, W. G., and Register, R. A. (1994). Rheology and the microphase separation transition in styrene-isoprene block copolymers. *Macromolecules*, 27:6026.

Adams, J. L., Quiram, D. J., Graessley, W. W., Register, R. A., and Marchand, G. R. (1996). Ordering dynamics of compositionally asymmetric styrene-isoprene block copolymers. *Macromolecules*, 29(8):2929.

Albersdörfer, A., Feder, T., and Sackmann, E. (1997). Adhesion-induced domain formation by interplay of long-range repulsion and short-range attraction force: a model membrane study. *Biophys. J.*, 73:245–257.

Alberts, B., Johnson, A., Lewis, J., Raff, M., Roberts, K., and Walter, P. (2002). *Molecular Biology of the Cell*. Garland, New York, 4th edition.

Almdal, K., and Bates, F. S. (1992). Order, disorder and fluctuation effects in an asymmetric pep-pee diblock copolymer. *J. Chem. Phys.*, 96:9122.

Almdal, K., Rosedale, J. H., Bates, F. S., Wignall, G. D., and Fredrickson, G. H. (1990). Gaussian-to stretched-coil transition in block copolymer melts. *Phys. Rev. Lett.*, 65:1112.

Anderson, P. W. (1972). More is different. *Science*, 177:393–396.

Angell, C. A. (1995). Formation of glasses from liquids and biopolymers. *Science*, 267(5206):1924.

Bagchi, B., Cerjan, C., and Rice, S. A. (1983). Theoretical analysis of the achievement of random close packing of hard spheres and a conjecture on spinodal decomposition. *Phys. Rev. B*, 28(11):6411.

Bahiana, M., and Oono, Y. (1990). Cell dynamical system approach to block copolymers. *Phys. Rev. A*, 41(12):6763–6771.

Balsara, N. P., Garetz, B. A., Newstein, M. C., Bauer, B. J., and Prosa, T. J. (1998). Evolution of microstructure in the liquid and crystal directions in a quenched block copolymer melt. *Macromolecules*, 31(22):7668.

Baltimore, D., Ludish, H., Berk, A., Zipursky, L. S., Matsudaira, P., and Darnell, J. (2003). *Molecular Cell Biology*. Freeman and Company, New York, 5th edition.

Barrat, J.-L., and Fredrickson, G. H. (1991). Collective and single-chain correlations near the block copolymer order-disorder transition. *J. Chem. Phys.*, 95:1281.

Bates, F. S., Cohen, R. E., and Berney, C. V. (1982). Small-angle neutron scattering determination of macrolattice structure in a polystyrene-polybutadiene diblock copolymer. *Macromolecules*, 15:589.

Bates, F. S., and Fredrickson, G. H. (1990). Block copolymer thermodynamics: theory and experiment. *Annu. Rev. Phys. Chem.*, 41:525.

Bates, F. S., and Fredrickson, G. H. (1999). Block copolymers–designer soft materials. *Phys. Today*, 52(2):32.

Bates, F. S., Rosedale, J. H., and Fredrickson, G. H. (1990). Fluctuation effects in a symmetric diblock copolymer near the order-disorder transition. *J. Chem. Phys.*, 92:6255.

Bates, F. S., Schulz, M. F., Khandpur, A. K., Förster, S., and Rosedale, J. H. (1994). Fluctuations, conformational asymmetry and block copolymer. *Faraday Discuss.*, 98.

Baudry, J., Bertrand, E., Lequeux, N., and Bibette, J. (2004). Bio-specific recognition and applications: From molecular to colloidal scales. *J. Phys. Condens. Matter*, 16:R469–R480.

Bell, G. I. (1978). Models for the specific adhesion of cells to cells. *Science*, 200:618.

Bell, G. I., Dembo, M., and Bongrand, P. (1984). Cell adhesion: Competition between nonspecific repulsion and specific bonding. *Biophys. J.*, 45:1051–1064.

Berg, J. M., Tymoczko, J. L., and Stryer, L. (2002). *Biochemistry*. W. H. Freeman, New York, 5th edition.

Bermúdez, H., Hammer, D. A., and Discher, D. E. (2004). Effect of bilayer thickness on membrane bending rigidity. *Langmuir*, 20:540–543.

Bongrand, P. (1999). Ligand-receptor interactions. *Rep. Prog. Phys.*, 62:921.

Boulbitch, A., Guttenberg, Z., and Sackmann, E. (2001). Kinetics of membrane adhesion mediated by ligand-receptor interaction studied with a biomimetic system. *Biophys. J.*, 81:2743–2751.

Brazovskii, S. A. (1975). Phase transition of an isotropic system to a nonuniform state. *Sov. Phys. JETP*, 41:85.

Bruinsma, R., Behrisch, A., and Sackmann, E. (2000). Adhesive switching of membranes: Experiment and theory. *Phys. Rev. E*, 61(4):4253–4267.

Bruinsma, R., and Sackmann, E. (2002). Cell adhesion as wetting transition? In Flyvbyerg, H., Ormos, P., and David, F., Eds. *Physics of Biomolecules and Cells*, Vol. 75 of *Les Houches Summer School*, Springer, pp. 287–309.

Canham, P. B. (1970). The minimum energy of bending as a possible explanation of the biconcave shape of the human red blood cell. *J. Theor. Biol.*, 26(1):61–81.

Carignano, M. A., and Szleifer, I. (2003). Controlling surface interactions with grafted polymers. *Interface Science*, 11:187–197.

Chen, C.-C., and Dormidontova, E. E. (2005). Architectural and structural optimization of the protective polymer layer for enhanced targeting. *Langmuir*, 21:5605–5615.

Choi, S., Lee, K. M., Han, C. D., Sota, N., and Hashimoto, T. (2003). Phase transitions in sphere-forming PS-PI-PS copolymer and its blends with homopolymer. *Macromolecules*, 36:793.

Coluzzi, B., Parisi, G., and Verrocchio, P. (2000). Thermodynamical liquid-glass transition in a lennard-jones binary mixture. *Phys. Rev. Lett.*, 84(2):306–309.

Coniglio, A. N., Stanley, H. E., and Klein, W. (1979). Site-bond correlated percolation problem: A statistical mechanical model of polymer gelation. *Phys. Rev. Lett.*, 42(8):518–522.

Coniglio, A. N., Stanley, H. E., and Klein, W. (1982). Solvent effects on polymer gel. *Phys. Rev. B*, 25(11):6805–6821.

Coombs, D., Dembo, M., Wolfsy, C., and Goldstein, B. (2004). Equilibrium thermodynamics of cell-cell adhesion mediated by multiple ligand-receptor pairs. *Biophys. J.*, 86:1408–1423.

Cornwall, J. M., Jackiw, R., and Tomboulis, E. (1974). Effective action for composite operators. *Phys. Rev. D*, 10(8):2428.

Cuvelier, D., and Nassoy, P. (2004). Hidden dynamics of vesicle adhesion induced by specific stickers. *Phys. Rev. Lett.*, 93:228101.

Cuvelier, D., Vezy, C., Viallat, A., Bassereau, P., and Nassoy, P. (2004). Mimicking cell/extracellular matrix adhesion with lipid membranes and solid substrates: Requirements, pitfalls and proposals. *J. Phys. Condens. Matter*, 16:S2427–S2437.

de Gennes, P. G. (1979). *Scaling Concepts in Polymer Physics*. Cornell University Press, Ithaca.

de la Cruz, M. O. (1991). Transitions to periodic structures in block copolymer melts. *Phys. Rev. Lett.*, 67:85.

Debenedetti, P. G., and Stillinger, F. H. (2001). Supercooled liquids and the glass transition. *Nature*, 410:259.

Dembo, M., and Bell, G. I. (1987). The thermodynamics of cell adhesion. *Current Topics in Membranes and Transport*, 29:71–89.

Discher, B. M., Won, Y.-Y., Ege, D. S., Lee, J. C.-M., Bates, F. S., Discher, D. E., and Hammer, D. A. (1999). Polymersomes: Tough versicles made from diblock copolymers. *Science*, 284:1143–1146.

Dobrynin, A. V., and Erukhimovich, I. Y. (1991). Fluctuation effects in the theory of weak supercrystallization in block copolymer systems of complicated chemical structure. *J. Phys. II France*, 11:1387.

Doi, M. (1996). *Introduction to Polymer Physics*. Clarendon Press, Oxford.

Doi, M., and Edwards, S. F. (1986). *The Theory of Polymer Dynamics*. Oxford University Press.

Dormidontova, E. E., and Lodge, T. P. (2001). The order-disorder transition and the disordered micelle regime in sphere-forming block copolymer melts. *Macromolecules*, 34:9143.

Drolet, F., and Fredrickson, G. H. (1999). Combinatorial screening of complex block copolymer assembly with self-consistent field theory. *Phys. Rev. Lett.*, 83:4317–4320.

Drolet, F., and Fredrickson, G. H. (2001). Optimizing chain bridging in complex block copolymers. *Macromolecules*, 34:5317.

Dustin, M. L., Ferguson, L. M., Chan, P.-Y., Springer, T. A., and Golan, D. E. (1996). Visualization of CD2 interaction with LFA-3 and determination of the two-dimensional dissociation constant for adhesion receptors in a contact area. *J. Cell. Bio.*, 132(3):465–474.

E, W., Ren, W., and Vanden-Eijnden, E. (2002). String method for the study of rare events. *Phys. Rev. E.*, 66:052301.

Edwards, S. F., and Anderson, P. W. (1976). Theory of spin glasses II. *J. Phys. F*, 6(10):1927.

Eniola, A. O., Willcox, P. J., and Hammer, D. A. (2003). Interplay between rolling and firm adhesion elucidated with a cell-free system engineered with two distinct receptor-ligand pairs. *Biophys. J.*, 85:2720–2731.

Evans, E., and Ritchie, K. (1999). Strength of a weak bond connecting flexible polymer chains. *Biophys. J.*, 76(5):2439.

Finger, E. B., Puri, K. D., Alon, R., Lawrence, M. B., von Andrian, U. H., and Springer, T. A. (1996). Adhesion through L-selectin requires a threshold hydrodynamic shear. *Nature*, 379:266–269.

Flory, P. J. (1953). *Principles of Polymer Chemistry*. Cornell University Press, Ithaca and London.

Flyvbjerg, H., Hertz, J., Jensen, M. H., Mouritsen, O. G., and Sneppen, K., Eds. (1997). *Physics of Biological Systems: From molecules to species*. Springer Verlag.

Fraaije, J. G. E. M., van Vlimmeren, B. A. C., Maurits, N. M., Postma, M., Evers, O. A., Hoffman, C., Altevogt, P., and Goldbeck-Wood, G. (1997). The dynamic mean-field density functional method and its application to the mesoscopic dynamics of quenched block copolymer melts. *J. Chem. Phys.*, 106:4260.

Fredrickson, G. H., and Binder, K. (1989). Kinetics of metastable states in block copolymer melts. *J. Chem. Phys.*, 91:7265.

Fredrickson, G. H., Ganesan, V., and Drolet, F. (2002). Field-theoretic computer simulation methods for polymers and complex fluids. *Macromolecules*, 35:16–39.

Fredrickson, G. H., and Helfand, E. (1987). Fluctuation effects in the theory of microphase separation in block copolymers. *J. Chem. Phys.*, 87:697.

Fredrickson, G. H., and Leibler, L. (1989). Theory of block copolymer solutions: Nonselective good solvents. *Macromolecules*, 22(1238-1250).

Garcia, A. J. (2006). Interfaces to control cell-biomaterial adhesive interactions. *Adv. Polym. Sci.*, 203:171–190.

Geissler, P. L., and Reichman, D. R. (2004). Nature of slow dynamics in a minimal model of frustrated-limited domains. *Phys. Rev. E*, 69(2):021501(9).

Gido, S. P., and Thomas, E. L. (1994). Lamellar diblock copolymer grain boundary morphology. 4. Tilt boundaries. *Macromolecules*, 27(21):6137.

Götze, W. (1989). Aspects of structural glass transitions. In Hansen, J. P., Levesque, D., and Zinn-Justin, J., editors, *Liquids, Freezing and Glass Transition, Part I*, Vol. 51 of *Les Houches*. North-Holland.

Grakoui, A., Bromley, S. K., Sumen, C., Davis, M. M., Shaw, A. S., Allen, P. M., and Dustin, M. L. (1999). The immunological synapse: A molecular machine controlling t cell activation. *Science*, 285:221–227.

Grousson, M., Krakoviack, V., Tarjus, G., and Viot, P. (2002a). Langevin dynamics of the coulomb frustrated ferromagnet: A mode-coupling analysis. *Phys. Rev. E*, 66(2):026126.

Grousson, M., Tarjus, G., and Viot, P. (2001). Monte carlo study of the three-dimensional coulomb frustrated ising ferromagnet. *Phys. Rev. E*, 64(3):036109.

Grousson, M., Tarjus, G., and Viot, P. (2002b). Evidence for "fragile" glass-forming behavior in the relaxation of coulomb frustrated three-dimensional systems. *Phys. Rev. E*, 65(6):065103.

Guttenberg, Z., Lorz, B., Sackmann, E., and Boulbitch, A. (2001). First-order transition between adhesion states in a system mimicking cell-tissue interaction. *EuroPhys. Lett.*, 54(6):826–832.

Hall, R. W., and Wolynes, P. G. (1987). The aperiodic crystal picture and free energy barriers in glasses. *J. Chem. Phys.*, 86(5):2943.

Hamley, I. W. (1998). *The Physics of Block Copolymers*. Oxford University Press.

Hamley, I. W., Ed. (2004). *Developments in Block Copolymer Science and Technology*. John Wiley and Sons.

Hammer, D. A. and Tirrell, M. (1996). Biological adhesion at interfaces. *Annu. Rev. Mater. Sci.*, 26:651.

Han, C. D., Vaidya, N. Y., Kim, D., Shin, G., Yamaguchi, D., and Hashimoto, T. (2000). Lattice disordering/ordering and demicelliation/micellization transitions in highly asymmetric PS-PI copolymers. *Macromolecules*, 33:3767.

Helfrich, W. (1973). Elastic properties of lipid bilayers: theory and possible experiments. *Z. Naturforsch. C*, 28(11):693–703.

Hiddessen, A. L., Rodgers, S. D., Weitz, D. A., and Hammer, D. A. (2000). Assembly of binary colloidal structures via specific biological adhesion. *Langmuir*, 16:9744–9753.

Hohenberg, P. C., and Swift, J. B. (1995). Metastability in fluctuation-driven first-order transitions: Nucleation of lamellar phases. *Phys. Rev. A*, 52:1828.

Ikkai, F., and Shibayama, M. (1999). Static inhomogeneities in thermoreversible physical gels. *Phys. Rev. Lett*, 82(24):4946–4949.

Ishida, M., and Tanaka, F. (1997). Theoretical study of the postgel regime in thermoreversible gelation. *Macromolecules*, 30(13):3900–3909.

Israelachvili, J. N. (1992). *Intermolecular and Surface Forces*. Academic Press, 2nd edition. (3rd edition to be published by Elsevier in 2008.)

Jeppesen, C., Wong, J. Y., Kuhl, T. L., Israelachvili, J. N., Mullah, N., Zalipsky, S., and Marques, C. M. (2001). Impact of polymer tether length on multiple ligand-receptor bond formation. *Science*, 293:465.

Kauzmann, W. (1948). The nature of the glassy state and the behavior of liquids at low temperatures. *Chem. Rev.*, 43:219.

Kielhorn, L., and Muthukumar, M. (1997). Fluctuation theory of diblock copolymer/homopolymer blends and its effect on the lifshitz point. *J. Chem. Phys.*, 107(14):5588.

Kim, J. K., Lee, H. H., Sakurai, S., Aida, S., Masamoto, J., Nomura, S., Kitagawa, Y., and Suda, Y. (1999). Lattice disordering and domain dissolution transitions in polystyrene-block-poly(ethylene-co-but-1-ene)-block-polystyrene triblock copolymer having a highly asymmetric composition. *Macromolecules*, 32(20):6707.

Kim, W. G., Chang, M. Y., Garetz, B. A., Newstein, M. C., Balsara, N. P., Lee, J. H., Han, H., and Patel, S. S. (2001). Effect of quench depth on grain structure in quiescently ordered block copolymers. *J. Chem. Phys.*, 114(22):10196.

Kirkpatrick, T. R., and Thirumalai, D. (1989). Random solutions from a regular density functional hamiltonian: a static and dynamical theory for the structural glass transition. *J. Phys. A: Math. Gen.*, 22:L149.

Kirkpatrick, T. R., Thirumalai, D., and Wolynes, P. G. (1989). Scaling concepts for the dynamics of viscous liquids near an ideal glassy state. *Phys. Rev. A*, 40(2):1045.

Kirkpatrick, T. R., and Wolynes, P. G. (1987). Connections between some kinetic and equilibrium theories of the glass transition. *Phys. Rev. A*, 35(7):3072.

Kloboucek, A., Behrisch, A., Faix, J., and Sackmann, E. (1999). Adhesion-induced receptor segregation and adhesion plaque formation: a model membrane study. *Biophys. J.*, 77:2311–2328.

Komura, S., and Andelman, D. (2000). Adhesion-induced lateral phase separation in membranes. *Euro. Phys. J. E*, 3:259–271.

Kudlay, A., and Stepanow, S. (2003). Short-range fluctuations in the Hartree theory of diblock copolymer melts. *J. Chem. Phys.*, 118(9):4272.

Kumar, S. K., and Douglas, J. F. (2001). Gelation in physically associating polymer solutions. *Phys. Rev. Lett.*, 87(18):188301.

Kumar, S. K., and Panagiotopoulos, A. Z. (1999). Thermodynamics of reversible associating polymer solutions. *Phys. Rev. Lett.*, 82(25):5060–5063.

Kuo, S. C., and Lauffenburger, D. A. (1993). Relationship between receptor/ligand binding affinity and adhesion strength. *Biophys. J.*, 65:2191–2200.

Lauffenburger, D. A., and Linderman, J. J. (1993). *Receptors: Models for Binding, Trafficking and Signaling*. Oxford University Press, New York.

Laughlin, R. B., Pines, D., Schmalian, J., Stojkovic, B. P., and Wolynes, P. (2000). The middle way. *Proc. Natl. Acad. Sci.*, 97(1):32–37.

Lawrence, M. B., and Springer, T. A. (1991). Leukocytes roll on a selectin at physiologic flow rates: Distinction from and prerequisite for adhesion through integrins. *Cell*, 65:859–873.

Lee, S.-J. E., Hori, Y., and Chakraborty, A. K. (2003). Low t cell receptor expression and thermal fluctuations contribute to formation of dynamic multifocal synapses in thymocytes. *Proc. Natl. Acad. Sci.*, 100(8):4383–4388.

Leibler, L. (1980). Theory of microphase separation in block copolymers. *Macromolecules*, 13:1602.

Lin, J. J., Bates, F. S., Hammer, D. A., and Silas, J. A. (2005). Adhesion of polymer versicles. *Phys. Rev. Lett.*, 95:026101.

Lin, J. J., Silas, J. A., Bermúdez, H., Milam, V. T., Bates, F. S., and Hammer, D. A. (2004). The effect of polymer chain length and surface density on the adhesiveness of functionalized polymersomes. *Langmuir*, 20:5493–5500.

Ling, D. D., Friman, B., and Grinstein, G. (1981). First- and second-order transitions in models with a continuous set of energy minima. *Phys. Rev. B*, 24(5):2718.

Lipowsky, R. (1994). Discontinuous unbinding transitions of flexible membranes. *J. Phys. II France*, 4:1755–1762.

Lipowsky, R. (1995). Generic interactions of flexible membranes. In Lipowsky, R. and Sackmann, E., Eds. *Structure and Dynamics of Membranes* G*eneric and Specific Interactions*, Handbook of Biological Physics (ab), Elsevier Science (North Holland), p. 521.

Lipowsky, R. (1996). Adhesion of membranes via anchored stickers. *Phys. Rev. Lett.*, 77(8):1652–1655.

Lipowsky, R., and Dimova, R. (2003). Domains in membranes and vesicles. *J. Phys. Condens. Matter*, 15:S31–S45.

Lipowsky, R., and Leibler, S. (1986). Unbinding transitions of interacting membranes. *Phys. Rev. Lett.*, 56(23):2541–2544.

Manghi, M., and Aubouy, M. (2003). Mobile polymer connectors. *Euro. Phys. J. E*, 11:243–254.

Martin, J. I., Zhang, C.-Z., and Wang, Z.-G. (2006). Polymer-tethered ligand-receptor interactions between surfaces. *J. Polym. Sci. Part B Polymer Physics*, 44:2621–2637.

Matsen, M. W., and Bates, F. S. (1996). Unifying weak- and strong-segregation block copolymer theories. *Macromolecules*, 29:1091.

Matsen, M. W., and Schick, M. (1994). Stable and unstable phases of a diblock copolymer melt. *Phys. Rev. Lett.*, 72:2660.

Maurits, N. M., and Fraaije, J. G. E. M. (1997). Mesoscopic dynamics of copolymer melts: From density dynamics to external potential dynamics using nonlocal kinetic coupling. *J. Chem. Phys.*, 107:5879.

Mézard, M., and Parisi, G. (2000). Statistical physics of structural glasses. *J. Phys. Condens. Matter*, 12:6655.

Mézard, M., Parisi, G., and Virasoro, M. A., Eds. (1987). *Spin Glass Theory and Beyond*. World Scientific.

Monasson, R. (1995). Structural glass transition and the entropy of the metastable states. *Phys. Rev. Lett.*, 75:2847–2850.

Moore, N. W., and Kuhl, T. L. (2006). The role of flexible tethers in multiple ligand-receptor bond formation between curved surfaces. *Biophysical J.*, 91:1675–1687.

Moreira, A. G., Jeppesen, C., Tanaka, F., and Marques, C. M. (2003). Irreversible vs. reversible bridging: When is kinetics relevant for adhesion? *EuroPhys. Lett.*, 62(6):876–882.

Moreira, A. G., and Marques, C. M. (2004). The role of polymer spacers in specific adhesion. *J. Chem. Phys.*, 120(13):6229–6237.

Müller, M., Katsov, K., and Schick, M. (2006). Biological and synthetic membranes: What can be learned from a coarse-grained description. *Phys. Rept.*, 434:113–176.

Nap, R., and Szleifer, I. (2005). Control of carbon nanotube-surface interactions: The role of grafted polymers. *Langmuir*, 21:12072–12075.

Nelson, D., Piran, T., and Weinberg, S., Eds. (2004). *Statistical Mechanics of Membranes and Surfaces*. World Scientific, Singapore, 2nd edition.

Nussinov, Z. (2004). Avoided phase transitions and glassy dynamics in geometrically frustrated systems and non-abelian theories. *Phys. Rev. B*, 69(1):014208.

Nussinov, Z., Rudnick, J., Kivelson, S. A., and Chayes, L. N. (1999). Avoided critical behavior in $O(n)$ systems. *Phys. Rev. Lett.*, 83(3):472.

Ohta, T., and Kawasaki, K. (1986). Equilibrium morphology of block copolymer melts. *Macromolecules*, 19:2621.

Orsello, C. E., Lauffenburger, D. A., and Hammer, D. A. (2001). Molecular properties in cell adhesion: A physical and engineering perspective. *Trends in Biotechnology*, 19(8):310–316.

Palmer, R. G. (1982). Broken ergodicity. *Adv. Phys.*, 31(6):669.

Peliti, L. (1994). Amphiphilic membranes. In David, F., Ginzparg, P., and Zinn-Justin, J., Eds. *Fluctuating Geometries in Statistical Mechanics and Field Theory*, Vol. 62 of *Les Houches Summer School*, Elsevier, pp. 195–286.

Peliti, L., and Leibler, S. (1985). Effects of thermal fluctuations on systems with small surface tension. *Phys. Rev. Lett.*, 54(15):1690–1693.

Petka, W. A., Harden, J. L., McGrath, K. P., Wirtz, D., and Tirrell, D. A. (1998). Reversible hydrogels from self-assembling artificial proteins. *Science*, 281.

Phillips, R., and Quake, S. R. (2006). The biological frontier of physics. *Phys. Today*, 59(5):38–43.

Pochan, D. J., Gido, S. P., Pispas, S., and Mays, J. W. (1996). Morphologies of microphase-separated a(2)-b simple graft-copolymers. *Macromolecules*, 29(22):5099.

Qi, S.-Y., Groves, J. T., and Chakraborty, A. K. (2001). Synaptic pattern formation during cellular recognition. *Proc. Natl. Acad. Sci.*, 98(12):6548–6553.

Rädler, J., and Sackmann, E. (1993). Imaging optical thicknesses and separation distances of phospholipid vesicles at solid surfaces. *J. Phys. II Paris*, 3:727–748.

Rädler, J. O., Feder, T. J., Strey, H. H., and Sackmann, E. (1995). Fluctuation analysis of tension-controlled undulation forces between giant vesicles and solid substrates. *Phys. Rev. E*, 51(5):4526–4536.

Raphaël, E., Gay, C., and de Gennes, P. G. (1997). Progressive construction of an "Olympic" gel. *J. Stat. Phys.*, 89(1/2):111–118.

Raychaudhuri, S., Chakraborty, A. K., and Kardar, M. (2003). Effective membrane model of the immunological synapse. *Phys. Rev. Lett.*, 91(20):208101.

Ren, S. Z., and Sorensen, C. M. (1993). Relaxations in gels: Analogies to α and β relaxations in glasses. *Phys. Rev. Lett.*, 70(11):1727–1730.

Rosedale, J. H., and Bates, F. S. (1990). Rheology of ordered and disordered symmetric PEP-PEE diblock copolymers. *Macromolecules*, 23:2329.

Sackmann, E. (1996). Supported membranes: Scientific and practical applications. *Science*, 271:43–48.

Sackmann, E. (2006). Thermo-elasticity and adhesion as regulators of cell membrane architecture and function. *J. Phys. Condens. Matter*, 18:R785–R825.

Sackmann, E., and Bruinsma, R. F. (2002). Cell adhesion as wetting transition? *Chem. Phys. Chem.*, 3:262–269.

Sackmann, E., and Goennenwein, S. (2006). Cell adhesion as dynamic interplay of lock-and-key, generic and elastic forces. *Prog. Theo. Phys. Suppl.*, 165:78–99.

Safran, S. A. (1994). *Statistical Thermodynamics of Surfaces, Interfaces and Membranes*. Addison-Wesley Publishing Company.

Sain, A., and Wortis, M. (2004). Influence of tether dynamics on forced Kramers escape from a kinetic trap. *Phys. Rev. E*, 70:031102.

Schmalian, J., and Wolynes, P. G. (2000). Stripe glasses: Self-generated randomness in a uniformly frustrated system. *Phys. Rev. Lett.*, 85(4):836–839.

Schmalian, J., Wu, S., and Wolynes, P. G. (2003). cond-mat/0305420.

Schmid, F. (1998). Self-consistent-field theories for complex fluids. *J. Phys. Condens. Matter*, 19:8105–8138.

Schwab, M., and Stühn, B. (1996). Thermotropic transition from a state of liquid order to a macrolattice in asymmetric diblock copolymers. *Phys. Rev. Lett.*, 76:924.

Segrè, P. N., Prasad, V., Schofield, A. B., and Weitz, D. A. (2001). Glasslike kinetic arrest at the colloidal-gelation transitiion. *Phys. Rev. Lett.*, 86(26):6042-6045.

Semenov, A. N. (1989). Microphase separation in diblock-copolymer melts: Ordering of micelles. *Macromolecules*, 22:2849.

Semenov, A. N., Joanny, J. F., and Khokhlov, A. R. (1995a). Associating polymers: Equilibrium and linear viscoelasticity. *Macromolecules*, 28(4):1066–1075.

Semenov, A. N., Nyrkova, I. A., and Cates, M. E. (1995b). Phase equilibria in solutions of associating telechelic polymers: Rings vs. reversible network. *Macromolecules*, 28(23):7879–7885.

Semenov, A. N., and Rubinstein, M. (1998a). Thermoreversible gelation in solutions of associative polymers 1. statics. *Macromolecules*, 31(4):1373–1385.

Semenov, A. N., and Rubinstein, M. (1998b). Thermoreversible gelation in solutions of associative polymers 2. linear dynamics. *Macromolecules*, 31(4):1386–1385.

Shankar, R. (1994). Renormalization-group approach to interacting fermions. *Rev. Mod. Phys.*, 66(1):129.

Shen, W., Zhang, K., Kornfield, J. A., and Tirrell, D. A. (2006). Tuning the erosion rate of artificial protein hydrogels through control of network topology. *Nature Mat.*, 5:153–158.

Shibayama, M., Tsujimoto, M., and Ikkai, F. (2000). Static inhomogeneities in physical gels: Comparison of temperature-induced and concentration-induced sol-gel transition. *Macromolecules*, 33(21):7868–7876.

Simson, R., Wallraff, E., Faix, J., Nienöhner, J., Gerisch, G., and Sackmann, E. (1998). Membrane bending modulus and adhesion energy of wild-type and mutant cells of *Dictyostelium* lacking talin or cortexillins. *Biophys. J.*, 74:514–522.

Singh, Y., Stoessel, J. P., and Wolynes, P. G. (1985). Hard-sphere glass and the density-functional theory of aperiodic crystals. *Phys. Rev. Lett.*, 54(10):1059–1062.

Sota, N., Sakamoto, N., Saijo, K., and Hashimoto, T. (2003). Phase transition from disordered sphere to hex-cylinder via transient ordering into bcc-sphere in SIS triblock copolymer. *Macromolecules*, 36(12):4534.

Springer, T. A. (1990). Adhesion receptors of the immune system. *Nature*, 346:425–434.

Springer, T. A. (1994). Traffic signals for lymphocytes recirculation and leukocyte emigration: Multistep paradigm. *Cell*, 76:301–314.

Stauffer, D., Coniglio, A., and Adam, M. (1982). Gelation and critical phenomena. *Adv. Polym. Sci.*, 44:103–158.

Swift, J., and Hohenberg, P. C. (1977). Hydrodynamic fluctuations at the convective instability. *Phys. Rev. A*, 15:319.

Szleifer, I., and Carignano, M. A. (1996). Tethered polymer layers. *Adv. Chem. Phys.*, 94:165–260.

Tanaka, F. (1989). Theory of thermoreversible gelation. *Macromolecules*, 22(4):1989–1994.

Tanaka, F. (1990). Thermodynamic theory of network-forming polymer solutions. 1. *Macromolecules*, 23(16):3784–3789.

Tanaka, F., and Matsuyama, A. (1989). Tricriticality in thermoreversible gels. *Phys. Rev. Lett.*, 62(23):2759–2762.

Tanaka, F., and Stockmayer, W. H. (1994). Thermoreversible gelation with junctions of variable multiplicity. *Macromolecules*, 27(14):3943–3954.

Tanaka, M., and Sackmann, E. (2005). Polymer-supported membranes as models of the cell surface. *Nature*, 437:656–663.

Tanaka, T., Swislow, G., and Ohmine, I. (1979). Phase separation and gelation in gelatin gels. *Phys. Rev. Lett.*, 42(23):1556–1559.

Torney, D. C., Dembo, M., and Bell, G. I. (1986). Thermodynamics of cell adhesion II. freely mobile repellers. *Biophys. J.*

Tzeremes, G., Rasmussen, K. O., Lookman, T., and Saxena, A. (2002). Efficient computation of the structural phase behavior of block copolymers. *Phys. Rev. E*, 65(4):041806.

Uneyama, T., and Doi, M. (2005). Density functional theory for block copolyer melts and blends. *Macromolecules*, 38:196–205.

Volmer, A., Seifert, U., and Lipowsky, R. (1998). Critical behavior of interacting surfaces with tension. *Euro. Phys. J. B*, 5:811–823.

Wang, J., Wang, Z.-G., and Yang, Y. (2005). Nature of disordered micelles in sphere-forming block copolymer melts. *Macromolecules*, 38(5):1979.

Wang, X., Dormidontova, E. E., and Lodge, T. P. (2002). The order disorder transition and the disordered micelle regime for poly(ethylenepropylene-b-dimethylsiloxane) spheres. *Macromolecules*, 35:9687.

Wang, Z.-G. (2002). Concentration fluctuation in binary polymer blends: χ parameter, spinodal and Ginzburg criterion. *J. Chem. Phys.*, 117(1):481.

Weikl, T. R., Andelman, D., Komura, S., and Lipowsky, R. (2002). Adhesion of membranes with competing specific and generic interactions. *Euro. Phys. J. E*, 8:59–66.

Westfahl, H., Schmalian, J., and Wolynes, P. G. (2001). Self-generated randomness, defect wandering, and viscous flow in stripe glasses. *Phys. Rev. B*, 64(17):174203(16).

Wong, J. Y., Kuhl, T. L., Israelachvili, J. N., Mullah, N., and Zalipsky, S. (1997). Direct measurement of a tethered ligand-receptor interaction potential. *Science*, 275:820.

Wood, S. M., and Wang, Z.-G. (2002). Nucleation in binary polymer blends: A self-consistent field study. *J. Chem. Phys.*, 116(5):2289–2300.

Wu, S., Schmalian, J., Kotliar, G., and Wolynes, P. G. (2004). Solution of local-field equations for self-generated glasses. *Phys. Rev. B*, 70:024207.

Wu, S., Westfahl, Jr., H., Schmalian, J., and Wolynes, P. G. (2002). Theory of microemulsion glasses. *Chem. Phys. Lett.*, 359:1.

Xia, X., and Wolynes, P. G. (2000). Fragilities of liquids predicted from the random first-order transition theory of glasses. *Proc. Natl. Aca. Sci.*, 97(7):2990–2994.

Zhu, C., Bao, G., and Wang, N. (2000). Cell mechanics: Mechanical response, cell adhesion and molecular deformation. *Annu. Rev. Biomed. Eng.*, 2:189–226.

Zilman, A. G. and Safran, S. A. (2002). Thermodynamics and structure of self-assembled networks. *Phys. Rev. E*, 66(5):051107.

Zinn-Justin, J. (2002). *Quantum Field Theory and Critical Phenomena*. Clarendon Press, Oxford, 4th edition.

Zukerman, D., and Bruinsma, R. (1995). Statistical mechanics of membrane adhesion by reversible molecular bonds. *Phys. Rev. Lett.*, 74(19):3900–3903.